Numerical Investigation and Evaluation of Applying PPCI Combustion in A HSDI Diesel Engine

Bin Liu

A thesis submitted in partial fulfilment of the requirements of the University of Sussex for the degree of Doctor of Philosophy in Engineering

UNIVERSITY OF SUSSEX

September, 2013

UNIVERSITY OF SUSSEX

BIN LIU, DOCTOR OF PHILOSOPHY IN ENGINEERING

NUMERICAL INVESTIGATION AND EVALUATION OF APPLYING PPCI COMBUSTION IN A HSDI DIESEL ENGINE

SUMMARY

In this study, the Partially Premixed Compression Ignition (PPCI) combustion strategy in the high-speed, direct-injection diesel engine was investigated numerically by KIVA-3V code coupled with detailed chemistry, aiming to find the solution to meet the increasingly stringent emission regulations. Using split-injection, the parameters including injection timing, split-proportion, spray angle and injection pressures have been studied for their effects on combustion performance and emissions. The effects of swirl ratio, EGR rate and boost pressure are evaluated for improving the mixing and combustion of PPCI. The Homogeneity Factor (*HF*) was proposed for evaluating the quality of mixing and for quantitatively investigating the effects of injection parameters and in-cylinder air motion on mixture formation. Relationships between the quality of mixing and combustion performance and emissions were discussed using this factor. The results showed that HF had well revealed overall quality of mixture and the effects of operating parameters explicitly.

Different EGR compositions with varied fractions of CO_2 or H_2O were applied in PPCI combustion in order to evaluate the effects of EGR constituents on the combustion performance and emissions. Moreover, the parametric study was conducted under a sweep of the 2nd injection timing and EGR rate, for the understanding of the effects of CO_2 and water vapour in EGR at different operating modes

The speed range and load range for the PPCI diesel combustion using split injection was investigated. The results showed that the high level of EGR rate limited the implementation of PPCI combustion at high engine load, while the engine speed was limited by increased CO emissions. The application of high level cooled EGR had the potential for extending operating limits. The proposed Premixed Rate (*PR*) has revealed the correlations between the degree of premixed combustion and ignition delay, together with overall equivalence ratio. Good responses in fuel consumption have been shown with increase *PR*. And the significant reduce in *PR* indicated low degree of premixed at high engine load.

Acknowledgements

It is a pleasure to thank those who made this thesis possible. First and foremost, my gratitude goes to Dr. Zhijun Peng, my supervisor, for his constant encouragement and guidance. He leads me to go through all the stages of my DPhil study since 2007. Without his consistent and illuminating instructions, this thesis could not have reached its present form.

Secondly, I owe my heartfelt gratitude to Professor Yunqing Li, who guided me into the academic research of automotive engine, and gave me consistent helps without reservation. It is a great sorrow that now he is unable to witness my completion of this thesis. But I know he certainly would be extremely happy for me as he also did at every step of my progress.

I would also like to thank Professor Abdulnaser Sayma and Dr William Wang. As my co-supervisors, they have made available their support in a number of ways. Thanks are due to Dr. Ming Jia who was a research fellow from 2007 to 2009 at the University of Sussex, and now is at the Dalian University of Technology, China. He kindly provided the modified version of KIVA-3V code which was used though out this thesis. And the other faculty and research students in the School of Engineering and Informatics, University of Sussex also play an essential role in assisting me to overcome obstacles through this adventure.

I am also immensely grateful to Professor Hua Zhao of the Brunel University and Dr. Evgeny Petrov of the University of Sussex as they kindly accepted to be my examiners and for their constructive comments.

Lastly, I am indebted to my family, for their love, patience, encouragement and support all through these years. They are the source that confers the meanings on every piece of my life.

Contents

List of Tables

List of Figures

Nomenclature

Abbreviations

ABDC	After Bottom Dead Center ATDC
ATDC	After Top Dead Center BBDC
BBDC	Before Bottom Dead Center
BMEP	Break Mean Effective Pressure
CFD	Computational Fluid Dynamics
CO	Carbon Monoxide
CA	Crank Angle
DPF	Diesel Particulate Filter EGR
EGR	Exhaust Gas Recirculation
EVC	Exhaust Valve Closing
EVO	Exhaust Valve Opening
FTIR	Fourier Transform Infra-Red
GA	Genetic Algorithm
HCCI	Homogeneous Charge Compression Ignition
HRR	Heat Release Rate
HSDI	High Speed Direct Injection
IMEP	Indicated Mean Effective Pressure
IVC	Intake Valve Closing
IVO	Intake Valve Opening
ISFC	Gross Indicated specific fuel consumption [g/kW-hr]
LNT	Lean NOx Trap
LTC	Low Temperature Combustion
MK	Modulated Kinetics
NADI	Narrow Angle Direct Injection
NEDS	New European Drive Cycle

NO	Nitric Oxide
PCCI	Premixed Charge Compression Ignition
PPCI	Partially Premixed Compression Ignition
PREDIC	PREmixed lean DIesel Combustion regime
ROI	Rate of Injection
SOI	Start of Injection
SR	Swirl ratio
TAB	Taylor Analogy Breakup
TDC	Top Dead Center
UNIBUS	UNIforrn Bulky combustion System
UHC	Unburned Hydro Carbon
VCO	Valve Covered Orifice

Equations

L	Liquid length
ρ_f	Liquid fuel density
ρ_a	Surround air density
C_a	Orifice area-contraction coefficient
θ	Spray cone angle
d	Orifice diameter
T_a	Surround air temperature
P_a	Surround air pressure
T_f	Fuel temperature
h_a	Enthalpy of surround air
h_f	Enthalpy of fuel
T_s	Saturated fuel vapor temperature
P_s	Saturated fuel vapor pressure
η_{fc}	Fuel conversion efficiency

η_{tc}	Thermal conversion efficiency
η_{hl}	Heat loss efficiency
η_{comb}	Combustion efficiency
η_{hr}	Heat rejection efficiency
W	Gross Indicated work
m_f	Fuel mass injected per cycle
Q_{LHV}	Lower heating value of fuel
Q_{chem}	Total chemical heat release
Q_{hl}	Heat transfer losses
P_{in}	Intake boost pressure [kPa]
$\dot{m}_{fuel}$	Fuel mass injected per cycle [mg/cyc]
T_{in}	Intake air temperature [℃]
P_{inj}	Injection pressure [MPa]

Chapter 1 Introduction

Diesel engine is a power source for in automotive industry because of its superior economy than gasoline engine. However, its intrinsic drawback of high level of NO_x and soot emissions generated during the diffusion combustion processes limit the spread of using diesel engine on passenger cars in many countries. Fortunately, the research and develop on diesel engine have not been abandoned in Europe.

In recent decades, diesel engine becomes attractive again because it offers lower fuel consumption and generates lower CO_2 output compared with gasoline engine due to its higher compression ratio and leaner operating conditions. As the main constituent of green house gas, CO_2 now is one of the most important target pollutions in much legislation and regulations of environment protecting. And the increasingly raised oil price also drives more attentions on the application and optimizing of diesel engine on passenger cars and boosts the growth of diesel engine industry. Meantime, the developed electronic controlled fuel injection system makes it feasible to realize multiple-injection and high-pressure injection, which is helpful for the implementation of advanced combustion strategies.

Various combustion strategies have been proposed aiming to reduce NO_x and soot emissions without massive sacrifices in fuel consumption. The research of Kamimoto and Bae [1988] evaluated the effects of equivalence ratio (ϕ) and temperature (T) on the formation of NO_x and soot. The representative $\phi - T$ map presented by Kamimoto and Bae have become the basis for the studies about diesel combustion strategies for low emissions .As shown in Figure 1.1, simultaneously reduced NO_x and soot emission is possible to realize if the regions favorable for forming emissions can be avoid during combustion.

Homogeneity Charge Compression Ignition (HCCI) combustion and Partially Premixed Compression Ignition (PPCI) combustion are two typical strategies derived from this concept. HCCI combustion shows great capability in simultaneously reducing NO_x and soot emissions. However, to acquire homogeneous mixture, extremely early injection (before -60 ^{o} ATDC) or fuel-air pre-mixing out of cylinder is utilized, which leads to significant wall wetting due to the inferior volatility of diesel and consequently deteriorated combustion efficiency and increased HC and CO emissions in HCCI combustion. Moreover, with uniform distribution of equivalence ratio the combustion in HCCI is dominated by chemical reaction kinetics. Therefore, the control over combustion phase is difficult for HCCI combustion.

In comparison with HCCI, PPCI is more practical and adopts moderately early fuel injection to reduce wall wetting. A Large amount of EGR is introduced to prolong ignition delay and suppress the combustion temperature avoid the formation regions of NO_x and soot. Though the

mixture is still stratified prior to ignition, combustion takes place at much higher fraction of premixed combustion compared with the conventional diesel combustion process. Increased proportion of fuel burned under leaner equivalence ratio and lower combustion temperature results improved NO_x and soot emissions. More important, the control over combustion through injection strategy is feasible in PPCI combustion.

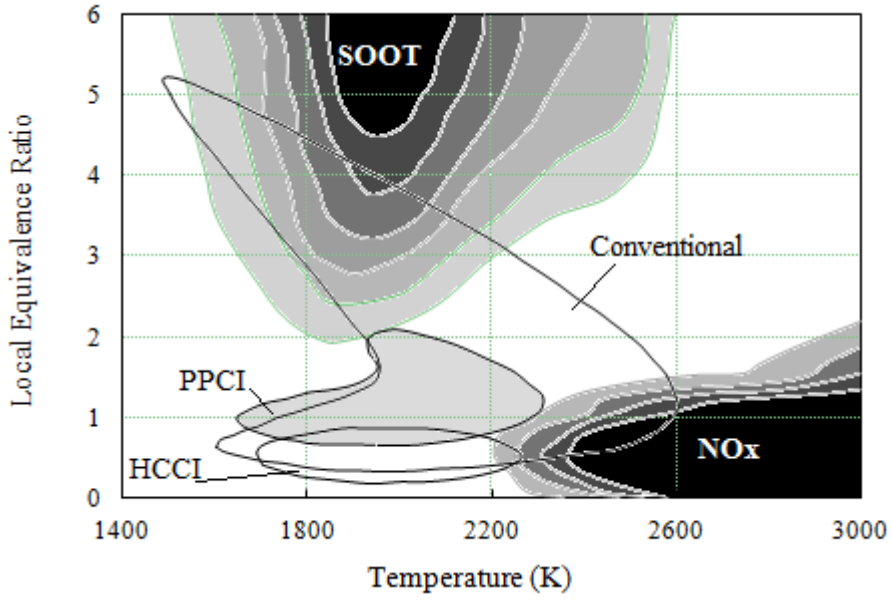

Figure 1.1 Simplified diesel combustion strategies in $\phi - T$ map, modified from the work of Kamimoto and Bae [1988]

PPCI combustion is not limited to extremely lean mixtures, then improving fuel-air mixing is the most important pathway to drastically reduce NO_x and soot emissions and avoid acceptable fuel economy penalty. Split-injection that has been commonly used in conventional diesel engines shows potentials to enhance the fuel-air mixing by appropriately increasing the in-cylinder temperature during the evaporation of the main injected fuel [Kook et al., 2006]. The pertinent literatures available demonstrated that fuel consumption and the output of CO and UHC can be improved by utilizing a pilot injection, where the simultaneously low NO_x and soot are achieved at the same level of PPCI combustion with single-injection [Koci et al., 2009; Park and Bae, 2011]. However, most of the PPCI research has been constrained to single-injection, while the knowledge about the engine performance and emission mechanisms of PPCI using split-injection is lacking.

In the meantime, the quality of mixing in PPCI combustion is difficult to evaluate directly or individually. Based on the same overall equivalence ratio, the homogeneity of mixture is evaluated through the comparison of conditions for mixing, like the length of ignition delay, injection pressure, the intensity of in-cylinder air motion, or through the data of combustion

performance and the formation of emissions. Limited pertinent literatures have discussed the definition of homogeneity but in primary stage [Nandha and Abraham, 2002]. Their definitions are not generalized, the relationships between homogeneity and engine performance and emission mechanism have not be investigated in their studies.

Because a significantly large amount of EGR is introduced into intake air for the implementation of PPCI diesel combustion, the effect of EGR and contributions of each constituent on engine performance and emission mechanism need to be discussed thoroughly. The dilution effect and thermal effect of EGR are the major factors that influence the mixing and combustion processes of PPCI combustion. Two major constituents in EGR, i.e. CO_2, and water vapor, show different results in dilution and thermal effect [Ladommatos et al., 1997]. Therefore, different EGR compositions with varied faction of CO_2 or H_2O may result in different effects in PPCI combustion, if same amount of EGR is introduced.

The high EGR requirement limits the power output, whilst the operating speed is constrained because the preparation of mixture requires appropriate ignition delay. It is of great interest to push the current limit of PPCI combustion to higher speed and loads level and eventually make it approaching the requirement of the engine in a passenger car. Meantime, for real implementation of PPCI combustion the thermal conversion efficiency has to be improved. Normally, the combustion phase of PPCI locates away from the TDC, where is usually considered as the thermodynamically efficient location. Therefore, the relations between the location of combustion phase and the thermal conversion efficiency need to be investigated in PPCI diesel combustion.

It is important to notice that PPCI combustion processes in stratified mixture rather than completely homogeneous charge. Though, the level of premixed combustion is much higher than in conventional diesel combustion, diffusion combustion, which is controlled by mixing, still exists in PPCI combustion. Currently, the evaluations of the degree of premixed combustion are conducted through qualitative analysis of heat release rate. This approach is adequate for comparing the level of premix between cases with similar engine configurations. However, it is difficult to clearly discuss the relations between the degree of premix combustion and engine responses without clear definition. Therefore, the proper definition of the degree of premixed combustion will be helpful for the investigation of PPCI combustion.

The objectives of present study can be summarized into following aspects: 1) to gain sufficient understandings about the combustion characteristics and emission mechanisms of PPCI diesel combustion with split-injection; 2) to propose a definition about the degree of homogeneity to evaluate the quality of mixture providing for PPCI combustion; 3) to evaluate the effects of EGR compositions on combustion performance and emission formations in PPCI diesel

combustion; 4) to explore the operating range of PPCI combustion with split-injection and evaluate the control methods for optimizing the thermal conversion efficiency in PPCI combustion; 5) to quantitatively define the degree of premix in PPCI combustion.

The structure of this thesis is: Chapter 2 gives the review of pertinent literature regarding the PPCI combustion, EGR, homogeneity of mixture, the degree of premixed combustion and other research area involved in this study. The numerical method and models used in this study are introduced in Chapter 3. Chapter 4 illustrates the parametrical investigation about the effects of split-injection strategy, swirl ratio, EGR rate and boost pressure on the combustion performance and emission formations in PPCI diesel combustion. Meantime, definition of the Homogeneity Factor (*HF*) is presented, together with discussions about the relations between the homogeneity of mixture and combustion characteristics or emissions are given in this chapter. The evaluation for the effects of EGR compositions on combustion performance and emission formations in PPCI diesel combustion is given in Chapter 5. The speed and load limits are explored in Chapter 6, together with the control methods for optimizing the thermal conversion efficiency in PPCI combustion. Moreover, the definition and discussions about Premixed Ratio (*PR*) are given here. Finally, the conclusions of this study and recommendation for future investigation are presented in Chapter 7.

Chapter 2 Literature Review

2.1 PPCI Combustion

As briefly discussed in Chapter 1, PPCI diesel combustion is considered as a promising strategy to simultaneously reduce NO_x and soot emissions and retain the control over combustion through injection. This section will give more information about the mechanisms, advantages and limitations of PPCI diesel combustion. Moreover, typical implementation of PPCI combustion will be presented.

2.1.1 Introduction to PPCI combustion

PPCI combustion is characterised by increased fraction of fuel burned in premixed combustion stage compared to conventional diesel combustion [Keeler and Shayler, 2008]. According to Figure 1.1, the combustion temperature is suppressed by large amount of EGR to avoiding region of NO_x formation [Kamimoto and Bae, 1988]. Meantime, the reduced bulk-air temperature during compression stroke delays the auto ignition of mixture and prolongs the time for mixing. The increased ignition delay leads to more uniform fuel distribution and reduced local equivalence ratios, which help the combustion to avoid the formation of soot.

Unlike HCCI combustion, PPCI combustion utilize moderately early injection timing initial for the purpose of reducing the wall wetting of fuel [Kong et al., 2005]. Though prolonged ignition delay allows more time for mixing, the completely homogeneous mixture is impossible to achieve with this moderately early injection. Thus, despite relatively low local equivalence ratio is achieved, fuel-air mixture features significant gradients in equivalence ratio. Although, partially mix-controlled combustion may be resulted, the gradient of equivalence ratio implies the possibility to control the combustion of PPCI by injection strategy [Park and Bae, 2011].

Since the level of premixed charge is increased in PPCI combustion, the reaction rate is much faster than that in conventional diesel combustion. The relatively rapid combustion leads to shorter combustion duration and increased level of combustion noise [Keeler and Shayler, 2008]. Also, the moderate advanced injection timing and shorter combustion duration causes the location of combustion phase away from the TDC, which is unbeneficial for thermal conversion efficiency. In order to increase the time for the flammable mixture reaching ignition limit, the in-cylinder temperature and pressure are suppressed by introducing large amount of cool EGR and reduced compression ratio, respectively. Wall impinging results in higher output of unburned hydrocarbon and increased fuel consumption due to the longer spray penetration and slower evaporation in the environment of lower temperature and pressure. Moreover, the reduced combustion temperature in PPCI combustion is not favourable for the oxidation of CO. Therefore, penalty in fuel economy and increased CO and UHC emissions challenge the

implementation of PPCI combustion.

2.1.2 Operating Limits and Implementation of PPCI Combustion

The operating limit is one of the major concerns for the implementation of PPCI diesel combustion. As shown in Figure 1.1, PPCI combustion is not constrained to extremely lean mixture. However, the power output is limited due to the high EGR requirement for suppressing temperature. Meantime, the engine speed is also limited since adequate time is required for achieving sufficient mixing in PPCI combustion.

Lewander et al. [2009] investigated the operating range of PPCI combustion in a heavy duty engine referring to the criteria shown below. The criteria are based on the assumption that after treatment is utilized to reduce smoke, while the NOx output is original. Constrained to the criteria, 30% of maximum load of conventional combustion can be achieved at low speed; whilst 21% of maximum load of conventional combustion can be achieved at high speed. Since the the time for mixing is reduced, the load limit decrease linearly with increased engine speed. They also showed that reducing EGR temperature can increase the operating range significantly.

sNO_x <= 0.3 g/kW h

Smoke <= 2FSN

bfsc < $bsfc_{baseline} \times 1.05$

Keeler and Shayler [2008] studied the constraints on fuel injection and EGR strategies for PPCI diesel combustion. In their study, the limits on speed and load in PPCI combustion are attributed to oxygen availability. Based on this conclusion, they suggested improving mixing, increasing boost pressure and further intake cooling to allow higher limits of speed and load. The load output of 9 bar IMEP was achieved with an intake pressure of 2.6 bar, where the overall equivalence ratio is 0.7. They also considered the combustion noise as an indicator limited the operating range of PPCI combustion. Increasing EGR rate or utilizing a pilot injection was suggested as effective measures to limit noise. Moreover, pilot injection with appropriate timing was found favourable for reducing soot output, which also beneficial for extending the limits of operation.

Helmantel [2008] pointed out that excessively increased boost pressure to extend the load limits could results in high combustion temperature which exceeded the limit of PPCI combustion, though high EGR rate (50%) is used. In this study, the load up to 13 bar IMEP have been achieved by PPCI combustion, with boost pressure of 2 bar, intake temperature of 60℃ and EGR rate up to 46%. Also, increased injection pressure (1800 bar) and intensive in-cylinder air motion were used to enhance fuel-air mixing. This high level of boost pressure is difficult to

realize in a practical application. Moreover, they suggested alternative valve opening strategies to increase swirl ratio to improve the soot output under relatively high combustion temperature.

Within the current limits on engine speed and load, there are some typical implementations of PPCI combustion strategy need to be noted:

Although with retarded injection, which is different from the method utilized in this study, the Modulated Kinetics (MK) is a promising implementation to achieve simultaneously reduced NO_x and soot emissions under PPCI combustion concept [Kimura et al., 1999; 2001]. Increased EGR rate and injection pressure, together with high swirl ratio were adopted to improve mixing. Kimura et al. [1999] found that the operating range could be extended to cover the Japanese test cycle (10-15 mode) by using high pressure injection and injector with large nozzle hole. Thereafter, near stoichiometric combustion was released by Kimura et al. [2001] using MK strategy with low compression ratio and cool EGR. They showed soot emission could be avoid if the injection finished within ignition delay and allow sufficient for fuel-air mixing. However, the requirement for complex intake port structure and considerably high injection pressure impeded MK strategy to be practically used. The investigations for developing MK strategy are still continuing.

Lee and Reitz [2006a] experimentally studied the characteristics of PPCI combustion in a single cylinder diesel engine under a representative operating condition for small bore HSDI engines in the New European Drive Cycle (NEDC). Their results demonstrate that combustion performance and emissions are strongly affected by injection timing. They proposed that there was a boundary of injection timing between conventional diesel and PPCI combustion in their study. They also indicated that spray targeting at the surface of piston bowl directly impacted the formation of emissions. In their opinion, start-of-injection timing could not explain the emission trends in PPCI combustion independently but with spay including angle. They considered the spray targeting point which was located near the edge of piston bowl as the optimum for PPCI combustion through different engine operating conditions because an excellent NOx and soot trade-off, together with better CO emissions could be achieved then.

The study of Lee et al. [2006b] showed that diesel stoichiometric operation can be realized by PPCI combustion with acceptable increase of fuel consumption (7%) compared to the conventional diesel combustion of best fuel economy, while sufficient reductions in NO_x (0.1 g/kW ћ) and soot (0.2 g/kW ћ) emissions were achieved. They also suggested higher fuel injection pressure and boost pressure for the future improvement of fuel consumption under stoichiometric diesel operation. Moreover, the realization of stoichiometric operation made it is possible to use three-way catalyst for the after treatment of emissions. However, the temperature of exhaust gas needs to be check for reaching the lighting-up limit of catalyst.

Kerschgens et al [2009] numerically studied the influence of combustion chamber geometry on mixture formation and pollutant emissions of PPCI combustion with CFD-Multi-Zone approach. The simulation was operated at part-load conditions with a speed of 2000 rpm and external EGR rate of 30%. Three piston-bowl shapes with original, reduced and stretched bowl diameters were simulated under same operating condition and with different injection timing in order to find the way to optimize the piston-bowl design for PPCI combustion. Their results showed that narrow bowl would trap the fuel inside and leading to incomplete combustion, while wide bowl would abate the effecting of air motion on mixing and leading to increased CO emissions. This suggested that an intermediate bowl diameter had to consider both pray targeting and fuel-air interaction.

Kokjohn et al [2010] investigated the potential of controlling PPCI combustion through varying fuel-reactivity. The dual-fuel strategy using port-injection gasoline and direct-injection diesel was adopted to realize variable fuel-reactivity stratification aiming to control combustion phase under a medium load of 9 bar net IMEP in their study. According to their results, fuel-reactivity stratification working with equivalence ration stratification could extend the combustion duration and reduce the rate of pressure rise compared to single fuel PPCI combustion. Additionally, fuel-reactivity stratification played a larger role in these effects than equivalence ratio stratification. They also stated that engines using this dual-fuel PPCI strategy could easily meet US EPA 2010 heavy-duty NO_x and PM emissions regulations without after-treatment, while reaching a net indicated thermal efficiency of 53%.

2.2 Emission Control Techniques in Diesel Engine

Apart from the alternative combustion strategies, many other techniques have been applied on diesel engine in order to reduce the emissions. The most commonly used and well developed techniques are including Exhaust Gas Recirculation (EGR), advanced injection systems, variable in-cylinder motion and pressure charging VGT. Some of them are important for the implementation and improvement of PPCI diesel combustion. This section will introduce these techniques and their applications on PPCI combustion.

2.2.1 Exhaust Gas Recirculation (EGR)

Exhaust gas recirculation (EGR) is considered one of the most effective techniques for NO_x control in diesel engines [Lapuerta et al., 1995]. Meantime, the impacts on fuel consumption and other emissions (soot, CO, UHC) can be massive because the application of changes the oxygen concentration and thermodynamic properties of intake air. Azetsu and Ito [2005] simplified the investigation about the effects of EGR by using CO_2 and N_2 to mix into ambient air, where intermittent spray combustion took place. The results from the optical study showed that both the ignition delay and combustion duration became longer with increased mixing gas,

whilst the combustion temperature decreased at the same time. They attributed these effects to the decreased O_2 concentration and higher heat capacity of CO_2. However, the effects of actual EGR are more complicated to understand.

A series of studies conducted by Ladommatos et al. [1996a; 1996b; 1997a; 1997b] tried to isolate the effects of EGR: 1) the dilution effect by replacing oxygen from intake air; 2) the thermal effect due to the higher heat capacity of EGR gas; 3) the chemical effect resulting from the dissociation of CO_2 or H_2O. The results showed that the reduced oxygen concentration was the main contributor to impact emissions. Increased dilution effects resulted reduced NO_x emission and increased output in soot, CO and UHC. The thermal effects of EGR were majorly responsible for the increased ignition delay and reduced combustion temperature. The effect of dissociation were minor compared to other two effects and did not act under low temperature combustion. However, small decrease of both NO_x and soot were obtained due to the dissociation of CO_2. They also compared the effects of CO_2 or H_2O in each aspect. Since the amount of CO_2 is almost twice as much as H_2O in EGR, CO_2 showed enlarged contribution in dilution effects and overall effects. With same mass, H_2O showed higher thermal effects due to its higher specific heat capacity. More chemical effects were observed in CO_2.

For PPCI diesel combustion, EGR is an effective way to achieve simultaneous low NOx and soot emission through prolonged ignition delay and reduced combustion temperature. However, the oxidation rate may reduce due to the lower oxygen availability at high EGR rate. Increased CO and UHC could be resulted from the decreased combustion efficiency. Meantime, the decreased combustion temperature due to the increased heat capacity by introducing EGR is not favorable for the oxidation of CO, and may leads to further increased of CO emissions. Therefore, higher CO outputs are often observed in PPCI combustion [Kook et al., 2006]. Moreover, internal EGR, which is feasible to realize without much cost in the re-structure of engine system, is found not suitable for apply in PPCI combustion due to its high temperature [Neely et al., 2005]. Thus, more pressure has been laid on the cooling system.

Kiplimo et al. [2012] investigated the effects of EGR on the combustion and emission characteristics of a PPCI diesel engine with a volume of 781.7 cm^3. The results for two EGR rates, i.e. 0% and 40%, were compared. With increased EGR rate, the excess air ratio reduced from 4.5 to 3.0, where the equivalence ratio was still in the lean area. Simultaneously reductions of NO_x and soot emissions were observed in the high EGR case. Though increased HC and CO emissions were detected in the high EGR case, the fuel efficiency and IMEP were improved. This indicated increased thermal conversion efficiency resulting from the shorter combustion duration and less advanced combustion phase location.

Hardy and Reitz [2006] performed the study of the effects of high EGR on a heavy-duty engine

at high speed (1737 rpm) and loads up to 60% of full load for PPCI combustion. With the earliest injection timing at -60 ºATDC, EGR level up to 75% was introduced and resulted in equivalence ratios up to 0.95. The results showed that increasing EGR rate to such a high level could still achieve reductions in soot, NO_x and CO with slightly increase in HC. Moreover, combustion noise intended to reduce at each load since the pressure rise rate dropped with increased EGR rate. BSFC decreased due to the decreased thermodynamic efficiency when the combustion phase retarded further after TDC.

2.2.2 Injection Strategies

Advanced injection strategies, like complex multiple injections, are developed base on the techniques of common rail and electronic control which allow injecting with high pressure and precisely respond. As discussed in previous section, improved fuel-air mixing is a major method to enhance fuel efficiency and reduce emissions in PPCI diesel combustion. Therefore, injection strategy significant impacts the responds of PPCI in both fuel consumption and emissions since it highly determines the mixing process. Following, the literature about the effects of injection timing, injection pressure, spray angle and split-injection on the characteristics of PPCI combustion are introduced.

Park and Bae [2011] explored the optimal injection timing for PPCI combustion by experiments on a single-cylinder direct injection diesel engine which was modified from diesel passenger car engine. With intake temperature of 80 ºC, ignition delay started to increase as injection timing was advance to more than -20 ºATDC. They also showed that start of combustion was governed by injection timing when it in the range of 0 ~ -30 ºATDC. Therefore, the injection timing between -20 ºATDC to -30 ºATDC was chosen for PPCI combustion in order to realize sufficient timing for mixing and controlling over combustion by injection. Meantime, they investigated the effects of pilot injection on PPCI combustion with split ratio of 10% to 30% at -35 ºATDC. The results showed that applying of pilot injection was effective for increasing IMEP and reducing emissions in PPCI diesel combustion.

Lee and Reitz [2006a] investigated the effects of spray targeting on exhaust emissions in PPCI combustion with a single-cylinder HSDI diesel engine, through sweeps of injection timing with several nozzles having different spray angles ranging from 50 ºto 154 º. The results demonstrated that there were optimal targeting spot on piston for low soot and CO emissions, while NO_x emissions were not affected by targeting. Cases using narrow spray angle showed high soot and CO emissions in conventional combustion region. However, CO decreased significantly in PPCI combustion region for narrow spray angle cases.

Kong et al [2009] numerically studied the performance of low pressure injector (15 MPa) and high pressure injector (190 MPa) in PPCI combustion based on the modified KIVA code

coupled with CHEMKIN. Their results showed that both extremely early injecting by low pressure injector and retarded injecting (-5 º ATDC) by high pressure injector could achieve efficiently reduced emissions. Opat et al. [2007] investigated the mixing effects on HC/CO emissions for PPCI combustion in a light duty diesel engine through varied injection pressures ranged from 600 to 1120 bar. Decreased CO output was observed with increased injection pressure in their study. In fact, due to the enhanced air entrainment by increased injection pressure reduced soot could be achieved [Keeler and Shayler, 2008].

Kokjohn [2008] discussed a two-stage combustion (TSC) concept where the fuel injection per cycle was split into two portions. One portion was fully premixed with air to achieve homogeneous condition in cylinder at the beginning of compression process, and the second portion of fuel was injected directly into combustion chamber near TDC. Then two combustion modes were combined in the combustion process, which were ideally HCCI combustion in the first stage and diffusion dominated combustion in the second stage. In the study, six objectives including improving NO_x, soot, CO, HC, ISFC, and peak pressure rise rate (PRR) were optimized by adjusting four parameters including boost pressure, EGR rate, fraction of premixed fuel, and start-of-injection timing. His results demonstrated that low NOx and soot with a low peak PRR of 4.3 bar/deg could be achieved by utilizing a high EGR (54%), low IVC pressure (1.74 bar), premixing rate of 36%, and late injection timing of 2.9 ºCA ATDC.

Koci et. al. [2009] experimentally investigated the emission mechanisms and engine performance with multiple injections in low temperature combustion (LTC) at a light to medium load condition of 5.5 bar net IMEP at 2000 rev/min. An optimal split ratio was proposed to minimize the UHC and CO emissions in their study. Meanwhile their research suggested the noise could be effectively suppressed by spreading the heat release through equally split injections. Nevertheless, increased injection pressure led to reduced soot emission for all split fuel injection ranges.

Horibe et al. [2009] conducted the study for extending the operating range in PPCI diesel combustion by utilizing split-injection. According to their results, fuel fraction in the first injection should be reduced to avoid noise. Lower EGR level was suggested for split-injection cases in order to suppress unburned species emissions. They also suggested different splitting strategies for low load and high load. At low engine load, the second injection was suggested start before the combustion of the fuel in the first injection. At high load, the first injection was recommended to advance for reducing the soot emissions; while the second injection was suggested to be located near TDC for higher thermal efficiency.

2.2.3 Swirl Ratio

The large scale in-cylinder flows mainly include swirl, tumble and squish motion, which have

been found significantly influence the combustion performance and emission mechanism in diesel engine. Swirl flow usually generates during the intake stroke and reaches the peak value of its kinetic energy at the close of intake valve timing. With the rotating movement around the vertical axis of cylinder, swirl flow has been proved having the capability to enhance fuel-air mixing and to reduce soot emissions and fuel consumption for conventional diesel combustion in several studies [Miles, 2000]. As introduced above, the study of MK combustion strategy cited that swirl motion was important for reducing soot and UHC emissions in PPCI diesel combustion [Kimura et al., 2001].

Moreover, because the applications of high EGR rate the oxidation of CO is reduced due to the decreased oxygen availability and combustion temperature in PPCI diesel combustion. Therefore, improvement in fuel-air mixing is required for suppressing the CO output. Kook et al. [2006] investigated the effects of swirl ratio on CO emissions and fuel consumption in a PPCI combustion engine through both numerical simulations and optical experiments. Swirl ratios ranged of 1.44 to 7.12 were tested over a broad range of injection timing. The results showed that there was optimal swirl ratio with certain injection timing for minimum CO emission and fuel consumption. They attributed these improvements to the enhanced mixing after premixed combustion stage. They also considered advanced injection timing had more influence on the pre-combustion mixing than swirl ratio.

Opat et al. [2007] studied the effects of swirl ratio on mixing in PPCI combustion by 3D in-cylinder CFD simulations. Their work showed that vaporization rate increased with swirl ratio. However, no improvement on fuel consumption was observed with high swirl ratio. The image from simulation showed that the excessive increased swirl ratio constrained the reactants in bowl area and impeded the entering of the oxygen available in the squish region. Therefore, the oxidation of CO was reduced due to the poor mixing resulted from excessive swirl ratio. Moreover, enhanced swirl flow increased heat loss to cylinder wall during compression stroke, and further led to decreased fuel efficiency.

For the implementation of stoichiometric operation in PPCI combustion, Lee [2006] tried to improve the fuel economy by enhanced mixing. However, high swirl ratio resulted sacrificed fuel consumption in the range of 1.8 to 3.3. According to the discussion of Miles [2000], secondary flow structures generated from high swirl flows during compression stroke which were not beneficial for fuel-air mixing. Nevertheless, they considered the pre-ignition mixing significantly affected by swirl motion.

2.3 Homogeneity of Mixture

Because of the limited time for mixing, stratified fuel-air mixture is common in PPCI combustion [Hardy and Reitz, 2006]. Therefore, the mixture formation and its distribution

influence the ignition and the phase of combustion and hence its control. Thus, the method to evaluate the mixing quality of fuel-air mixture in PPCI engine is required to be discussed.

When evaluating the mixing characteristics two aspects usually are considered: the overall degree of mixing – homogeneity, and the detailed structure of mixture in cylinder. In a great majority of previous studies about the PPCI or standard diesel engine the distribution of equivalent ratio was used to illustrate the mixing characteristics of mixture [Okude et al., 2004]. The distribution of equivalent ratio was usually given as sectional views showing by counter lines or images. This method is sufficient in the explanation of the details of mixture pattern at a current crank angle, and it also can be considered as good evidence when the comparisons are between the similar engines and similar testing conditions. However, there is lack of explicit criterions or indicators to explain the overall degree of mixing in cylinder.

Similar to the distribution of equivalent ratio, the mixture fraction gradient is usually used to explain the mixing characteristics of mixture in a similar way. Hu et al [2008] proposed a factor of the mixture fraction gradient as an indicator of homogeneity of gas mixture when they constructed an extended flamelet time scale combustion model. In their study, scalar dissipation rate χ is regarded as an indicator of homogeneity of mixture since it is proportional to the squared magnitude of mixture fraction gradient. χ is defined as:

$$\chi = 2D\left(\frac{\partial Z}{\partial x_i}\right)\left(\frac{\partial Z}{\partial x_i}\right) = 2D\left|\frac{\partial Z}{\partial x_i}\right|^2 \tag{2.1}$$

where Z is mixture fraction; D is a molecular diffusivity.

However, Hu and et. al did not give any results about the degree of homogeneity using this factor.

Nandha and Abraham [2002] utilized two methods to describe the fuel-air mixing characteristics. In the first method, the total injected fuel at any instant was divided into three parts: lean, flammable and rich. The series of fractions for the fuel mass in each part over the total fuel mass were used to indicate the quality of mixing. Though the definitions are arbitrary, it is useful to monitor the mixing process. In the second method, they proposed the degree of heterogeneity (DOH (θ)) through a standard deviation of the equivalence ratio normalized by the overall equivalence ratio. At any crank angle θ after injection:

$$DOH(\theta) = \frac{\sqrt{\sum_i^{N_{cells}} \frac{[(\phi_i - \phi_o)^2 \delta m_i]}{M}}}{\phi_o} \tag{2.2}$$

$$\phi_o = \frac{\sum_i^{N_{cells}} \phi_i \delta m_i}{M} \tag{2.3}$$

Where

$$M = \sum_{i}^{N_{cells}} \delta m_i \tag{2.4}$$

Where, ϕ_i is the equivalent ratio; and δm_i is the mass of the mixture in any computational cell, i, at a given angle θ; and N_{cells} is the total number of computational cells. The DOH (θ) provides the non-uniformity in cylinder. Completely homogeneous is believed to achieve when DOH (θ) approaching zero. This method is considered particularly useful for the quantitative evaluation of mixing in PPCI or HCCI combustion.

Richter et al. [2005] proposed a measure of homogeneity index for OH distribution during the study of the combustion process with simultaneous formaldehyde and OH PLIF in a direct-injected HCCI engine. Based on the image data acquired, the homogeneity index was calculated by counting the number of shifts between signal and on signal in a digitalized image by scanning the image in rows and columns. Through dividing the shifts number of an image in homogeneous condition, the number of shifts in a data image was normalized to be the index of homogeneity. When it approaches 1, the uniform distribution of OH is considered achieved. This method to evaluate homogeneity is straight but only in 2-D. Moreover, it is difficult to be used in CFD simulation studies.

In the numerical analysis of fuel spray mixing in a single-cylinder optical research engine using Narrow Angle Direct Injection (NADI) technique, the Uniformity Index *UI(x)* was proposed in order to express the homogeneity of mixture by Kaario et al. [2009]. The index was calculated on a cut plane and given as:

$$UI(x) = 1 - \sqrt{\frac{\sum_i (x_i - \bar{x})^2 A_i}{\bar{x}^2 A}} \tag{2.5}$$

where x_i is the local fuel vapour mass fraction; $\bar{x}$ is the average fuel vapor mass faction in the cut plane; A_i is the local cell face area; and A is the total cut plane area. The index approaches unit when homogeneity is achieved. It has to be notice that the results of *UI(x)* are highly determined by the locations selected for extracting the plane. Therefore, it is difficult to compare the homogeneity between different engines using this index.

A large number studies in material science proposed a range of method to evaluate the homogeneity in material, such as alloy. Most of them are based on a concept similar to Nandha and Abraham [2002]'s method which is using the standard deviation of species' fraction as the core factor for the formula evaluating the homogeneity or heterogeneity [Torralba et al., 1996; Munnik et al., 2000; Held et al.;1999]. Besides of the similar concept, these methods often add some uncertainty contribution for homogeneity or heterogeneity to represent the influence from sampling. Obviously, this addition is not necessary for the evaluation of homogeneity of mixture

in engine.

2.4 Degree of Premix in PPCI Combustion

Unlike HCCI combustion, PPCI diesel combustion is applied using direct injection with moderately advanced injection timing. The mixture is not completely premixed before ignition and features considerable equivalence ratio gradient. Therefore, though the level of premixed combustion is much higher than in conventional diesel combustion, mix-controlled combustion still exists of certain fraction in PPCI diesel combustion. The method to evaluate the degree of premix combustion is required to discuss.

For conventional diesel combustion, the premixed combustion phase is easy to be distinguished in the diagram of heat release rate, since the combustion is mainly controlled by mixing and the fuel amount burned in the premixed combustion phase is small and fast [Heywood, 1988]. Then it is possible to calculate the premixed combustion rate by the area of premixed combustion phase and the total area of the entire heat release process for the conventional diesel combustion, or by mass fraction directly. Watson's model [1980] for predicting the degree of premixed combustion in conventional diesel combustion will be discussed in detail in Chapter 6.

For PPCI combustion, it is normally difficult to identify the premix combustion stage from the entire combustion process in the curve of heat release rate. The typical heat release rate diagram of PPCI combustion does not exhibit distinct premixed and diffusion burns as in conventional diesel combustion. Based on the literature review within the research about PPCI combustion, it is found that the current studies mostly evaluated the degree of premixed combustion by comparisons in quality rather than in quantity [Husberg et al., 2005; Keeler and Shayler, 2008]. Therefore, a quantitative definition about the degree is required and will be introduced in Chapter 6.

2.5 Summary

In this chapter, the concept of PPCI combustion has been introduced together with its advantages and constraints. Following, some typical implementations of PPCI combustion have been reviewed. It is shown that PPCI diesel combustion potentially offers the solution to suppress NO_x and soot emissions without significant penalty in fuel consumption. However, the operating limit and the increased CO and UHC emissions hinder the application of PPCI combustion in passenger cars. Improving fuel-air mixing is considered as the major pathway to improve the performance of PPCI combustion.

The review about the emission control techniques provides some possible solutions to reduce the emission level in PPCI combustion and to improve its fuel economy. Split-injection is considered as one of the effective methods to reduce the CO emission and fuel consumption in

PPCI combustion, but the strategy for splitting need to be investigated. Introduction of high EGR is effective to reduce NO_x emissions by reducing oxygen availability and suppressing combustion temperature. However, the operating range is limited by the high EGR rate, and CO emissions may increase due to the reduced oxygen concentration. Cooled EGR is suggested to extend the operating range of PPCI diesel combustion. Appropriately increased swirl ratio is beneficial for mixing and favorable for improve the fuel economy in PPCI combustion. Nevertheless, the selection of swirl ratio must be careful and refers to the injection strategy and geometry of combustion chamber.

The factors indicating the homogeneity of mixture and the degree of premixed combustion are important and helpful for the investigation of PPCI combustion. However, no adequate information can be acquired for the definition of premixed degree from the pertinent literature. Meantime, the definition for the homogeneity of mixture needs to be improved for generalizing.

Chapter 3 Numerical Model and Validation

3.1 Model description

With the developments of computational technologies over last decades it has become more feasible to use computational fluid dynamics (CFD) for simulating complex flow and combustion phenomena in internal combustion (IC) engines. However, in-cylinder flow modeling is particularly difficult because the flow is transient, multi-phase, turbulent, and chemically reacting under high pressure and temperature. In the present study, an improved KIVA-3V2 code coupled with CHEMKIN is employed for simulating the in-cylinder flow phenomena and combustion process of a light-duty diesel engine. KIVA-3V2 is a transient, multi-phase, multi-dimensional, structured-mesh, and finite-volume CFD program which has been widely used to confine in-cylinder flows in IC engines [Amsden, 1999]. CHEMKIN is a robust and mature chemistry simulation tool [Kee et al, 1996] which can be implemented into KIVA-3V2 for solving the chemical processes by detailed chemical kinetic rather than common combustion models such as used by conventional CFD simulation of combustion process. In the following sections, the primary models used in this study will be introduced [Amsden et al., 1989; Amsden, 1993, 1997, 1999].

3.1.1 Governing Equations

A. Continuity Equation

The continuity equation for species *m* is

$$\frac{\partial \rho_m}{\partial t} + \nabla \cdot (\rho_m \mathbf{u}) = \nabla \cdot \left[\rho D \nabla \left(\frac{\rho_m}{\rho}\right)\right] + \dot{\rho}^c_m + \dot{\rho}^s \delta_{m1} \qquad (3.1)$$

where, ρ_m is the mass density of species m, ρ the total mass density, and **u** the fluid velocity. D is the diffusion coefficient, $D = \mu_{eff}/\rho S_c$, where S_c is Schmidt number, and μ_{eff} is the effective viscosity as the sum of laminar and turbulent viscosity, $\mu_{eff} = \mu_l + \mu_t = \mu_l + C_\mu \rho k^2/\varepsilon$, where k is turbulent kinetic energy, ε is turbulent dissipation and C_μ=0.09 an empirical constant. $\dot{\rho}^c_m$ and $\dot{\rho}^s$ are the source terms due to chemistry and spray, respectively.

B. Momentum Equation

The momentum equation for the fluid mixture is

$$\frac{\partial(\rho \mathbf{u})}{\partial t} + \nabla \cdot (\rho \mathbf{u}\mathbf{u}) = -\frac{1}{a^2}\nabla p - A_0 \nabla \left(\frac{2}{3}\rho k\right) + \nabla \cdot \boldsymbol{\sigma} + \mathbf{F^s} + \rho \mathbf{g} \qquad (3.2)$$

where p is the fluid pressure. The dimensionless quantity a is used in conjunction with the Pressure Gradient Scaling (PGS) Method. The quantity A_o is 0 in laminar calculations or 1 in turbulence calculations. $\mathbf{F}^s$ is the rate of momentum gain per unit volume due to the spray. The

specific body g is assumed constant. The viscous stress tensor $\boldsymbol{\sigma}$ is Newtonian in form:

$$\boldsymbol{\sigma} = \mu[\boldsymbol{\nabla}\mathbf{u} + (\boldsymbol{\nabla}\mathbf{u})^T] + \lambda\boldsymbol{\nabla}\cdot\mathbf{u}\mathbf{I} \quad (3.3)$$

where μ and λ are the first and second coefficients of viscosity, respectively. The superscript T denotes the transpose and $\mathbf{I}$ is the unit dyadic.

C. Energy Equation

The internal energy equation is

$$\frac{\partial(\rho I)}{\partial t} + \boldsymbol{\nabla}\cdot(\rho\mathbf{u}I) = -p\boldsymbol{\nabla}\cdot\mathbf{u} + (1-A_0)\boldsymbol{\sigma}:\boldsymbol{\nabla}\mathbf{u} - \boldsymbol{\nabla}\cdot\mathrm{J} + A_0\rho\varepsilon + \dot{\boldsymbol{Q}}^{\boldsymbol{c}} + \dot{\boldsymbol{Q}}^{\boldsymbol{s}} \quad (3.4)$$

where I is the specific internal energy, exclusive of chemical energy. The heat flux vector J is the sum of contributions due to heat conduction and enthalpy diffusion:

$$\mathrm{J} = -K\boldsymbol{\nabla}T - \rho D\sum_m h_m\boldsymbol{\nabla}(\rho_m/\rho) \quad (3.5)$$

where T is the fluid temperature and h_m the specific enthalpy of species m. $\dot{\boldsymbol{Q}}^{\boldsymbol{c}}$ and $\dot{\boldsymbol{Q}}^{\boldsymbol{s}}$ are the source terms due to chemical heat release and spray interactions, respectively.

D. Equations of State of Ideal Gas

The state relations are assumed to be those of an ideal gas mixture. Therefore,

$$p = R_0T\sum_m(\rho_m/W_m) \quad (3.6)$$

$$I(T) = \sum_m(\rho_m/\rho)I_m(T) \quad (3.7)$$

$$c_p(T) = \sum_m(\rho_m/\rho)\,c_{pm}(T) \quad (3.8)$$

And

$$h_m(T) = I_m(T) + R_0T/W_m \quad (3.9)$$

where R_0 is the universal gas constant; W_m, the molecular weight of species m; $I_m(T)$, the specific internal energy of species m; and c_{pm}, the specific heat at constant pressure of species m.

3.1.2 Turbulence Model

Besides the standard k--ε turbulence model, KIVA-3V2 offers the Renormalization Group (RNG) theory variant of k--ε model proposed by Han and Reitz [Han and Reitz, 1995]. This formulation takes the effects of compressibility in to considering through a rapid distortion analysis. This modified RNG k--ε model shows better accuracy for the reproduction of in-cylinder flow structure compared to the standard k--ε turbulence model. This RNG k--ε model is expressed as:

$$\frac{\partial(\rho k)}{\partial t}+\boldsymbol{\nabla}\cdot(\rho\mathbf{u}k)=-\frac{2}{3}\rho k\boldsymbol{\nabla}\cdot\mathbf{u}+\boldsymbol{\sigma}:\boldsymbol{\nabla}\mathbf{u}+\boldsymbol{\nabla}\cdot\left[\left(\frac{\mu}{Pr_k}\right)\boldsymbol{\nabla}k\right]-\rho\varepsilon+\dot{W}^s \quad (3.\ 10)$$

$$\frac{\partial(\rho\varepsilon)}{\partial t}+\nabla\cdot(\rho\mathbf{u}\varepsilon)=-\left(\frac{2}{3}C_{\varepsilon1}-C_{\varepsilon3}+\frac{2}{3}C_\mu C_\eta\frac{k}{\varepsilon}\boldsymbol{\nabla}\cdot\mathbf{u}\right)\rho\varepsilon\boldsymbol{\nabla}\cdot\mathbf{u}+\boldsymbol{\nabla}\cdot\left[\left(\frac{\mu}{Pr_\varepsilon}\right)\boldsymbol{\nabla}\varepsilon\right]$$

$$+\frac{\varepsilon}{k}\left[\left(C_{\varepsilon1}-C_\eta\right)\boldsymbol{\sigma}:\boldsymbol{\nabla}\mathbf{u}-C_{\varepsilon2}\rho\varepsilon+C_s\dot{W}^s\right] \quad (3.\ 11)$$

where $\dot{W}^s$ is the source terms due to the fluid compressibility and the interaction between the flow and spray, and

$$C_{\varepsilon3}=0.41333+(-1)^\delta 0.06899C_\eta\eta \quad (3.\ 12)$$

$$C_\eta=\frac{\eta(1-\eta/\eta_0)}{1+\beta\eta^3} \quad (3.\ 13)$$

$$\eta=\frac{k}{\varepsilon}(2S_{ij}S_{ij})^{1/2} \quad (3.\ 14)$$

$$S=\frac{1}{2}\left(\frac{\partial \mathrm{u}_i}{\partial x_j}+\frac{\partial \mathrm{u}_j}{\partial x_i}\right) \quad (3.\ 15)$$

the coefficients: C_μ=0.0845; $C_{\varepsilon1}$=1.42; $C_{\varepsilon2}$=1.68; Pr_k=1.39; Pr_ε=1.39; η_0=4.38; β=0.012.

3.1.3 Fuel Spray Models

Modelling for the dynamics of a spray and its interactions with surrounding gas is an extremely complicated problem. The essence of spray modelling is the modelling of gas phase and liquid phase and the interactions between them. In KIVA-3V2, spray behaviour is modelled by Discrete Droplet Model (DDM), where each computational parcel represents a number of droplets with uniform properties. The probability distributions that govern the assignment of droplet properties are determined by using a Monte Carlo technique. The ordinary differential equations governing droplets trajectories and the rates of mass, momentum, and energy exchange between the gas and spray are solved by Lagrangian method [Amsden et al, 1989]. Meanwhile, several sub models are included in the code to simulate spray atomization, breakup, collision, vaporization and spray-wall interaction.

Reitz and Diwakar proposed 'Blobs' model for the modeling of liquid fuel injection and atomization [Reitz, 1987]. This method assumes that atomization and drop breakup are indistinguishable processes within the dense spray near the nozzle exit. The initial spray droplets are prescribed a size equal to the nozzle exit diameter, and the amount of droplets is calculated base on the injecting flow rate.

A. Break-up Model

A Kelvin-Helmholtz Rayleigh-Taylor (KH-RT) model is used to simulate the break-up process of injected droplets. The KH-RT model is derived from the wave model [Reitz and Bracco, 1986;

Reitz, 1987], which is based on a linear instability analysis of liquid jets. The wave model sets a limit of stability and if droplets have existed long enough to become unstable, breakup occurs and the characteristics of the new droplets is based on the wave length and frequency of the instability that brought about the breakup. Based on Kelvin-Helmholtz (KH) instabilities, the breakup time, which accounts for two conditions including bag breakup at low Weber numbers and stripping breakup at high Weber numbers [Reitz and Diwakar, 1987], is given below.

$$\tau = \frac{3.788 B_1 r}{\Omega_{wave} \Lambda_{wave}} \tag{3. 16}$$

where B_1 is empirical coefficient; r is the radius of the droplet; Λ_{wave} and Ω_{wave} represent the wavelength and the frequency of the fast growing wave, respectively. And they are obtained through curve fits from the solutions of dispersion equation which describes the KH instability growing on the surface of a cylindrical liquid jet penetrating into stationary incompressible gas [Jia et al., 2008a]. The frequency and wavelength of the fastest growing wave are given by Reitz [1987] as

$$\Omega_{wave} = \frac{0.34 + 0.38 We^{1.5}}{(1+Z)(1.4T^{0.6})} \sqrt{\frac{\sigma}{\rho_l r^3}} \tag{3. 17}$$

$$\Lambda_{wave} = \frac{9.02 r \left(1 + 0.45\sqrt{Z}\right)(1 + 0.4T^{0.7})}{(1 + 0.865 We^{1.67})^{0.6}} \tag{3. 18}$$

where $We = (\rho_g u_r^2 r) / \sigma$, is the Weber number for the gas; $Z = \sqrt{We_l}/Re_l$, the Ohnesorge number; and $T = ZWe^{1/2}$, the Taylor number. u_r is the magnitude of the relative velocity; We_l is the liquid Weber number similar to We except the liquid density used; Re_l is the liquid Reynolds number.

It defines the breakup drop radius, r_c, as

$$r_c = B_0 \Lambda_{wave} \tag{3. 19}$$

The change rate of the droplet radius is given as

$$\frac{dr}{dt} = \frac{r - r_c}{\tau} \tag{3. 20}$$

The wave model only calculates the stripping events of droplets, which is resulted from the growth of KH instability on the droplet surface due to the relative velocity between the gas phase and liquid phase. To enhance this wave model, the Rayleigh-Taylor (RT) model is added to account for the sudden catastrophic breakup due to the deceleration of the droplets [Patterson and Reitz, 1998; Ricart et al., 2000]. In the RT model, the breakup time is given by

$$\tau_{\mathrm{RT}} = C_\tau / \Omega_{\mathrm{RT}} \tag{3. 21}$$

where C_τ is a constant and Ω_{RT} is the frequency of the fastest growing wave, given by Bellman and Pennington [Bellman and Pennington, 1953] as

$$\Omega_{\mathrm{RT}} = \sqrt{\frac{2}{3\sqrt{3\sigma}} \frac{\left[-\mathrm{g_t}(\rho_l - \rho_\mathrm{g})\right]^{3/2}}{\rho_l + \rho_g}} \tag{3. 22}$$

when considering surface tension and neglecting viscosity. The corresponding wavelength, Λ_{RT}, is

$$\Lambda_{\mathrm{RT}} = 2\pi \sqrt{-\frac{3\sigma}{\mathrm{g}_t(\rho_l - \rho_\mathrm{g})}} \tag{3. 23}$$

where g_t is the acceleration in the direction of travel. The breakup drop radius are given by

$$r = C_{3,\mathrm{RT}} \Lambda_{\mathrm{RT}} / 2 \tag{3. 24}$$

where, $C_{3,RT}$ is a constant.

In current KH - RT model, both KH and RT models are considered once the breakup length has been reached. In the KH model, the breakup implies shedding-off smaller droplets and creating a new computational parcel; while, in the RT model, it indicates complete breakup into smaller droplets [Ricart et al., 2000]. Within the jet breakup length near the nozzle exit only KH instabilities are considered [Ricart et al., 2000].

B. Collision Model

Consistent with the manners of DDM for spray modeling, droplet collisions are computed by the stochastic particle method. In order to limit the demand for computer storage, instead of calculating the probable number of droplets in parcel A that undergo collisions, KIVA only uses the collision frequency to calculate the probability P that a droplet in parcel A will undergo a collision with a droplet in other parcel [Amsden et al., 1989]. Since all the droplets in parcel A are with uniform properties and behaving, they either do or do not collide, and the probability of collision event is P. After this collision, no new parcels are generated. Owing to this parcel-based method, the major requirement of collision model is an appropriated solution of the collision probability P.

The original collision model in KIVA was proposed by O'Rourke [Amsden et al., 1989]. O'Rourke's model [1981] will conduct the collision computing if and only if two parcels are in the same computational cell and the probability for collision is higher than a threshold value based on the collision frequency. The definition of the collision frequency is:

$$\nu = \frac{\pi}{V} N_{n,small} (r_{small} + r_{large})^2 \left| \mathbf{v}_{n,small} - \mathbf{v}_{n,large} \right| E_{12} \tag{3. 25}$$

where E_{12} is the collision efficiency, which is set to be 1.0 in KIVA. The subscripts small and large refer to the properties of the droplets with smaller radius and larger radius. $N_{n,small}$ is the number of droplets in parcel small, and V is the volume of the cell where the pair of parcels are.

$\mathbf{v}_{n,small/large}$ is the velocity of droplets.

Basing on this hypothesis and the expression above, the O'Rourke's collision model is seriously grid dependent. Collision events are not significant unless the liquid volume fraction is large in cell under this model. Another weakness is O'Rourke's model neglects the fact of whether the parcels are moving towards or away from each other if they are in the same cell. Then the chance of collision inside cell is over predicted, while the chance of collision is neglected between cells. These inaccuracies of predictions will be serious for cases with complex geometries.

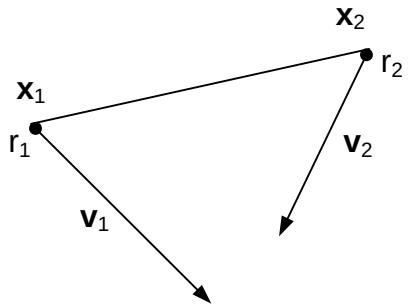

Figure 3.1 Two parcels travelling towards each other.

For the concern of both accuracy and computational cost, the collision model developed by Nordin [2001] is integrated into the KIVA-3V2. In Nordin's model, collision between two parcels occurs if their trajectories intersect and the intersection point is reached within the integration step. In order to reduce computational demanding, two prerequisites were proposed for eliminating the impossible collisions. First, as shown in Figure 3.1, two parcels have to travel towards each other, or $\mathbf{v}_{12} > 0$, where

$$\mathbf{v}_{12} = (\mathbf{v}_1 - \mathbf{v}_2) \cdot \frac{\mathbf{x}_2 - \mathbf{x}_1}{|\mathbf{x}_2 - \mathbf{x}_1|} \tag{3. 26}$$

The second prerequisite is that the distance between parcels should be shorter than the parcels' relative displacement in one time step Δt, as

$$\mathbf{v}_{12}\Delta t = |\mathbf{x}_2 - \mathbf{x}_1| - (r_1 + r_2) \tag{3. 27}$$

The parcels which meet these two prerequisites have the chance of collision and the probability P is

$$P = \left(\frac{r_1 + r_2}{max(r_1 + r_2, \Delta_{12})}\right)^{C_1} e^{-C_2|\alpha_0 - \beta_0|/\Delta t} \tag{3. 28}$$

where $\alpha_0 \in [0, \Delta t]$ and $\beta_0 \in [0, \Delta t]$ are the solutions to the system

$$\mathbf{z}_1 = \mathbf{x}_1 + \alpha \mathbf{v}_1$$

$$\mathbf{z}_2 = \mathbf{x}_2 + \beta \mathbf{v}_2 \tag{3. 29}$$

$$\frac{\partial|\mathbf{z}_2-\mathbf{z}_1|}{\partial\alpha,\beta}(\alpha_0,\beta_0)=0 \tag{3. 30}$$

and $\Delta_{12} = |\ \mathbf{z}_2(\beta_0) - \mathbf{z}_1(\alpha_0)\ |$ is the minimum distance between the two trajectories. C_1 and C_2 are model constants. If a random number $\xi \in [0,1]$, is less than the collision probability P, the collision will occur.

C. The Spray-Wall Interaction Model

The full spray-wall interaction model was first included into KIVA by O'Rourke and Amsden [2000]. This model includes only two regimes of stick and splash. The HXT model in our study was developed by Han et al. [2000], which improved O'Rourke and Amsden's model by adding another two regimes of rebound and spread. The transition criteria for these regimes are

Stick: $We_n \le 5$ (3. 31)

Rebound: $5 < We_n \le 10$ (3. 32)

Spread: $We_n \ge 10$ and $We_n\, Re_n^{0.5} < H_{cr}$ (3. 33)

Splash: $We_n\, Re_n^{0.5} \ge H_{cr}$ (3. 34)

where Re_n and We_n are Reynolds number and Weber number of the incident droplet. H_{cr} is the splash threshold, as

$$H_{cr}=\left(1500+\frac{650}{\beta^{0.42}}\right)[1+0.1Re_n^{0.5}\min(\delta,0.5)] \tag{3. 35}$$

where β is non-dimensional surface roughness, $\beta = r_s / D$. r_s is the surface roughness height, and D is the diameter of the incident droplet. δ is the non-dimensional film thickness, $\delta = h / D$, where h is the film thickness. Therefore, in HXT model, the wall conditions of film thickness and roughness have been considered into the calculation.

After the splashing, the ratio of the total secondary droplet's mass m over the incident drop mass M is given as

$$\frac{m}{M}=0.75\{1-\exp[-10^{-7}(H-H_{cr})^{1.5}]\} \tag{3. 36}$$

Where H is the dimensionless parameter, $H = We_n\, Re_n^{0.5}$. The mean size of the secondary droplets, d_m, is given as

$$\frac{d_m}{D}=\frac{3}{We^{0.5}Re^{0.25}}\sqrt{\frac{\rho_l}{\rho_g}} \tag{3. 37}$$

To explain the size distribution for the secondary droplets, one type of Nukiyama-Tanasawa function is used:

$$f(d) = \frac{2}{3}\frac{d^2}{d_m^3}\exp\left[-\left(\frac{d}{d_m}\right)^{3/2}\right] \tag{3. 38}$$

Then, the SMD, d_{32}, can be stated as:

$$d_{32} = \frac{\Gamma(4)}{\Gamma(4/3)}d_m = 2.16d_m \tag{3. 39}$$

where Γ is the gamma function.

The secondary droplet velocity $\boldsymbol{w}$ is given as

$$\boldsymbol{w} = w\boldsymbol{n} + v\zeta\left(\cos\varphi\boldsymbol{e}_{\mathrm{t}} + \sin\varphi\boldsymbol{e}_{\mathrm{p}}\right) \tag{3. 40}$$

where $\boldsymbol{n}$ is the unit normal to the wall surface; $\boldsymbol{e}_{\mathrm{t}}$ and $\boldsymbol{e}_{\mathrm{p}}$ is the tangential component and parallel component of unit vector, respectively. The value w is the normal velocity component and is determined from the following Nukiyama-Tanasawa function:

$$P(w) = \frac{4}{\sqrt{\pi}}\frac{w^2}{w_{\mathrm{m}}^3}\exp\left[-\left(\frac{w}{w_{\mathrm{m}}}\right)^2\right] \tag{3. 41}$$

where the distribution mean w_{m} changes with incident angle α and azimuthal angle φ,

$$w_{\mathrm{m}} = (0.1 + \xi\cos\varphi)w_0 \tag{3. 42}$$

where the function ξ is given as

$$\xi = \frac{0.1}{90}\alpha \tag{3. 43}$$

The tangential velocity v of the secondary droplet is chosen from the following normal distribution as

$$N(v) = \frac{1}{\sqrt{2\pi}\delta}\exp\left[-\frac{(v-\bar{v})^2}{2\delta^2}\right] \tag{3. 44}$$

where

$$\delta = 0.1v_0 + 0.02306w_0 \tag{3. 45}$$

$$\bar{v} = \sqrt{0.7v_0^2 + 0.03w_0^2} \tag{3. 46}$$

The azimuthal angle is chosen from the distribution introduced by Naber and Reitz [1988]

$$\varphi = -\frac{\pi}{\gamma}\ln[1 - \mathrm{P}(1 - \mathrm{e}^{-\gamma})] \tag{3. 47}$$

where P is a random number in the interval [0, 1] and γ is a parameter related to angle α by

$$\sin\alpha = \frac{\mathrm{e}^{\gamma}+1}{\mathrm{e}^{\gamma}-1}\frac{\gamma^2}{\gamma^2+\pi^2} \tag{3. 48}$$

The function ζ is introduced to reflect the trend of the oblique impingement due to the non-uniform tangential velocity distribution, as

$$\zeta = \frac{\sin^2\left[(\pi/2)(1-2\alpha/\pi)^{(1-|\varphi|/\pi)}\right]}{\cos^2\alpha}\exp\left(-\frac{\gamma}{\pi}|\varphi|\right) \quad (3.\ 49)$$

D. The Wall Heat Transfer Model

Instead of the original model in KIVA introduced by Launder and Spalding [1974], the wall heat transfer is modeled using the method proposed by Han and Reitz [1997]. This model includes the variations of fluid density and turbulent Prandtl number into computing, since the density-variable turbulent flows are commonly found in the boundary layer. In this model, the heat flux is proportional to the logarithm of the ratio of the flow temperature to the wall temperature rather than the arithmetic difference which is used in the models for incompressible flow [Launder and Spalding, 1974].

The temperature profile equation is given as

$$T^+ = 2.1\ln(y^+) + 2.1G^+y^+ + 33.4G^+ + 2.5 \quad (3.\ 50)$$

where y+ is dimensionless distance, $y^+ = u^*y/v$. And y is the distance to the wall; u^* is friction velocity; v is kinematic viscosity. G^+ is the dimensionless source term, $G^+=Gv/q_w u^*$. And G is the source term in energy equation; q_w is the heat flux from the wall, as

$$q_w = \frac{\rho c_p u^* T\ln(T/T_w) - (2.1y^+ + 33.4)Gv\ /\ u^*}{2.1\ln(y^+) + 2.5} \quad (3.\ 51)$$

where T_w is the wall temperature. This wall heat transfer model was found to be independent of grid resolution and to achieve results that satisfactory agreement with measured heat fluxes [Han and Reitz, 1997; Jafari and Hannani, 2006].

3.1.4 Combustion and Emission Models

A. N-heptane mechanism

In this study, main objectives are to investigate the combustion process of PPCI as a kind of low temperature combustion and its influence on emissions in diesel engines. For achieving adequate premixed mixture before ignition, relatively large amount of fuel amount during pilot injection is applied in most engine combustion cases, and the pilot injection timing is advanced to - 40 ° CA ATDC. Therefore, the ignition and the substantial portion of combustion in most cases are more controlled by chemical kinetics. Because the detailed chemical kinetic reaction mechanisms for realistic diesel fuels are very complicated and currently not available, an n-heptane chemistry mechanism with 29 species and 52 reactions is used for present calculations owing to its similar ignition characteristics to those of diesel fuel. This skeletal reaction mechanism developed by Patel et al. [2004] is derived from Golovitchev's mechanism [2000], which is more detailed and includes the reactions of polycyclic aromatic. Quantities of

validations in constant-volume and various engines have been conducted for this skeletal n-heptane mechanism, and the results showed very good agreement and computational efficiency [Patel et al., 2004; Kong et al., 2005a; Jia et al., 2009]. Though this skeletal n-heptane mechanism is suitable for the chemical reactions of diesel fuel, the physical properties of heptane (e.g. density) are different from those of diesel fuel. Then the diesel fuel model DF2, i.e. the $C_{12}H_{26}$ Cummins model [Amsden, 1989], is used to simulate the non-chemical-kinetic processes of diesel fuel, e.g. transport and spray.

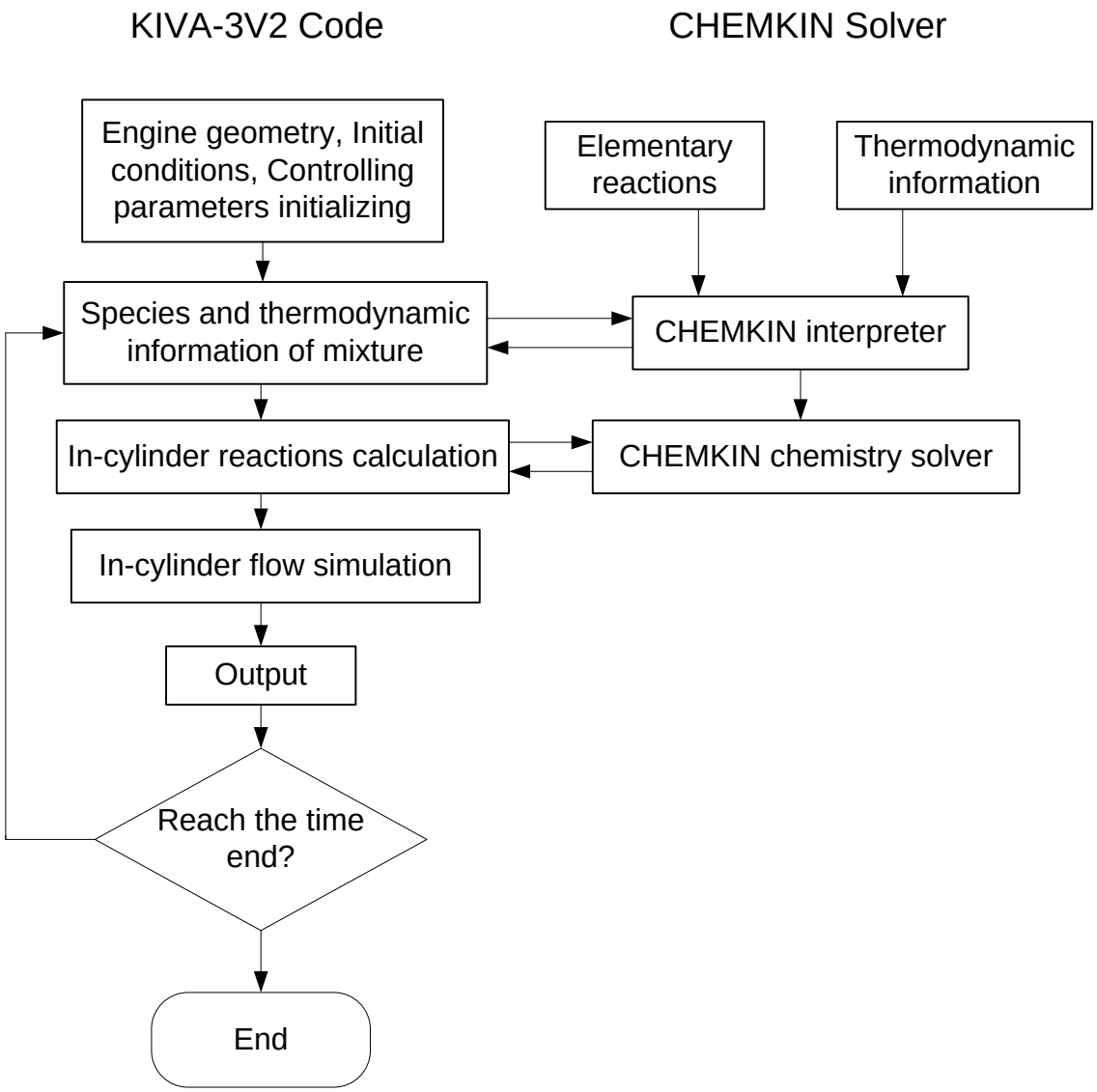

Figure 3.2 The sketch of the mechanism of the coupling of KIVA-3V2 code and Chemkin [Kong et al., 2001].

The CHEMKIN solver is integrated into the KIVA-3V2 code for solving the skeletal n-heptane reaction mechanism during the multidimensional engine simulations. The mechanism of the coupling of CHEMKIN and KIVA-3V2 is given in Figure 3.2. The turbulence is modeled by RNG k--ε model here, and then the sub-grid scale turbulence-chemistry interaction is not

considered. Further details of the mechanisms and the validations can be found in the relevant references [Patel et al., 2004; Golovitchev, 2000; Kong et al., 2005a; Opat et al., 2007; Jia et al., 2009]

B. NO_x model

NO_x emissions are calculated by a reduced NO_x mechanism of Golovichev that was derived from the Gas Research Institute (GRI)'s NO mechanism [Smith et al., 2000]. Four additional species (N, NO, NO2, N2O) and 13 reactions from Golovichev mechanism [Golovichev, 2002] are added to the n-heptane chemistry mechanism. In these reactions, only the thermal NO_x formation is calculated, while the prompt NOx formation is neglected. Three of these 13 reactions are the extended Zeldovich reactions, which are favorable for the prediction of high temperature NOx formation. The other 10 reactions account for NOx formation through NO2 and N2O reactions pathway are also included for the conditions of low temperature combustion, which is common in PPCI combustion. This reduced NO_x mechanism has been validated by many studies [Jia and Xie, 2006; Kong et al., 2005a; Kokjohn, 2008], and the reactions are shown below in Table 3.1:

Table 3.1 The reduced NO_x mechanism [Golovichev, 2002]

1. $N + NO = N_2 + O$	2. $N + O_2 = NO + O$
3. $N + OH = NO + H$	4. $N + CO_2 = NO + CO$
5. $N_2O + O = N_2 + O_2$	6. $N_2O + O = NO + NO$
7. $N_2O + H = N_2 + OH$	8. $N_2O + OH = N_2 + HO_2$
9. $N_2O + M = N_2 + O + M$	10. $NO + HO_2 = NO_2 + OH$
11. $NO_2 + O = NO + O_2$	12. $NO_2 + H = NO + OH$
13. $NO + O + M = NO_2 + M$	

C. Soot model

In this study, soot emissions are predicted by an improved phenomenological model developed by Jia [2009], which is based on the work of Tao et al. [2006]. As shown in Figure 3.2 [Jia et al., 2009], the complex soot formation and oxidation processes are described into several global steps. Acetylene (C_2H_2) is chosen as the inception species for soot formation rather than the parent fuel molecule because C_2H_2 is the species that affects soot formation most in

hydrocarbon fuel [Kong et al., 2005b]. Instead of using global reaction to describe the conversion of fuel to C_2H_2 in the work of Tao et al. [2006], the formation and oxidation of C_2H_2 are simulated through the detailed chemical mechanism in this study. The species of C_2H_2 and 13 additional reactions for the formation and oxidation of C_2H_2 are added to the original n-heptane mechanism, as shown in Table 3.2.

Table 3.2 The C_2H_2 formation and oxidation mechanism [Jia et al., 2009]

1. $CH_2 + CH_2 = C_2H_2 + H_2$	2. $CH_2 + CH_2 = C_2H_2 + H + H$
3. $C_2H_4 + M = C_2H_2 + H_2 + M$	4. $C_2H_2 + O_2 = HCO + HCO$
5. $C_2H_2 + O = CH_2 + CO$	6. $C_2H_2 + H + M = C_2H_3 + M$
7. $C_2H_3 + H = C_2H_2 + H_2$	8. $C_2H_3 + OH = C_2H_2 + H_2O$
9. $C_2H_3 + CH_2 = C_2H_2 + CH_3$	10. $C_2H_3 + C_2H_3 = C_2H_2 + C_2H_2$
11. $C_2H_3 + O = C_2H_2 + OH$	12. $C_2H_2 + OH = CH_3 + CO$
13. $C_2H_3 = C_2H_2 + H$	

The expressions for 6 global reactions in Figure 3.3 are given in Table 3.3. The reaction rate for precursor formation, particle inception, particle surface growth, and particle oxidation are computed in form of global Arrhenius expressions. The rate of particle coagulation (R_4) is given as

$$\dot{R}_4 = \frac{1}{2}\beta N^2 \tag{3.52}$$

where N is the soot number density and β is the collision frequency constant which is given by the Kazakov and Foster model [1998]. The rates of particle surface oxidation by O_2 and OH are determined from NSC oxidation model [Nagle and Strickland-Constable, 1962; Walls and Strickland-Constable, 1964] and the oxidation model of Neoh et al. [1985], respectively. In Jia's soot model, soot precursor and soot particle are assumed have only carbon atoms, and the numbers of carbon atoms in precursor and initial soot nucleus are set to be 50 and 100, respectively. This soot model has been validated by the shock tube experiments and diesel engine experiments, and the results have shown very good agreement between predictions and experiment data [Jia et al., 2009]. More details about this soot model and its validations can be found in the references of Tao et al. [2006] and Jia et al. [2009].

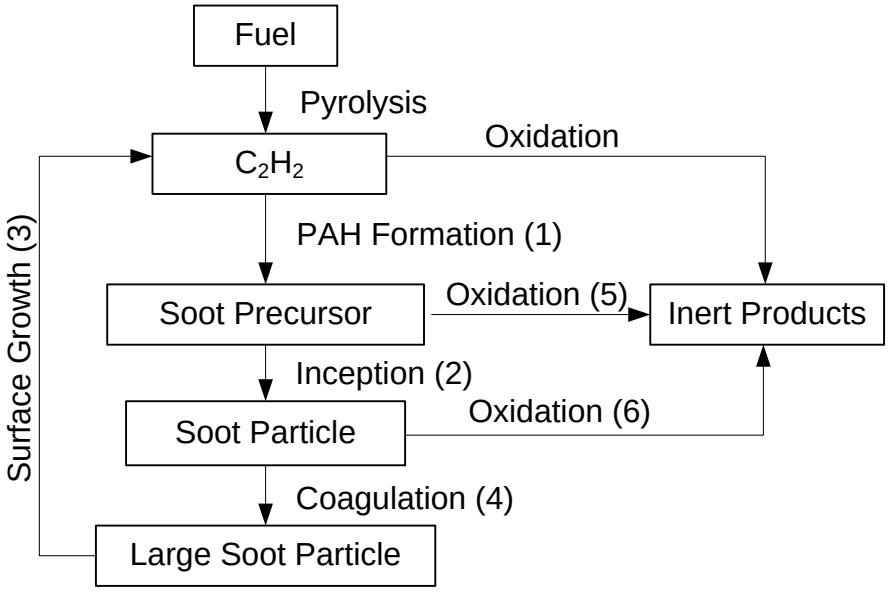

Figure 3.3 Schematic representation of the improved phenomenological soot model [Jia et al., 2009]

Table 3.3 The global steps of soot formation [Jia et al., 2009]

	Description	Reaction
R_1	Precursor species formation	$C_2H_2 \rightarrow 0.04C(PR)_{50} + H_2$
R_2	Particle inception from Precursor species	$C(PR)_{50} \rightarrow 0.5C(S)_{100}$
R_3	Particle surface growth	$C(S)_m + C_2H_2 \rightarrow C(S)_{m+2} + H_2$
R_4	Particle coagulation	$nC(S)_m \rightarrow C(S)_{n*m}$
R_5	Precursor species oxidation	$C(PR)_{50} + 25O_2 \rightarrow 50CO$
R_6	Particle surface oxidation	$C(S)_m + O_2 \rightarrow C(S)_{m-2} + 2CO$
		$C(S)_m + 2OH \rightarrow C(S)_{m-2} + 2CO + H_2$

C(PR) and C(S) represent the soot precursor species and soot particles, respectively.

3.2 Model Validation

The validation work focus on the accuracy of the integrated computational model rather than any individual sub-model. The details of the validations of the sub-models can be found in the related literatures which have been indicated in the sections above. For the modified spray models, the prediction accuracy of the break-up model was assessed by Jia et al. (2008a) base

on the experimental results from constant volume in terms of spay penetration, droplet diameter, droplet velocity and vapour distribution. And the KH-RT model showed good predictions in all aspects. Meantime, Jia et al. (2008b) validated the spray-wall interaction model by the experimental data under the conditions related to the diesel PPCI combustions. Through comparing the spray pattern, droplet mass, size and velocity after impingement, the thickness of the wall film and vapour distribution with the experimental data, the HXT model showed better accuracy in predictions owing to its consideration of the gas density. However, for clarification, the coefficients of these sub-models, which are constants during the simulations, are given in the Table 3.4.

Table 3.4 The coefficients for the break-up model and the collision model

Sub	Model	Coefficients	Explanation	Value
Break-up	KH-RT	C	Jet break-up length	30
		B_0	Product droplet radius for KH	0.61
		B_1	Time scale for KH	18
		$C_{3,RT}$	Product droplet radius for RT	2.5
		C_τ	Time scale for RT	1.0
Collision	Nordin	E_{12}	Collision efficiency	1.0
		C_1	Spatial probability decay	1.0
		C_2	Temporal probability decay	0.2

For the simulation of combustion, the details of the skeletal reaction mechanism of n-heptane can be found in the work of Patel et al. [2004], which gives the species, the reactions and the reaction rates' constants of the mechanism in its appendix. For the mechanism of NO_x formation that has been briefly described in the previous section, its constants of the reaction rates are given in the Table 3.5. And the constants of the rates of the C_2H_2 formation/oxidation and the global steps of soot formation are given in the Table 3.6 and the Table 3.7, respectively. These combustion model and the emission models have been validated by Jia et al. (2006, 2008c, 2009) under the operating conditions of diesel PCCI or PPCI combustion on a diesel engine with similar parameters of the engine in current study.

Table 3.5 The constants of reaction rates in the NO_x mechanism according to the Table 3.1

Reaction number	$k = AT^b exp\ (-E/RT)$		
	A (cm^3/mol s)	b	E (kcal/mol)
1	3.50×10^{13}	0.0	330.0
2	2.65×10^{12}	0.0	6400.0
3	7.33×10^{13}	0.0	1120.0
4	1.90×10^{11}	0.0	3400.0
5	1.40×10^{12}	0.0	10,810.0
6	2.90×10^{13}	0.0	23,150.0
7	4.40×10^{14}	0.0	18,880.0
8	2.00×10^{12}	0.0	21,060.0
9	1.30×10^{11}	0.0	59,620.0
10	2.11×10^{12}	0.0	- 480.0
11	3.90×10^{12}	0.0	- 240.0
12	1.32×10^{14}	0.0	360.0
13	1.06×10^{20}	-1.4	0.0

Table 3.6 The constants of reaction rates in the C_2H_2 mechanism according to the Table 3.2

Reaction number	$k = AT^b exp\ (-E/RT)$		
	A (cm^3/mol s)	b	E (kcal/mol)
1	1.20×10^{13}	0.0	800.0
2	1.20×10^{14}	0.0	800.0
3	1.50×10^{15}	0.0	55,800.0
4	4.0×10^{12}	0.0	28,000.0
5	1.02×10^{7}	2.0	1,900.0
6	5.54×10^{12}	0.0	23,150.0
7	4.00×10^{13}	0.0	0.0
8	3.00×10^{13}	0.0	0.0
9	3.00×10^{13}	0.0	0.0
10	1.45×10^{13}	0.0	0.0
11	1.00×10^{13}	0.0	0.0
12	4.83×10^{-4}	4.0	- 2,000.0
13	4.60×10^{e}	- 8.8	46,200.0

Table 3.7 The constants of reaction rates in the soot mechanism according to the Table 3.3

Reaction number	$k = AT^b exp\ (-E/RT)$		
	A (cm^3/mol s)	b	E (kcal/mol)
R_1	1.00×10^{11}	0.0	39.74
R_2	8.00×10^{10}	0.0	61.597
R_3	1.05×10^{4}	0.0	6.1597
R_4	Kazakov-Foster model [1998]		
R_5	NSC model [1962] and Neoh et al. model [1985]		
R_6	1.00×10^{9}	0.0	39.74

Since split-injection is applied to all the cases in this study, the model predictions of the single injection is not the emphasis here. PPCI engine experiments with split-injection performed by Lee et al. [2006a; 2006b] are used for computational model validation. Because the numerical investigation of diesel engine combustion in this study is conducted on an engine with the parameters similar to Lee's engine, the accuracies of both grid resolution and condition parameters are also well tested in this validation. Therefore, the validation according to the work of Lee et al. [2006a; 2006b] will be introduced in details. Moreover, the experiments by Hu and Rutland [2006] are also be recalculated to complete the validation of the computational model in different combustion modes. The results of the validation base on Hu's and Rutland's experiments are briefly discussed in the final stage of this section.

3.2.1 Introduction of Validating Experiments

The test engine in Lee's experiments is developed from a Ricardo Hydra single-cylinder engine [Ricardo, 2006] with a cylinder head which is modified from a Fiat 2.4 L five-cylinder engine. In order to achieve accurate control and measurement, a complex testing system has been constructed by Lee [2006a; 2006b] with a lot of instruments and sensors and more detailed information about the experimental set-up can be found in the publications of Lee.

A. Engine Specifications

The single-cylinder engine used by Lee is a typical high-speed direct-injection (HSDI) diesel engine with a volume of 0.477L. A relatively low compression ratio is designed to suppress the peak pressure and temperature in cylinder in order to reduce combustion noise and NO_x

formation. The cylinder head consists of two intake ports and two exhaust ports, and its schematic diagrams are given is Figure 3.4. The combination of directed and helical intake ports enables the adjustment of swirl ratio from 1.8 to 3.3. Specifications of the engine are summarized in Table 3.8. The injection in Lee's experiment is conducted using a Bosch common-rail injection system which can realize accurate multi-injection control. The nozzle has 8 orifices with a spray included angle of 130 °. The specifications of the injection system can be seen in Table 3.9.

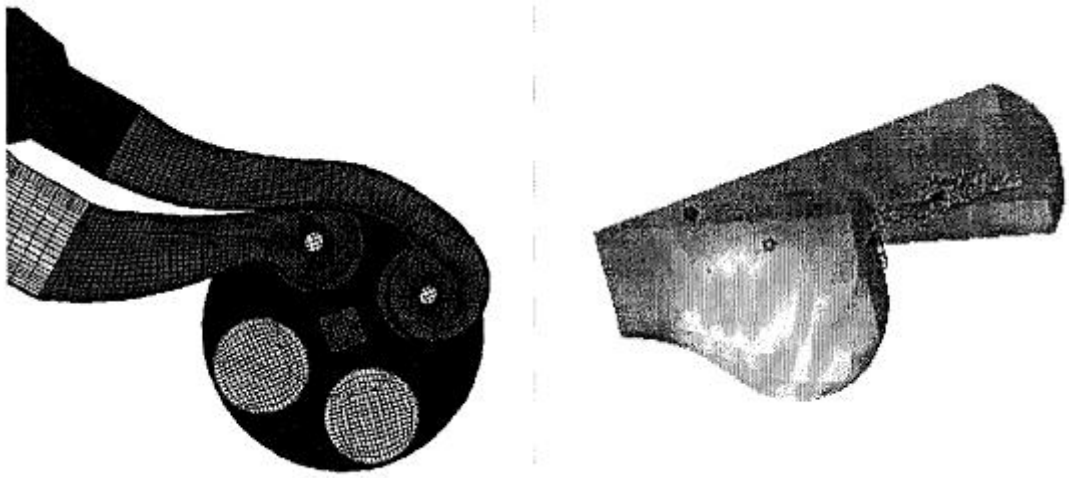

Figure 3.4 The Schematic diagrams of the intake port and piston bowl of Ricardo Hydra engine

Table 3.8 Engine specifications [Lee, 2006a]

Volume	0.477 L
Bore	82.0 mm
Stroke	90.4 mm
Squish Height	1.61 mm
Combustion Chamber Geometry	Open Crater Type Bowl
Compression Ratio	16.0 : 1
IVO / IVC	10 °CA BTDC / 38 °CA ABDC
EVO / EVC	38 °CA BBDC / 8.5 °CA ATDC
Swirl Ratio (at IVC)	1.83

Table 3.9 Injection system specifications [Lee, 2006a]

Design	Common Rail
Injector	Bosch DSLA 144 PV3 377623
Number of Orifices	8
Spray Included Angle	130 °
Diameter of Orifice	0.133 mm

B. Grid Resolution

Since the diesel injector used in Lee's experiment has 8 equally spaced orifices, a 45° sector of the full mesh with periodic boundaries is used for simulation. The intake and exhaust ports are not included in the grid because the simulation starts at the IVC and ends at the EVO. The plots of the grid at TDC and at IVC are given in the Figure 3.5.

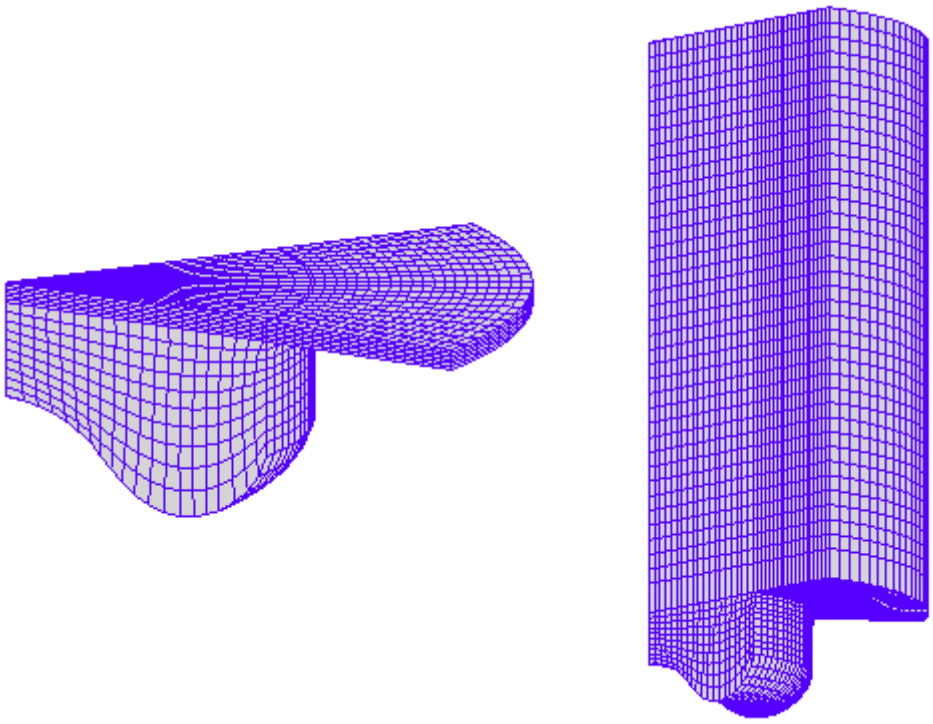

Figure 3.5 The computational grids at TDC (left) and at the IVC, i.e. -142 °CA ATDC (right)

This grid has approximately 44,000 hexahedral cells whose typical scale is smaller than 2 mm. The average cell dimensions are 0.9 to 1.1 mm in radial direction, and 0.5 to 2.3 mm in vertical direction. Moreover, Abani et al. [2008] used similar spray model computing on a set of grids, and their results showed no obvious differences between the fine grids and coarse grids around

this level of cell scale. The research of Kim et al. [1999] also showed some confidence of precision when using relatively coarser grids (2.2 × 2.2 × 3.0 mm^3). Jia and Xie [2006] also observed that a resolution of 2 mm in the axial direction did not affect the results and the difference was less than 5 percent in spray vaporization. Therefore, the grid used in our study is considered fine enough to yield sufficient accuracy for prediction.

C. Operating Conditions

The operating conditions in Lee's split-injection engine experiments are given in Table 3.10. The condition is highly diluted using EGR rate near 40% to suppress the in-cylinder temperature and to retard the ignition. In the split-injection strategy, the fraction of fuel in the 1st injection is chosen to be 25%, and the timing of the 1st injection is fixed at -35 °CA ATDC. In order to examine the effect of mixing on combustion and emission, the 2nd injection (75% fuel) timings varied from - 25 °to - 5 °CA ATDC are simulated. The injection pressure is fixed, and fuel mass rate is around 17 mg per cycle. The simulations are conducted from the IVC to the EVO, so the initial pressure and initial temperature are set to be the value at IVC. More details about the test conditions and experiments set-up can be found in references [Lee, 2006].

Table 3.10 The operation conditions [Lee, 2006]

Engine Speed	2000 rpm
IMEP	≈ 5.5 bar
Intake Pressure / Exhaust Pressure	1.3 bar / 1.48 bar
EGR	≈ 40%
Intake Air Temperature	90 ℃
Injection Pressure	1500 bar
Start of 1st Injection (SOI_1st)	-35 °CA ATDC
Start of 2nd Injection (SOI_2nd)	-25 °~ -5 °CA ATDC
Fuel in 1st Injection (in fraction)	25%
Swirl Ratio	1.83
Fuel Temperature	60 ℃

3.2.2 Validating Results

The comparisons between simulated and experimental profiles of pressure and hear release rate for three representative conditions are given in Figure 3.6. The profiles of injection pulse are also approximately sketched in Figure 3.6. It can be seen that the combustion timing and duration are accurately predicted. The simulation reproduces the delay of combustion timing and the increase of combustion duration when the 2nd injection timing retards. Though the peak value of heat release rate is a little over predicted, a good agreement is achieved between simulated and experimental heat released rate. The in-cylinder pressure is also predicted well, and only small and acceptable discrepancies exist between simulated and experimental results.

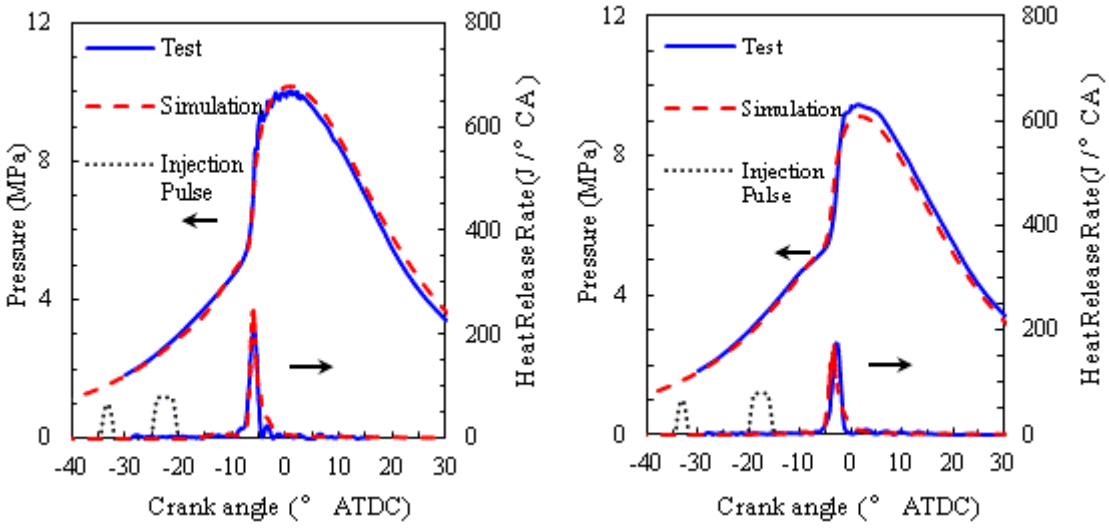

SOI_2nd = 25 °CA BTDC

SOI_2nd = 20 °CA BTDC

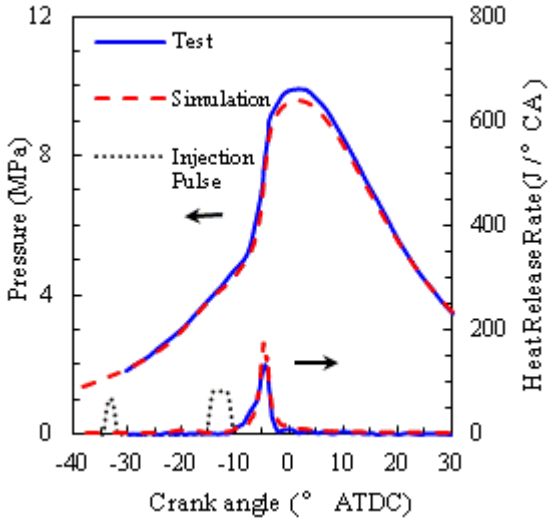

SOI 2nd = 15 °CA BTDC

Figure 3.6 The comparisons between experimental [Lee, 2006] and simulation results for the pressure and the heat release rate with different SOI_2nd timings.

Figure 3.7 shows the comparisons between predicted and experimental NO_x and soot emissions. The trends of NO_x and soot captured by experiments are predicted well by simulation. As SOI_2nd moves closer to TDC, NOx emission decreases, while soot emission increases. For the latest SOI_2nd (-5 °CA ATDC) the discrepancy between prediction and experimental results is relatively large. When SOI_2nd is near TDC, the time and space for mixing is limited. Serious wall film and insufficient combustion is resulted owing to the under-mix and low combustion temperature caused by the high EGR level and low compression ratio [Jia, 2009]. Therefore, the combustion is not very steady in this case.

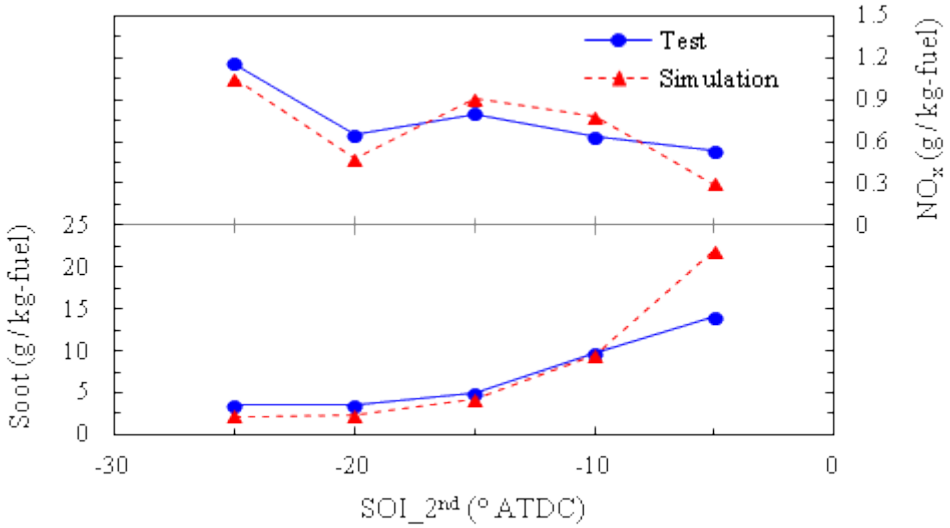

Figure 3.7 The comparisons between experimental [Lee, 2006] and simulation results for NOx and soot with different SOI_2nd timings.

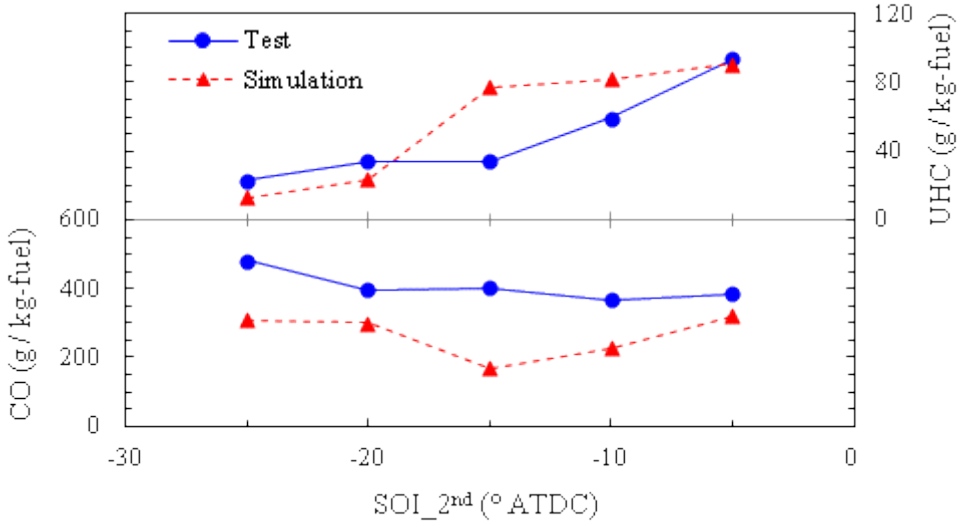

Figure 3.8 The comparisons between experimental [Lee, 2006] and simulation results for UHC and CO with different SOI_2nd timings.

As shown in Figure 3.8, Lee's PPCI diesel engine with split injections has very high CO output,

and CO formation decreases when SOI_2nd delays. The simulation results show some under-prediction in CO emission, while the overall trend of experimental profile is reprodeced well. The under prediction for CO formation can be regarded as another respect of the over prediction for heat release rate. The results from both simulation and experiment show that unburn hydrocarbon (UHC) formation increases as the injection timing is retarded. Relatively large discrepancies between the simulation and experimental results are observed for SOI_2nd is -15 ° CA ATDC and -10 ° CA ATDC. These discreoancies can be regarded as a results of the limitations of the wall film model [Han et al., 2000]. Nevertheless, the prediction can qualitatively reveal the trend of UHC.

3.2.2 Validation with Traditional Diesel Combustion Mode

A relatively large range of operating conditions will be involved during this study for diesel engine, though the major problem is the investigation about PPCI combustion. As stated in prior chapter, unlike HCCI combustion, in PPCI combustion the fuel does not have entirely uniform distribution in cylinder. In the operating conditions with relative late injection, large fraction of fuel is oxidized in mix-controlled combustion, which is the feature of traditional diesel engine. To ensure adequate accuracies for the large range of operating conditions, the validation on traditional diesel engine is conducted and briefly introduced below.

The experiments on a traditional diesel engine in the publication of Hu and Rutland [2006] are used for validation. The test engine is a single-cylinder version of the Caterpillar 3400 series diesel engine. The engine specifications and operating conditions are listed in Table 3.11 and 3.12. As shown in Figure 3.9, both pressure and heat release rate are predicted with acceptable accuracy.

Table 3.11 Engine specifications of HU and Rutland's experiments [2006]

Volume	2.44 L
Bore / Stroke	137.6 mm / 165.1 mm
Compression Ratio	15.1 : 1
Number of Orifices	6
Diameter of Orifice	0.259 mm
Spray Included Angle	55 °
IVC	- 147 °CA ATDC

Table 3.12 Operating conditions of HU and Rutland's experiments [2006]

Engine Speed	1600 rpm
Load	75%
Injected Mass	129 g/min
Injection Pressure	90 MPa
SOI	- 9 °CA ATDC
Duration of Injection (DOI)	21 °CA

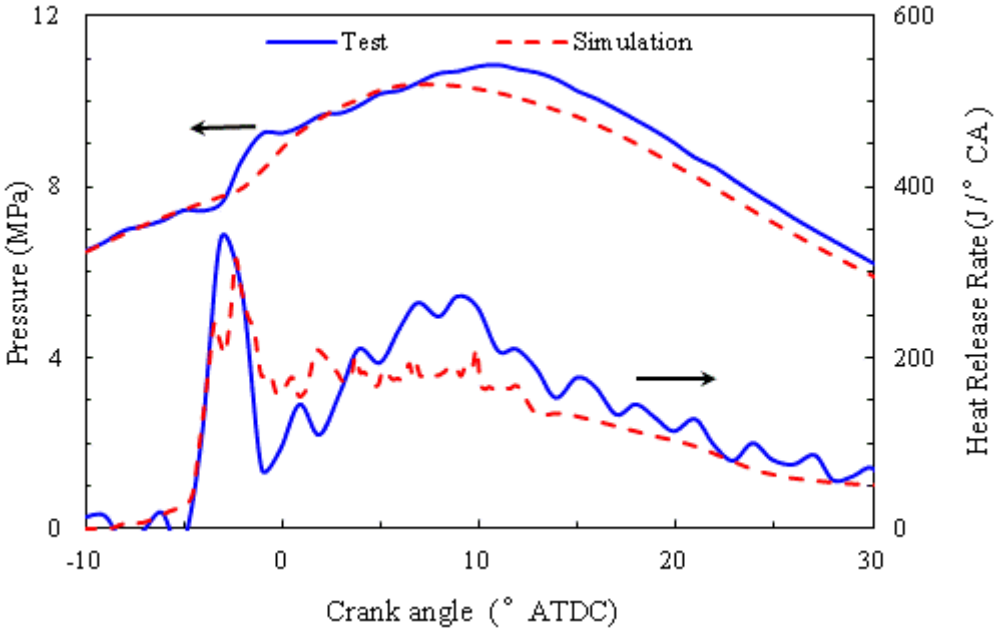

Figure 3.9 The comparisons between experimental [Hu and Rutland, 2006] and simulation results for the pressure and the heat release rate.

3.3 Summary

In this chapter, the numerical models used in this study and validations are mainly introduced. An improved KIVA-3V2 code [Amsden, 1999] coupled with CHEMKIN [Kee et al, 1996] is used to simulate the in-cylinder flow phenomena and combustion process. For improving the modeling of spray, a KH-RT model [Jia et al., 2008] is used to simulate the break-up process of injected droplets, and the droplets' collision is calculated by Nordin's model [2001]. Moreover, the spray-wall interaction is modeled by HXT model [Han et al., 2000]. The heat flux through wall is simulated by a grid-independent wall heat transfer model developed by Han and Reitz [1997]. Skeletal reaction mechanism for n-heptane with 29 species and 52 reactions [Patel et. al.,

2004] is used to simulate diesel fuel chemistry in this study. Four additional species (N, NO, NO2, N2O) and 13 reactions from Golovichev mechanism [Golovichev, 2002] are added to this n-heptane chemistry mechanism in order to calculate the formation of NO_x. For the prediction of soot formation, an improved phenomenological model developed by Jia [2009], which is based on the work of Tao et al [2006], is employed. Meanwhile, the inception species for soot formation, i.e. C_2H_2, and 13 related reactions are added to the original n-heptane chemistry mechanism. Then the model of soot formation and the chemical kinetic reaction mechanism is connected.

Validations on a PPCI diesel engine [Lee, 2006] and a traditional diesel engine [Hu and Rutland, 2006] are conducted for testing the accuracy of the models. For the validation with PPCI diesel combustion mode, very good agreement is achieved for the prediction of in-cylinder pressure and heat release rate. Also, the characteristics of NO_x and soot formation of this PPCI diesel engine are captured well by simulation. Though there are some discrepancies between the experimental data and the prediction for CO and UHC emission, the trend of CO and UHC can be qualitatively revealed through simulation. Moreover, the validation with the tradational diesel combustion shows that the prediction is capable to reproduce the characteristics of combustion in traditional diesel engines.

In summary, the numerical approach used here is of adequate accuracy for the investigation of split-injection diesel engine's combustion conducted in this study.

Chapter 4 Diesel PPCI Combustion with Split-Injection and Homogeneity Factor Study

4.1 Diesel PPCI Combustion with Split-Injection

The objectives of this study are to investigate the effects of operating parameters on combustion performance and emission in PPCI combustion using split-injection. The strategy of split-injection is the primary field to be examined. Therefore, the investigations about the effects of the 2nd injection timing (SOI_2), the fuel split proportion, the spray angle and injection pressure of this split-injection strategy are conducted to obtain comprehensive understanding about the characteristics of mixing and combustion in PPCI combustion with split-injection. Moreover, the impacts of swirl ratio, EGR rate and boost pressure are examined to develop the operating range of PPCI engine. In the meantime, in order to evaluating the quality of mixing, the Homogeneity Factor (*HF*) is proposed to quantitatively characterize mixing. Also, the relations between the quality of mixing and characteristics of combustion and emissions are tried to describe quantitatively using this factor.

4.1.1 Operating Conditions

The study in this section is performed on the engine with the same parameters of the engine in Chapter 3 [Lee and Reitz, 2006] but using a different injector. The new injector has 6 orifices with the diameter of 0.11mm. The simulation in this chapter is at the speed of 2500 rpm, the initial in-cylinder temperature at IVC of 360 K. While the fuel mass per cycle is kept as 23 mg, the maximum achieved torque output can be around 100 N·m. And the timing of first injection (SOI_1) is fixed at - 40 °CA ATDC. Other parameters, i.e. the 2nd injection timing (SOI_2), the split proportion, the spray angle, the injection pressure, the swirl ratio, the EGR rate and boost pressure are varied for testing the characteristics of PPCI combustion with split-injection, which can be found in Table 4.1. The value underlined in these variable parameters is the setting of baseline condition.

Table 4.1 The operating conditions for PPCI combustion using split-injection

Engine Speed	2500 rpm
Maximum Torque	100 N·m
Temperature at IVC	360 K
Boost Pressure	0.60 bar, 1.00 bar, 1.40 bar
The Fraction of Fuel in the 2nd Injection	20%, 50%, 80%
Start of the 1st Injection (SOI_1)	-40 °CA ATDC
Start of the 2nd Injection (SOI_2)	-30 °~ -5 °CA ATDC
Injection Pressure	70 MPa, 110 MPa, 150 MPa
Spray Included Angle	90 °, 120 °, 150 °
Swirl Ratio	1.4, 1.8, 2.2
EGR Rate	20%, 35%, 50%
* The value underlined is the setting for baseline condition.	

4.1.2 Data Processing Method

A. Specific Fuel Consumption

The specific fuel consumption is a useful parameter to evaluate the fuel economy of engine by giving the fuel flow rate per unit power out. In this study, the gross indicated specific fuel consumption (ISFC) is adopted because the power output, *W*, calculated by simulation is the gross indicated power. In this thesis, the ISFC indicated the gross fuel efficiency when it is mentioned, and it is given as:

$$ISFC = \frac{m_f}{W} \tag{4.1}$$

where, m_f and W are the fuel mass and power output per cycle, respectively.

B. Fuel Conversion Efficiency

The fuel conversion efficiency represents the overall efficiency of the supplied fuel energy converting into the work produced per cycle. It is defined as:

$$\eta_{fc} = \frac{W}{m_f Q_{LHV}} \tag{4.2}$$

where , η_{fc} is the indicate fuel conversion efficiency; W, m_f, and Q_{LHV}, represent the gross indicated work per cycle, the fuel mass injected per cycle, and the lower heating value of fuel, respectively.

During the conversion of the fuel energy into work, a series of energy losses happens. These energy losses can be generally concluded as the incomplete combustion, the heat loss and the thermodynamic loss, which are represented as the combustion efficiency, the heat loss efficiency and the thermal conversion efficiency, respectively. The relation between these efficiencies and the fuel conversion efficiency is given in below:

$$\begin{aligned} \eta_{fc} &= \eta_{tc}\eta_{hl}\eta_{comb} \\ &= \left(\frac{W}{Q_{chem} - Q_{hl}}\right)\left(\frac{Q_{chem} - Q_{hl}}{Q_{chem}}\right)\left(\frac{Q_{chem}}{m_f Q_{LHV}}\right) \\ &= \left(\frac{W}{Q_{chem} - Q_{hl}}\right)\left(\frac{Q_{chem} - Q_{hl}}{m_f Q_{LHV}}\right) \\ &= \eta_{tc}\eta_{hr} \end{aligned} \tag{4.3}$$

where, η_{tc} is the thermal conversion efficiency; η_{hl} is the heat loss efficiency; η_{comb} is the combustion efficiency. In this equation, Q_{LHV}, Q_{chem} and Q_{hl} represent the lower heating value of fuel, the total chemical heat release during combustion, and the heat transfer loss, respectively.

The second term in the equation 4.3 indicates the heat rejection efficiency (η_{hr}), according to the definition of Lee et al. [2006b] and Kook et al. [2005]. The heat rejection efficiency indicates how much and how well the chemical energy of fuel is released, and concludes the effect of the combustion efficiency, the heat transfer losses and the gas exchange losses in it. The thermal conversion efficiency indicates how effectively the heat release is converted to the mechanical work.

It has to be noticed that the efficiencies used in this thesis are the gross indicated efficiencies, since they are calculated by using the gross indicated work output.

4.1.3 The Effects of the 2nd Injection Timing

A preliminary study is conducted to gain an initiatory understanding of the split-injection in diesel engine through a sweep of the 2nd injection timing. The 2nd injection timing varies from -30 °CA ATDC to -5 °CA ATDC with an interval of 5 °CA, and other parameters is setting as the baseline condition. With the spray angle of 120 °, the earliest injection timing is determined

by the assurance that the spray will be kept in the piston bowl. While the latest injection timing is held before TDC because the combustion will be unstable with this high level of EGR rate (35%) and low combustion temperature when the injection timing is near TDC [Lee and Reitz, 2006]. 20% of the total fuel is injected in the 1st injection, while 80% in the 2nd injection. The injection pressure is set to be a medium value, i.e. 110 MPa, for the purpose of moderating the wall wetting and oil dilution problem.

From Figure 4.1, it can be seen that the combustion is significantly affected by the 2nd injection (80% fuel) timing. Though using relative early first injection, no observable heat release can be found until - 20 ° CA ATDC for each case. This suggests that the in-cylinder pressure and temperature are not sufficiently high for ignition until - 20 ° CA ATDC. Since the injection finishes before ignition, it is difficult to distinguish the heat release from the two stages of injection when the 2nd injection timing is - 30 ° CA ATDC, because the fuel of both injections has been mixed with air and might oxidize simultaneously. However, for other cases with later 2nd injection timing, the heat release from the 1st and the 2nd injection displays separately. The peak value of heat release rate decreases as the 2nd injection timing is retarded, as shown in Figure 4.1. And the efficiency of combustion is apparently deteriorated when the 2nd injection timing is moved close to TDC.

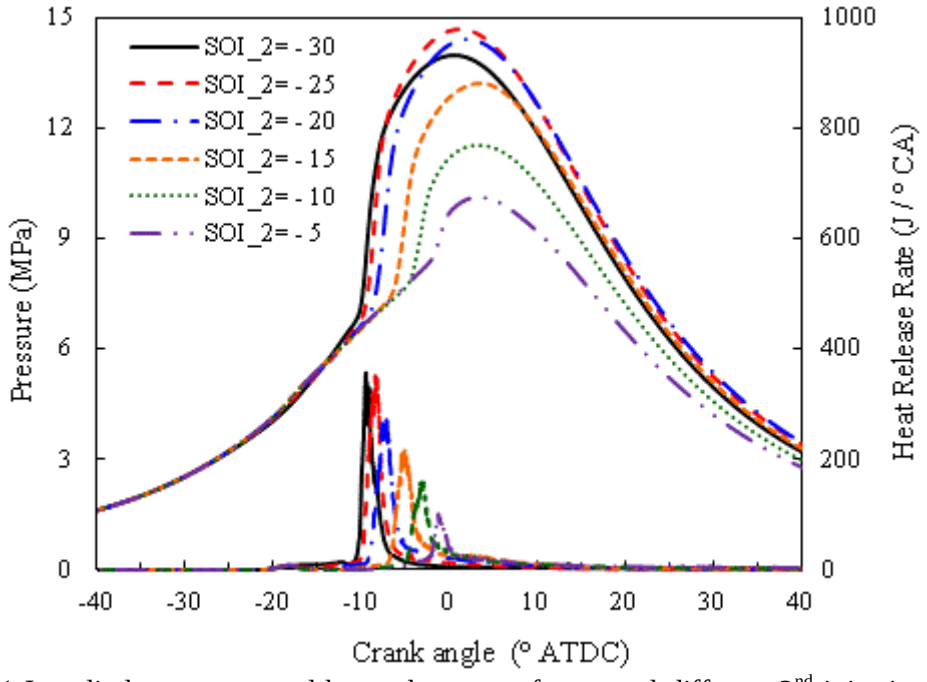

Figure 4.1 In-cylinder pressure and heat release rate for several different 2nd injection timings (SOI_2)

The conclusion of Lee [2006], which proposes short combustion duration as the character of PPCI combustion that can be used to distinguish PPCI combustion from standard diesel combustion, is also observed in this study. In Figure 4.2, the 10% accumulative fuel burnt

location is chosen as the start of combustion since it is typical located near the onset of the main heat release [Opat et al., 2007], while the location of 50% fuel burnt and 90% fuel burnt represents the location of entire combustion phase and the end of combustion, respectively. It is shown that though the start of combustion retards as the 2nd injection timing moving to TDC, the variation is not significant until the 2nd injection timing is after - 20 ° CA ATDC. And the combustion starts before injection ends (EOI) when the 2nd injection timing (SOI_2) is later than - 25 ° CA ATDC. Therefore, the mixing process controls the combustion of the cases with relatively late 2nd injection timing. Moreover, the combustion duration (crank angle between 10% and the 90% burnt location) increases as the 2nd injection is retarded. And this phenomenon proves the statement of Lee [2006] that the combustion in PPCI mode is faster than in standard diesel mode. However, the phases of PPCI combustion with early injection locate far before the TDC, and this will have negative effect on the power output, as shown in the profiles of pressure in the Figure 4.1.

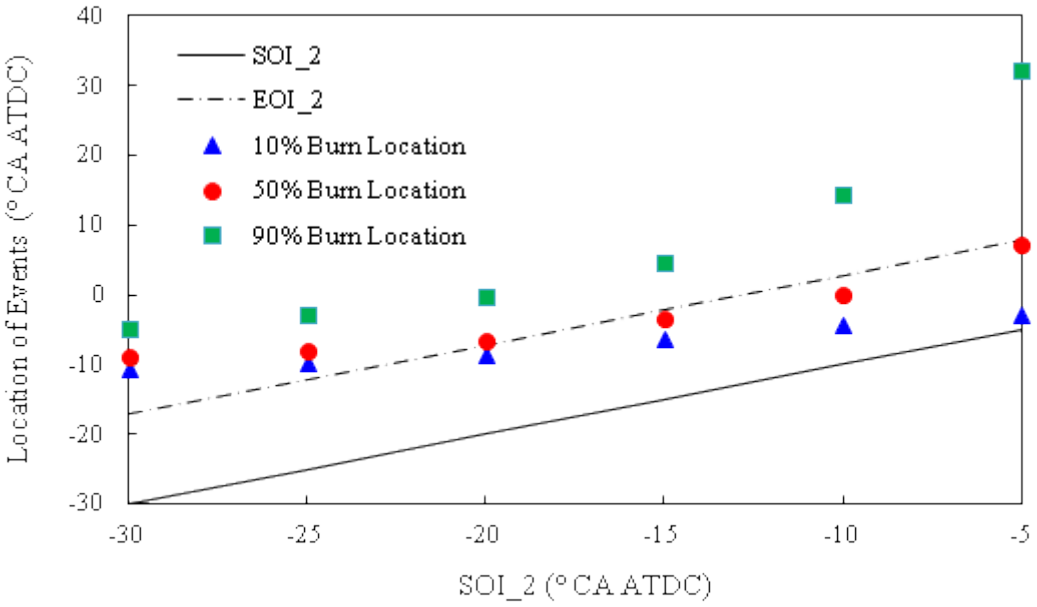

Figure 4.2 The 10%, 50% and 90% burn location of the cases with different 2nd injection timing

Figure 4.3 and Figure 4.4 show the variation of emissions as for different the 2nd injection timings. At the earliest 2nd injection timing (-30 ° CA ATDC), moderately high level of soot, CO and unburned hydrocarbon (UHC) are observed. The low combustion temperature is considered as the reason of low combustion efficiency which can be proved by the high level of CO and UHC output. Although the mixing time in this case is longer than others, the relatively low in-cylinder temperature increases the difficulty for fuel evaporation and results in long spray penetration, and these eventually lead to serious wall wetting. During the combustion, the fuel adhered to the cylinder wall is usually an important source for soot formation. The highest NO_x is observed when the 2nd injection timing is -25 ° CA ATDC. Though, the ignition delay is

shorter than in the case of the earliest 2nd injection timing, higher in-cylinder temperature enhances mixing process in this case and promotes the combustion. Sharper pressure raising slope and shorter combustion duration are reached for the case with the 2nd injection timing of -25 °CA ATDC, as shown in Figure 4.1 and 4.2. Moreover, Figure 4.4 shows the reduction of CO and UHC in this case comparing with the earliest injection, and this reduction implies the improvement of combustion efficiency. Moreover, the high combustion temperature in this promoted combustion causes the high level of NO_x formation in the case with the 2nd injection timing of -25 °CA ATDC. The lowest level of soot, CO and UHC emission is achieved when the 2nd injection timing is -20 °CA ATDC, and NO_x output starts to decrease at the same time. As the 2nd injection timing is retarded further, the output of soot, CO and UHC increase dramatically because the under-mix of air and fuel is getting serious under this high level of EGR rate. Meanwhile, since the fuel enrolled in combustion reduces, the combustion temperature is suppressed, and the NO_x formation decreases as the 2nd injection timing moving to TDC. A sudden drop of soot emission is observed when the 2nd injection timing is retarded to -5 °CA BTDC, though its mixing condition is the worst compared with the former cases.

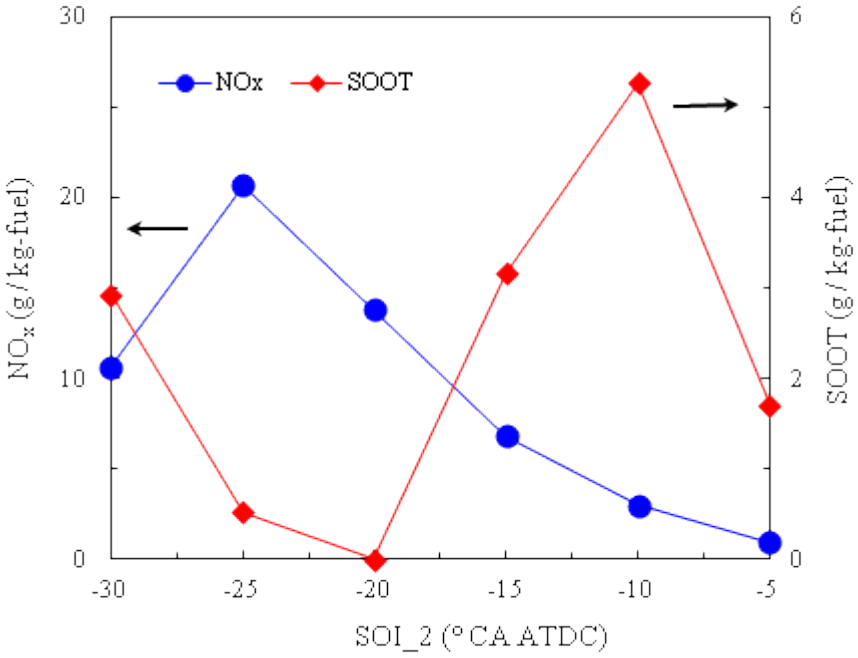

Figure 4.3 Effects of the 2nd injection timing on NO_x and soot emission

The reduction of soot for this case is resulted from the low combustion temperature, and serious incomplete combustion is implied from the high level of UHC and CO output, as shown in Figure 4.4. Figure 4.5 shows the distribution of equivalence ratio before the start of combustion, which is at -15 °CA ATDC when SOI_2= -30 °CA ATDC, or at -5 °CA ATDC when SOI_2= -10 ° ATDC. For the case with the 2nd injection timing of -30 ° CA ATDC, a high equivalence ratio area exists near the surface of piston bowl before the combustion starts, as given in Figure

4.5(a). And after 10 crank angles, though the combustion is almost finished according to Figure 4.2, high equivalence ratio is still detected in bowl area for this case. Therefore, the relatively high soot and UHC output of the case with SOI_2= -30 °CA ATDC can be considered derived from this rich area near the surface of piston bowl and fuel adhered on piston. For the case with the 2nd injection timing of -10 °CA ATDC, the injection dose not finish when the combustion starts, and very poor fuel-air mixing could be observed in cylinder, as shown in Figure 4.5(b). Considering the relatively high temperature at -5 °CA ATDC, the poor mixture formation is considered as the reason for the high level of soot and UHC output.

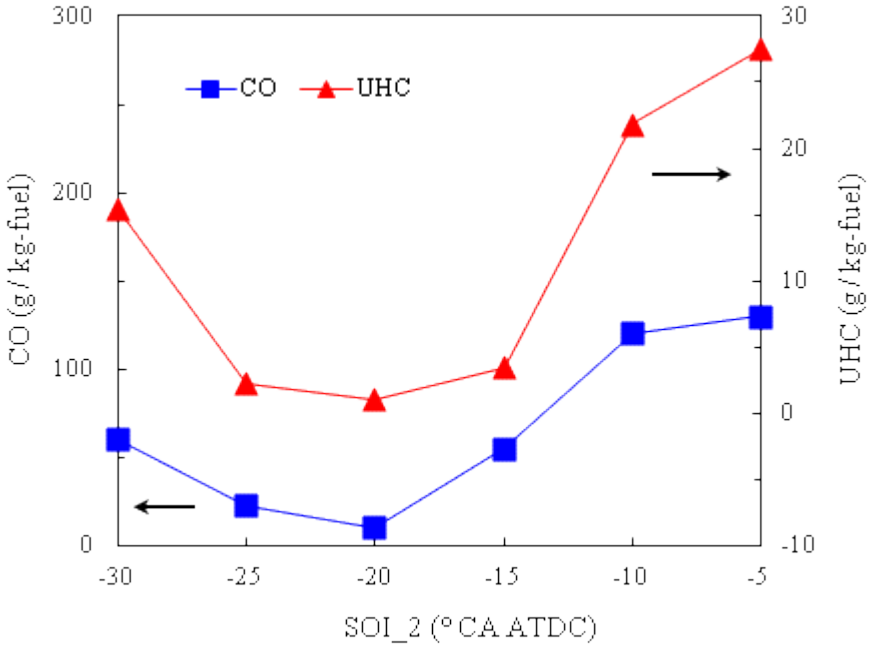

Figure 4.4 Effects of the 2nd injection timing on CO and UHC emission

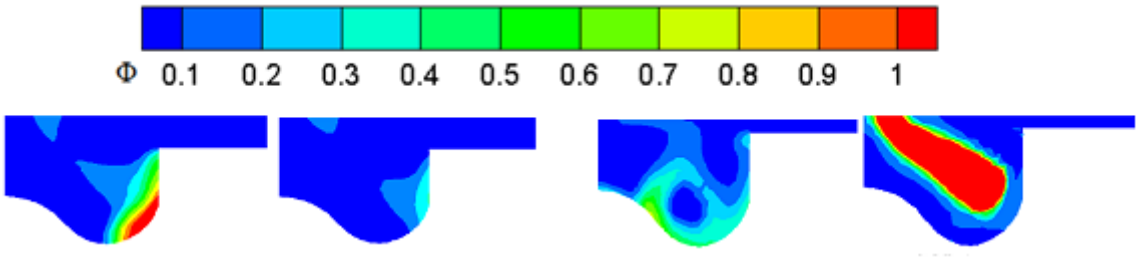

SOI_2= -30 °ATDC SOI_2= -10 °ATDC SOI_2= -30 °ATDC SOI_2= -10 °ATDC

(a) at -15 °CA ATDC (b) at -5 °CA ATDC

Figure 4.5 Equivalence ratio distribution prior to the ignition (at -15 °CA ATDC and at -5 °CA ATDC), when SOI_2= -30 °CA ATDC and -10 °CA ATDC.

4.1.4 The Effects of Fuel Splitting Proportion

Two more fuel splitting strategies, which are 50% and 80% of fuel in the 1st injection, are added to the simulation to study the effects of fuel split proportion. For the most cases, with a certain

2nd injection timing, as the fraction of fuel in the 1st injection increases, the start of combustion moves forward and the duration of combustion (DOC) become shorter, as shown in Figure 4.6. Raising the fuel amount in the earlier 1st injection will certainly enhance the mixing before ignition and increase the amount of mixture. For the cases with 80% of fuel delivered in the 1st injection, their combustion durations are all very short, and the shortest one is around 4 ° CA. According to Lee's study [2006], this short level of combustion duration is a typical characteristic of PPCI combustion. Moreover, as the fraction of fuel in the 1st injection increases, the variation of the start of combustion and the combustion duration over different 2nd injection timing becomes relatively less obvious, though the trends for these 3 different fuel splitting strategies are similar.

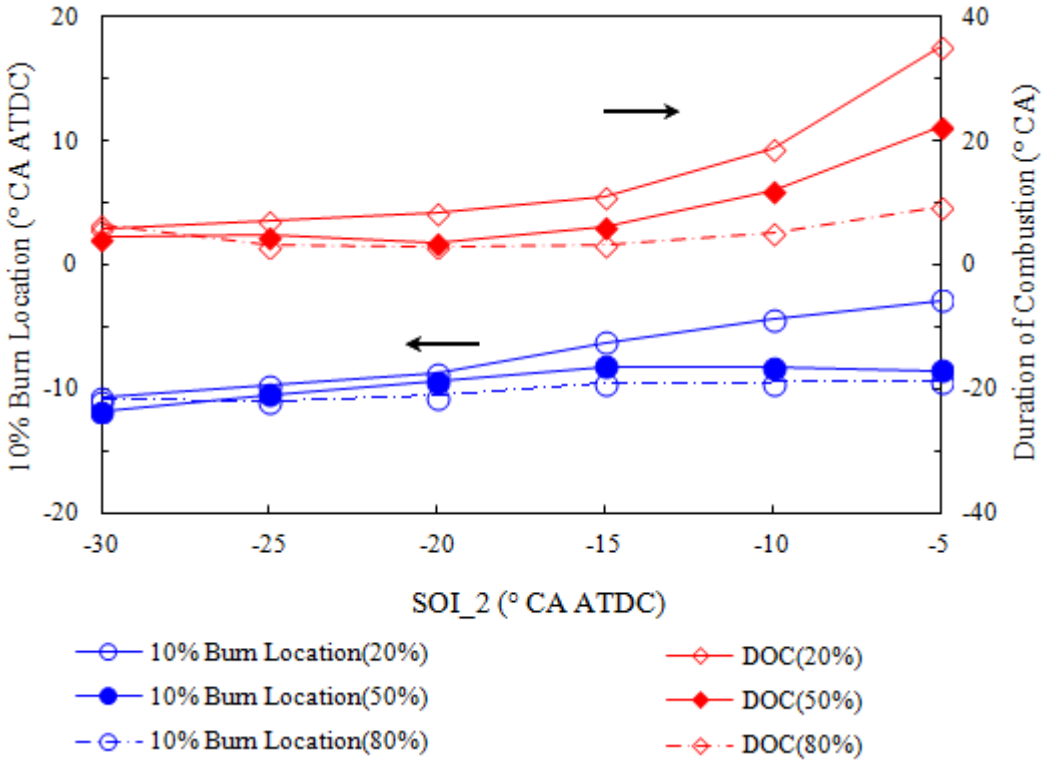

Figure 4.6 The 10% burn location and combustion duration for the cases of different 2nd injection timings with different fuel splitting proportions

The 50% burn location is not significantly affected by the 2nd injection timing and is around -9 ° CA ATDC to -7 ° CA ATDC, when the 80% of fuel is delivered into the cylinder through the 1st injection, as shown in the Figure 4.7. However, when increasing the portion of fuel injected in the 2nd injection, a steeply increasing slope of 50% burn location with respect to the 2nd injection timing is observed. With earliest 2nd injection timing at -30 ° CA ATDC, the highest ISFC is resulted when 80% of fuel is delivered in the 1st injection; while similar high level of ISFC is observed as the 2nd injection timing is retarded to - 5 ° CA ATDC when 20% of fuel is in the 1st injection. The high fuel consumption in the former case is considered stemming from the

under-mix owing to the low temperature during early injection. And the later one results from the incomplete combustion during the mix-control phase. When the 2nd injection timing is before -15 ° CA ATDC, the ISFC is higher as the portion of fuel in the 1st injection increases. Once the 2nd injection timing is retarded after -15 ° CA ATDC, the ISFC raises dramatically as the 2nd injection moving to the TDC when only 20% or 50% of fuel is delivered in the 1st injection. Then higher level of ISFC is observed when less fuel is in the 1st injection.

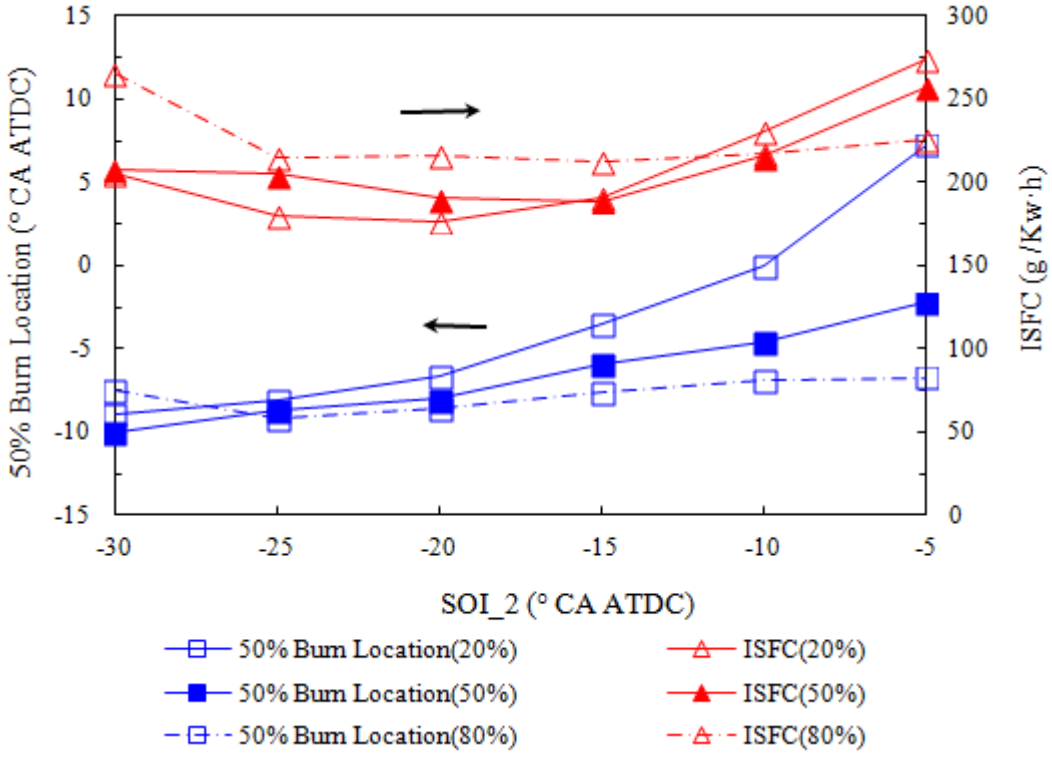

Figure 4.7 The 50% burn location and ISFC for the cases of different 2nd injection timings with different fraction of fuel in the 1st injection

As shown is Figure 4.8 and Figure 4.9, the trends of emission over different 2nd injection timing are significantly affected by the fuel splitting strategy. The peak NO_x of the splitting strategy with more fuel delivered through the 1st injection appears closer to the TDC. When major portion of fuel (80%) is in the 1st injection, the NO_x formation still maintains a relatively high level even the 2nd injection is retarded to after -15 ° CA ATDC, while sudden drop of NO_x output is observed in other two fuel splitting strategies. This is because, when 80% of fuel is delivered through the 1st injection, the combustion temperature is higher during the later stage of combustion process since more fuel has been burnt before the 2nd injection starts. The soot emission can be efficiently suppressed when transferring the major portion of fuel to the 1st injection. As 80% of fuel has been injected before -30 ° CA ATDC, the soot output is smaller than 1 g per kg fuel for all 2nd injection timings, as shown in Figure 4.8. With this level of soot, the diesel engine can be considered working under ‘smokeless’ condition.

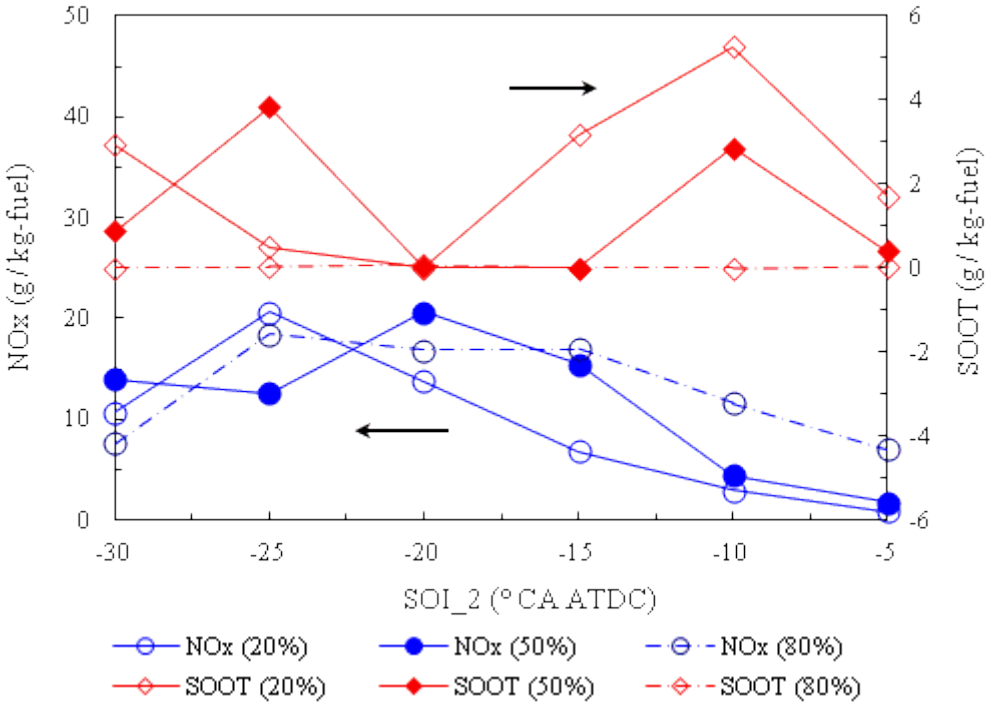

Figure 4.8 The NO_x and soot emission for the cases of different 2nd injection timings with different fraction of fuel in the 1st injection

Though using early injection with major fraction of fuel seems to be a measure to resolve the smoke issue of diesel engine, the UHC is much higher than the cases whose 1st injection carries smaller amount of fuel when the 2nd injection timing is before -10 ° CA ATDC. Since most of fuel is injected more than 30 ° CA before TDC, which is about 20 ° CA before the combustion starts, more and richer mixture is achieved because of the longer ignition delay. Then premixed combustion is considered playing major role in the whole combustion process. However, the low in-cylinder temperature during the early injection is unfavourable for evaporation and the following low temperature combustion also causes high UHC emission. Once the 2nd injection timing retards after -10 ° CA ATDC, the UHC output increases sharply when major portion of fuel is in the 2nd injection because the under-mixing causes seriously incomplete combustion in the mix-controlled combustion phase. The CO emission keeps lower than others as 80% of fuel in the 1st injection since its relatively sufficient mixing. The dramatic increase of CO emission for the cases with large amount of fuel in the late 2nd injection implies that the incomplete combustion results from under-mixing, low temperature in mix-controlled burn phase is the reason for the high level of CO emission in the diesel engine under this high EGR rate [Lee, 2006; Opat et al., 2007; Koci et al., 2009].

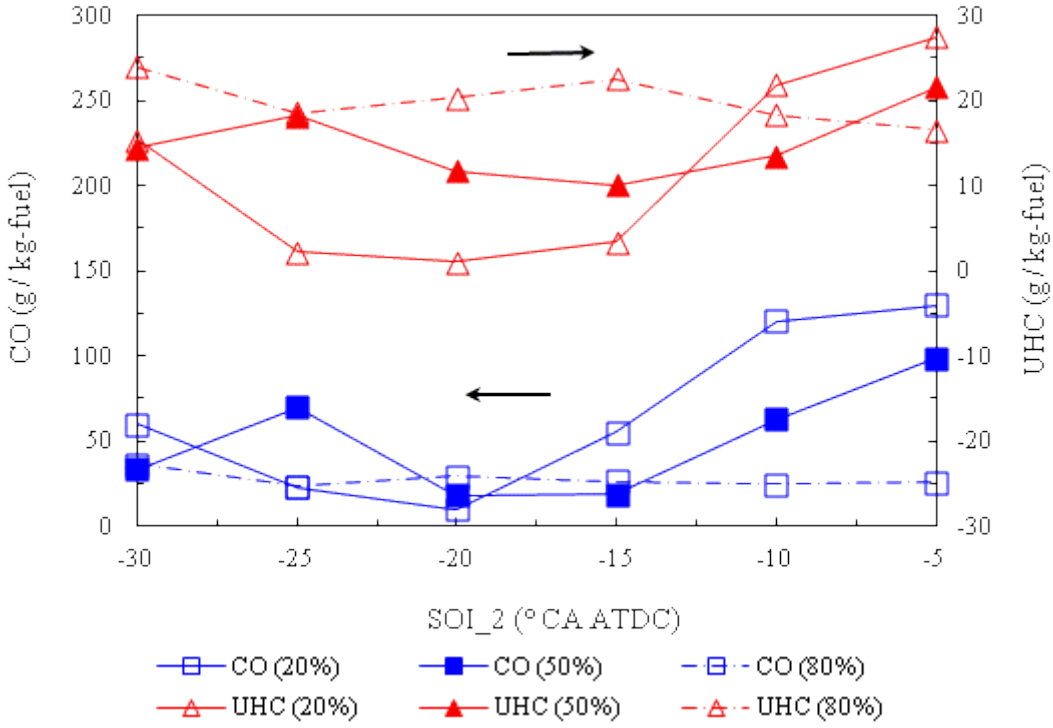

Figure 4.9 The CO and UHC emission for the cases of different 2nd injection timings with different fraction of fuel in the 1st injection

4.1.5 The Effects of Spray Angle

The spray angle is considered massively affect the performance and emissions of the diesel engine through its influence on the equivalence ratio distribution in cylinder. Meanwhile, the research of Martin et al. [2008] and Walter at al. [2002] showed that the implementation of narrow angle direct injection (NADI) had the potential to operate a diesel engine under HCCI/PPCI combustion with satisfied emissions and acceptable fuel consumption because it could suppress the wall impinging. To study the effect of spray included angle on performance and emissions, three nozzles with different spray angle (90°, 120°, and 150°) are examined for both PPCI combustion and standard diesel combustion.

As shown in Figure 4.10, the effect of spray angle on the start of combustion is not significant. The largest discrepancy of combustion start's timing for different spray angle appears when the 2nd injection timing is -5° CA ATDC. Therefore, the influence of spray targeting on the distribution of equivalence ratio and temperature could be more obvious when using late 2nd injection. The combustion duration is prolonged as the spray included angle getting narrow, and the discrepancy of combustion duration for different spray angle is enlarged as the 2nd injection timing retarded. This phenomenon implies that the spray angle affects the mixing process significantly. With the shape of piston top in this study, more fuel intends to be captured in the bowl area as the spray angle getting narrow, as shown in Figure 4.11. Under the EGR level of

35%, it increases the difficulties for fresh air to enter into fuel in this area of piston bowl. Then the increase of fuel fraction in this rich area results in the prolonged combustion duration when using narrow spray angle.

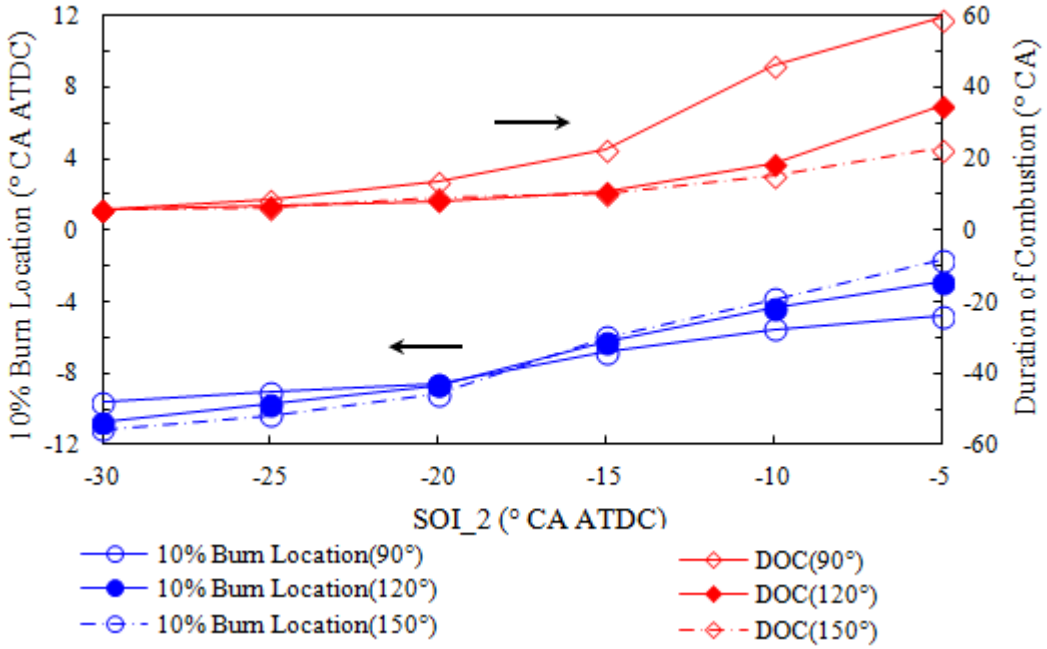

Figure 4.10 The 10% burn location and combustion duration for the cases of different 2nd injection timings with different spray angle.

And the Figure 4.11 also shows that the insufficiency of fuel and air mixing in the bowl area gets more serious when the 2nd injection timing retards closer to TDC. Hence, appropriated amount of fuel in the squish region is beneficial for combustion. Opat et al.[2007] showed, for single injection diesel engine, there is an optimal spray targeting to achieve desired combustion. For split-injection, it is complicated to find the optimal spray targeting.

No obvious discrepancy in the 50% burn location can be seen for different spray angle until the 2nd injection timing retards to later than -10 °CA ATDC, as shown in Figure 4.12. The case using narrow spray angle (90 °) has the latest 50% burn location when the 2nd injection timing is -5 ° CA ATDC. Referring to Figure 4.11, it is can be found that the discrepancies in combustion duration are due to the 50% to 90% burnt duration. From the Figure 4.12, it is can be seen that the ISFC is significantly affected by the spray included angle. Lower fuel consumption and stable level of ISFC for different 2nd injection timing can be achieved when using wider spray angle. Due to the lack of available O_2 in piston bowl area, the fuel economy of diesel engine is deteriorated if narrow spray angle is applied. And the effect of the 2nd injection timing on ISFC is intensified for the cases with narrow spray angle.

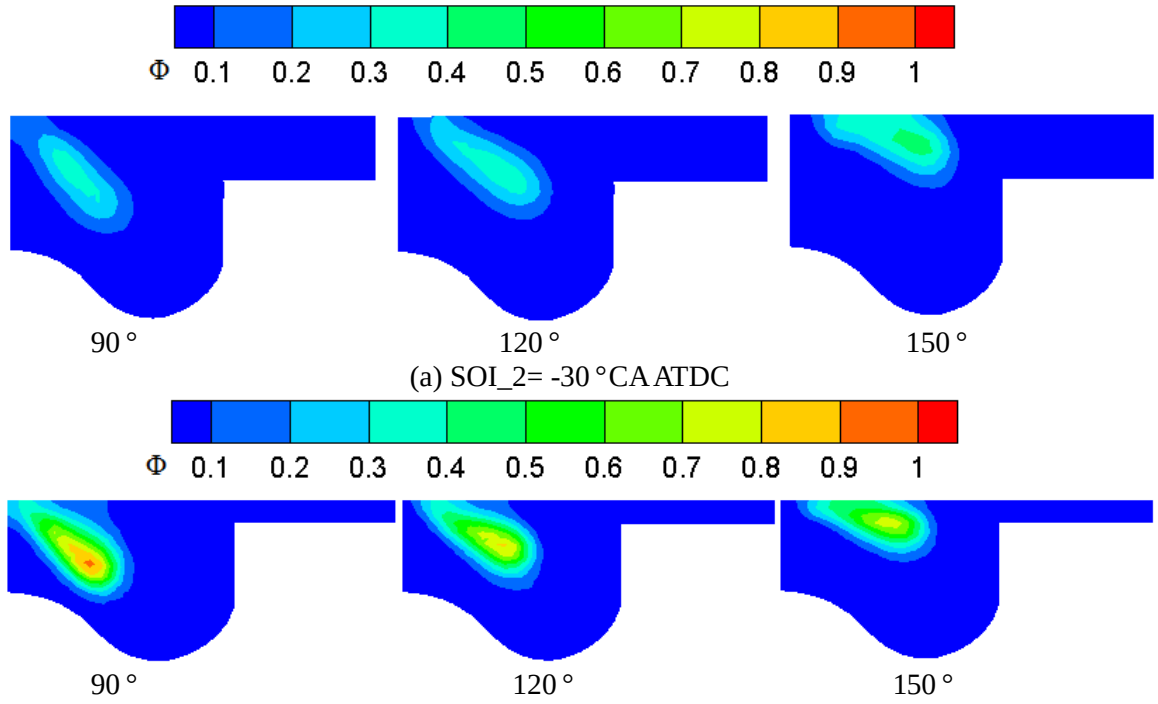

(a) SOI_2= -30 °CA ATDC

(b) SOI_2= -15 °CA ATDC

Figure 4.11 Equivalence ratio distribution at 5 ° CA after the 2nd injection for the cases with different spray angle, when SOI_2= -30 °CA ATDC and -15 °CA ATDC.

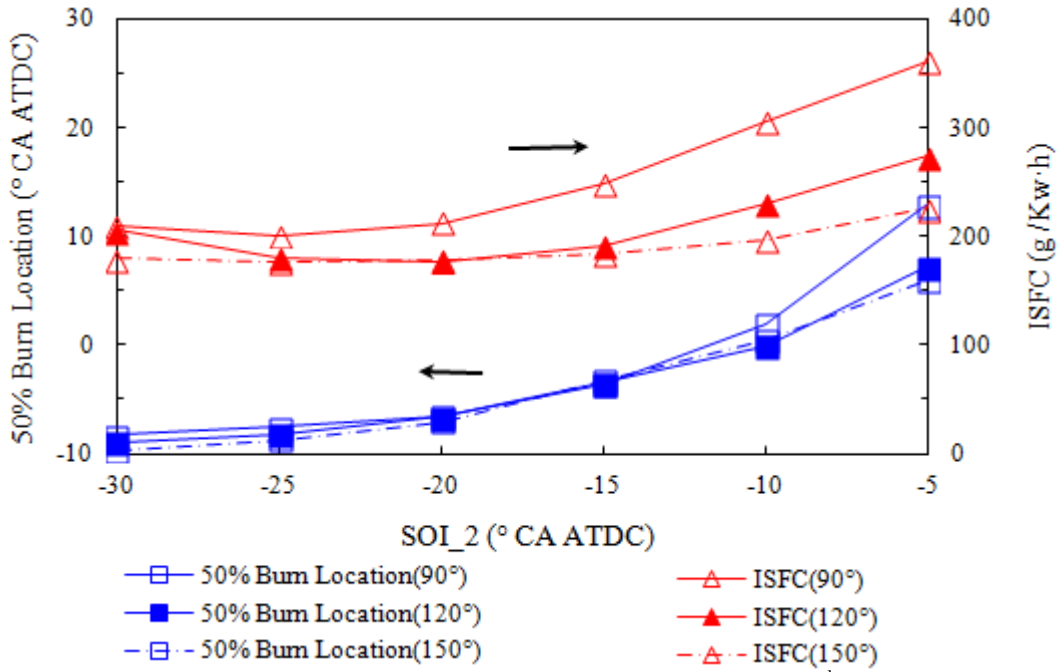

Figure 4.12 The 50% burn location and ISFC for the cases of different 2nd injection timings with different spray angle

As shown in Figure 4.13, no significant change of NO_x can be seen for most cases with different 2nd injection timing until the spray angle is reduced to 90 °. The reduction of NO_x for the cases with spray angle of 90 ° is considered as the result of the reduction of area with relatively high

O_2 concentration and the decrease of oxidation temperature owing to the incomplete combustion. According to the data shown in Figure 4.13, almost zero or very low soot emission can be achieved using the spray angle of 150° and 120°, respectively. Because of the seriously insufficient mixing, the soot emission raises dramatically when the spray angle is reduced to 90°. Figure 4.14 gives the soot mass distributions at 120° ATDC for the cases with SOI_2= -15° CA ATDC and-5° CA ATDC. When using spray angle of 90°, soot mainly appears in the center of cylinder and piston bowl area owing to the poor mixing. With SOI_2= -15° CA ATDC, the area near injector is the place where the soot concentrates when spray angle is 150°, while as the start of 2nd injection is retarded to -5° CA ATDC, soot mainly appears in the squish region.

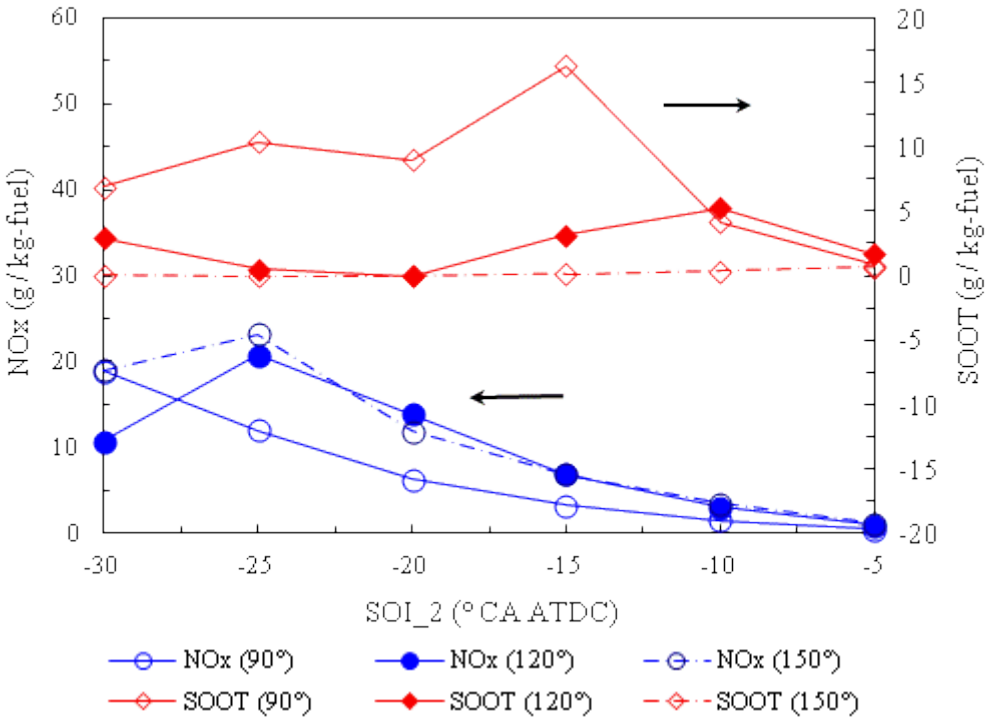

Figure 4.13 The NO_x and soot emission for the cases of different 2nd injection timings with different spray angle

With wider spray angle (150° and 120°), both CO and UHC can be suppressed under an acceptable level. Once the spray angle is reduced to 90°, CO and UHC output increase dramatically. This implies the combustion efficiency is deteriorated when the spray angle is narrow. Moreover, the effect of the 2nd injection timing on UHC is enhanced when the spray angle is reduced to 90°. Therefore, the spray targeting, which is the result of the codetermination of spray angle and injection timing, affects the combustion and emission of diesel engine significantly.

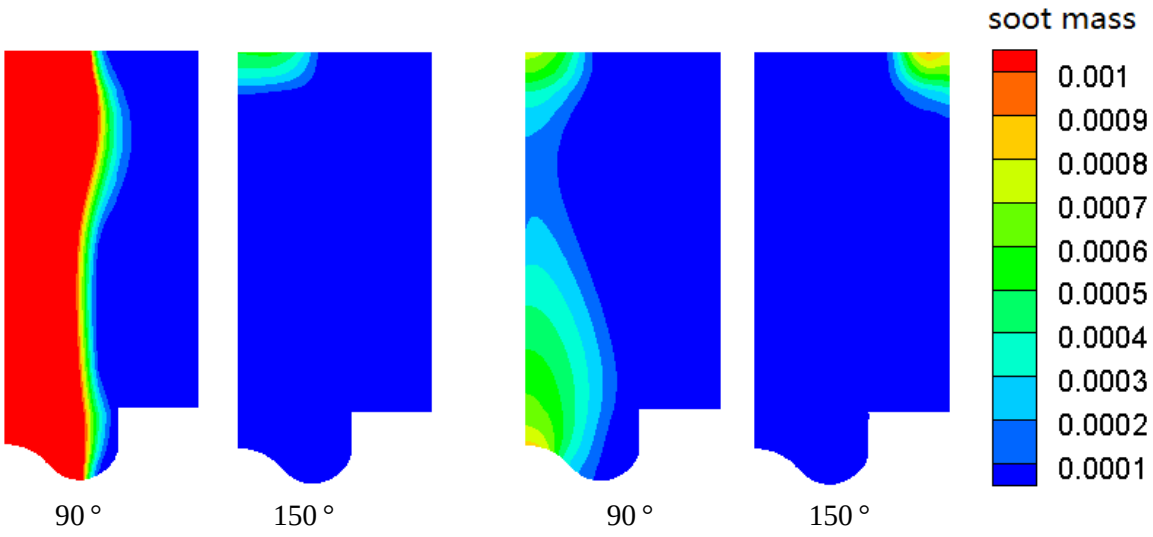

(a) SOI_2= -15 °CA CA ATDC (b) SOI_2= -5 °CA CA ATDC

Figure 4.14 Soot mass distribution at 120 °CA ATDC for the cases with different spray angle, when SOI_2= -15 °CA ATDC and -5 °CA ATDC

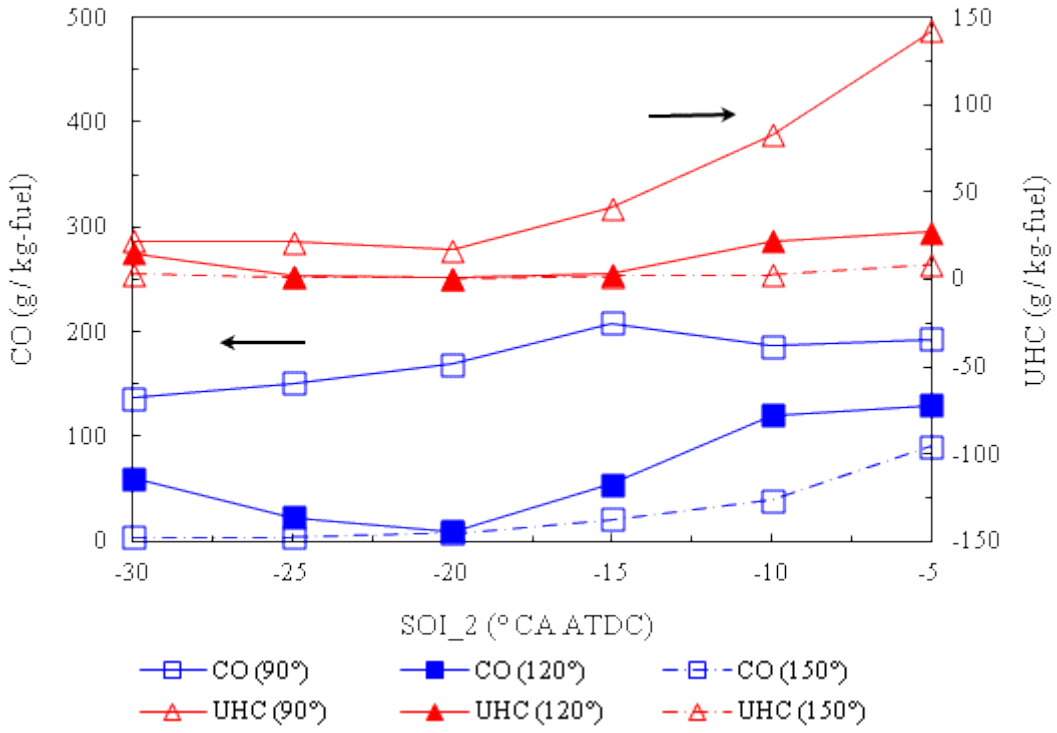

Figure 4.15 The CO and UHC emission for the cases of different 2nd injection timings with different spray angle

4.1.6 The Effects of Injection Pressure

The injection pressure is considered significantly impact the fuel distribution in PPCI / standard diesel engine [Koci et al., 2009; Kong et al., 2005]. According to the study of Xu and Hiroyasu [1992], the spray penetrates faster and further in the combustion chamber when the injection

pressure is increased. With the increased injection velocity and shorter injection duration, the injected fuel intents to target more in the squish region for same injection timing [Siewert, 2007]. Moreover, the increased spray penetration leads to an enhancing of cylinder wall impingement. In order to make further understanding about the effects of injection pressure on the mixing and combustion processes, three different injection pressures (70 MPa, 110 MPa and 150 MPa) are simulated in this study.

The trend of the timing of combustion start is similar for different injection pressure. As given in Figure 16, the obvious difference of 10% burn location can be seen when the 2nd injection timing is very early because the relatively large volume of cylinder is favourable for the diversity of equivalence ratio distribution when the injection pressure is different. Minimal differences in the trend of combustion duration are seen at the highest injection pressure as the 2nd injection timing is varied. When the injection pressure is decreased, the combustion duration is prolonged and the increase getting significant as the 2nd injection timing is retarded. Therefore, when the combustion is majorly controlled by mixing, the effects of injection pressure on combustion seem more significant.

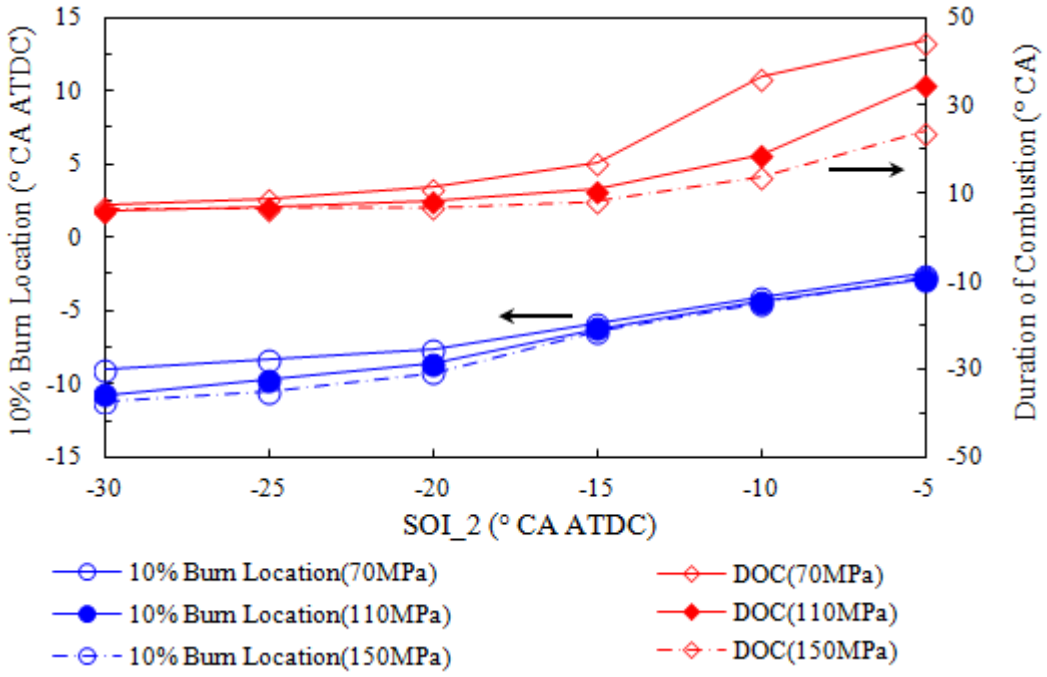

Figure 4.16 The 10% burn location and combustion duration for the cases of different 2nd injection timings with different injection pressures

As shown in Figure 4.17, the trends of 50% burn location are almost parallel for three different injection pressures. Referring to the combustion duration in Figure 4.13, it is found that the effect of injection pressure on combustion speed is more significant in the latter half stage of combustion rather than in the former half, especially when the combustion is majorly controlled by mixing. With early 2nd injection timing, the fuel consumption is lower when using low

injection pressure because the wall impingement is mitigated. While as the 2nd injection timing is retarded to near TDC, the fuel consumption decreases when the injection pressure increases due to the enhanced the fuel evaporation and mixing. When the injection pressure is increased, the spray penetrates faster and further into the combustion chamber and the spray targeting moves up, as shown in Figure 4.18. Moreover, larger area is covered by richer mixture in the case using higher injection pressure. These could be considered beneficial for efficient evaporation due to the faster injection, which leads to faster and more completed combustion.

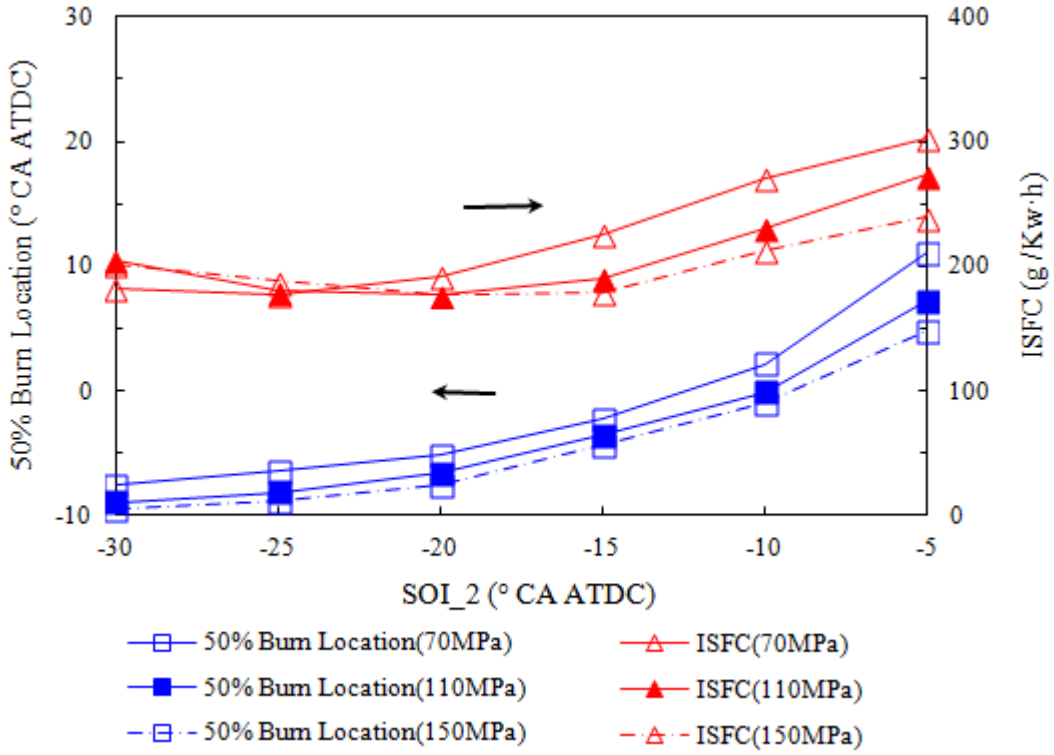

Figure 4.17 The 50% burn location and ISFC for the cases of different 2nd injection timings with different injection pressures

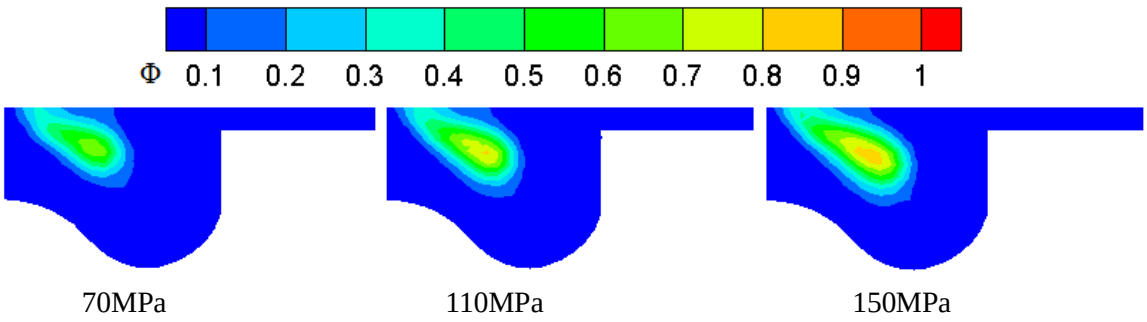

Figure 4.18 Equivalence ratio distribution at 5 ° CA after the 2nd injection for the cases with different injection pressures, when SOI_2= -15 °CA ATDC.

NO_x is generally increased as the injection pressure is raised, as shown in Figure 4.19. According to the simulation results, the relations between the soot emission and injection

pressure are not clear. Nevertheless, in general, the cases using moderate injection pressure have the relatively low soot emission. Though, the increased injection pressure can make the spray penetration and air entrainment greater, and possibly reduce the local equivalence ratio, the high level of soot is observed when the 2nd injection timing is retarded after –10 °CA ATDC when the injection pressure is 150 MPa. Serious impingement on piston and the relatively high in-cylinder pressure are considered as the reasons of this high soot emission.

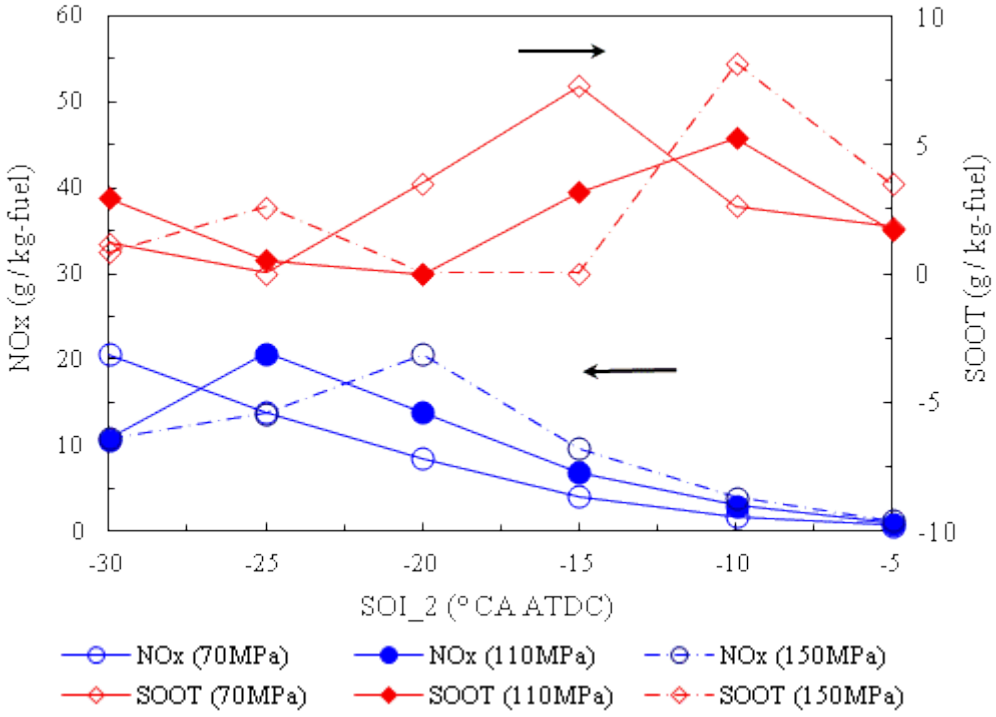

Figure 4.19 The NO_x and soot emission for the cases of different 2nd injection timings with different injection pressures

Raising injection pressure is expected to reducing CO and UHC emission through promoting fuel / air mixing [Opat et al., 2007; Koci et al., 2009]. As shown in Figure 4.20, when the 2nd injection timing is retarded later than -20 °CA ATDC, both the CO and UHC emission decrease as the injection pressure increases. For the cases with relatively early 2nd injection timing, serious wall impingement would be source of CO and UHC emission when using high injection pressure. Moreover, the location of the lowest CO is retarded as the injection pressure increases. And minimal differences in the trend of UHC are seen at the highest injection pressure.

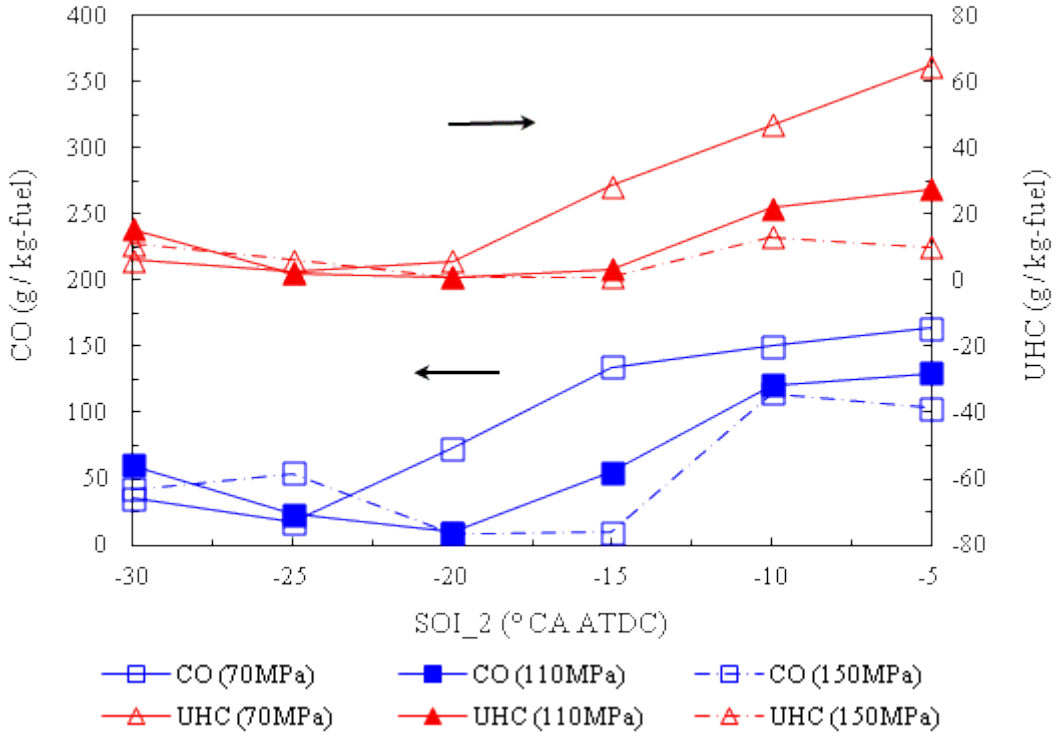

Figure 4.20 The CO and UHC emission for the cases of different 2nd injection timings with different injection pressures

4.1.7 The Effects of Swirl Ratio

Higher swirl ratio is usually expected to intensify the turbulence production and mixing processes, and further leading to more rapid and complete combustion [Kook et al., 2006]. However, some studies show that excessive swirl is possible to impede mixing [Opat et al., 2007]. Meantime, the impeding of excessive swirl ratio on mixing by limiting jet penetration is shown not significant for the typical HSDI diesel engine which is usually with small bore diameter and high injection pressure [Opat et al., 2007]. For the further understanding about the effects of swirl ratio, three different swirl ratios (1.4, 1.8, and 2.2) are simulated in this study.

As shown in Figure 4.21, there are almost no effects of swirl ratio on the start of combustion. The effects of swirl ratio on combustion duration are not obvious until the 2nd injection timing is retarded later than - 15 °CA ATDC. With the relatively late 2nd injection timing, the combustion duration is prolonged as the swirl motion is stronger. Therefore, the increased swirl ratio doesn't accelerate the combustion rate according to the data of this study.

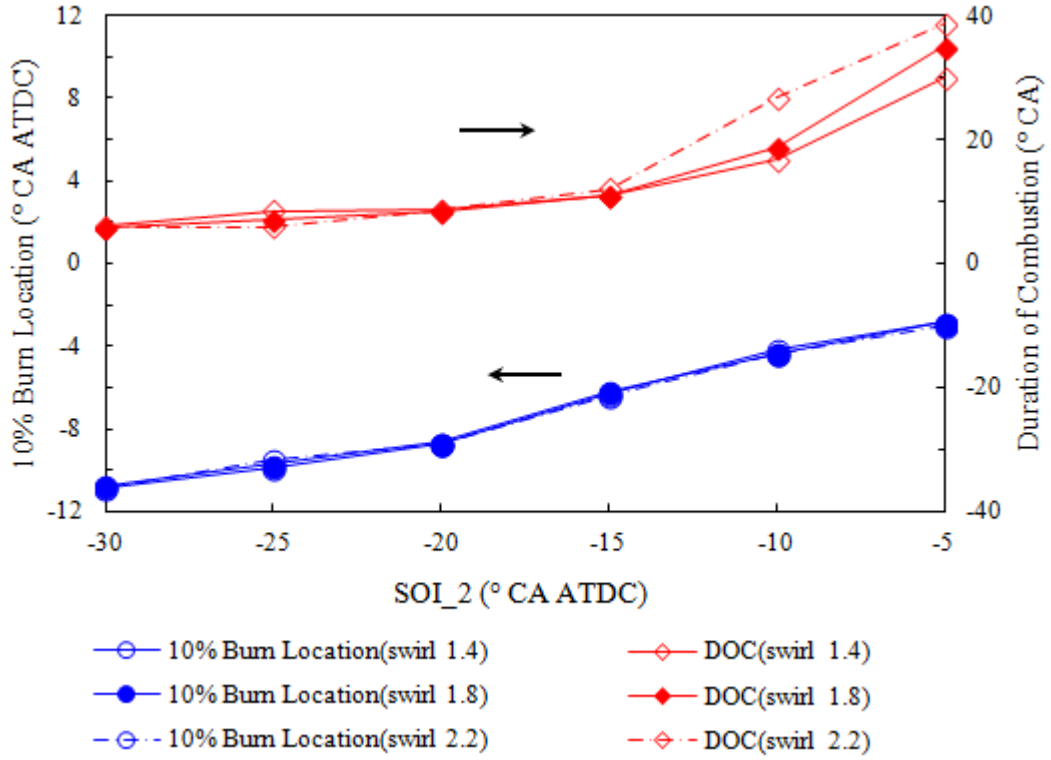

Figure 4.21 The 10% burn location and combustion duration for the cases of different 2nd injection timings with different swirl ratios

Little difference can be seen for the 50% burn location when the swirl ratio is varied, as shown in Figure 4.22. Then, for the cases with relatively late 2nd injection timing, the effect of swirl ratio on combustion speed majorly exists in the latter half stage of combustion rather than in the former half. With early 2nd injection timing, where the fuel is largely premixed, small discrepancies in the ISFC trends can be seen for different swirl ratios, and the fuel consumption decreases when the swirl ratio increases. When the 2nd injection timing is retarded to later than -20 ° CA ATDC, the ISFC increases with the swirl ratio rising. Meanwhile, the influence of the swirl ratio becomes more significant. Therefore, for different combustion mode, the effects of swirl ratio are not coherent.

As shown in Figure 4.23, NO_x emission increases as the swirl ratio is raised when the 2nd injection timing is earlier than -20 ° CA ATDC. When the 2nd injection timing is retarded further, the trends of NO_x emission for different swirl ratio get similar. The effects of swirl ratio on soot emission are more significant, especially when the 2nd injection timing is retarded over -20 °CA ATDC. Soot emission increase as the swirl ratio gets higher with early injection timing, while this trend is reversed when the 2nd injection timing is later than -20 ° CA ATDC. The highest soot emission appears when using the highest swirl ratio and the 2nd injection timing at -15 °CA ATDC. In Figure 4.24, the equivalence ratio distribution at 5 °CA after the 2nd injection gets more concentrate as the swirl ratio increases, when SOI_2= -15 ° CA ATDC. Therefore,

instead of enhancing the mixing, the increased swirl ratio traps the fuel from the air. As a result of the trapping, increased fuel consumption and high soot emission are detected.

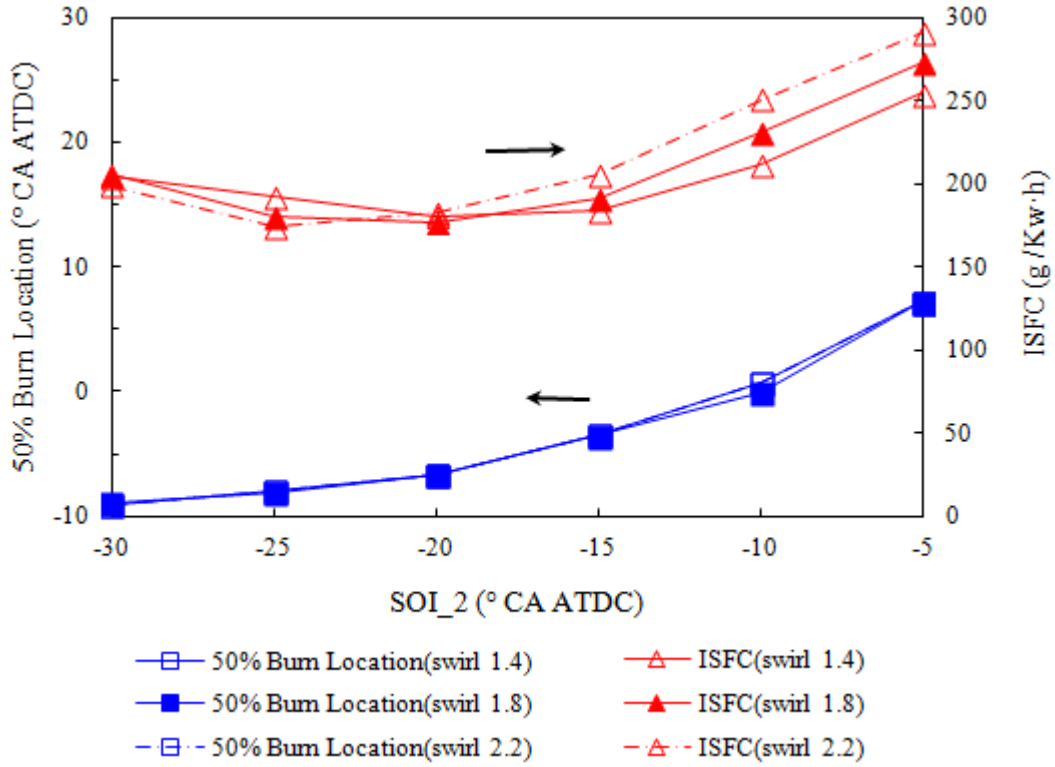

Figure 4.22 The 50% burn location and ISFC for the cases of different 2nd injection timings with different swirl ratios

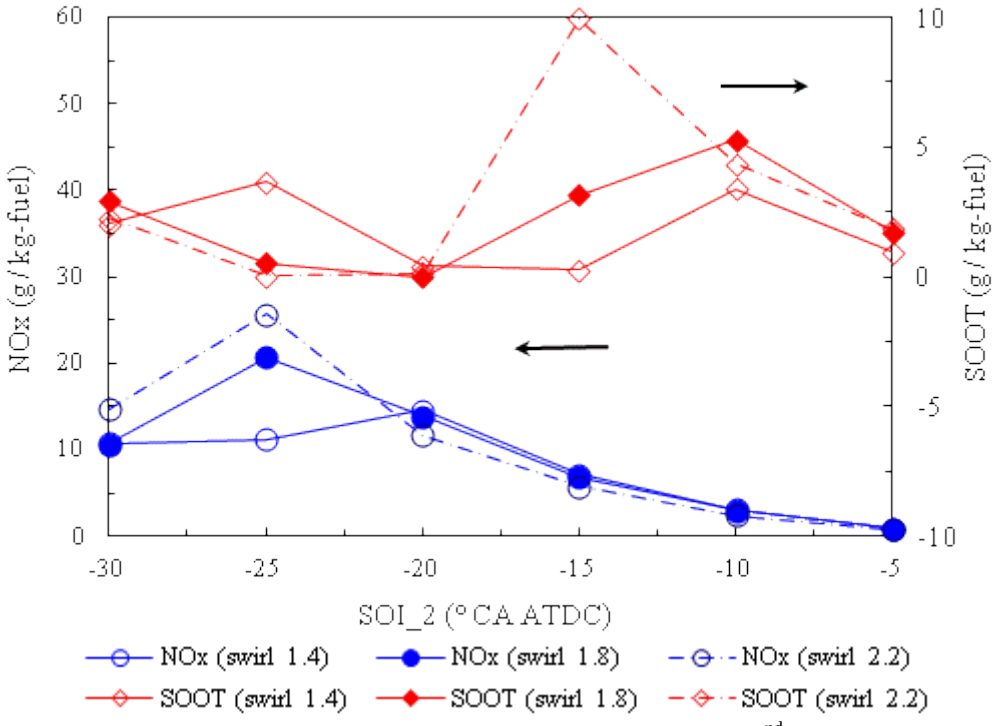

Figure 4.23 The NO_x and soot emission for the cases of different 2nd injection timings with different swirl ratios

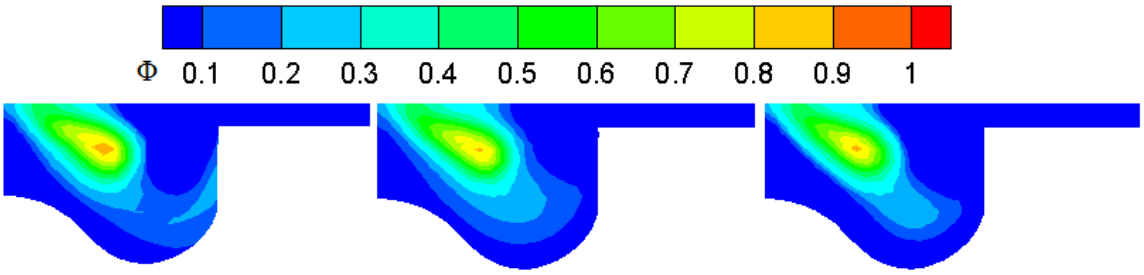

swirl 1.4 swirl 1.8 swirl 2.2

Figure 4.24 Equivalence ratio distribution at 5 °CA after the 2nd injection for the cases with different swirl ratios, when SOI_2= -15 °CA ATDC.

The effects of swirl ratio on CO and UHC show the similar trends, as given in Figure 4.25. With the relatively early 2nd injection timing, both CO and UHC emission decrease when the swirl ratio is elevated. It seems that intense swirl motion is beneficial for combustion efficiency when the fuel is largely premixed during the combustion, referring to Figure 4.22 and Figure 4.25. Nevertheless, with further retarded 2nd injection timing, elevated swirl ratio results in more serious CO and UHC emission. Therefore, the increased swirl ratio is not favourable for the mixing during the mix-controlled combustion stage, where the CO emission is considered to stem predominantly from the under-mixed fuel [Kook et al., 2006].

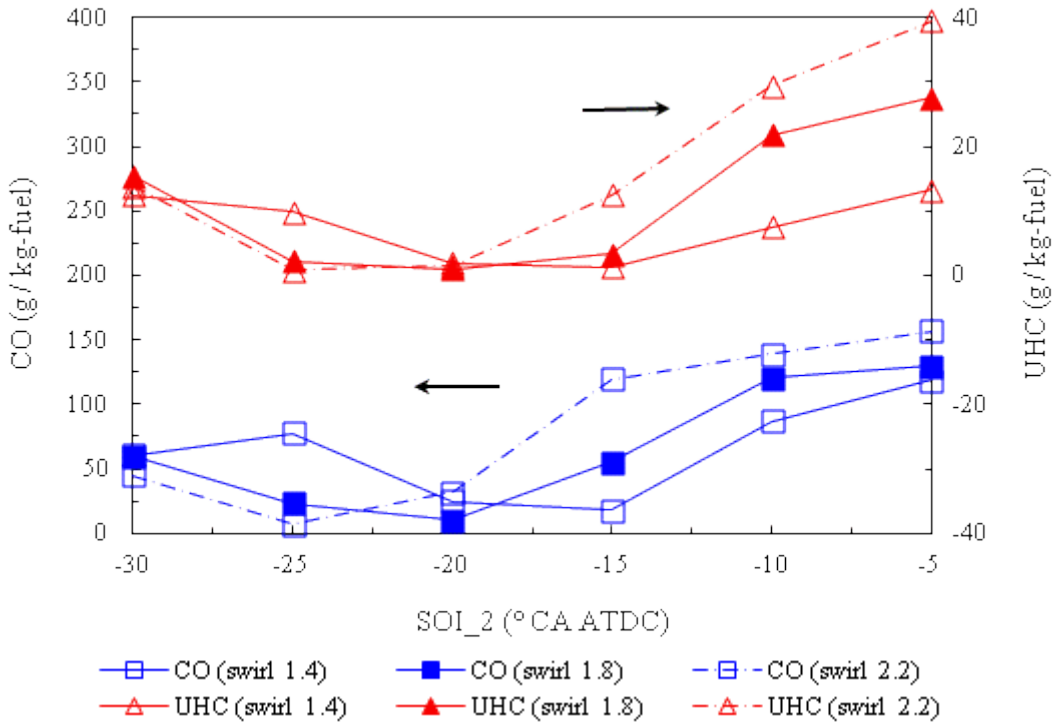

Figure 4.25 The CO and UHC emission for the cases of different 2nd injection timings with different swirl ratios

4.1.8 The Effects of EGR Rate and Boost Pressure

EGR and turbo-charging intake system are the most effective and widely applied ways to implement the performance control and emission optimization in diesel engine. EGR has been found an effective manner to reduce NO_x emission since its dilution effect which providing lower oxygen availability. Meantime, the use of EGR will impact the soot emission and fuel economy. The boost pressure is considered significantly influence the fuel consumption as its effects on ignition timing and equivalence ratio. To discuss the characteristics of the diesel engine with split-injection, three EGR rates (20%, 35%, and 50%) and three intake pressures (1.6 bar, 2.0 bar, and 2.4 bar) are investigated here.

As shown in Figure 4.26, it can be seen that the addition of EGR results in delayed start of combustion. When the EGR rate is increased to 20% from 35%, the delay of the combustion start is not large, and the trends of combustion start for these two levels of EGR rate are nearly parallel. Once the EGR rate is increased further to 50%, the delay of combustion start is prolonged, and the prolonging increases as the 2nd injection timing is retarded. Therefore, with the EGR rate of 50%, the increase in the time for mixing is much more significant for the case whose 2nd injection timing is relatively late. When the 2nd injection timing is before -15 °CA ATDC, the effect of EGR rate on combustion duration is not significant. With the further retarded 2nd injection, the combustion duration decreases as the level of EGR rate is elevated. In the case with the high EGR rate (50%), the variation of combustion duration is small with different 2nd injection timing. It means, if using high EGR rate, even with late injection timing short combustion duration can still be achieved owing to the significantly increased ignition delay.

Before the 2nd injection timing is retarded to -5 °CA ATDC, the trends of 50% burn location are nearly parallel for different EGR rate, though the 50% burn location is retarded as a result of the addition of EGR, as given in Figure 4.27. With the 2nd injection timing at -5 °CA ATDC, increasing the EGR rate leading to relatively advanced 50% burn location. The effect on fuel consumption is not significant until the EGR rate is increased to 50%. When the 2nd injection timing is earlier than -10 °CA ATDC, ISFC is much higher if using 50% EGR rate because the in-cylinder oxygen availability is significantly reduced. Nevertheless, using 50% EGR rate, lower fuel consumption is observed in the cases with the relatively late 2nd injection. Referring to Figure 4.26, it seems that using high level of EGR rate can improving the mixing in the cases whose 2nd injection timing are close to TDC by prolonging the ignition delay. Therefore, shorter combustion duration and lower fuel consumption is possibly achieved in these cases. This phenomenon is similar to the feature of MK diesel combustion unless the injection timings in these cases are not retarded after TDC.

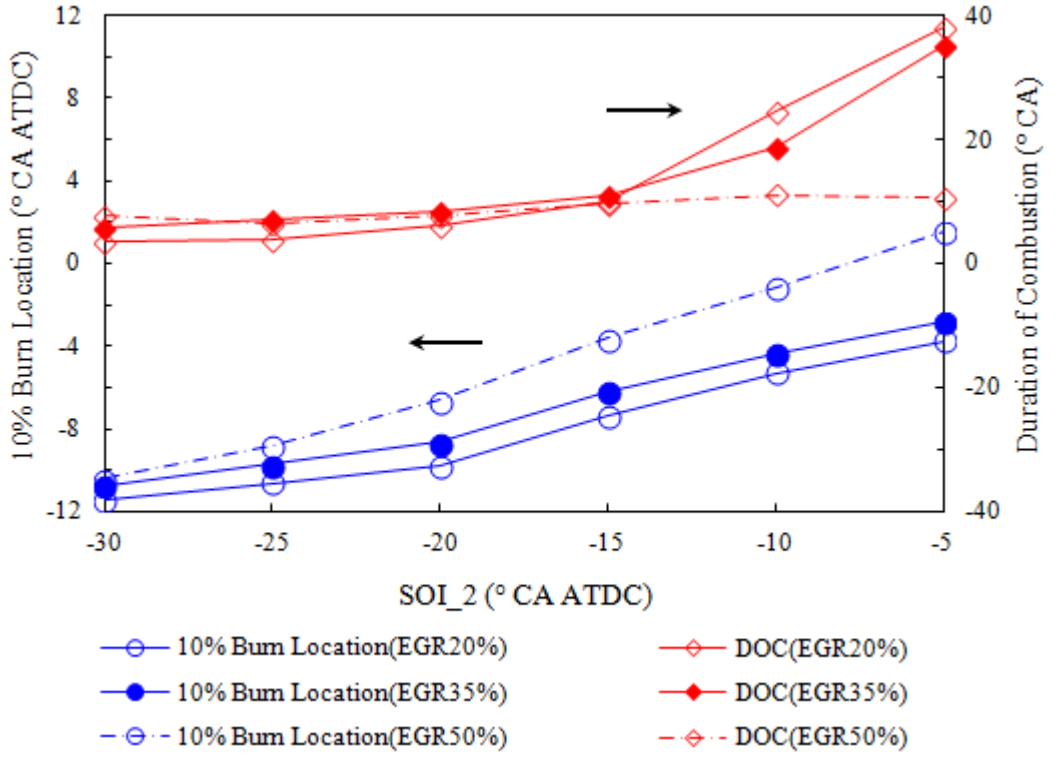

Figure 4.26 The 10% burn location and combustion duration for the cases of different 2nd injection timings with different EGR rates

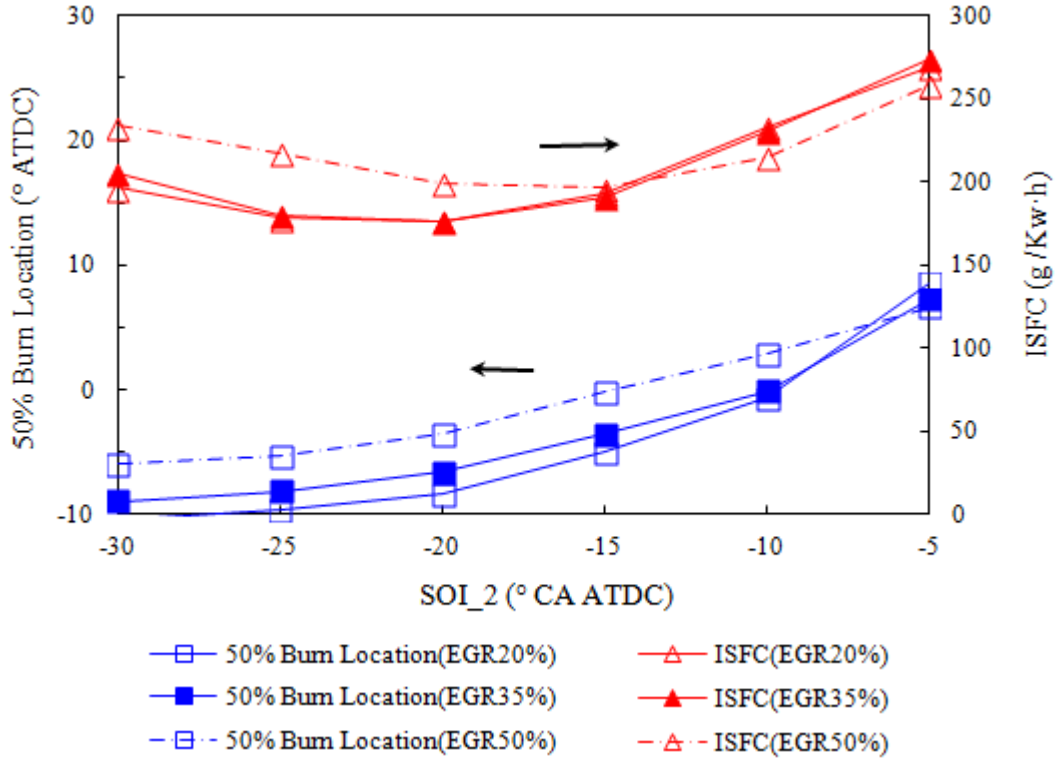

Figure 4.27 The 50% burn location and ISFC for the cases of different 2nd injection timings with different EGR rates

From Figure 4.28, it can be seen that increasing EGR rate can efficiently suppress NO_x emission.

The NO_x emission is almost reduced to zero when utilizing 50% EGR. By raising the EGR rate from 20% to 35%, a massive reduction in NO_x emission is observed, while the soot emission increase slightly. And massive growth of soot can be seen when using 50% EGR. Meanwhile, as shown in Figure 4.29, both CO and UHC increase significantly once the EGR rate is beyond 50%. Therefore, the incomplete combustion and soot formation due to the low oxygen availability is the major problem to be solved if utilizing high EGR to control NO_x. Nevertheless, moderate level of EGR rate (35%) can efficiently reduce NO_x emission and affect the soot, CO and UHC emissions little in the meantime.

Because the ignition timing is determined by the pressure and the temperature in combustion chamber, the start of combustion is advanced as the boost pressure is elevated, as shown in Figure 4.30. Therefore, the increased boost results in reduced time for pre-ignition mixing. For the cases with early 2nd injection timing (before -15 ° CA ATDC), slightly reduction in combustion duration can be seen when increasing the boost pressure. When the 2nd injection timing is retarded further, where the mixing majorly controls the combustion rate, elevating boost pressure leads to prolonged combustion duration. Therefore, high boost pressure is not beneficial for mixing when using relatively late 2nd injection.

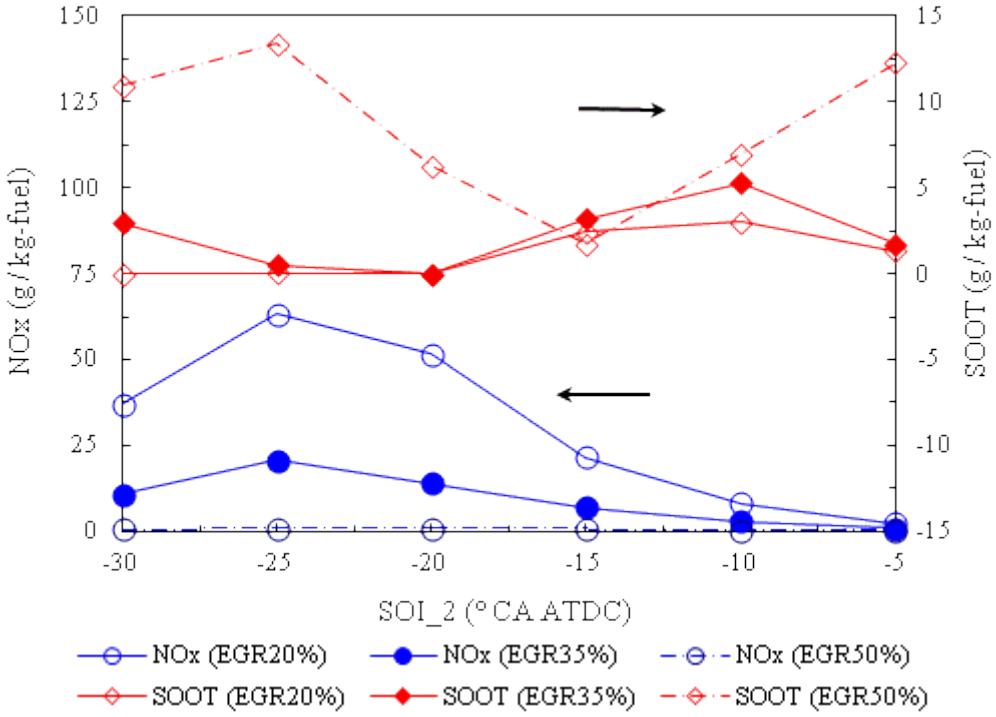

Figure 4.28 The NO_x and soot emission for the cases of different 2nd injection timings with different EGR rates

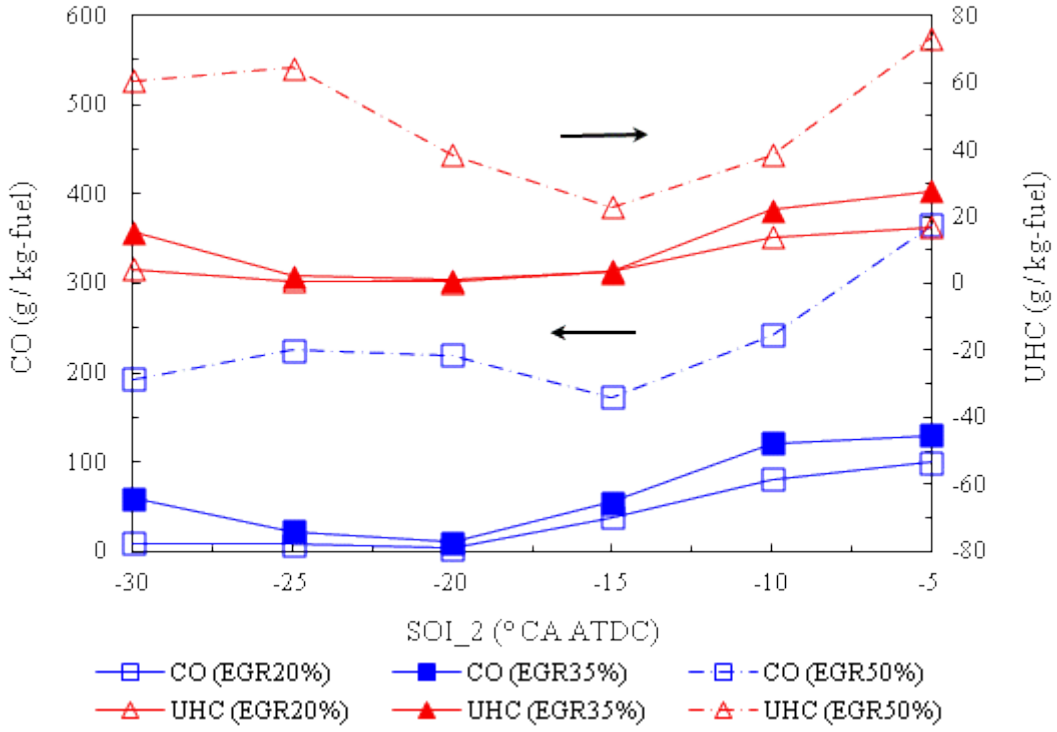

Figure 4.29 The CO and UHC emission for the cases of different 2nd injection timings with different EGR rates

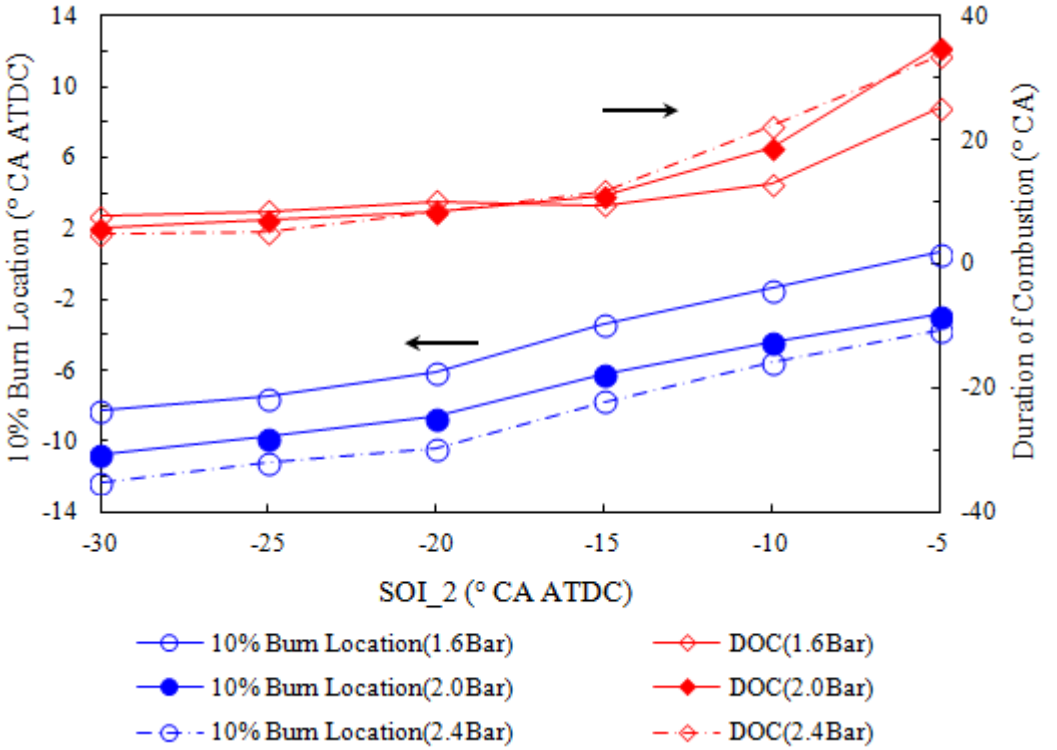

Figure 4.30 The 10% burn location and combustion duration for the cases of different 2nd injection timings with different intake pressures

As given in Figure 4.31, the 50% burn location is moved forward as the boost pressure is elevated before the 2nd injection timing is retarded to -5 ° CA ATDC. When the 2nd injection

timing is at -5 °CA ATDC, though the combustion starts earlier in the case with boost pressure of 2.0 bar, its 50% burn location is later than the case with boost pressure of 1.6 bar because its relatively slower combustion rate. The superior in fuel economy for the cases with higher boost pressure is deteriorated when the 2nd injection timing is retarded after -15 °CA ATDC. The lack of sufficient mixing is considered as the reason of relatively high ISFC in the cases with the boost pressure of 2.0 bar and 2.4 bar, when the 2nd injection timing is later than - 15 °CA ATDC.

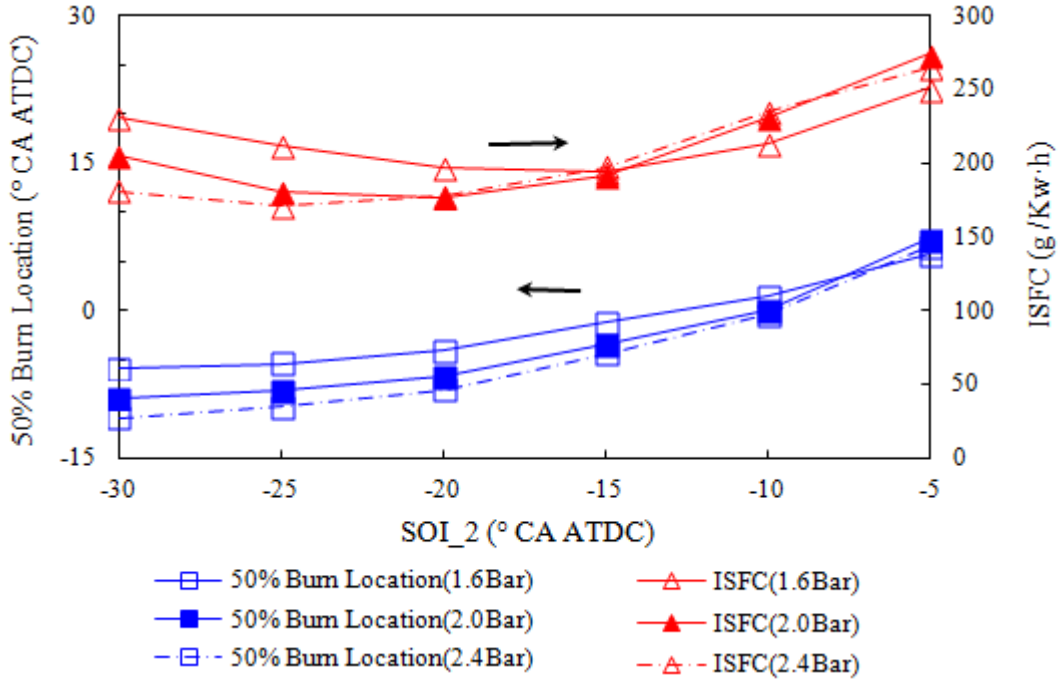

Figure 4.31 The 50% burn location and ISFC for the cases of different 2nd injection timings with different intake pressures

The smallest variation in the trends of NO_x is found in the cases utilizing the lowest boost pressure, as shown in Figure 4.32. As the boost pressure is elevated, the variation in the trends of NO_x over the 2nd injection timing is enlarged, and the level of NO_x gets higher. Small increase in the effective inlet oxygen mass flow occurs when the boost pressure is increased, because the oxygen concentration is nearly constant in the inlet air. Therefore, the global equivalence ratio is reduced when using higher boost pressure, and the increased inlet oxygen mass is favorable for the formation of NO_x. For most cases, higher level of soot emission is observed at lower boost pressure unless for the cases whose 2nd injection timing is at -15 °CA ATDC. In the conventional diesel combustion, the reduction of soot is expected because of the slightly decreased global equivalence ratio when the boost pressure is elevated. For the low temperature combustion, where large amount of EGR is utilized, there is study showing that increasing the boost pressure may result in locally richer regions which is favorable for soot formation [Koci et al., 2009].

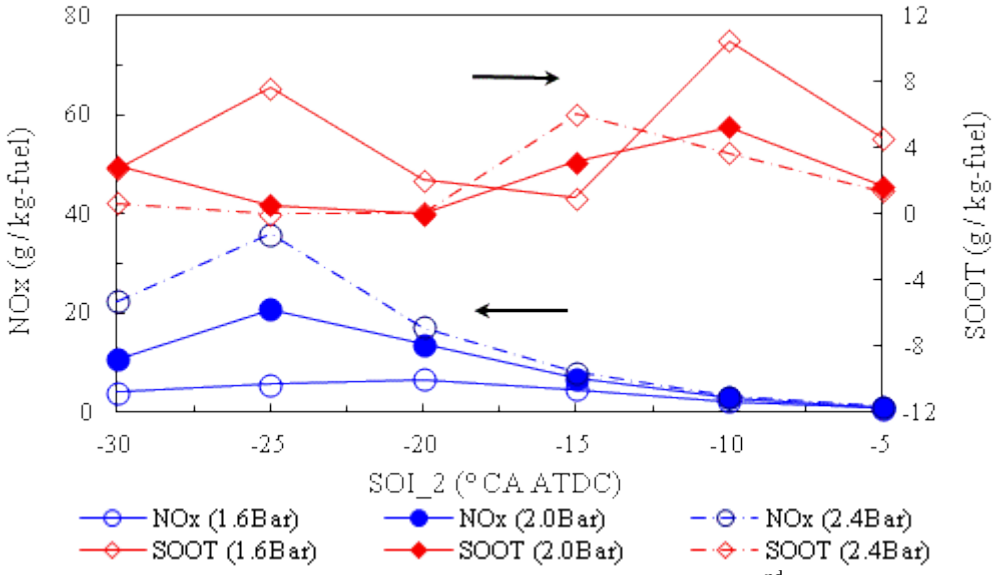

Figure 4.32 The NO_x and soot emission for the cases of different 2nd injection timings with different intake pressures

In general, increasing boost pressure is beneficial for suppressing CO and UHC emissions due to the reduction of equivalence ratio [Martin et al., 2008]. According to Figure 4.33, with earlier 2nd injection timing (before -15 ° CA ATDC), CO and UHC emissions decrease as the boost pressure is elevated. When the 2nd injection timing is retarded further, higher CO and UHC emissions are observed in the cases with boost pressure of 2.0 MPa. As motioned previously, the start of combustion moves forward and the ignition delay reduces as the boost pressure is increased. Therefore, with boost pressure of 2.0 MPa, higher CO and UHC emissions is considered resulting from the significantly insufficient mixing when using relatively late 2nd injection timing.

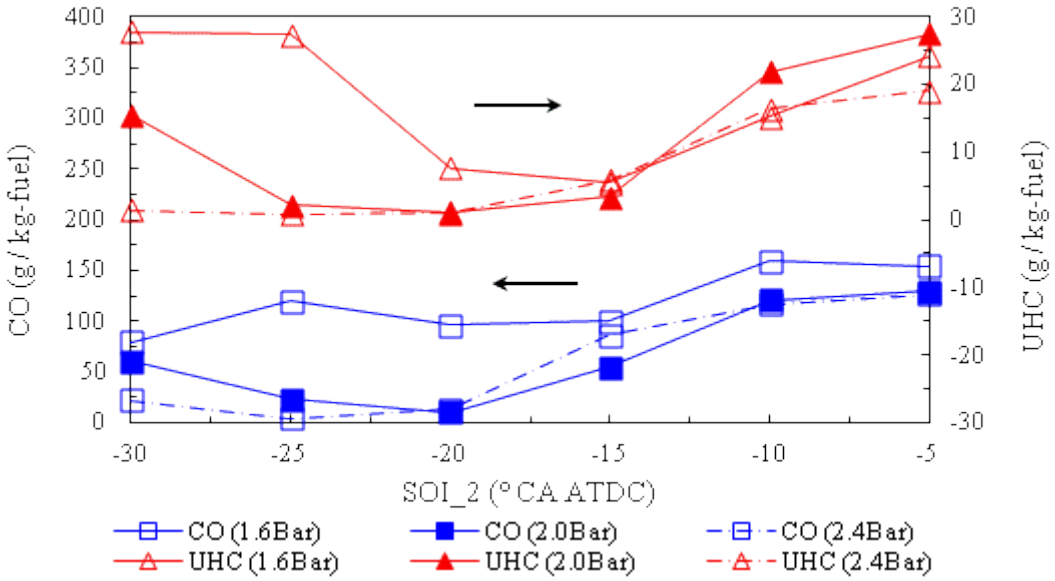

Figure 4.33 The CO and UHC emission for the cases of different 2nd injection timings with different intake pressures

4.2 Homogeneity Factor Study

The previously studies show that the mixture formation and its distribution influence the phase of combustion and its control [Nakagome et al., 1997; Harada et al., 1998; Akagawa et al., 1999]. Meanwhile, the mixture formation is considered to be affected by the strategy of injection and in-cylinder air motion [Kook et al., 2006]. In this study, early 1st injection timing and a broad range of 2nd injection timing are utilized. For most cases, because of the lack of time, partially mixed and stratified fuel / air mixture is common. Thus, a method to evaluate the quality of mixing is required for quantitatively investigating the effects of injection parameters and in-cylinder air motion on mixture formation. Moreover, the relations between the quality of mixing and characteristics of combustion and emissions can be described quantitatively if the method for evaluating the quality of mixing is established.

4.2.1 Definition and Formulas

Instead of the detailed structure of mixture distribution, an overall description for fuel/ air mixing characteristics named as homogeneity factor (*HF*) is proposed to characterize the process of mixture formation. The index of homogeneity is initially defined as

$$HF = 1 - HeterF \tag{4.4}$$

where *HeterF* is the degree of heterogeneity of the mixture, which is given as

$$HeterF = \frac{1}{2}\frac{\sum_{i=0}^{N_{cell}} \sqrt{\left(m_{fuel,i} - m_{fuel,0}\right)^2}}{M_{fuel}} \tag{4.5}$$

where the total fuel amount, M_{fuel} is given as

$$M_{fuel} = \frac{\Phi_0}{AFR_{st} + \Phi_0} M \tag{4.6}$$

Φ_0 is the overall equivalence ratio; AFR_{st} is the stoichiometric air/fuel ratio; M is the total amount of mixture mass.

The difference between the mass of fuel in computational cell i, $m_{fuel,i}$, and the averaged mass of fuel in this cell, $m_{fuel,0}$, can be given as

$$m_{fuel,i} - m_{fuel,0} = \frac{\Phi_i}{AFR_{st} + \Phi_i}\delta m_i - \frac{\Phi_0}{AFR_{st} + \Phi_0}\delta m_i = \frac{(\Phi_i - \Phi_0)AFR_{st}}{(AFR_{st} + \Phi_i)(AFR_{st} + \Phi_0)}\delta m_i \tag{4.7}$$

where Φ_i is the equivalence ratio and δm_i is the mixture mass in the computational cell i. Therefore, the formula (4.4) can be expressed as

$$HF = 1 - \frac{\sum_{i=0}^{N_{cells}} \frac{\sqrt{(\Phi_i - \Phi_0)^2}}{AFR_{st} - \Phi_i} AFR_{st} \delta m_i}{2 \cdot \Phi_0 M} \tag{4.8}$$

This *HF* approaches unity when the fully homogenous mixture is achieved; and it is close to zero if the logically extremely non-uniform happens. As this new definition can directly work as a method to quantitatively evaluate the quality of fuel/air mixing, it is expected to be used as a parameter for the adjustment of combustion phase. Therefore, the effects of the relevant operating parameters on *HF*, together with the relations between *HF* and the characteristics of combustion and emissions are discussed in this study. The *HF* at 5 ° CA ATDC is normally chosen here for evaluation because every case has finished its injection before 5 ° CA ATDC, even for the cases with the latest injection timing. However, in this study the start of combustion intends to happen before 5 ° CA ATDC because of the general use of early injection. Therefore, the mixture quality at 5 ° CA ATDC may be considered not representative of the mixture quality prior to ignition. On the other side, the ignition timings are of complicated variation for different operating conditions, and the average equivalence ratio at ignition timing is usually not same between cases. For simplicity reasons and requirement for comparability, 5 ° CA ATDC is chosen as the timing for the observing the mixing distribution.

4.2.2 The Characterization of Mixing in PPCI Engine

The trends of *HF* under baseline operating condition for various timings of the 2nd injection are given in Figure 4.34. After the 1st injection is finished, the *HF* keeps increasing until the 2nd injection is delivered. Though the decrease of the *HF* during the 2nd injection becomes larger as the 2nd injection is retarded, the *HF* gets substantial increase again after the 2nd injection ends. The *HF* grows faster as the 2nd injection is retarded when its timing is not later than -15 ° CA ATDC, imply that the mixing process is enhanced during the compression [Nandha and Abraham, 2002]. At 5 ° CA ATDC, higher *HF* is observed as the 2nd injection timing is advanced, and the highest value of *HF* is about 0.65. Although the starts of the combustion are varied between cases, it is can be prospected that the combustion processes in the mixture of higher homogeneity when the 2nd injection is advanced.

To explore the effects of injection parameters and in-cylinder air motion on mixing process, the *HF* at 5 ° CA ATDC is selected as the measure to inspect the mixing quality. The trends of *HF* are given in Figure 4.35 when different fraction of fuel is in the 1st injection. As shown in this figure, the *HF* is generally increased when larger fraction of fuel is injected during the 1st injection since there is more time for the mixing of the major part of fuel. When 80% of fuel is injected in the 1st injection which starts at - 30 ° CA ATDC, the *HF* decreases a little because of the critical wall impingement and deteriorated evaporation due to the low in-cylinder temperature. The variation of *HF* trend gets smaller as the fraction of fuel in the 1st injection is

increased. Therefore, the adjustment of *HF* through variable timing of the 2nd injection is remitted when the fraction of fuel in the 1st injection is increased.

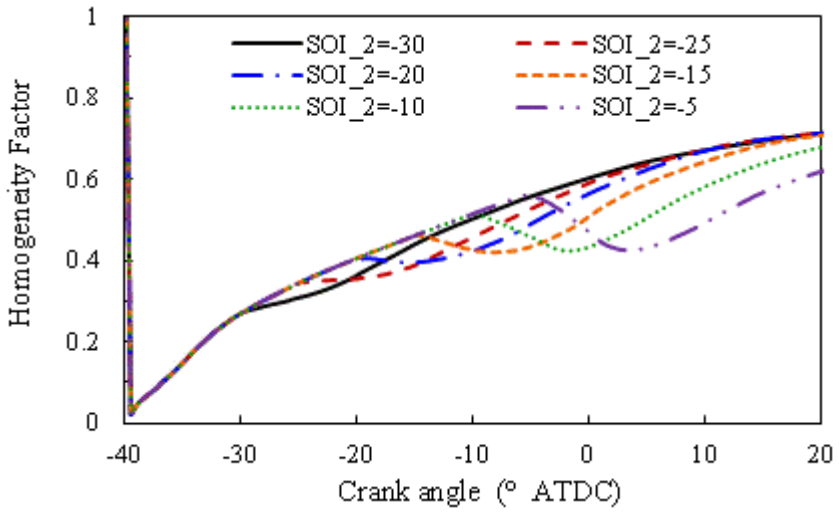

Figure 4.34 The plot of Homogeneity Factor for various timings of the 2nd injection.

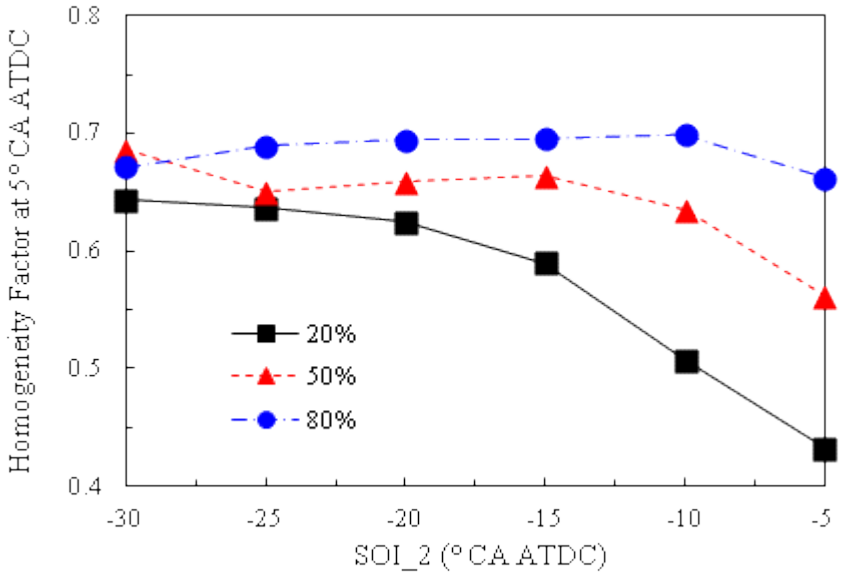

Figure 4.35 The effects of fuel fraction in the 1st injection on the *HF* for various timings of the 2nd injection.

The influences of injection pressure on the *HF* at 5 ° CA ATDC are given in the Figure 4.36. Under the current operation condition, significant improvement of mixing can be observed when the injection pressure is elevated from a low value (70 MPa) to a medium high level (110 MPa). Though increasing injection pressure can always improve mixing quality, the same amount increase of injection pressure does not contribute the same growth of the *HF* once the injection pressure is beyond 110 MPa. With high injection pressure, the wall impingement is aggravated due to the long spray penetration length. Therefore, when using high level of injection pressure (150 MPa), the raise of *HF* is limited for the cases of early timing of the 2nd

injection since the fuel is injected under relatively low air densities and low air temperature. Moreover, because of the constraint of space in the chamber in the cases with late timing of 2nd injection, the longer spray penetration is not favorable for enhancing the mixing of fuel and air.

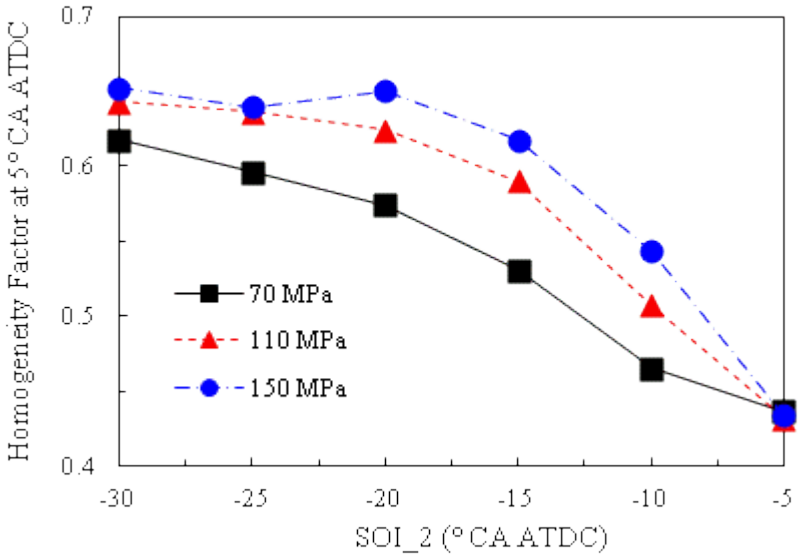

Figure 4.36 The effects of fuel injection pressure on the *HF* for various timings of the 2nd injection.

The influence of swirl ration on the *HF* is much smaller compared with those two former injection parameters, as given in Figure 4.37. A transformation of the trend for the *HF* over various 2nd injection timing is noticed when the timing of the 2nd injection is located at -15 °CA ATDC. With earlier 2nd injection timing, the *HF* is promoted by increased swirl ratio. For the cases with the 2nd injection timing later than -15 °CA ATDC, lower level of *HF* is observed with higher swirl ratio. As discussed in section 4.1.6, excessive swirl ratio will impede mixing when using relatively late 2nd injection timing.

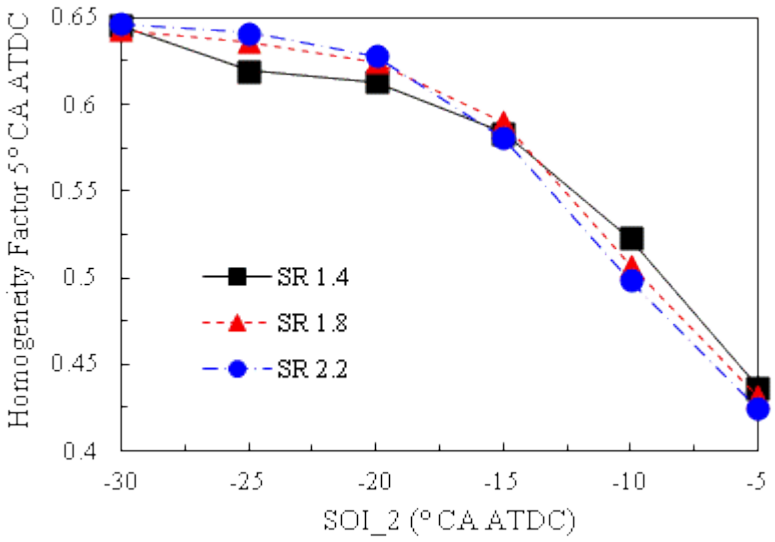

Figure 4.37 The effects of swirl ratio on the *HF* for various timings of the 2nd injection.

4.2.3 The Characterization of Combustion and Emissions in PPCI Combustion

Based on the definition of *HF* and the quantitative analysis of mixing, the relations between then characteristics of mixing and combustion or emission will be explored in this section. The start of combustion (10% burn location), the central location of combustion (50% burn location) and the fuel consumption (ISFC) is selected for monitoring the effect of *HF* on the combustion phase and efficiency. Meanwhile, the variations of NO_x, soot, CO and UHC with different *HF* are checked to explore the relation between the quality of mixing and the emissions. The expressions of these relations are studied for the possible method to realize the control of combustion and emissions in PPCI combustion engine.

The trends of the start of combustion over the *HF* under various injection conditions and intensity of in-cylinder air motion are given in Figure 4.38. In general, the 10% burn location is advanced when higher *HF* is achieved at 5 °CA ATDC. The trend line showing the correlation between 10% burn location and the *HF* is created as Y10= 420exp(-8.2*HF*)-12, as shown in Figure 4.38. Good following of this trend is observed until the *HF* reaches 0.65. The deviations appear in the cases having larger fraction of fuel (50% or 80%) injected in the 1st injection (-40 ° CA ATDC). Though, in the conventional diesel combustion, the start of combustion is significantly dependent on the mixture distribution; for the combustion processes in highly homogeneous condition, it cannot be considered majorly determined by the homogeneity of mixture. As many researches showed, in the HCCI/PPCI combustion, the start of combustion is determined by the temperature of mixture rather than the distribution of mixture or the timing of injection [Zhao, 2007; Agrell et al., 2003].

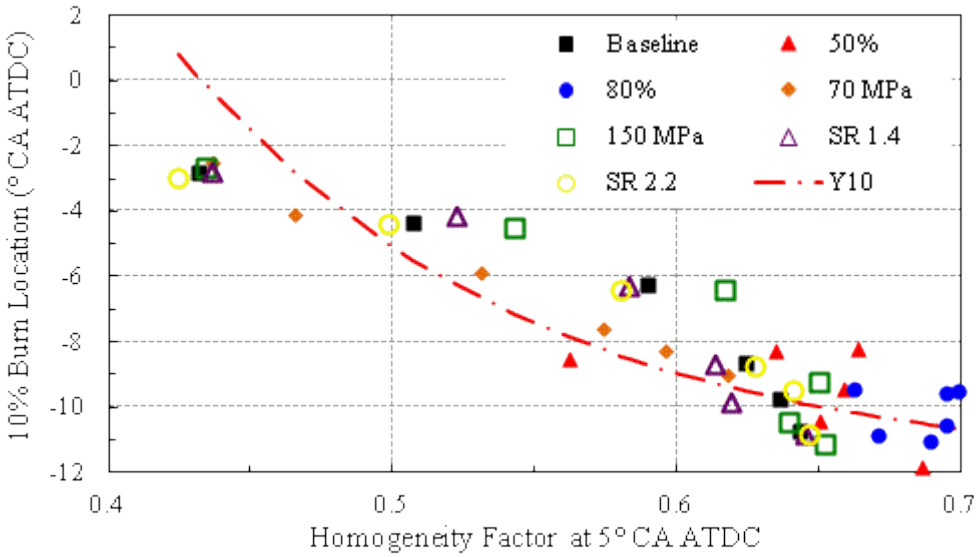

Figure 4.38 The effect of the *HF* on the 10% burn location under various operating conditions.

In this part, the 50% burn location is selected for evaluating the effect of *HF* on the combustion phase location, and the results are given in Figure 4.39. Similar to the trend of 10% burn

location, the 50% burn location is generally advanced when the *HF* increases. The trend line of 50% burn location with respect to the *HF* is given as Y50=2906exp(-11.3*HF*)-10 in Figure 4.39. Better agreement can be seen for this trend when compared to the condition in Figure 4.38, though some small deviations appear at high *HF* level. Although this correlation may be different for different operating conditions and engine structures, this at least suggests that the *HF* can be considered as a good parameter for the monitor of combustion phase location. And for current analytical cases shown in Figure 4.39, the *HF* value of 0.5 is required to maintain combustion phase location near TDC.

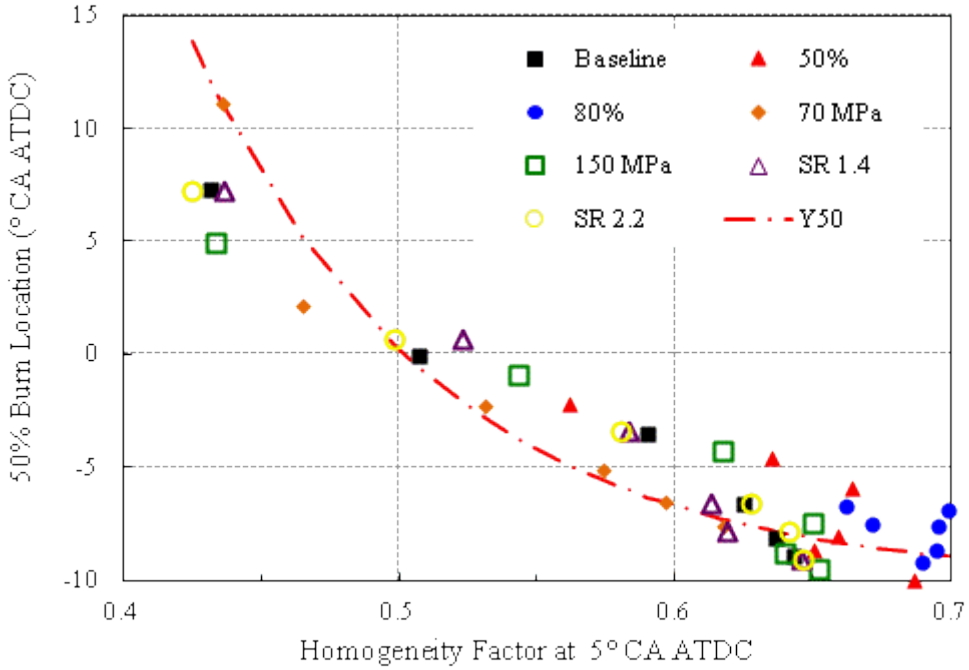

Figure 4.39 The effect of the *HF* on the 50% burn location under various operating conditions.

When *HF* can be used as an appropriate control parameter for indicating the combustion phase, its relation with the fuel consumption (ISFC) and emissions (NO_x, soot, CO and UHC) is another concern of this study. As shown in Figure 4.40, the trend of ISFC against *HF* shows that higher *HF* can result in the reduction of fuel consumption under specified injection or in-cylinder flow conditions. For varied proportion of fuel in the 1st injection, the trend line of fuel consumption moves to upper right area with the increase of fuel amount injected during the 1st injection, as given in Figure 4.40 (a). This is actually explained by the fact that the improvement of the air-fuel mixing will always be favourable for the complete combustion. Though higher *HF* is achieved as expected when the larger proportion of fuel is in the early injection, higher fuel consumption is observed due to the serious wall film, which cannot be revealed by *HF*. Moreover, with increased fuel in the 1st injection, the relatively earlier location of combustion phase (as shown in Figure 4.7 and 4.40) leads to deterioration of thermal conversion efficiency. Hence, the trend line of fuel consumption moves to upper right area when

using large part of early injection, although high *HF* is achieved. In Figure 4.40 (b), the discrepancy between the trend lines of fuel consumption under specified injection pressure is not significant, even the gap between highest and lowest injection pressure is up to 80 MPa. In Figure 4.40 (c), the swirl ratio shows some influence in the trend of fuel consumption in parallel. Therefore, it is possible to establish a generalized trend line of fuel consumption against *HF* for varied injection pressure and swirl ratio. While for the varied proportion of fuel amount in the 1st injection, the trend line of fuel consumption cannot be generalized.

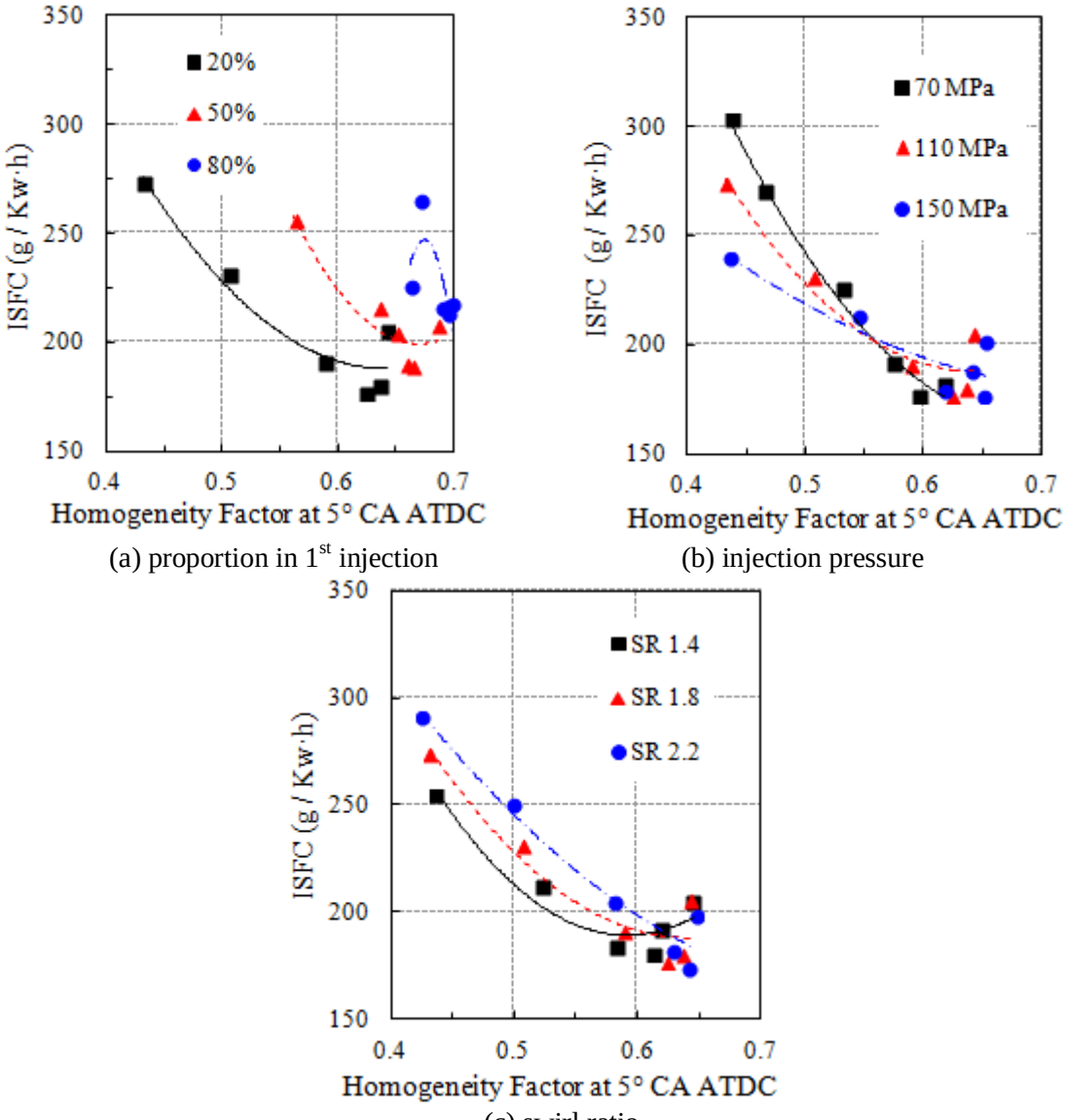

(a) proportion in 1st injection (b) injection pressure

(c) swirl ratio

Figure 4.40 The effect of the *HF* on the ISFC under various operating conditions.

In this study, higher *HF* will result in higher NO_x emission, as shown in Figure 4.41. This can be understood that higher *HF* will result in more complete combustion and higher combustion temperature, and then leads to higher NO_x emission. Though the fuel proportion in the 1st injection shows some influence on the trend line of NO_x-*HF* in parallel, the trends of all of these

data are obviously similar. For different injection pressures or swirl ratio, the discrepancies in trend are even less. Therefore, for NO_x emission, the *HF* is possible to be considered as a control parameter.

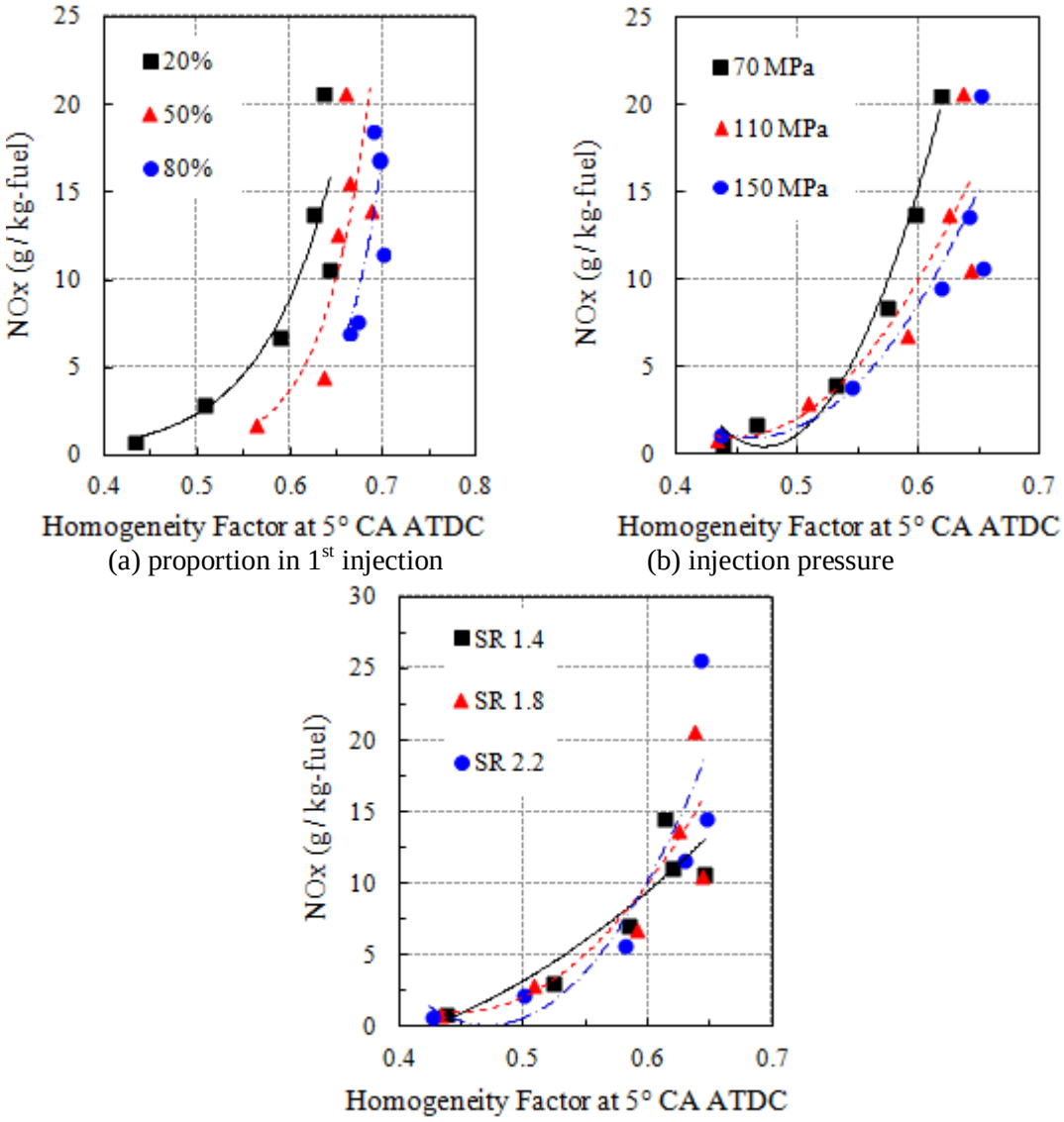

(a) proportion in 1st injection (b) injection pressure

(c) swirl ratio

Figure 4.41 The effect of the *HF* on the NO_x under various operating conditions.

The relationship between the *HF* and soot emission is complicated, as given in Figure 4.42. The peak value of soot emission appears at medium level of *HF*, while the lowest soot emission appears at the high level of *HF*. It has to be noticed that at low *HF* level, about 0.44, a relatively lower soot emission is achieved as unexpected. As state in section 4.1.2, this reduction of soot is considered as the result of low in-cylinder temperature under incomplete combustion. As the fuel amount in the 1st injection increases, the trend line of soot-*HF* shifts to the bottom-right corner, as shown in Figure 4.42(a). Though the trend lines are parallel for varied fuel proportion in the 1st injection, the discrepancies between lines are large. For varied injection pressure or

swirl ratio, the curvatures of the trend line of soot-*HF* are different. The influence of swirl ratio is more significant. Even though, the trends of all of these data are similar. A generalized trend line of soot-*HF* can be summarized with some discrepancy.

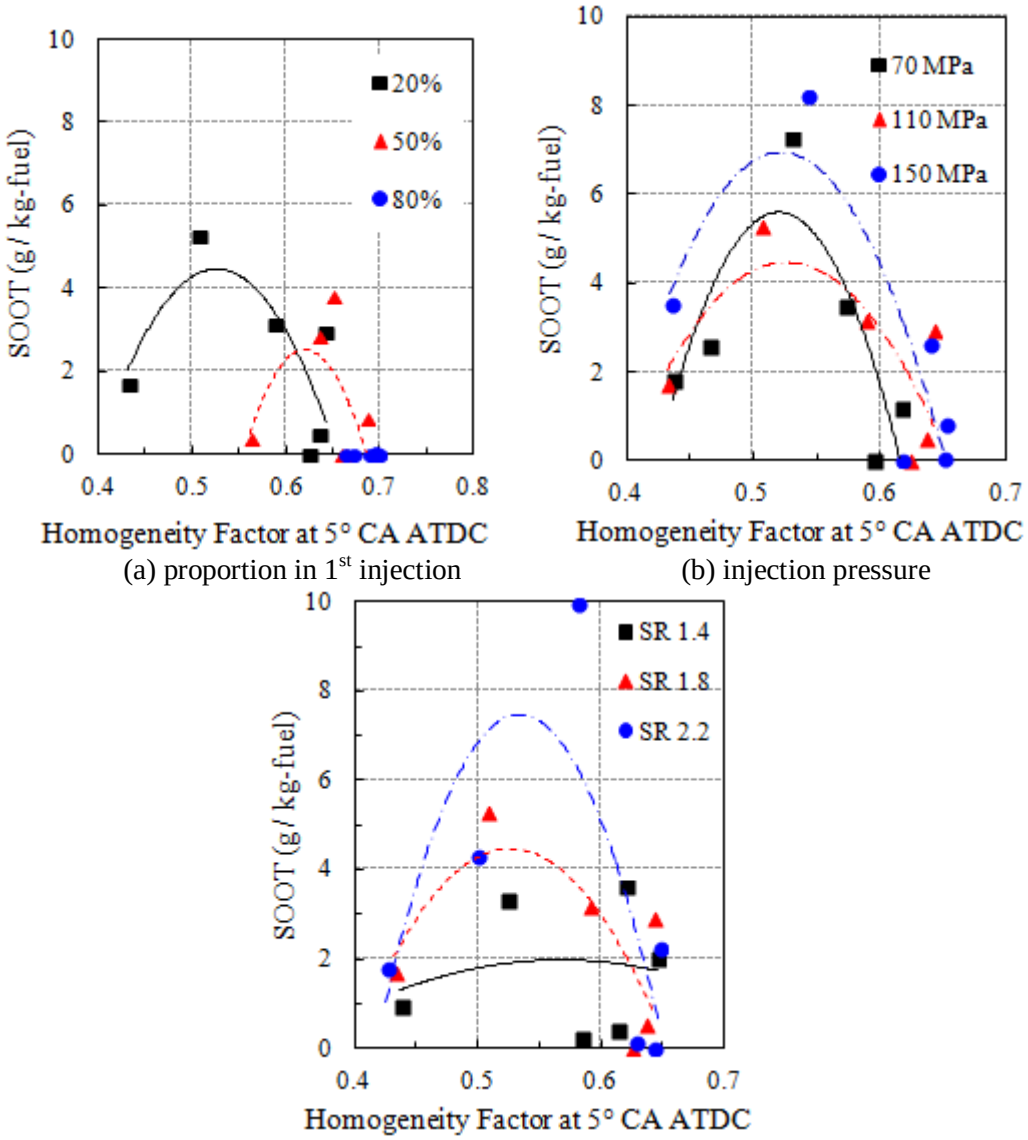

(a) proportion in 1st injection (b) injection pressure

(c) swirl ratio

Figure 4.42 The effect of the *HF* on the soot under various operating conditions.

As expected, the CO emission decreases when the *HF* increases, as shown in Figure 4.43. Similar to the view of Kook et al.[2006], under-mix is considered to be the major reason of CO emission. Also, in Figure 4.43, the trends of CO against *HF* are similar when the injection parameters or in-cylinder air motion are different. Therefore, the *HF* can be considered as a control factor for the CO emission.

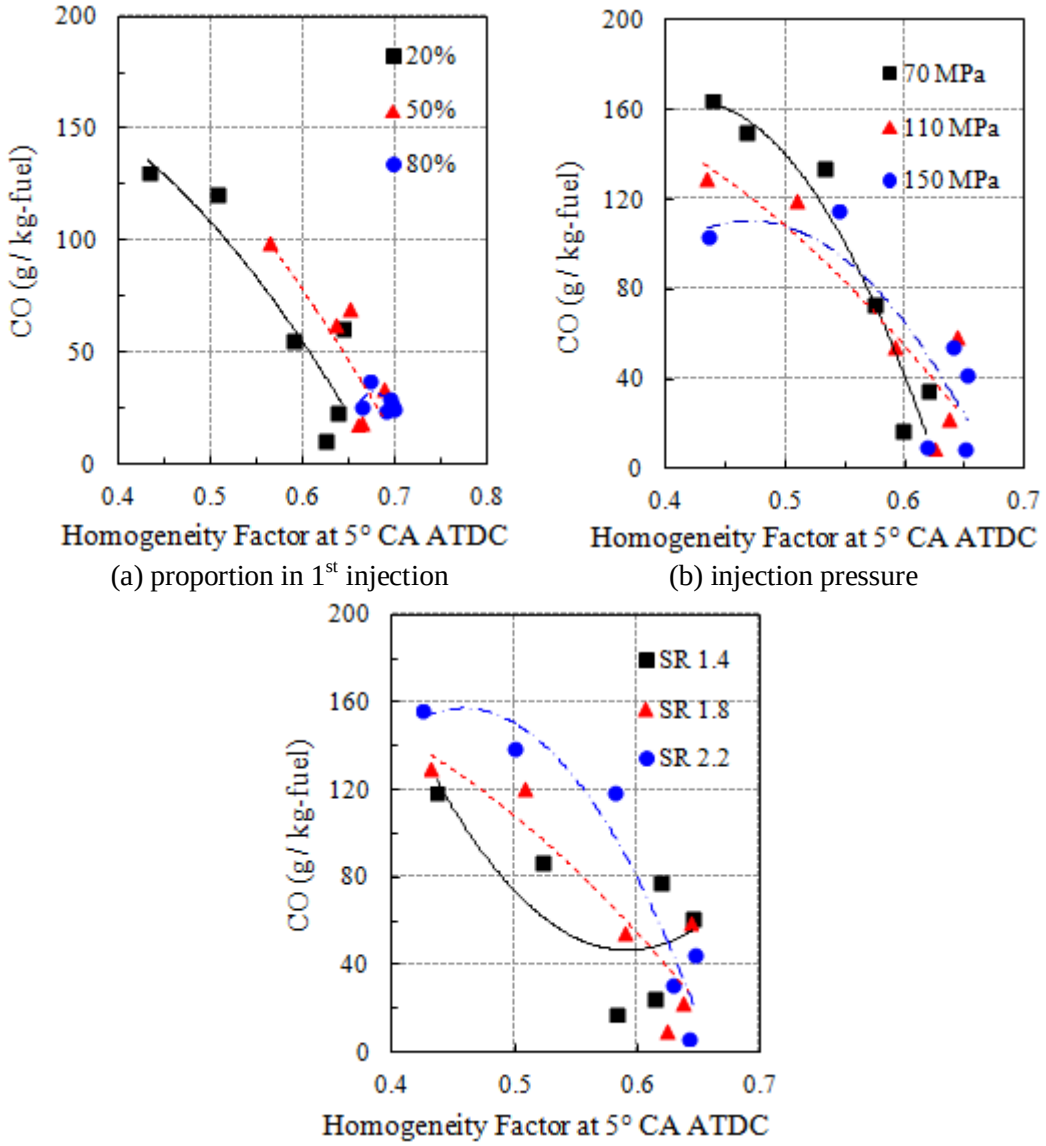

(a) proportion in 1st injection (b) injection pressure

(c) swirl ratio

Figure 4.43 The effect of the *HF* on the CO under various operating conditions.

For UHC emission, it normally decreases with higher *HF*, as given in Figure 4.44. However, the trend line of UHC-*HF* moves to the up-right when increasing the fraction of fuel in the 1st injection, as shown in Figure 4.44 (a). Referring to the trend of ISFC-*HF* shown in Figure 4.40 (a), this shift of the trend lines implies the fuel combustion efficiency decreases when increasing the fuel proportion in the 1st injection, although the homogeneity of mixture is improved. Moreover, the discrepancies between the trend lines of UHC-*HF* for different injection pressure are large. Hereby, other parameters are need if trying to monitor the output of UHC.

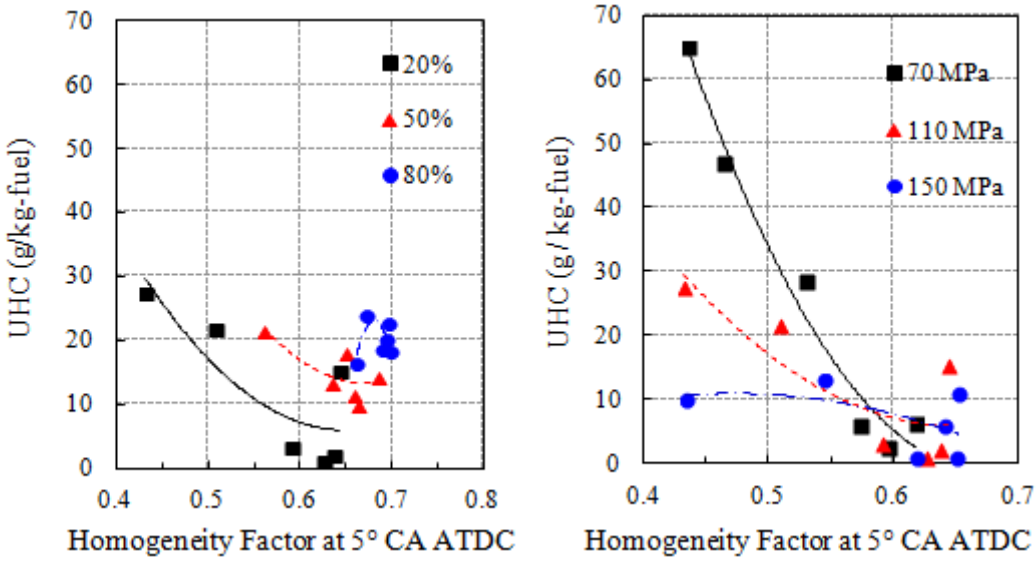

(a) proportion in 1st injection (b) injection pressure

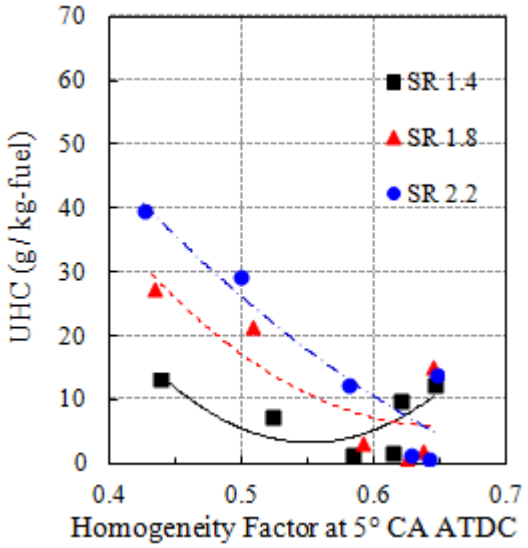

(c) swirl ratio

Figure 4.44 The effect of the *HF* on the UHC under various operating conditions.

4.3 Summary

This chapter numerically investigated the effects of operating parameters on combustion performance and emissions in PPCI combustion with split-injection, in a high-speed direct-injection diesel engine. The strategy of split-injection, including the 2nd injection timing, the fuel splitting proportion, the spray angle and the injection pressure, is examined primarily to obtain comprehensive understanding about the characteristics of mixing and combustion in PPCI combustion. Moreover, the impact of swirl ratio, EGR rate and boost pressure is examined to develop the operating range of PPCI engine. Meantime, the Homogeneity Factor (*HF*) is proposed for evaluating the quality of mixing and for quantitatively investigating the effects of injection parameters and in-cylinder air motion on mixture formation. Also, the relations between the quality of mixing and the characteristics of combustion and emissions are described

quantitatively using this factor.

The following conclusions have been derived from the investigations in this chapter:

1. The sweep of the 2nd injection timing shows that there is threshold of timing for a certain operating condition. Once the 2nd injection timing is much advanced than it, the engine operation is considered as PPCI diesel combustion; when the 2nd injection timing is retarded after it, the engine is considered working under conventional diesel mode. And the combustion duration is adopted to differentiate these two combustion mode of diesel. Moreover, under PPCI combustion, relatively low NO_x emission and soot emission can be achieved simultaneously with acceptable level of CO and UHC output. However, with the combustion phase far advanced to TDC, the thermal conversion efficiency of PPCI combustion is deteriorated.
2. The more fuel injected in the 1st injection, the more homogeneous the mixture is. In this study, the influence in NO_x emission is not significant when adjusting the fuel proportion in the 1st injection. Soot emission is successfully suppressed when increasing the fraction of fuel in the 1st injection. As more fuel injected in the 1st injection, UHC emission increases; while CO emission is reduced since the fuel-air mixing getting improved.
3. For the diesel engine used in this study, narrow spray angle is not beneficial for both combustion economic and emission control under PPCI combustion or conversional diesel combustion mode.
4. The effects of injection pressure are not significant on most combustion characteristics and emissions for PPCI diesel combustion, comparing to standard diesel combustion. However, the start of ignition is advanced as the injection pressure rising, while the fuel economic gets slightly improved.
5. The swirl ratio has significant influences on fuel economic and emissions, but it has little effects on other combustion characteristics. High swirl ratio is favourable for reducing ISFC, soot, CO and UHC under PPCI diesel combustion mode. In contrary, if the combustion is majorly controlled by mixing only NO_x emission decreases a little, while fuel consumption and other emissions increase dramatically with enlarged swirl ratio.
6. Both EGR rate and boost pressure have higher influence in the start of combustion rather than in the combustion duration. For fuel consumption and emissions, the effects of EGR rate are not significant until it reaches a certain level (50% in this study). When operating under PPCI diesel combustion, fuel consumption and emissions are more sensitive to the boost pressure.
7. The analysis of Homogeneity Factor (*HF*) quantitatively proves that, though the starts

of the combustion are varied, it can be prospected that the combustion processes in the mixture of higher homogeneity when the 2nd injection is advanced.

8. When increasing the fuel proportion in the 1st injection, the adjustment of *HF* through variable timing of the 2nd injection is not significant. High injection pressure is beneficial for achieve high *HF*. Excessive swirl ratio will impede mixing when using relatively late 2nd injection timing.
9. The correlation between 50% burn location and *HF* is apparent and it can be expressed with a simple exponent function. This suggests that *HF* can be considered as a parameter for the prediction of combustion phase location.
10. Accepted regressions can also be achieved for the relations between *HF* and NO_x/soot/CO. For fuel consumption and UHC, *HF* might not be the perfect parameter and other parameters are need for monitoring.

Chapter 5 Constituents of Exhausted Gas for Recirculation

For the application of EGR in PPCI diesel combustion, the studies are majorly about the overall effects of EGR on combustion characteristics and the operating range of PPCI combustion [Park and Bae, 2011; Horibe et al., 2009; Kiplimo et al., 2011]. The constituents of EGR are rarely considered in the study about PPCI diesel combustion. In this study, the effects of these two major constituents, i.e. CO_2 and water vapour, on combustion characteristics and emissions are numerically investigated to explore the potential measures to improve emission output in PPCI diesel combustion. The effects of EGR with different fraction of CO_2 or H_2O are explored to compare the influence of these two constituents. Moreover, the comparison is conducted under a sweep of the 2^{nd} injection timing and EGR rate, in order to achieve understanding of the effects of CO_2 and water vapor in EGR for different operation modes.

5.1 Test Methodology

In this chapter, the simulation is conducted for the engine with the same parameters of the engine in Chapter 4 [Lee and Reitz, 2006]. The operating condition is mostly same with the condition of baseline illustrated in Table 4.1, but with a lower speed of 1900 rpm and varied EGR rate. External EGR is assumed to apply here. Then, all the simulations are conducted at the inlet air temperature of 380K and a moderate level of boost pressure (0.6 bar) in order to ensure the vaporization of water. To evaluate the effect of each constituent, one constituent is replaced by other one proportionally by volume, as shown in Figure 5.1. It has to be noticed that Figure 5.1 just gives the schematics of the compositions for different EGR. The proportion of each area doesn't reveal the real fraction of each constituent. In fact, the other species has much larger fraction than it is shown in the figure. The different EGR constitutions simulated in this chapter and their abbreviation are given in Table 5.1, together with a simple introduction of operating conditions for simulation. Another fact need to be concern is that the mass of EGR is varied when the fraction of CO_2 over H_2O changes since the replacement is taken by volume. The sweep of the 2^{nd} injection timing and EGR rate are also conducted for different EGR constitutions aiming to get further understanding about the effects of each constituent in different combustion modes.

Table 5.1 Operating conditions and EGR constitutions

Engine Speed	1900 rpm
Maximum Torque	100 Nm
Temperature at IVC	380 K
Boost Pressure	0.6 bar
The Fraction of Fuel in the 2nd Injection	80%
Start of the 1st Injection (SOI_1)	-40 °CA ATDC
Start of the 2nd Injection (SOI_2)	-10 °CA ATDC (-20 °~ -5 °CA ATDC)
Injection Pressure	110 MPa
Spray Included Angle	120 °
Swirl Ratio	1.8
EGR Rate	40% (40 ~ 50%)
EGR constitutions and Abbreviation	Normal (Original EGR)
	x%H_2O_rp (x% of H_2O replaced by CO_2)
	x% CO_2_rp (x% of CO_2 replaced by H_2O)

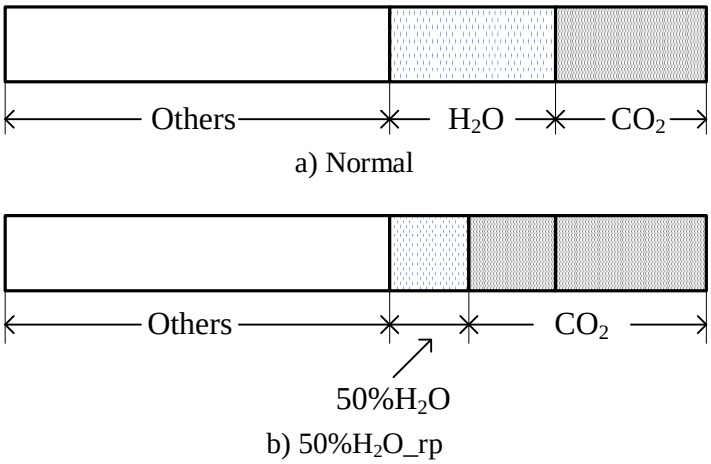

Figure 5.1 The EGR introduced into inlet air which is original: a) Normal; and 50% of water vapour has been replaced by CO_2: b) 50%H_2O_rp

5.2 The Effects of CO2 and Water Vapour in EGR

5.1.1 Combustion Process

For the methodology used in this study, the volume of inlet air and EGR keeps constant, and the concentration of O_2 by volume isn't affected by the EGR constitutions. Therefore, the EGR with the constitutions listed in Table 5.1 should show similar dilution effect at a certain EGR rate. As shown in Figure 5.2, when the CO_2 in EGR is completely replaced by H_2O, the curve of heat release rate moves forward. In contrary, the curve of heat release rate retards when the H_2O in EGR is completely replaced by CO_2. It is can be considered as the result of varied specific heat of EGR with different compositions. According to Figure 5.3, CO_2 has much higher molar heat capacity [Rogers and Mayhew, 1994]. Hence, lower in-cylinder temperature is expected when H_2O in EGR is replaced by CO_2, as given in Figure 5.4. With the injection timing and EGR rate used in this section, the combustion phases mainly locate after TDC. For the case where H_2O is completely replace by CO_2, the combustion occurs in the expansion stroke where the expanding volume further cools the in-cylinder temperature. Therefore, in Figure 5.4, the trace of in-cylinder temperature for the case using EGR with H_2O replaced by CO_2 retards and obviously decreases, comparing to the original case.

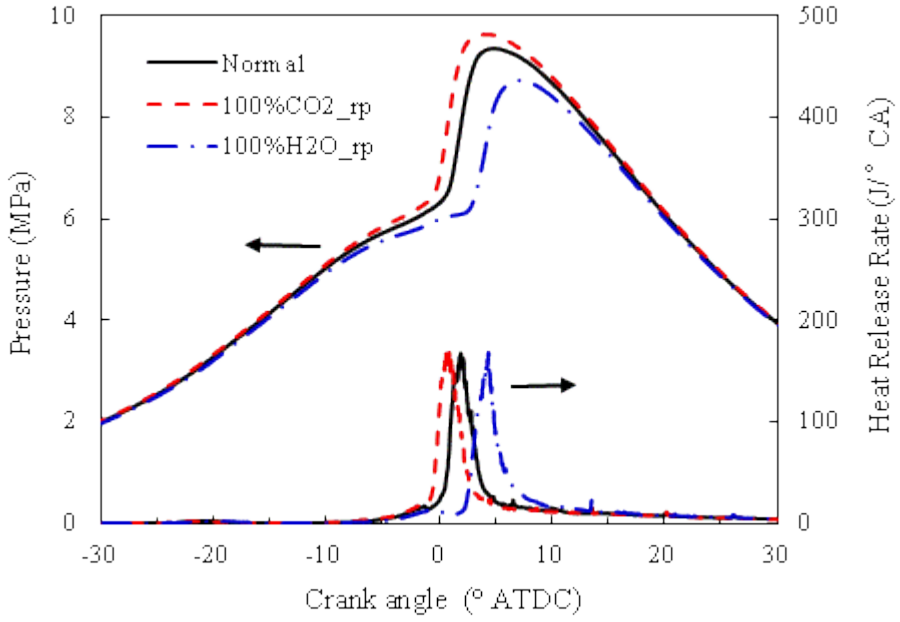

Figure 5.2 In-cylinder pressure and heat release rate of the cases with different EGR compositions

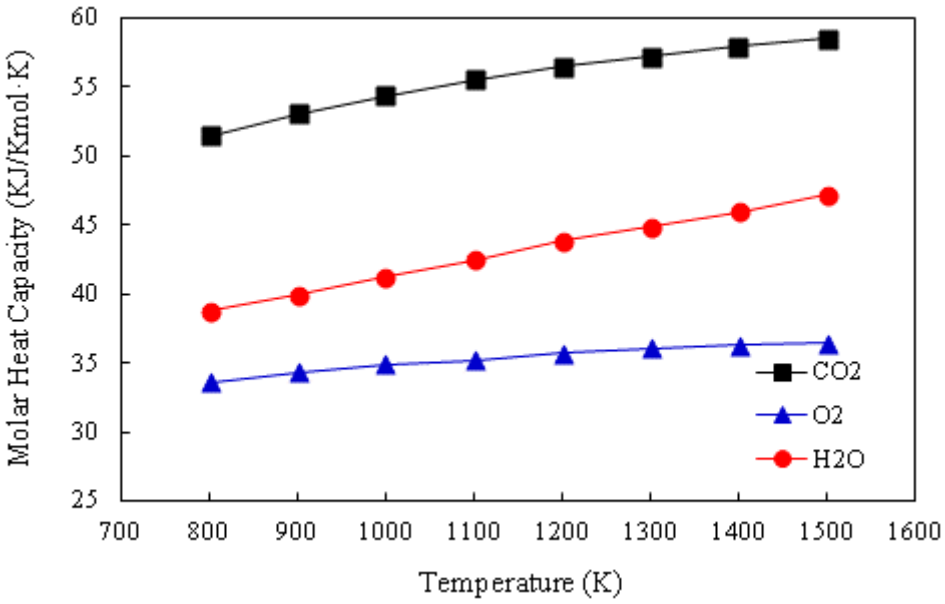

Figure 5.3Molar heat capacities of different gases. [Rogers and Mayhew, 1994]

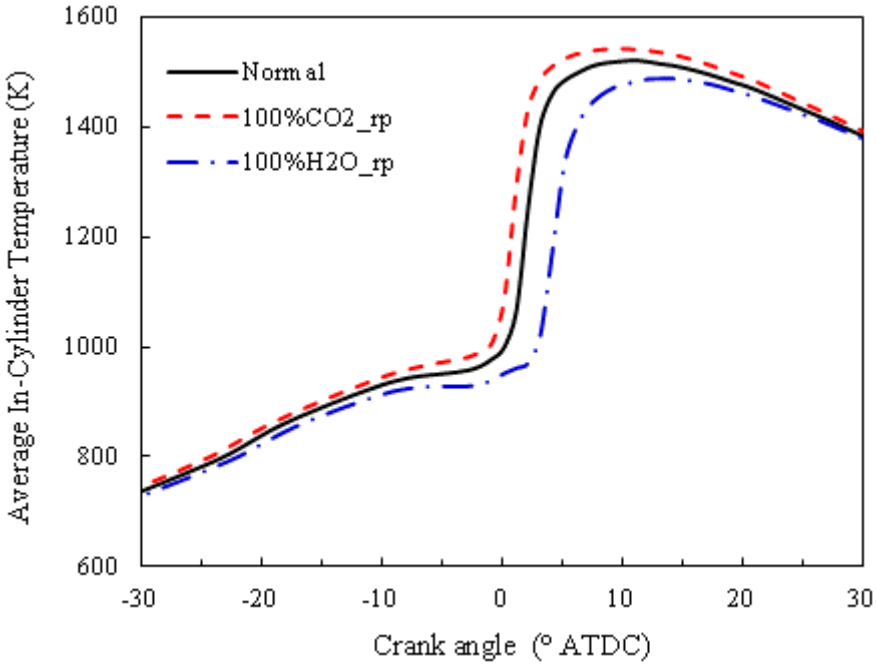

Figure 5.4 In-cylinder temperatures for the cases with different EGR compositions

Figure 5.5 gives how the start of combustion changes when CO_2 or water vapour in EGR is proportionally replace by other constituent. For CO_2 replacement, when the fraction increases the start of combustion is advanced. For H_2O replacement, the start of combustion retards as the fraction of CO_2 increases. Since the combustion of the original case starts almost at TDC, the starts of combustion for CO_2 replacement are all locate before TDC, while after TDC when H_2O is replaced. Therefore, larger ignition delay can be achieved through replacing H_2O in EGR by CO_2 of same volume owing to the higher specific heat. And the prolonged ignition delay allows

more time for mixing. Moreover, the increase of ignition delay resulted by H_2O replacement is much larger than the reduction of ignition delay resulted by CO_2 replacement. It may be considered that adding CO_2 has higher effect on the start of combustion than adding H_2O of same volume.

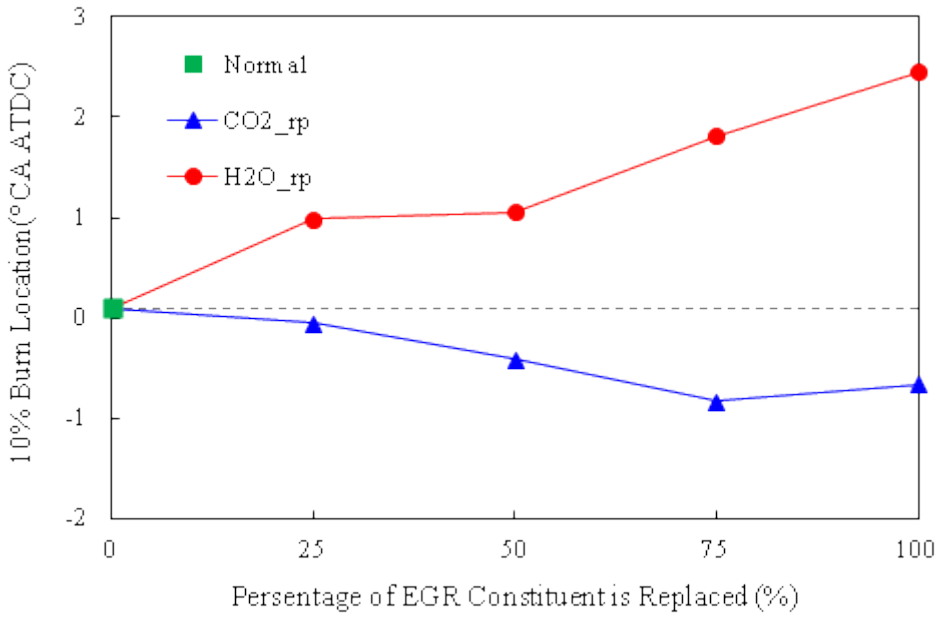

Figure 5.5 The starts of combustion for the cases with different EGR compositions

The durations of combustion for the cases exploiting different EGR compositions are shown in Figure 5.6. The durations of combustion, which are defined by the crank angles between the 10% and the 90% location of the accumulated heat release rate, are shortened in the cases using EGR of CO_2 replacement and H_2O replacement comparing to the original case. The increased in-cylinder temperature, which is resulted from the lower molar heat capacity of water vapour, accelerates oxidation reaction for the cases using EGR of CO_2 replacement. And the shortening of combustion duration is enlarged as the fraction of CO_2 replaced from EGR increases. However, an increase of combustion duration is seen when the replacement of CO_2 increases from 75% to 100%. Referring to Figure 5.5, the further shortened ignition delay leads to less time for mixing. Hence, more fuel intends to be burned during the mix-controlled combustion phase which normally has much slower combustion rate. When the replacement of CO_2 in EGR increases from 75% to 100%, the acceleration of oxidation reaction by increased temperature cannot compete with the slower combustion rate controlled by mixing, and increased combustion duration is resulted. For H_2O replacement cases, though the increased molar heat capacity and the late combustion phasing in expansion stroke cools the temperature for combustion, the enhanced mixing since the prolonged ignition delay results the shortening of combustion duration. However, because the competition between the lower temperature and enhanced mixing is complicated, the trend of combustion duration respected to the proportion of

H_2O replacement is not linear.

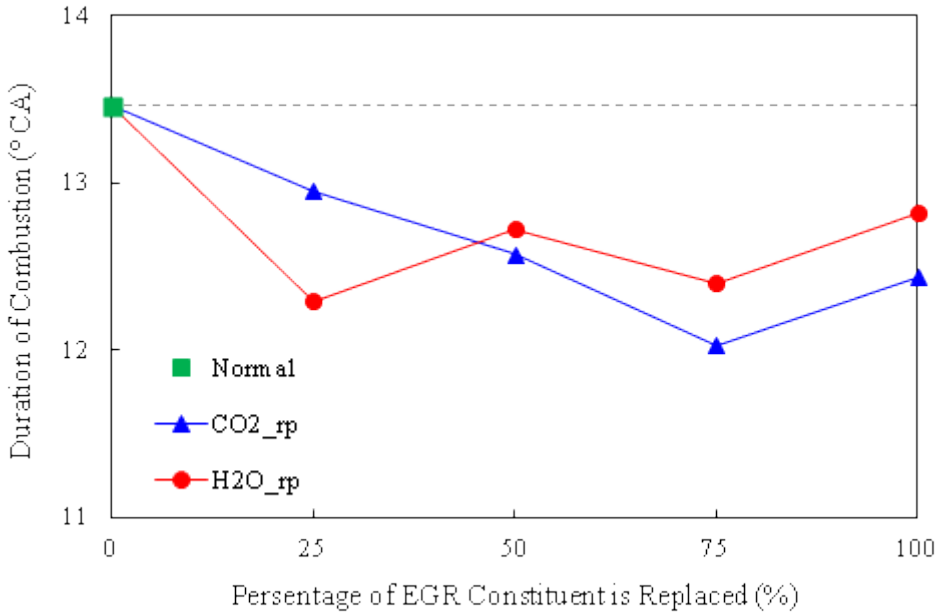

Figure 5.6 The durations of combustion for the cases with different EGR compositions

As stated in chapter 4, the 50% burn location is defined to represent the combustion phasing; while the ISFC indicates the fuel economy. The ISFC against the combustion phasing is shown in Figure 5.7 for the cases exploiting different EGR compositions. The combustion phasing is advanced to TDC as the CO_2 in EGR gradually replaced by H_2O owing to the decreased molecular heat capacity and increased in-cylinder temperature. And the fuel consumption increases with the advanced combustion phasing till 75% of CO_2 is replaced. When the CO_2 is entirely by H_2O, a considerable decrease of ISFC is observed with slightly advanced combustion phasing. The increased proportion of fuel's chemical energy released close to TDC is considered to be reason of the better fuel economy [Keeler and Shayler, 2008]. Conversely, increasing the fraction of H_2O replacement results in retarded combustion phasing. Significant increase in ISFC is detected when 25% H_2O replacement is exploited. Despite of this, the ISFC linearly increases with the retarded combustion phasing owing to the deteriorated thermal conversion efficiency when increasing H_2O replacement. Among the cases using EGR with different compositions, the lowest ISFC appears when using 25% CO_2 replacement, which locates at about 2.5 °CAATDC and has slightly shorter combustion duration than original.

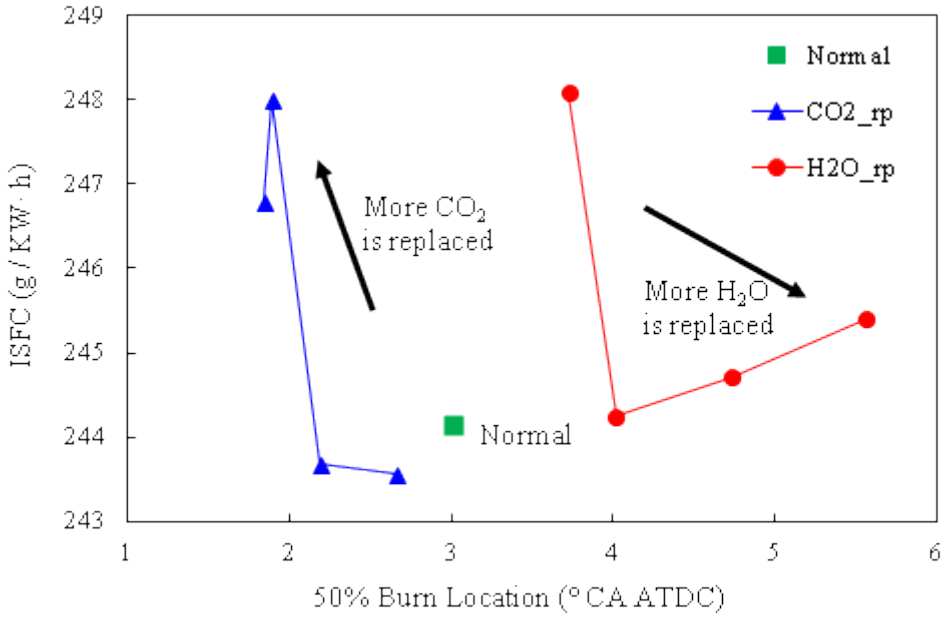

Figure 5.7 The ISFC respects to the combustion phase location for the cases with different EGR compositions

5.1.2 Emissions

Though introducing EGR is the most feasible method to suppressing NO_x emission of diesel engine, the increases in soot out comes at the same time for conventional diesel combustion. PPCI combustion is proposed as the strategy having the capability to simultaneously reduce NO_x and soot emissions. The PPCI diesel combustion is commonly implemented by introducing high level EGR and specific injection strategy rather than changing the hardware of modern HSDI diesel engine. Nevertheless, the penalty of fuel consumption and the increase of CO and unburned hydrocarbon (UHC) emission come owing to reduced oxygen availability and combustion temperature under high EGR rate. In this section, the trade-off between NO_x and other emissions, i.e. soot, CO and UHC is discussed. And the relation between NO_x and fuel consumption is illustrated in final.

In the previous studies about conventional diesel combustion, the trade-off between NO_x and soot emission is considered to be one major restraint for the optimization of diesel engine [L ázaro et al., 2002].In PPCI diesel combustion this trade-off still exists, but the outputs of NO_x and soot are usually simultaneously reduced to lower level comparing to the conventional combustion [Park and Bae, 2011; Horibe et al., 2009; Kiplimo et al., 2011]. Figure 5.8 illustrates the relation between NO_x and soot when using EGR of different compositions. In general, EGR with CO_2 replacement causes the trade-off of NO_x and soot shifting to a high level; while EGR with H_2O replacement can suppress this trade-off to lower level. Since the dilution effects are same for different EGR compositions according to the testing methodology discussed in section

5.1, the differences in thermal effect is considered as the reason for the shifting of NO_x -soot trade-off. Because of the higher heat capacity, NO_x emission decreases as the volume fraction of CO_2 in EGR rising owing to the lower flame temperature. Meantime, the prolonged ignition delay, as shown in Figure 5.5, allows more time for mixing and provides lower local equivalence ratios when combustion starts. Also, as given in Figure 5.4, when the increase the CO_2 fraction in EGR the in-cylinder temperature is lower since the combustion is retarded and starts in the expansion stroke. Therefore, soot emission is suppressed due to the higher homogeneity and lower combustion temperature. Overall, with same volume of EGR, the NO_x -soot trade-off can be improved if replacing the H_2O in EGR by CO_2.

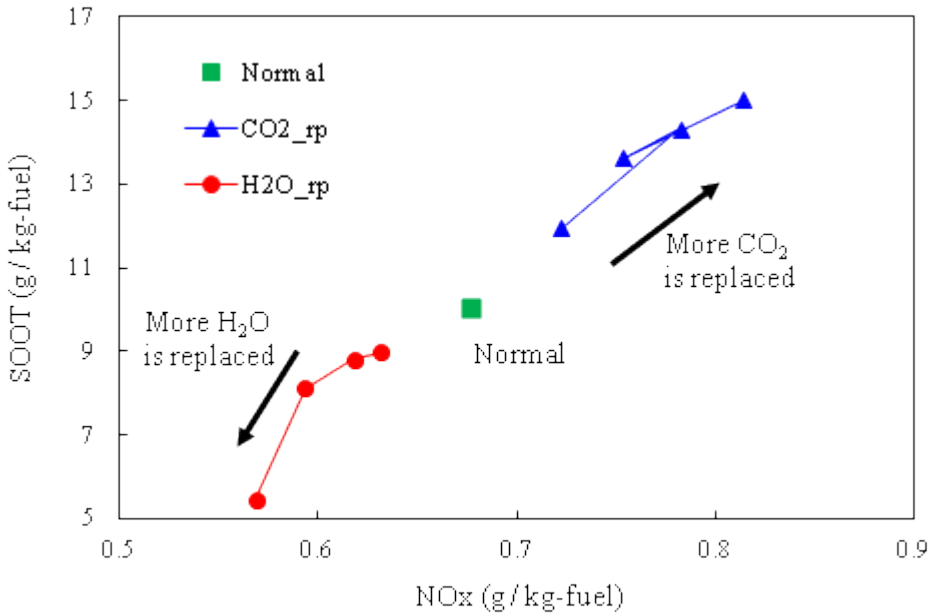

Figure 5.8 The trade-offs of NO_x and soot for the cases with different EGR compositions

The formation of CO is the consequence of incomplete combustion and generally considered from two primary sources. Firstly, the under-mixing of fuel, which may results locally or entirely lacking of oxygen for completing oxidation process, and leads to the generation of CO. Secondly, low combustion temperature has been found to be the reason for high CO level in lean region [Khan et al., 1973; Kim et al., 2008; Kook et al., 2006]. Both of these two reasons may exist in PPCI combustion when using large amount of EGR to realize the demanded NO_x -soot trade-off. Figure 5.9 shows the trade-off between NO_x and CO when using CO_2 or H_2O replacement in EGR. Lower level of CO is observed when the H_2O in EGR is replaced by CO_2, though the combustion temperature is lower comparing to the cases of CO_2 replacement, as shown in figure 5.4. Thus, the enhanced pre-combustion mixing due to longer ignition delay is considered as the reason for the reduction of CO output. As mentioned in Figure 5.8, lower NO_x is achieved in the same cases owing to the reduced flame temperature. Conversely, the case using EGR of CO_2 replacement results higher CO and NO_x emissions than the original case

because of higher combustion temperature and shorter ignition delay. Therefore, for the engine and operating condition used in this study, replacing the H_2O in EGR by CO_2 can improve the trade-off between CO and NO_x, though these two emissions behave in opposite measures with EGR rate and temperature.

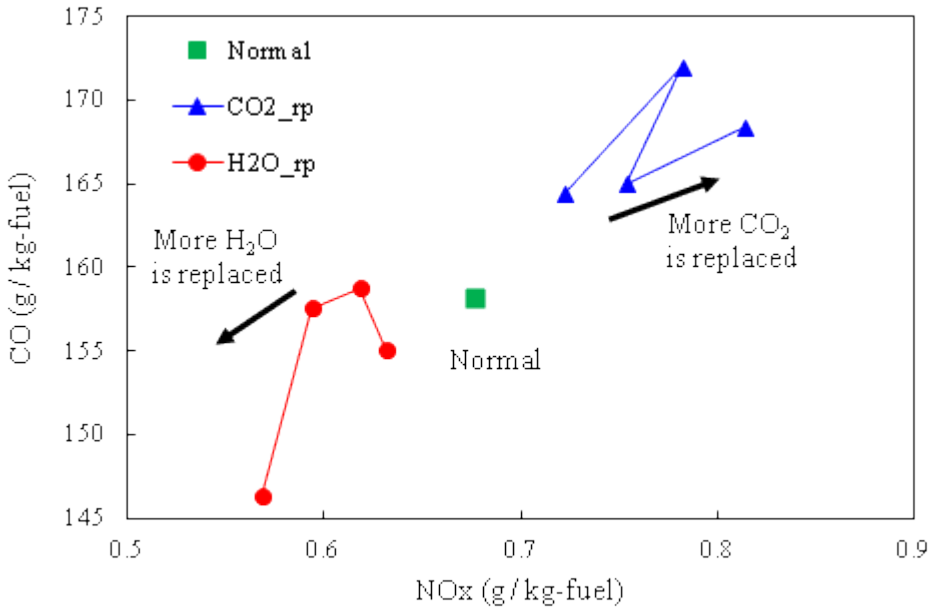

Figure 5.9 The trade-offs of NO_x and CO for the cases with different EGR compositions

For conventional diesel combustion, unburned hydrocarbons (UHC) are generally of very low level since the engines working with excess air. However, as dilution level is increased to suppress NO_x output, UHC increases significantly because of the reduced oxygen availability in PPCI combustion. Moreover, the lower combustion temperature, which is common in the high diluted combustion, is not favourable for the oxidation of hydrocarbon. The responds of UHC for different EGR compositions are given against NO_x, as shown in Figure 5.10. With the same dilution effect as discussed before, the NO_x -UHC trade-off shifts to lower-left in the plot when using EGR with H_2O replacement; while the NO_x -UHC trade-off shifts to high-right area of the plot when the CO_2 in EGR is replaced by H_2O. Since large amount of EGR is exploited, the UHC emission is majorly determined by the local equivalence ratio. Though the combustion temperatures are lower in the cases using EGR of H_2O replacement, the prolonged ignition delay allows more time for mixing and provides lower local equivalence ratio. This eventually results lower UHC emissions together with suppressed NO_x emissions in the H_2O replacement cases.

Though the Figure 5.7 gives the ISFC for different EGR compositions against the combustion phases, the trade-off between fuel consumption and NO_x emission is illustrated in Figure 5.11 for the discussion about possible measures to achieve low NO_x emission with acceptable compromising of fuel economy. Unfortunately, no obviously improvement of ISFC can be

detected when using EGR of CO_2 or H_2O replacement. Only slightly decrease of ISFC can be found when 25% and 50% of CO_2 in EGR is replaced by H_2O, together with sacrifice of NO_x emission. As mentioned in section 5.1.1, the fuel consumption is related to the combustion efficiency, combustion phasing and the combustion duration. Though, CO and UHC emission can be reduced by replacing H_2O in EGR by CO_2, as shown in Figure 5.9 and 5.10, the fuel consumption is not be improved because of the reduced thermal conversion efficiency since the combustion phase is more retarded from TDC. Therefore, it is failed to achieve an improved NO_x -ISFC trade-off by varying the EGR composition.

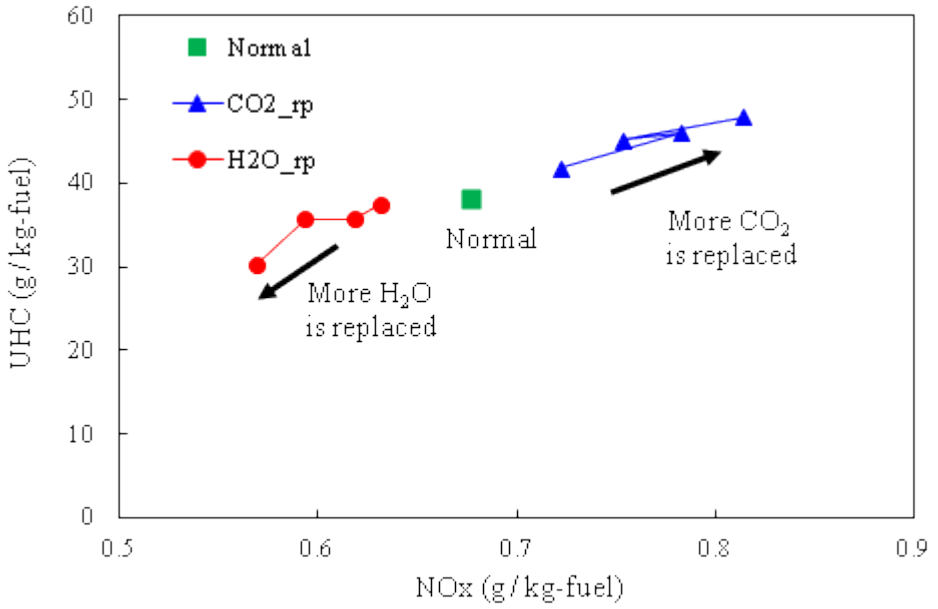

Figure 5.10 The trade-offs of NO_x and UHC for the cases with different EGR compositions

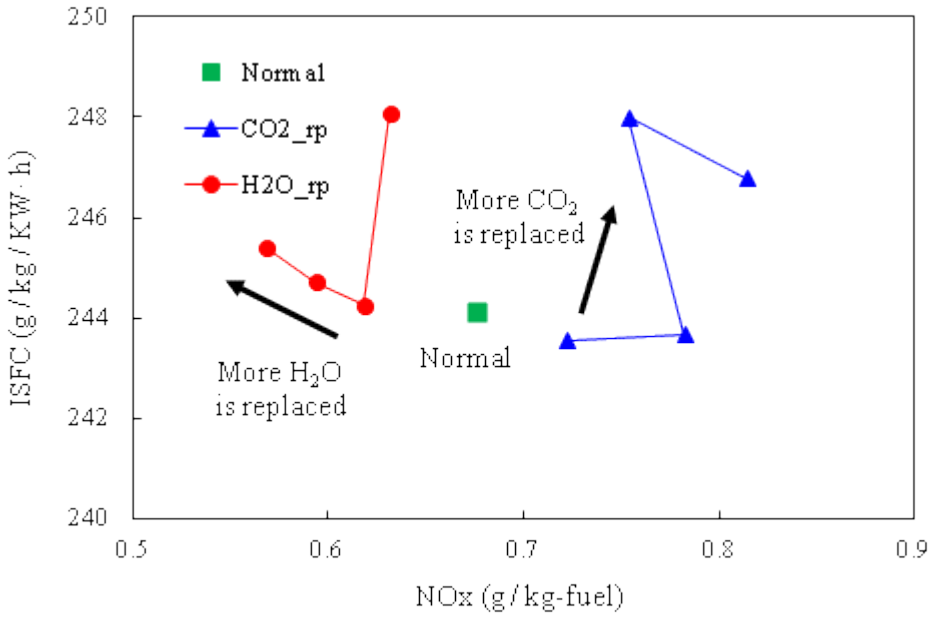

Figure 5.11 The trade-offs of NO_x and ISFC for the cases with different EGR compositions

5.2 Conditional Sensibility

In order to gain further understanding about the effects of EGR compositions, parametric study has been conducted in this section. Though the effects of CO_2 and water vapour in EGR have been discussed in detail, the operating condition in section 5.2 cannot represent the responds of typical PPCI diesel combustion since its long combustion duration and high soot output, as shown in Figure 5.6 and 5.8. Meantime, the effects of EGR composition when using higher diluted level are also need to be concerned. Thus, comparisons are conducted under the sweeps of the 2nd injection timing and EGR rate, in order to achieve understanding of the effects of CO_2 and water vapor in EGR for different operating mode.

5.2.1 Sensibility to the 2nd injection timing

As discussed in Chapter 4, the 2nd injection timing is considered significantly influence the combustion characteristics and emissions output of PPCI diesel combustion. It also has summarized that the combustion mode can be determined by the 2nd injection timing. For further estimating the effects of EGR composition, the condition using EGR with 100% CO_2 replaced, EGR with 100% H_2O replaced and the original EGR are simulated under the 2nd injection sweep from -20 °CAATDC to -5 °CAATDC. Meanwhile, a lower temperature of inlet air as 360 K is exploited to achieve prolonged ignition delay for PPCI combustion.

As shown in Figure 5.12, the start of combustion is linearly retarded as the 2nd injection timing moving towards TDC, while the EGR composition displays influences in parallel. With same 2nd injection timing and other conditions, advanced start of combustion is achieved when CO_2 in EGR is replaced by H_2O. Conversely, the EGR exploiting H_2O replacement results prolonged ignition delay. The discrepancy between CO_2 replacement case and H_2O replacement case is from 2 to 5 crank angles, and it increases as the 2nd injection timing retarding. As discussed before, the variation of combustion start is considered result by the differences between the thermal effect of water vapour and CO_2.

The effects of EGR composition in combustion duration are complicated, as given in Figure 5.13. For original case and the case exploiting EGR of CO_2 replacement, the combustion durations do not keep increasing once the 2nd injection timing is retarded after -15 °CA ATDC. The longest combustion duration for these cases is around 12 crank angles. However, the combustion duration increases linearly as the 2nd injection timing retarded when the H_2O in EGR is replaced by CO_2. Shorter combustion duration is detected in the H_2O replacement case when 2nd injection timing is earlier than -10 °CA ATDC. For these earlier 2nd injection timings, the enhanced mixing coming from prolonged ignition delay results shorter duration of combustion when using EGR of H_2O replacement. Meanwhile, because the starts of combustion are retarded more closely to TDC for these H_2O replacement cases, the conditions of higher

in-cylinder pressure and temperature also promote the combustion rate. After this timing, the combustion durations are longer in the cases exploiting EGR with H_2O replacement, comparing to the original cases and CO_2 replacement cases. When the 2nd injection timing is after -10 °CA ATDC, the higher molar heat capacity and the late combustion phasing in expansion stroke lead to cooler combustion temperature and lower combustion rate in H_2O replacement case. Referring to the discussions in chapter 4, when replace the H_2O in EGR by CO_2, the combustion can be promoted in premixed combustion region.

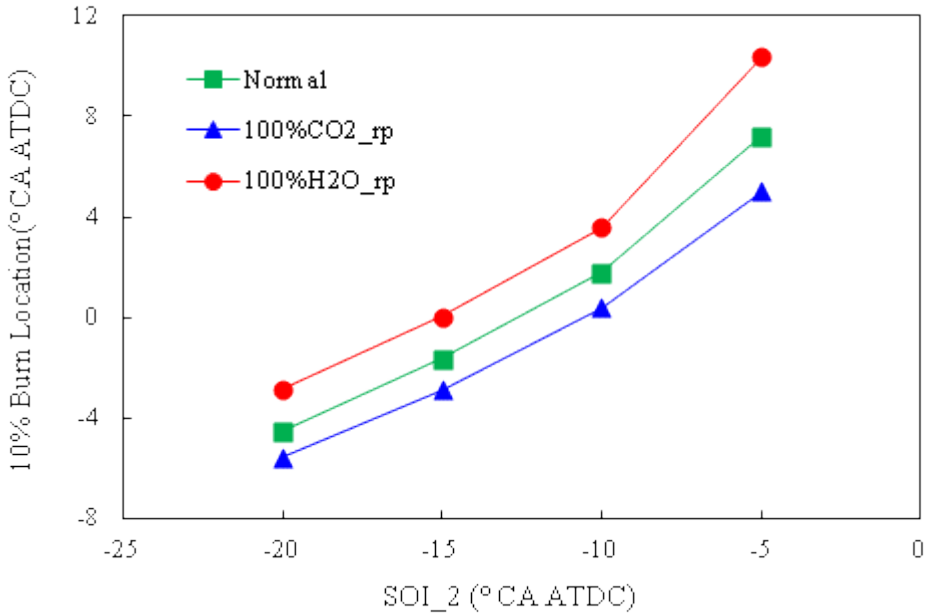

Figure 5.12 The starts of combustion for the cases with different EGR compositions and varied 2nd injection timing

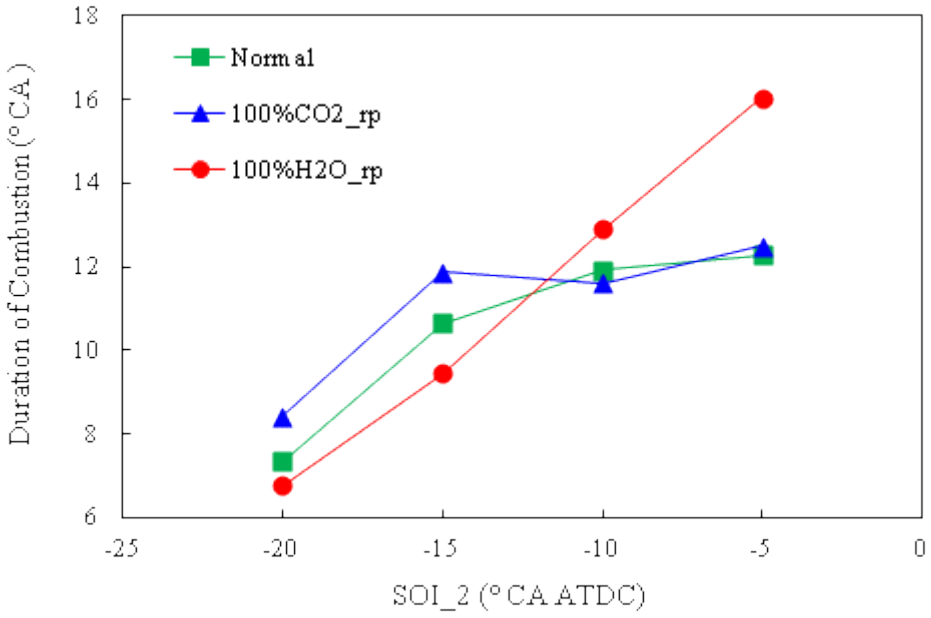

Figure 5.13 The durations of combustion for the cases with different EGR compositions and varied 2nd injection timing

In Figure 5.14, the combustion durations for different EGR compositions are illustrated in two stages, i.e. 10 to 50% burn duration and 50 to 90% duration. For each EGR composition, the 10 to 50% burn durations are varied slightly with the 2nd injection timing. It becomes slightly shorter when using EGR of CO_2 replacement due to the higher combustion temperature. Conversely, owing to the higher molar heat capacity of CO_2, prolonged 10 to 50% burn durations are observed since the reduce in-cylinder temperature when the H_2O in EGR is replaced by CO_2 of same volume. According to the discussion of Miles et al [2005] and LEE [2006], the above characteristics imply that 10 to 50% burn sections are majorly under premixed combustion region. The 50 to 90% burn durations for the cases using EGR of different composition show similar trend to the entire combustion durations. Unlike the trends of 10 to 50% burn duration, shorter 50 to 90% burn durations are observed in H_2O replacement cases, when the 2nd injection timing is earlier than -10 ° CA ATDC. The prolonged ignition delay and improved mixing before combustion are considered enlarge the premixed combustion part and then shorten the durations of the late combustion stages in H_2O replacement cases. For later 2nd injection timing, the combustion rates in 50 to 90% burn stages are suppressed in the H_2O replacement cases owing to the low combustion temperature and late combustion phase in compression stroke.

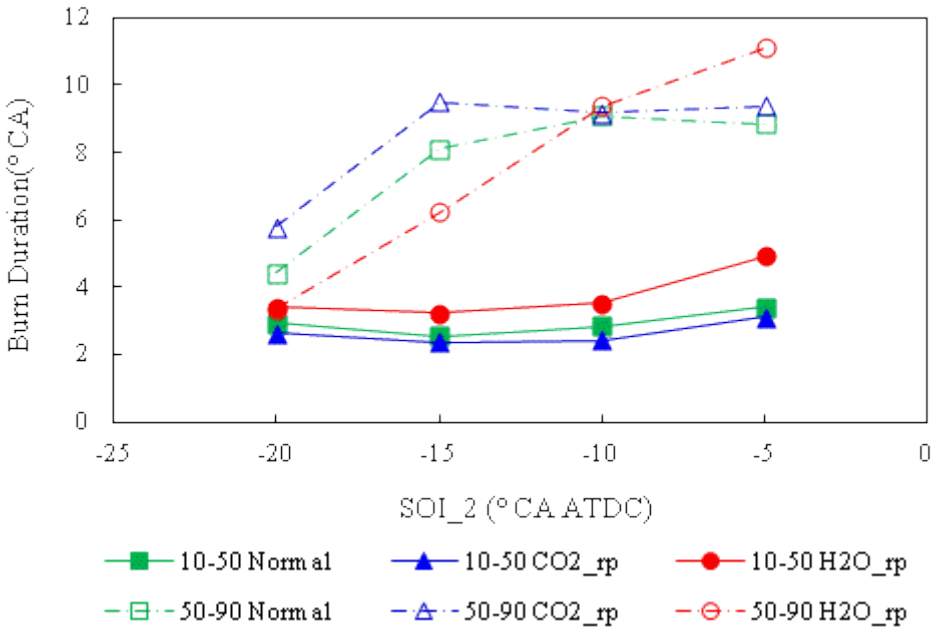

Figure 5.14 Detailed burn durations for the cases with different EGR compositions and varied 2nd injection timing

For varied 2nd injection timing, ISFC against combustion phasing is shown in Figure 5.15 for the cases exploiting different EGR compositions. With similar shape, the EGR composition influences the trends in parallel. When CO_2 in EGR is replaced by H_2O, advanced combustion

phase and reduced fuel consumption are observed due to the promoted combustion temperature by lower molar heat capacity. For H_2O replaced cases, the trend of ISFC against combustion phasing shifts to upper right area comparing to the trend of original cases. The effects of EGR composition on combustion phase location gets significant as the 2nd injection timing retarded forward TDC. However, the discrepancies of ISFC between cases using different EGR compositions get large when the 2nd injection timing is advanced. For the case with advanced 2nd injection timing, the deteriorated combustion efficiency is considered as the reason for higher ISFC when using EGR of H_2O replacement, because good thermal conversion efficiency is expected since its combustion phase is close to TDC.

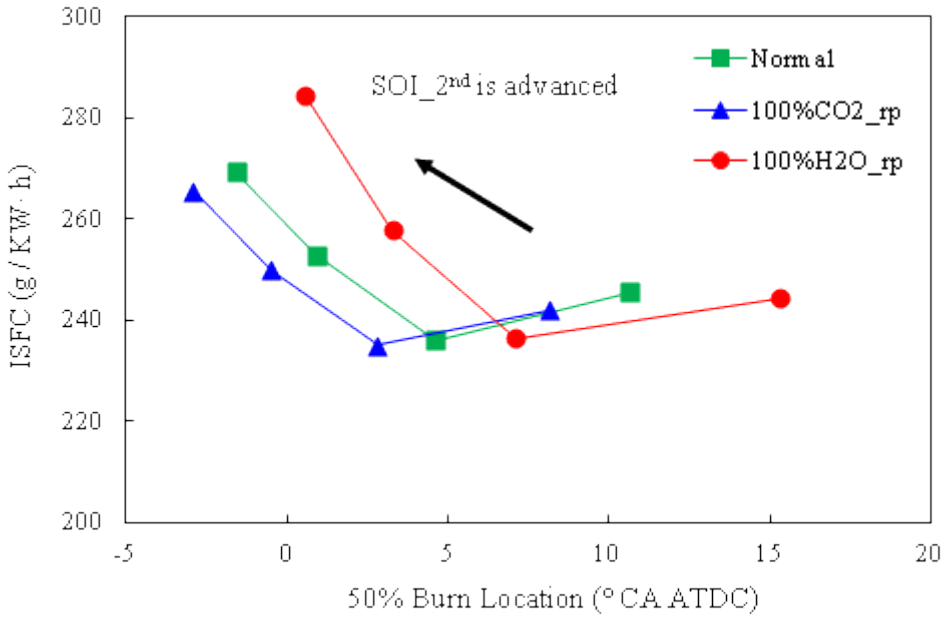

Figure 5.15 The ISFC respects to the combustion phase location for the cases with different EGR compositions and varied 2nd injection timing

For different EGR compositions, the trade-offs of the NO_x -soot are similar in trend for varied 2nd injection timing, as shown in Figure 5.16. When the 2nd injection timing is far advanced from TDC, higher NO_x is detected owing to the higher combustion temperature and relatively lower local equivalence ratio; while very low soot is observed since the mixing is improve due to the prolonged ignition delay. As the 2nd injection timing is retarded after -10 °CA ATDC, soot emission increases dramatically because of the poor mixing under this high dilution level; while NO_x is reduced to one third of the value for the case using the earliest 2nd injection timing. Over the entire range of the 2nd injection timings, EGR with H_2O replacement improves the trade-off of NO_x and soot to a lower level because of the suppressed combustion temperature and enhanced pre-combustion mixing resulting from the increased molar heat capacity of the EGR. Conversely, EGR with CO_2 replacement causes simultaneous increases of NO_x and soot when the 2nd injection timing and other parameters are same as the original case. The effects of EGR

composition on NO_x emission are of similar level for varied 2nd injection timing. For soot emission, the effects of EGR composition are more significant for the cases with relatively later 2nd injection timing, whose soot emission is high due to the poor mixing. The best trade-off is achieved in the H_2O replacement case when the 2nd injection timing is -15 °CA ATDC.

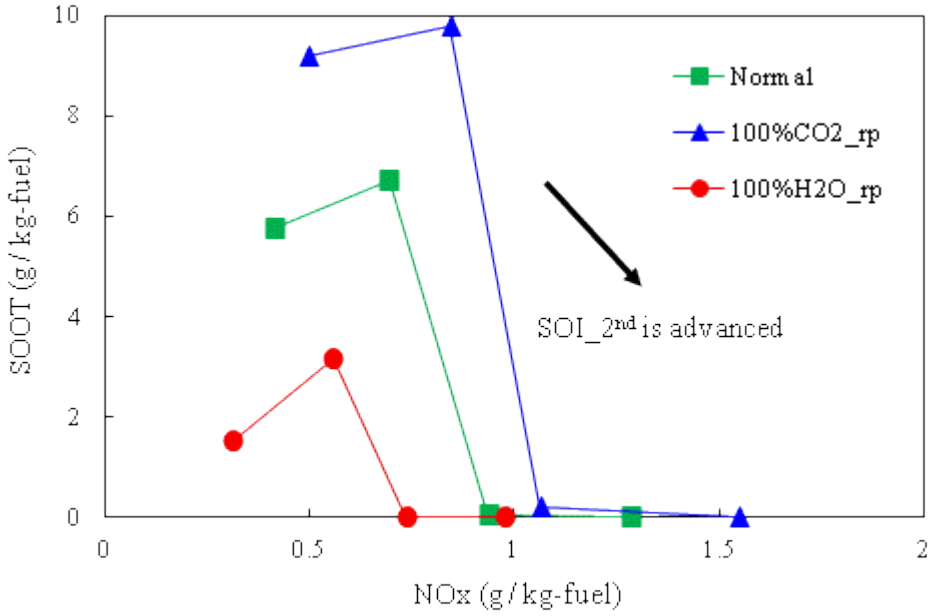

Figure 5.16 The trade-offs of NO_x and soot for the cases with different EGR compositions and varied 2nd injection timing

For each EGR composition, the CO and NO_x emissions respond in opposite ways with the 2nd injection timing, as shown in Figure 5.17. As discussed in chapter 4, the CO emission increases as the 2nd injection retarded because the time for mixing is reduced. Though the under-mix is considered as the reason for high CO output, EGR with H_2O replacement does not result lower CO level comparing to the original EGR. Lower CO emission is achieved by using EGR with CO_2 replacement, although shorter ignition delay is detected as given in Figure 5.12. According to the conclusion of Khan et al. [1973] and Kook et al. [2006], low combustion temperature is another reason for high CO output. Kim et al. [2008] also pointed out that high CO could be detected even in the area of low equivalence rate when the temperature is between 800 K and 1400 K. Thus, the increased molar heat capacity in H_2O replacement cases results in lower combustion temperature and leads to higher CO output eventually. Unfortunately, the improvement of the NO_x -CO trade-off cannot be achieved by adjusting the EGR composition because the increased combustion temperatures in the CO_2 replacement cases also promote the formation of NO_x output. The drop of CO output in the H_2O replaced case with 2nd injection timing at -5 °CA ATDC is tend to be explained as the sufficient improvement of mixing, since there are no evidences for elevated combustion temperature for its late combustion phase in compression stroke.

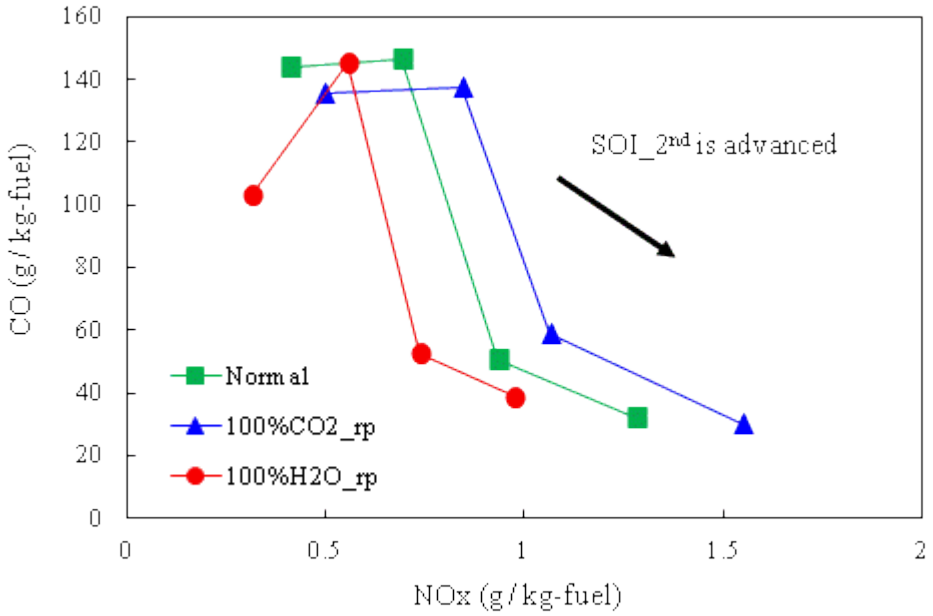

Figure 5.17 The trade-offs of NO_x and CO for the cases with different EGR compositions and varied 2nd injection timing

As given in Figure 5.18, though the unburned hydrocarbon also behaves reversed relation with NO_x emissions when varying the 2nd injection timing, the trade-off between NO_x and UHC can be improved by replacing the H_2O in EGR by CO_2 of same volume. With the 2nd injection timing after -15 °CA ATDC, the improvement is significant by the prolonged ignition delay and enhanced mixing. For the earliest 2nd injection timing, because the homogeneity of mixture is already at a relatively high level in the original case, the effect of EGR composition on mixing is less than the effect on combustion temperature. Therefore, the UHC is slightly lower in the CO_2 replaced case when the 2nd injection timing is advanced to -20 ° CA ATDC. The best trade-off between NO_x and soot is achieved in the H_2O replacement case when the 2nd injection timing is -15 °CA ATDC.

Figure 5.19 gives the ISFC for different EGR compositions against NO_x emission with varied 2nd injection timing. It is shown that adjusting EGR composition cannot achieve lower fuel consumption without elevated NO_x level. For earlier 2nd injection timing, significant reduction of NO_x is achieved together with notable sacrifice of ISFC about 20 g/KW ħ when the H_2O in EGR is replaced by CO_2. Referring to Figure 5.17 and 5.18, this significant increase of fuel consumption is derived from the reduced oxidation of CO owing to low combustion temperature. For the 2nd injection timing later than -10 ° CA ATDC, NO_x suppression can be achieved by using EGR of H_2O replacement without obviously increase of fuel consumption, because the unburned hydrocarbon is significantly reduced. Figure 5.17, Figure 5.18 and Figure 5.19 illustrate that the combustion efficiency is largely depended on the combustion temperature when using early 2nd injection timing where pre-combustion mixing is significant. The reduction

of NO_x with acceptable fuel economy penalty can only be realized by using EGR with H_2O replacement when the 2nd injection timing close to TDC, where mix-control takes the major part of combustion.

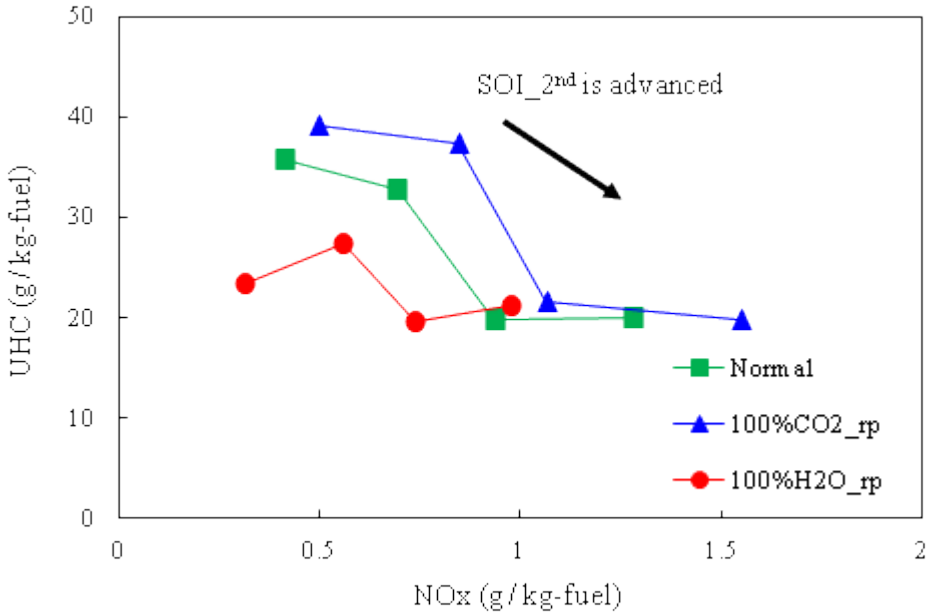

Figure 5.18 The trade-offs of NO_x and UHC for the cases with different EGR compositions and varied 2nd injection timing

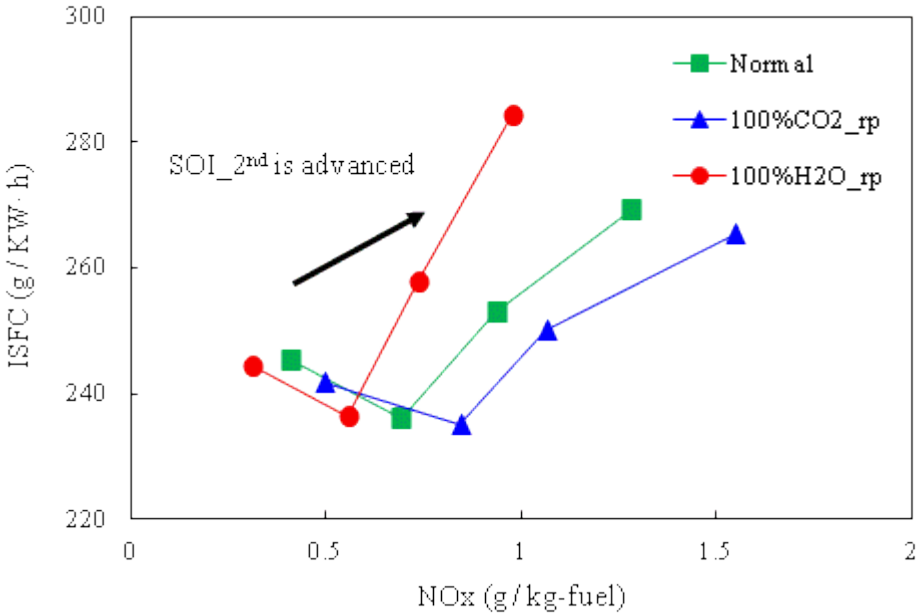

Figure 5.19 The trade-offs of NO_x and ISFC for the cases with different EGR compositions and varied 2nd injection timing

5.2.2 Sensibility to EGR Rate

For PPCI combustion, very high EGR rate is required to realizing the sufficiently prolonged

ignition delay and lower combustion temperature [Park and Bae, 2011]. Thus, the overall equivalence ratio in PPCI combustion is richer than that in conventional diesel combustion. Theoretically, according to the equivalence-temperature map introduced by Kamimoto and Bae [1988], intensively high EGR rate can be applied in PPCI combustion if it can be confined outside the NO_x -soot formation islands by suppressing the combustion temperature. The study of Akihama et al. [2001] showed that simultaneous avoidances of NO_x and soot were possible when the combustion temperature was suppressed by using EGR rate of 60%. Jacobs et al. [2005] demonstrated their automotive diesel engine running under PPCI combustion region with the overall equivalence ratio of 1.16. However, low operating load and high fuel economy sacrifice were also come up in these studies. In this section, the study about the effects of EGR composition is extended to two higher EGR level, i.e. 45% and 50%. The aiming is to find possible measures to achieve moderate fuel economic penalty under high diluted conditions.

The operating conditions for simulations are mostly same to that given in section 5.1, but with intake air of lower temperature, i.e. 360 K. Also, as mentioned above, the study is conducted under three EGR rates, which are 40%, 45% and 50%. They refer to three diluted levels whose equivalence ratios are 0.72, 0.81 and 0.95, respectively. With certain EGR rate, four cases with EGR constituent replacement (50% CO_2 / H_2O replacement, 100% CO_2 / H_2O replacement) and one original case are simulated for investigation. As stated in the studies of Ladommatos et al. [1996; 1997], the dilution effects was the most significant factor that influence the combustion characteristics. Accordingly, Figure 5.20 shows that the start of combustion is almost linearly retarded as the EGR rate is increased for each EGR composition. However, the contribution of the increased thermal effect cannot be neglected. Since CO_2 has higher thermal effect than H_2O of same volume, much steeper trend of the combustion start against EGR rate is observed as the fraction of CO_2 in EGR increases. When the CO_2 in EGR is completely replaced by H_2O, the difference of combustion starts between the highest EGR case and Lowest EGR case is about 1 crank angle. For the 100% H_2O replaced case, the difference of combustion starts is almost 3 crank angles. Meantime, the increased molar heat capacity results in prolonged ignition delay with same EGR rate when the H_2O in EGR is replace by CO_2 of same volume. As the EGR level is elevated, the increase of ignition delay is enhanced since the actual inlet charge specific heat is increased. It means, with same dilution level, the ignition delay can be adjusted for 3 to 4 crank angles by varied EGR compositions. With EGR level of 50%, a shortening of ignition delay is observed when the replacement of H_2O is increased to 100%. Actually, the accumulated heat release at its 10% burn location is much lower than in other cases because of incomplete combustion which will discusses bellow. For same level of accumulated heat release, its combustion start should be adjusted to around 7.5 °CA ATDC.

The effects of EGR composition on combustion duration are given under three EGR levels, as

shown in Figure 5.21. In the original case, the duration of combustion is shortened slightly when the EGR rate is increased from 40% to 45%. When the EGR rate is further increased to 50%, though the combustion duration is prolonged, it's shorter than that in 40% EGR case. It reveals that the combustion rate is accelerated owing to the enhanced pre-combustion mixing by prolonging ignition delay, though the reduced oxygen availability and higher specific heat capacity is resulted by elevated EGR rate. Similar trend of combustion duration respecting to EGR rate is observed in 50% CO_2 replaced case. When the CO_2 is completely replaced by H_2O, higher combustion temperature is implied due to the decreased heat capacity. In this case, combustion duration decreases linearly with the increased dilution level. For H_2O replacement case, the combustion duration is prolonged excessively when using higher EGR rate because of its thermal effect. With 50% EGR rate, 100% H_2O replacement results a significant long combustion duration about 40 crank angle. It implies excessively low combustion temperature, low heat release rate and low thermal conversion efficiency.

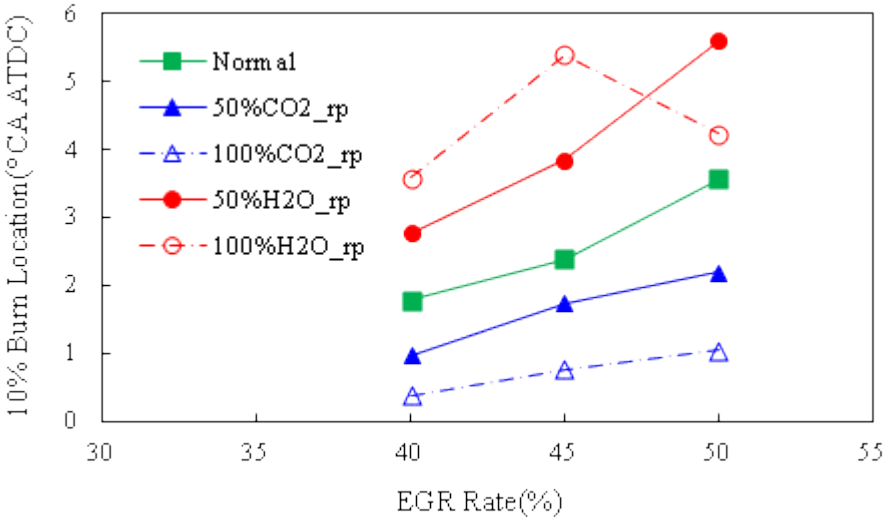

Figure 5.20 The effect of EGR composition on the start of combustion at three EGR rates

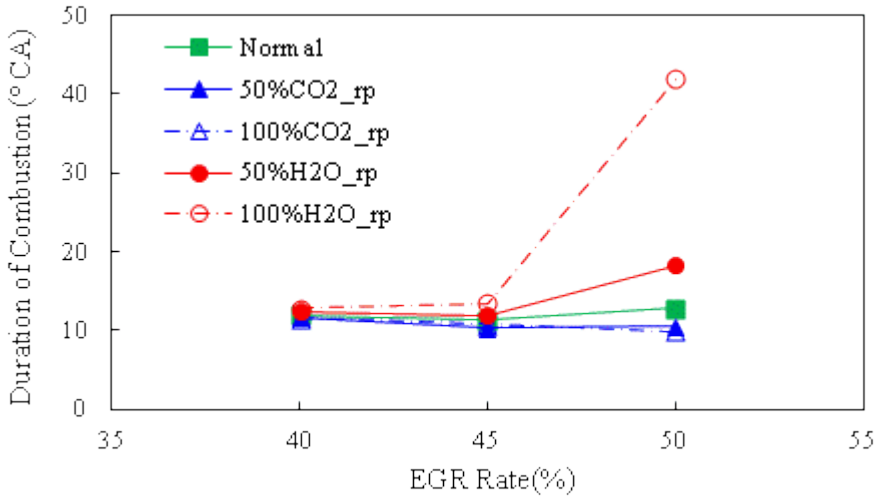

Figure 5.21 The effect of EGR composition on the duration of combustion at three EGR rates

The fuel consumptions are given against the combustion phase locations for different EGR compositions of three EGR rates, as shown in Figure 5.22. The effects of EGR rate and EGR composition on combustion phase location are similar to the conditions of combustion starts. Increased EGR rate results retarded combustion phase location; while the retardation is enhanced as the fraction of CO_2 in EGR is increased. Extremely retarded combustion phase is observed for EGR rate of 50%, when using 100% H_2O replacement, because its slow combustion rate owing to the very low combustion temperature. Though the combustion phase location gets more unfavorable for thermal conversion efficiency as the CO_2 fraction increases, low fuel consumptions are achieved in the case using 45% EGR rate with 50% H_2O replaced, and 50% EGR rate with 100% H_2O replaced. For relatively low dilution level of 40% EGR rate, fuel consumption can be improved by replacing CO_2 in EGR by H_2O. As mention before, the combustion efficiency is signification deteriorated when using 100% H_2O replacement at 50% EGR rate. In this highly diluted combustion, excessively reduced combustion temperature resulted by higher heat capacity and the cooling effect of combustion chamber volume expansion is considered as the reason for this poor combustion. Therefore, massive emissions from incomplete combustion are expected in this case.

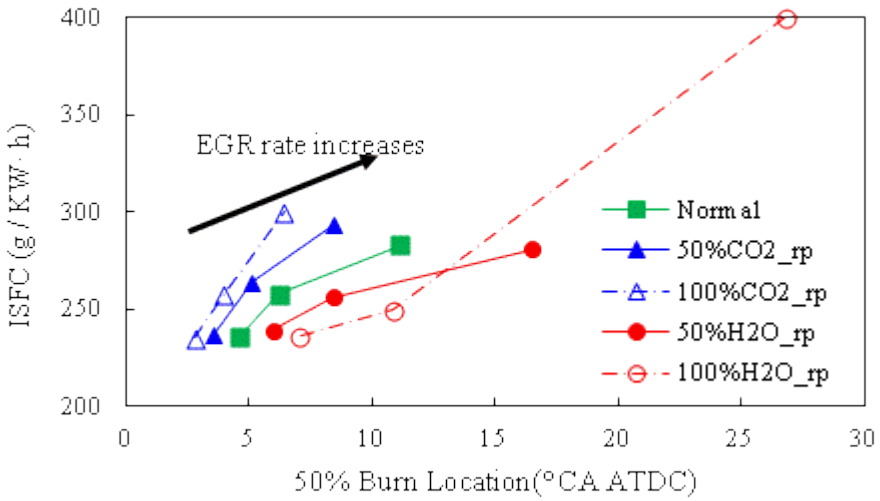

Figure 5.22 The ISFC respects to the combustion phase location for the cases with different EGR compositions of three EGR rates

As shown in Figure 5.23, the effects of EGR rate on the trade-offs between NO_x and soot are similar for different EGR compositions. When the EGR rate is increased from 40% to 45%, the NO_x emission is reduced significantly with the expense of slightly increased soot output. As the EGR rate further increased to 50%, simultaneously reduce of soot and NO_x is achieved. Meantime, the trade-off of NO_x and soot is shifted to lower level by using EGR of H_2O replacement. Referring to Figure 5.22, at EGR rate of 40%, around 30% reduction of NO_x and 50% reduction of soot are achieved by completely replacing the H_2O in EGR by CO_2, with only

small penalty in fuel consumption. Although near zero NO_x and soot is observed in 50% EGR case with 100% H_2O replacement, the dramatically high ISFC makes this case unacceptable.

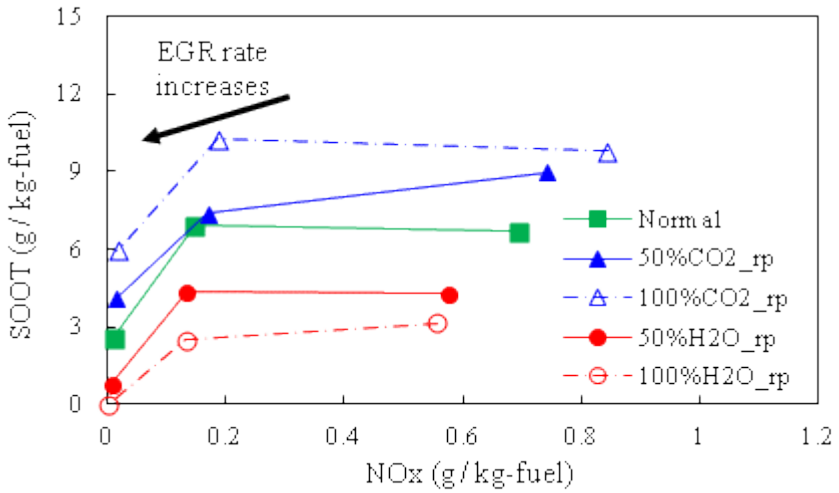

Figure 5.23 The effect of EGR composition on the trade-offs of NO_x and soot at three EGR rates

Figure 5.24, 5.25 and 5.26 give the trades-off of NO_x -CO, NO_x -UHC and NO_x -ISFC with varied EGR rate of different EGR compositions, respectively. The three trade-offs are similar since they all reveals the level of combustion completion. Higher dilution level always results reduced NO_x emission together with expense of increased incomplete combustion products or fuel consumption. By replacing the H_2O in EGR with CO_2, the trade-off can be shifted to lower level. Therefore, under same dilution level, the combustion completion level can be improved by increase the thermal effects of EGR, because the pre-combustion mixing is enhance by prolonged ignition delay owing to the higher heat capacity. However, with extremely high dilution which formatting near stoichiometric mixture, EGR of high heat capacity may result excessively low combustion temperature and seriously incomplete combustion. Therefore, high level outputs of CO and UHC are also detected in this case.

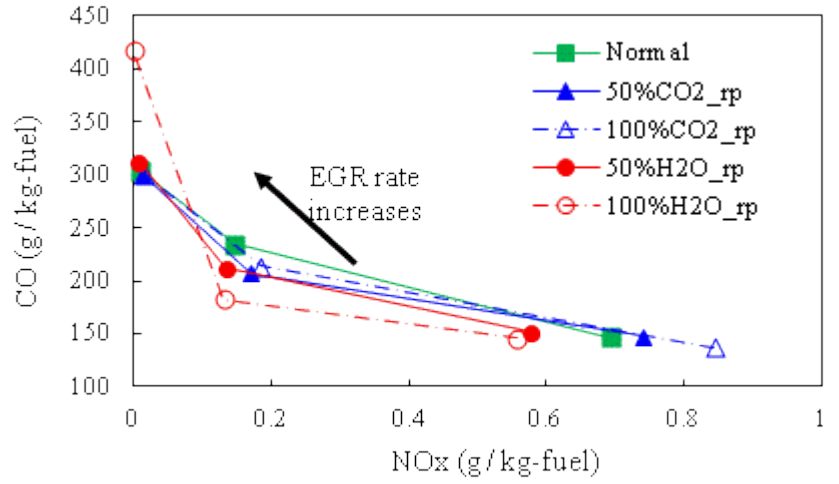

Figure 5.24 The effect of EGR composition on the trade-offs of NO_x and CO at three EGR rates

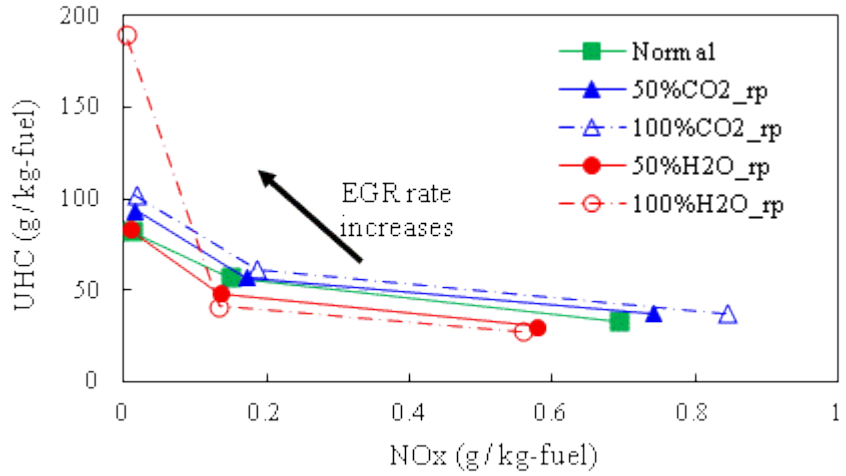

Figure 5.25 The effect of EGR composition on the trade-offs of NO_x and UHC at three EGR rates

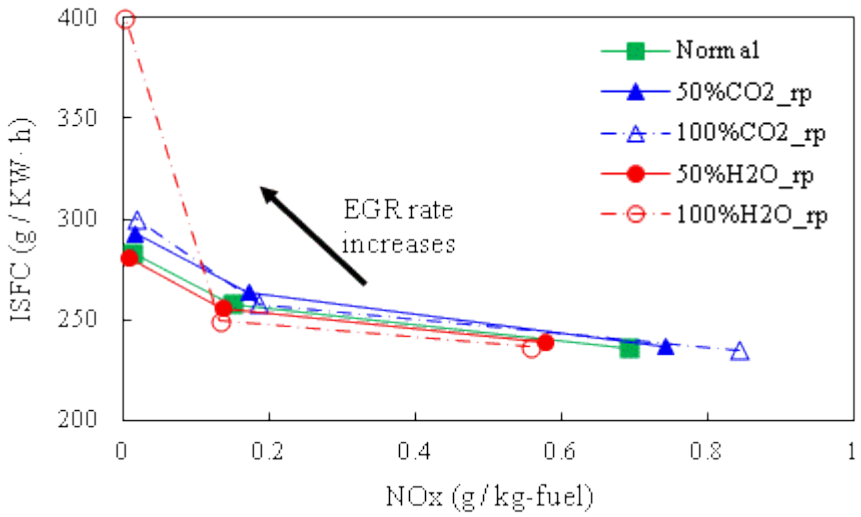

Figure 5.26 The effect of EGR composition on the trade-offs of NO_x and ISFC at three EGR rates

5.3 Summary

In this study, the effects of the two major constituents, i.e. CO_2 and water vapor, on combustion characteristics and emissions are numerically investigated. The effects of EGR with different fraction of CO_2 or H_2O are explored to compare the influence of these two constituents. Moreover, the parametric study is conducted under a sweep of the 2nd injection timing and EGR rate, in order to achieve understanding of the effects of CO_2 and water vapor in EGR at different operating modes.

The following conclusions have been derived from the investigations in this chapter:

1. Because of the higher molar heat capacity of CO_2, the start of combustion and combustion phase location are always retarded as the fraction of CO_2 in EGR is

increased. And a reduction of combustion temperature is detected. The effect of EGR composition on combustion duration is complicated because the combustion rate is determined by both mixing quality and combustion temperature. Though higher CO_2 fraction in EGR can result in prolonged ignition delay, the combustion rate may be suppressed by the reduced combustion temperature. Improved fuel consumption can be achieved by adjusting the EGR composition, but the parameter should be selected carefully according to the characteristics of combustion.

2. The trade-off between NO_x and soot can be improved by using EGR where the H_2O is replaced by CO_2 owing to the further reduced combustion temperature and enhance pre-combustion mixing. Accordingly, as the proportion of replacement increasing, the improvement becomes more significant. CO emission is not simply reduced by any constituent replacement unless the mixing enhancement is much more significant than the effect of reduced combustion temperature. Unburned hydrocarbon is reduced by H_2O replacement since the prolonged ignition delay intensified the mixing. Improved NO_x-ISFC trade-off is failed to achieve in this study because of the deteriorated thermal conversion efficiency due to poor combustion phasing.
3. For relatively early 2^{nd} injection timing, shortening of combustion duration can be achieved by H_2O replacement because the low-rate mix-controlled combustion region shrinks owing to the prolonged ignition delay. For late 2^{nd} injection timing, combustion rate is majorly determined by temperature. Thus, longer combustion durations are detected as the higher heat capacities in the H_2O replacement cases. Significant increase of fuel consumption is observed when the H_2O in EGR is replaced by CO_2 in typical PPCI combustion region. The deteriorated combustion efficiency owing to reduced combustion temperature is considered to be the reason.
4. The trade-off of NO_x -soot and the trade-off of NO_x -UHC are improved by using CO_2 replacing the H_2O in EGR. The improvement is significant when using relatively late 2nd injection timing, where the combustion is majorly controlled by mixing. The best trade-off of NO_x and soot is achieved in the H_2O replacement case when the 2nd injection timing is -15 °CA ATDC. The improvement of NO_x -CO trade-off is failed to achieve because the oxidation of CO requires higher combustion temperature.
5. For higher dilution level, the effects of EGR composition are enhanced. However, with extremely high dilution which formatting near stoichiometric mixture, EGR of high heat capacity may result in excessively low combustion temperature and seriously incomplete combustion.

Chapter 6 Operating Limits and Optimization of Thermal Conversion Efficiency in PPCI Combustion

The operating limit is one of the major concerns for the implementation of PPCI diesel combustion. In the meantime, plenty of studies have shown that one of the most important barriers for implementing PPCI in real car engine is its penalty in the fuel conversion efficiency because the combustion phase often locates away from the TDC since early or retarded injection timing is usually adopted. In this chapter, the speed range and load range for the PPCI diesel combustion using split injection are investigated. Based on the results of speed and load sweep, controlling method for adjusting the location of combustion phase is explored. Instead of varying the injection strategy, EGR rate and intake temperature are selected as the parameters to be adjusted for desired combustion location. With certain combination of EGR rate and intake temperature for adjusting combustion phase, the in-cylinder condition may not be perfect for realizing PPCI combustion and result in enlarged proportion of mixing-control combustion. To evaluate the degree of premixed combustion, the definition of Premixed Ratio (*PR*) is proposed in the last section of this chapter. Meantime, the relations between premixed ratio and fuel consumption or emissions are discussed.

6.1 Speed Transition

Firstly, the investigation about speed range is conducted at constant load in this section. As mentioned in the study of Lewander et al. [2009], the time for mixing is reduced when the speed increases. For same injection timing, injection pressure and fuel amount, the injection duration covers more crank angle, and the end of injection moves closer to TDC when increasing engine speed. These lead to different in-cylinder environment during injection and further affect the combustion process. Here, the effects of engine speed on combustion characteristics and emissions are discussed. Following, the EGR rate and intake temperature are adjusted to maintain the location of combustion phase at TDC.

6.1.1 Operating Conditions

The computational study in this section is conducted on the single cylinder HSDI diesel engine of same parameters as the one introduced in Chapter 4. The details of this engine are listed in Table 4.1.

The investigation on the speed limit is conducted by a sweep of speed at fix fuelling. The fuelling rate is 23 mg per cycle which can achieve maximum torque output around 100 N·m. The lowest speed is set to be 1500 rpm, and the engine speed is gradually increased to 2500 rpm with an interval of 200 rpm. The injection pressure is selected to be 110 MPa since it shows

overall advantages in all responses as discussed in Chapter 4. For split-injection strategy, both the 1st and 2nd injection timing are fixed, i.e. at - 40 °CA ATDC and -15 °CA ATDC, respectively. And 20% of the total fuel is injected in the 1st injection, while 80% in the 2nd injection. Initially, the moderate high level EGR rate of 40% is adopted with the intake air temperature of 380 K, which maintains the combustion phase location at TDC for the base case with speed of 1900 rpm. When adjusting the combustion phase location of another cases, the EGR rate and intake air temperature are varied. The detailed operating conditions for the speed tests are summarized in Table 6.1.

Table 6.1 The operating conditions for speed tests

Engine Speed	1500 ~2500 rpm (interval=200 rpm)
Maximum Torque	100 N ṁ
Boost Pressure	0.60 bar
The Fraction of Fuel in the 2nd Injection	80%
Injection timing	-40 °CA ATDC (1st), -15 °CA ATDC (2nd)
Injection Pressure	110 MPa
Spray Included Angle	120 °
Temperature at IVC	380 K (varied for adjustment)
EGR Rate	40% (varied for adjustment)

6.1.2 Speed Sweep

According to the operating conditions given in section 6.1.1, the overall equivalence ratio is constant during the speed sweep. Though the injection strategy and fuelling rate are also same, the developments of spray are different for varied engine speed. As speed increases, each crank angle covers shorter period in time domain. Therefore, since the injection duration takes same period in time domain, it increases in crank angle as the engine speeds up. For higher engine speed, larger piston moving distance and higher in-cylinder pressure and temperature in average are expected during injection. According to these factors, the ignition delay will shorten in time domain when engine speed increases. However, retardation in combustion phase is observed with increasing engine speed, as shown in Figure 6.1. Figure 6.2 gives the 10% burn locations (defined as start of combustion) and the ignition delays in time domain for different engine

speeds. The ignition delay decreases of about 0.15 ms from 1500 rpm to 2500 rpm. Meantime, the start of combustion retarded linearly respected to increased engine speed. Therefore, the time for mixing is less, and the combustion intends to take place in smaller chamber of higher pressure and temperature.

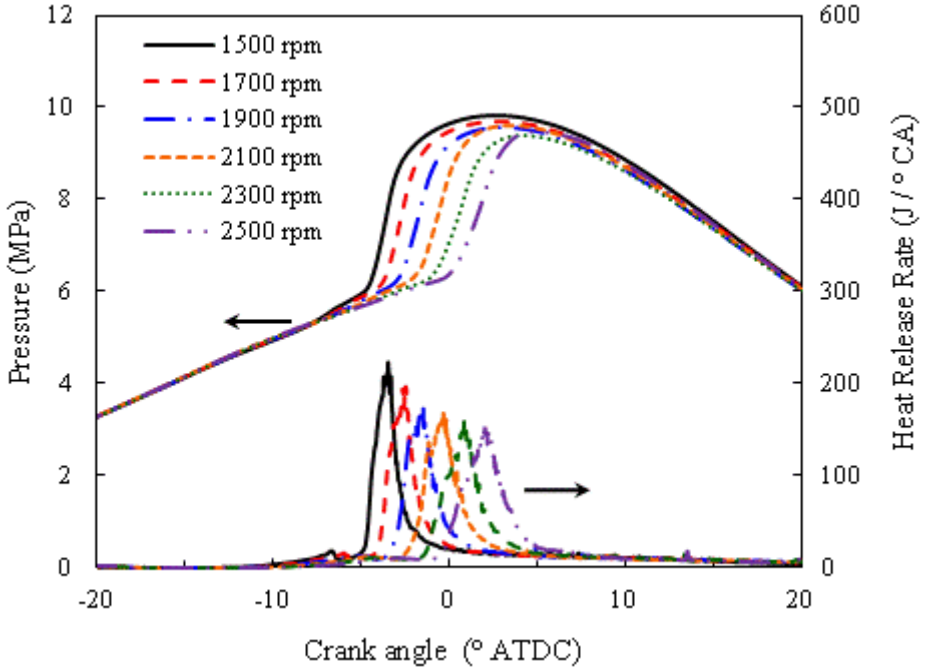

Figure 6.1 In-cylinder pressures and heat release rates at several different engine speeds

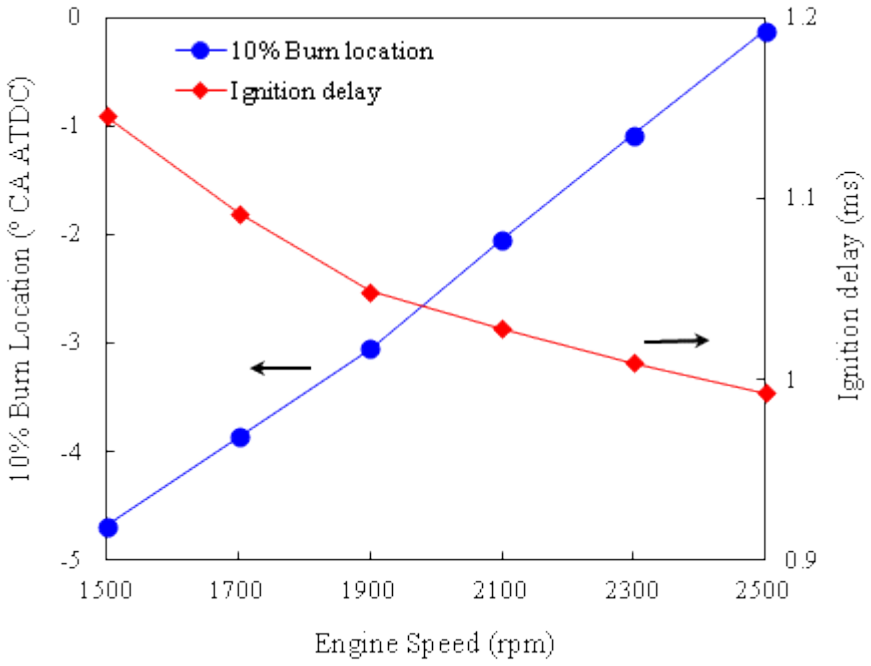

Figure 6.2 The starts of combustion and ignition delays at several different engine speeds

The peak pressures decreases slightly as engine speed increases, as shown in Figure 6.1. The

curve of pressure during combustion covers smaller range of crank angel for higher engine speed. This implies higher thermal conversion efficiency because the combustion conducts with smaller change of in-cylinder volume. When given in joule per crank angle, the heat release rate decreases, and its curve during combustion covers more crank angles as engine speed increasing. In the fact, because crank angle changes corresponding to a shorter period in time domain as engine speed increasing, the heat release rate is greater if plotted in J/ms for increased engine speed. For the same reason, the duration of heat release is shorter in time domain for higher speed. In average, the period covered by each crank angle decreases 40% as engine speed increasing from 1500 rpm to 2500 rpm. However, the reduction in peak heat release rate is around 30%, as shown in Figure 6.1. Therefore, more intensive heat release is expected for higher speed engine if the plot is given in J/ms.

The fuel consumptions for different engine speeds against combustion phase locations are shown in Figure 6.3. Generally, increased engine speed results in retarded combustion phase and decreased ISFC. As discussed above, the more intensive heat release is considered to be one of the major reasons for improved fuel economy at high engine speed. Though shorted ignition delay is shown in time domain, the process of injection is closer to TDC as engine speed increase. Therefore, the bulk-air has higher temperature which is beneficial for mixing and fuel evaporation. Also, enhance in-cylinder air motion coming from the accelerated piston speed improves the fuel-air mixing. As the combustion retards, the increased in-cylinder pressure improves combustion efficiency. Referring to Figure 6.1, higher thermal conversion efficiency is expected to further reduce the fuel consumption, because the combustion for higher engine speed processes under smaller change of in-cylinder volume.

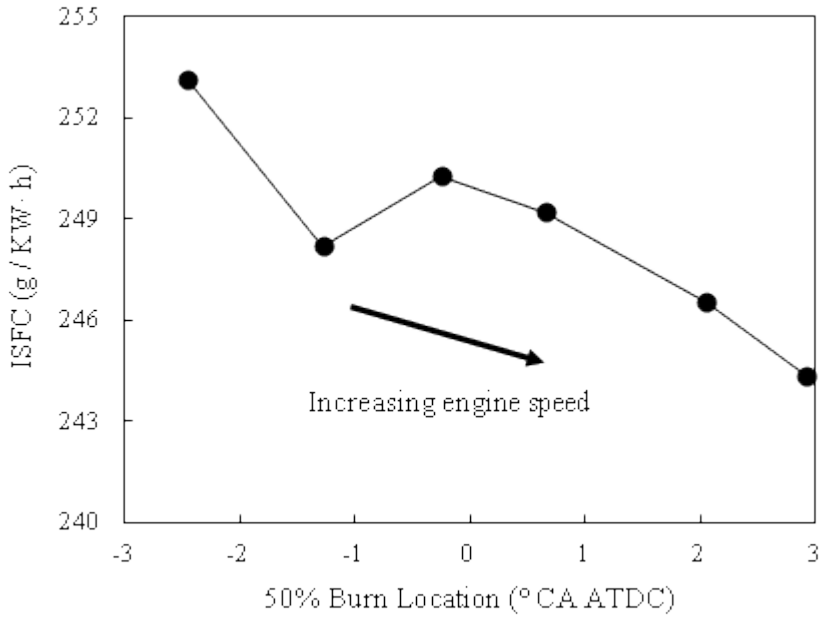

Figure 6.3 The ISFC respects to the combustion phase location for the cases at different speeds

Figure 6.4 illustrates the effect of engine speed on NO_x and soot emissions. Tranditional trade-off bewteen NO_x and soot is observed as engine speed increase. The NO_x emission decreases and the soot emission increases with engine speed. According to Figure 6.2, the decreased ignition delay in time domain leads to less time for mixing before ignition with increased engine speed. Moreover, the injection duration increases with engine speed, and the end of injection is closer to TDC. Thus, the injection takes place in a smaller volume which hinders the difussion of spray. The reduction of NO_x emission is detedted as the leaner area lessens with engine speed. The increased local equivalence ratio and together with the relatively higher in-cylinder temperature in average is respondsible for the increase of soot formation. Additionally, Keeler and Shayler [2008] considers that the shortened time period of reaction results decreased time for soot oxidation with increasing engine speed. As shown in Figure 6.5, the peak value of soot is only slightly higher at 1700 rpm and 2500 rpm, comparing to that at 1500 rpm. At 1900 rpm, 2100 rpm and 2300 rpm, the peak soot is even lower. However, the oxidation rate decreases significantly as the engine speed increases. And higher output of soot is eventually resulted due to the reduced oxidation rate with increased engine speed.

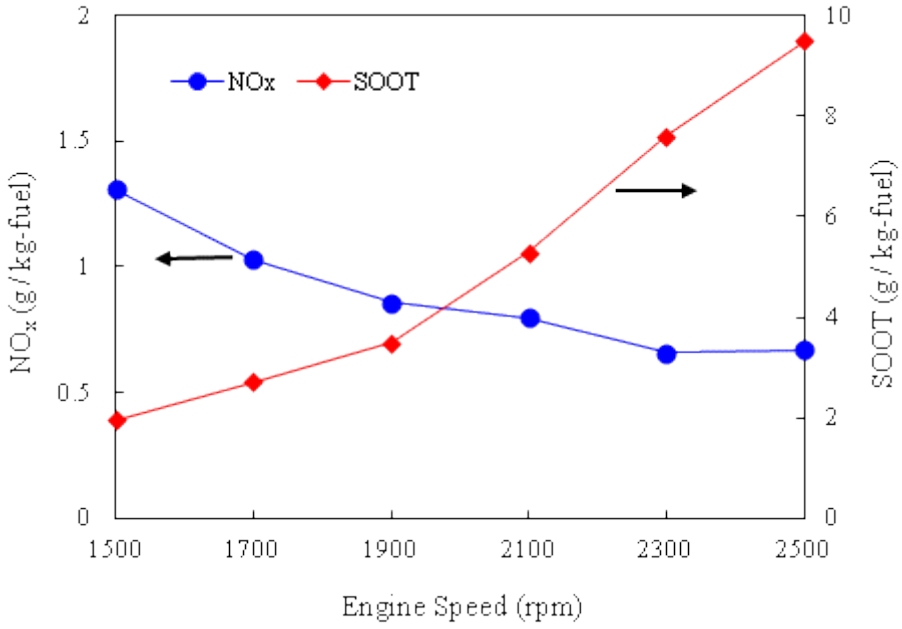

Figure 6.4 Effects of engine speed on NO_x and soot emissions

As shown in Figure 6.6, both CO and unburned hydrocarbon (UHC) increase with engine speed. The increasing of emission is almost 100% for CO and 40% for UHC when engine speed increases from 1500 rpm to 2500 rpm. With the significant increases of these two incomplete combustion emissions, reduced combustion efficiency is predicted, which is in contrary with the results shown in Figure 6.3. The decreased time for mixing in time domain is considered as the reason for the increases of CO and UHC. Similar to the formation of soot, the reduced time for oxidation is another reason for the increase in CO emission when engine speed increases. For

UHC emission, here only the fuel in cylinder is taken in count, while the fuel adhering to wall is not considered. In fact, because the injection takes place during more crank angles and in relatively higher in-cylinder temperature at higher engine speed, the fuel on cylinder wall is much less. This also explains why significant deterioration in fuel economic is not observed at high engine speed.

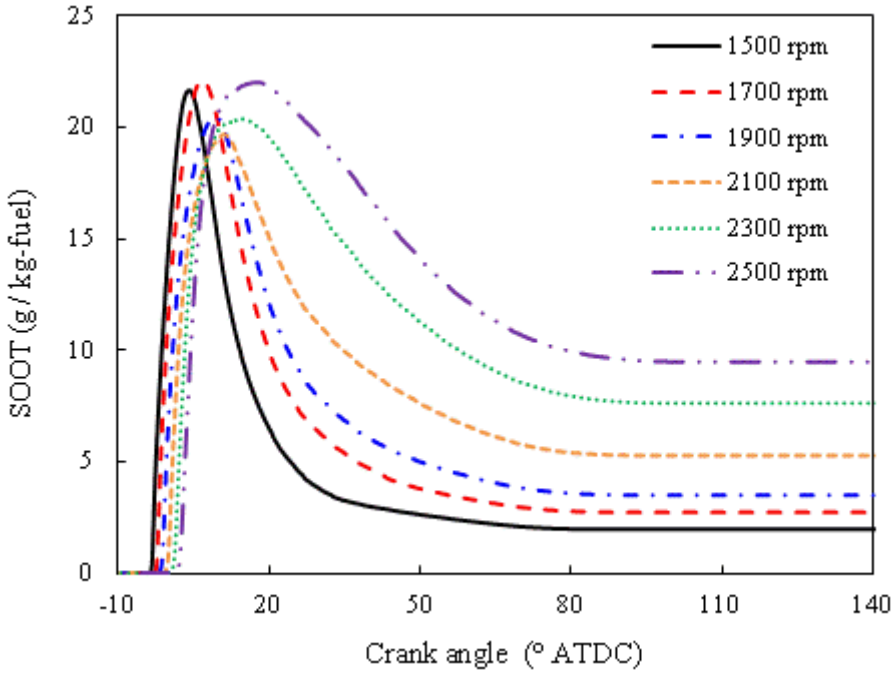

Figure 6.5 The traces of soot formation for different engine speeds

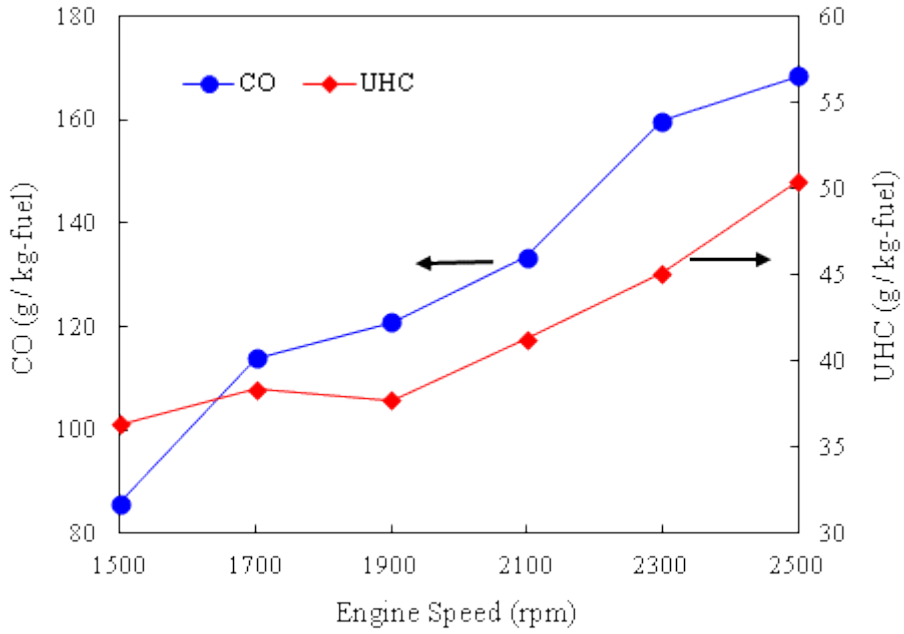

Figure 6.6 Effects of engine speed on CO and UHC emissions

6.1.3 Optimization for Speed Transition

Plenty of studies have shown that one of the most primary barriers for implementing PPCI in real car engine is the penalty in thermal conversion efficiency. Lee et al. [2006] shows that the thermal conversion efficiency is mostly determined by the location of combustion phase. They also show that slightly improvement of fuel consumption can be achieved by phasing optimization. Usually, TDC is considered to be the thermodynamically efficient location for combustion [Keeler and Shayler, 2008]. In this study, 50% burn location is adopted as the indicator of combustion phase. For this indicator, TDC is suitable for the optimal location. Normally, injection strategy is the most effective and commonly used method for adjusting combustion phase location. However, the combustion mode is also highly sensitive to injection strategy. For the PPCI diesel combustion achieved by early injection, the location of combustion is usually advanced from the TDC. If retarding the injection timing to delay the combustion, significant improvement in fuel consumption may not be realized since the combustion is likely to process under mix-controlled combustion [Lee, 2006]. Therefore, intake temperature and EGR rate are selected to be the factors to optimize the combustion phasing. The intake temperature influences the combustion phase location by adjusting the in-cylinder temperature which determines the timing for ignition. The EGR rate directly affects the global equivalence ratio and the heat capacity of mixture in cylinder, and further influences the ignition timing and combustion rate.

Table 6.2 gives the parameters for the adjustment of combustion location. The initial 50% burn location is resulted from the sweep of engine speed, as plotted in Figure 6.3. The combustion locates before TDC until the engine speed up to 2100 rpm. Thus, retarding combustion is the major object for these cases. By decreasing the intake temperature, it is possible to delay ignition. However, the combustion location is not very sensitive to the intake temperature. At 1500 rpm, about 70 K reduction is required to adjust the combustion location at TDC. Though increase intake air flow accompanies the reduced intake temperature, the reduced equivalence ratio does not improve the combustion efficiency because the excessively low temperature results serious wall film and reduced oxidation rate of CO. Then increased EGR rate is adopted to retard combustion phase location. For the engine speed higher than 2100 rpm, the original locations of combustion phases are retarded from TDC. Although increasing intake temperature may shorten the ignition delay, it also leads to reduced intake air flow. Consequently, the penalties in combustion efficiency and soot formation get serious due to the increased equivalence ratio. Therefore, the combustion phase locations are moved up by reducing the EGR rate. After the adjustment, with constant fuelling rate, the equivalence ratio decreases with engine speed.

Table 6.2 Parameters for adjusting combustion phase location at different engine speeds

Speed (rpm)	Intake temperature (K)	EGR rate (%)	Initial 50% burn location (ºCA ATDC)	Equivalence ratio
1500	370	45	-2.46	0.853
1700	380	42	-1.28	0.823
1900	380	40	-0.25	0.785
2100	380	40	0.65	0.785
2300	380	35	2.05	0.711
2500	380	25	2.92	0.618

The thermal conversion efficiency represents the fraction of thermal energy that converses to mechanical work. As shown in Figure 6.7, for the original sweep of engine speed, no significant variations are observed in thermal conversion efficiencies which range from 44% to 45%. In fact, the thermal conversion efficiencies are less than real because the simulations are conducted between the IVC till the exhaust valves opening. Therefore, more than 44% of thermal energy is converted into mechanical work for these cases. Minor increase of thermal conversion efficiency can be found with increased engine speed, which is about 0.5% for the combustion phase location range from - 2.46 ºATDC to 2.92 ºATDC.

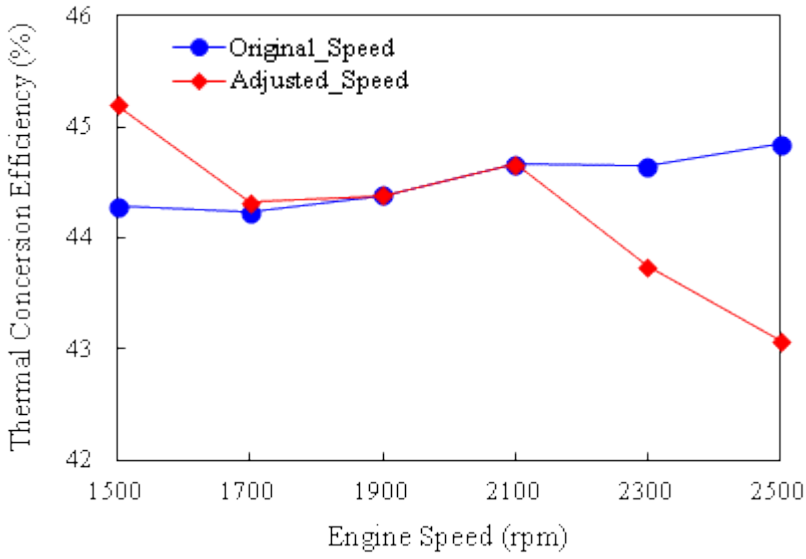

Figure 6.7 Thermal conversion efficiencies at different speeds for the cases of original and after adjustment

After the optimization of combustion phase location, the improvements in thermal conversion efficiency are not that efficient as expected. About 1% in improvement is detected at 1500 rpm, whose combustion location is retarded for about 2.4 crank angles. 1% and 1.5% decreases in thermal conversion efficiency are shown at 2300 rpm and 2500 rpm respectively after advancing their combustion phase locations. According Figure 6.8, the combustion duration is increased for about 20% after adjustment at 2500 rpm. This means less heat is released closer to TDC as expected. Therefore, the extended combustion duration deteriorates the gain from optimal combustion phase location.

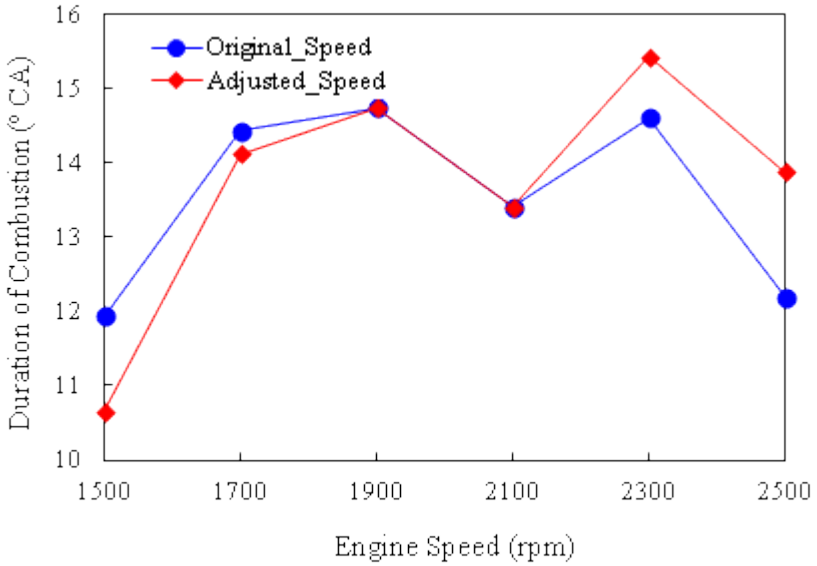

Figure 6.8 Combustion durations at different speeds for original engine speed sweep and after adjustment

Besides the thermal conversion efficiency, the influences of optimizing combustion phase location on fuel consumption and emissions are important for investigation. The fuel combustion can represent the overall efficiency of engine operation. Figure 6.9 gives the ISFC at different speeds after the optimization of combustion phase location. Unfortunately, the variations of fuel consumption from original cases show inverse responds of thermal conversion efficiency. Therefore, the efficiency which represents the fraction of fuel energy converted to thermal energy need to be discussed. The heat rejection efficiency is the sum of combustion efficiency and heat loss efficiency. It represents the quantity and quality of the thermal energy released. As shown in Figure 6.10, no significant variations of heat rejection efficiency are observed for the original sweep of engine speed. And the largest variation is about 1.5%. Referring to Figure 6.7, small variations in both heat rejection efficiency and thermal conversion efficiency result the small changes in fuel consumption in the original sweep of engine speed, as shown in Figure 6.3. During the adjustment, the increased EGR rates lead to the reduction of heat rejection efficiency at 1500 rpm and 1700 rpm. The decreased combustion

efficiency due to increased equivalence ratio and reduced combustion temperature is deemed to responsible for it. Conversely, improved heat rejection efficiencies are achieved by reducing EGR rates at 2300 rpm and 2500 rpm. Therefore, the larger changes in heat rejection efficiency determine the trend of variations in fuel consumption.

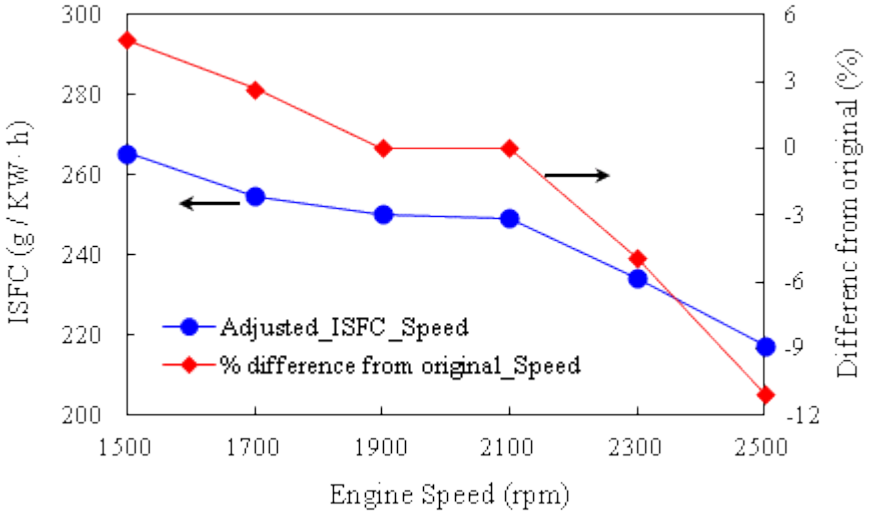

Figure 6.9 Fuel consumptions at different speeds after adjustment and their differences from original

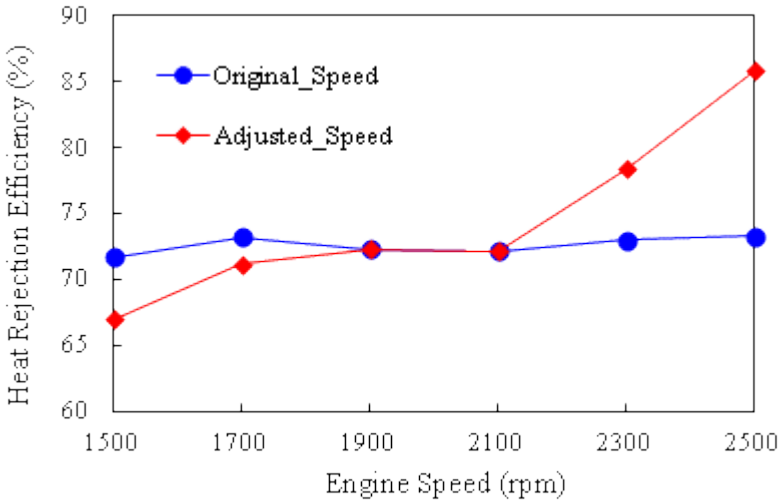

Figure 6.10 Heat rejection efficiency at different speeds for original engine speed sweep and after adjustment

Figure 6.11 to Figure 6.14 give the major emission at different speeds after the optimization of combustion phase location. Because NO_x emission is highly sensitive to the oxygen availability, the reduced EGR rates result significant increase of NO_x at 2300rpm and 2500 rpm, as shown in Figure 6.11. Therefore, NO_x emission constrains the optimization of combustion phase location with varied engine speed. Soot emission is reduced no matter the combustion phase is advanced or retarded during the optimization, as given in Figure 6.12. Increased EGR rate suppresses soot

formation by lowing combustion temperature, while reduced EGR rate achieves soot reduction by increase oxygen availability. The trends of CO emission and UHC emission are similar to that of ISFC, as shown in Figure 6.13, Figure 6.14 and Figure 6.9, respectively. The combustion efficiency is determined on the formation of these products of incomplete combustion, which are highly sensitive to EGR rate. Therefore, the optimization of combustion phase location is constrained by NO_x formation and combustion efficiency.

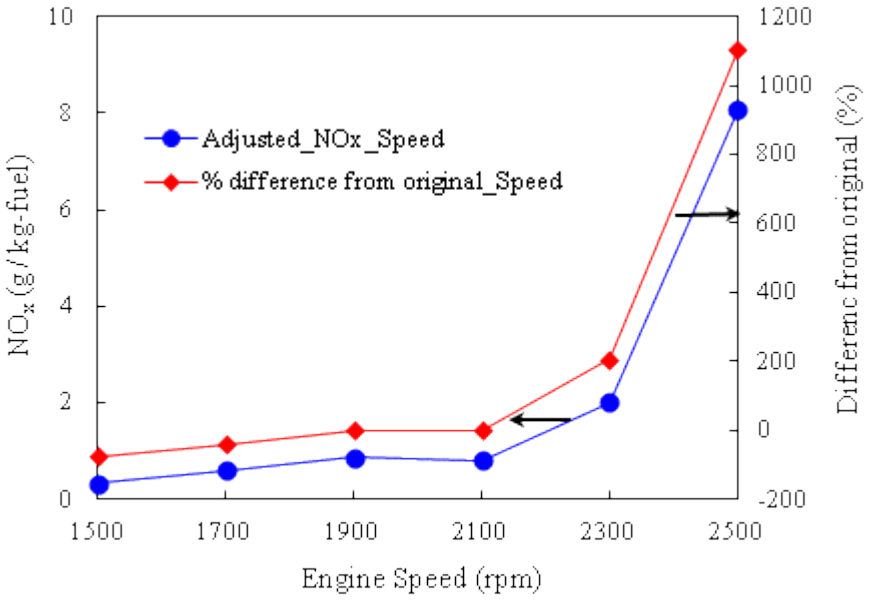

Figure 6.11 NO_x emissions at different speeds after adjustment and their differences from original

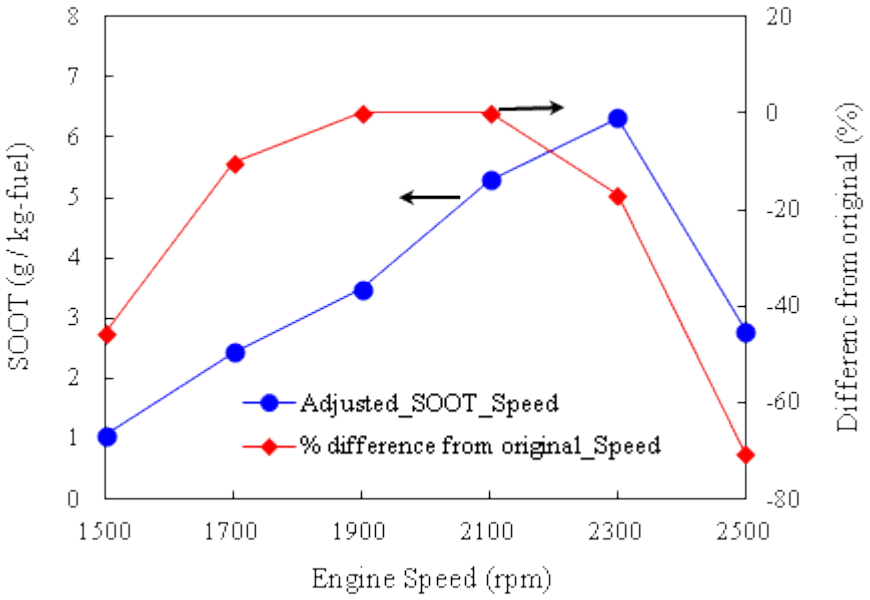

Figure 6.12 Soot emissions at different speeds after adjustment and their differences from original

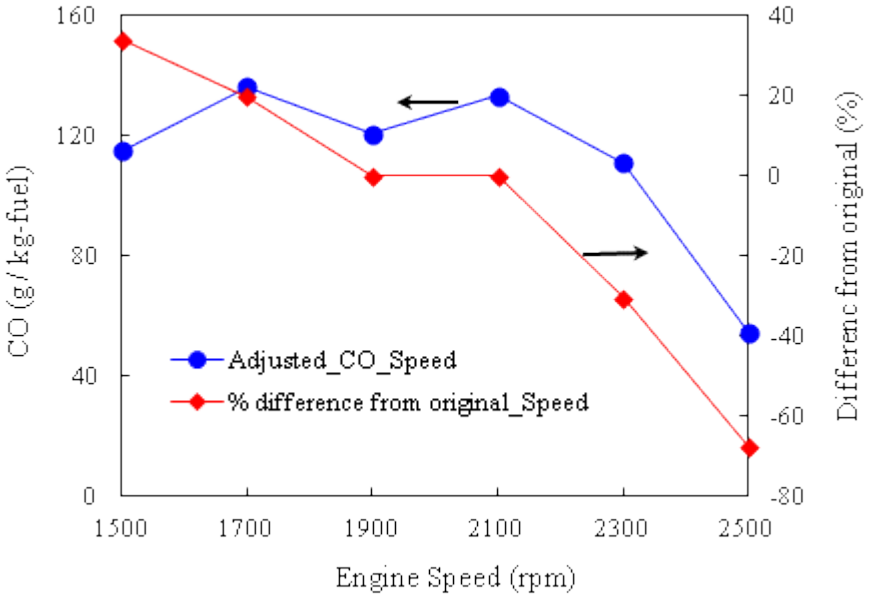

Figure 6.13 CO emissions at different speeds after adjustment and their differences from original

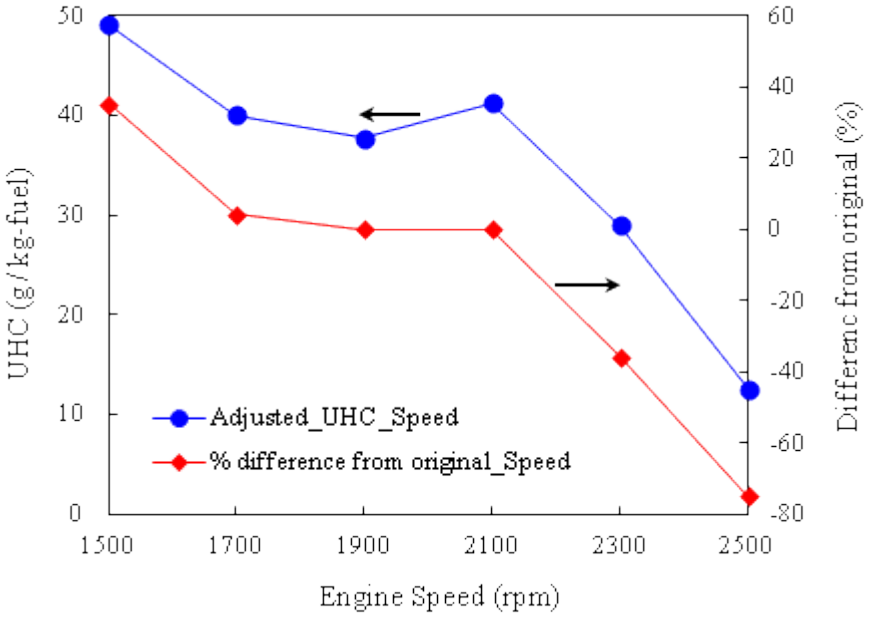

Figure 6.14 UHC emissions at different speeds after adjustment and their differences from original

6.2 Load Transition

Because the application of high level EGR, the engine load is limited for PPCI diesel combustion due to the relatively lower combustion temperature and the reduced oxygen availability. Although PPCI combustion can realize rich combustion with simultaneously reduced NO_x and soot emission by restricting the temperature inside fuel jet, the fuelling rate is still suppressed [Friedrich et al., 2006]. Therefore, the studies about PPCI combustion are

mostly conducted under part load. The study of Lewander et al. [2009] has proved that the PPCI operating range is limited by the emission criteria. In their study, 30% of maximum load as conventional combustion at low speed and 21% of maximum load as conventional combustion at high speed are achieved in PPCI diesel combustion. More importantly, they show that reducing EGR temperature can enlarge the operating range significantly. In this section, the effects of engine load on combustion characteristics and emissions are discussed. Similar to the study of speed limit, the EGR rate and intake temperature are adjusted to maintain the location of combustion phase at TDC for different engine loads.

6.2.1 Operating Conditions

For the numerical study of engine load, most of the operating conditions are similar to those listed in the Table 6.1 but with varied fuelling rates. Besides the standard load level of 100 N·m, both lower load and higher load output are intended to consider. However, With same intake temperature and EGR rate listed in the Table 6.1, the equivalence ratio of the case will over 1 once the load is higher than 120 N·m. Large fraction of unburned fuel and significant low combustion efficiency will come out in the cases with load higher than 120 N·m. Therefore, only three levels of load, i.e. 50 N·m, 75 N·m and 100 N·m, are studied during the sweep of load. The cases with higher level of load, i.e. 125 N·m and 150 N·m, will be investigated in the section of the optimization for load. All of these engine loads will be studied at three typical engine speeds, which are 1500 rpm, 1900 rpm and 2500 rpm, represent low speed, moderately high speed and excessively high speed. The injection strategy is kept same as that given in Table 6.1, but the fuel amounts in the 1^{st} injection and 2^{nd} injection are different for varied engine loads. With same injection pressure and similar in-cylinder environment, the injection duration increases with engine load. High level EGR is maintained in order to achieve long ignition delay and low combustion temperature.

6.2.2 Load Sweep

The in-cylinder pressures and heat release rates for increased fuelling rate at 1900 rpm are illustrated in Figure 6.15. Retarded combustion is observed as the fuelling rate increases. Though more fuel is injected in both 1^{st} injection and 2^{nd} injection, the enriched mixture does not accelerate the oxidation reaction. The increased fuel absorbs more heat during evaporation and leads to decrease of in-cylinder temperature which eventually results delaying of ignition. The pressure increases with load since more heat is released during combustion and the location of combustion is much closer to the TDC.

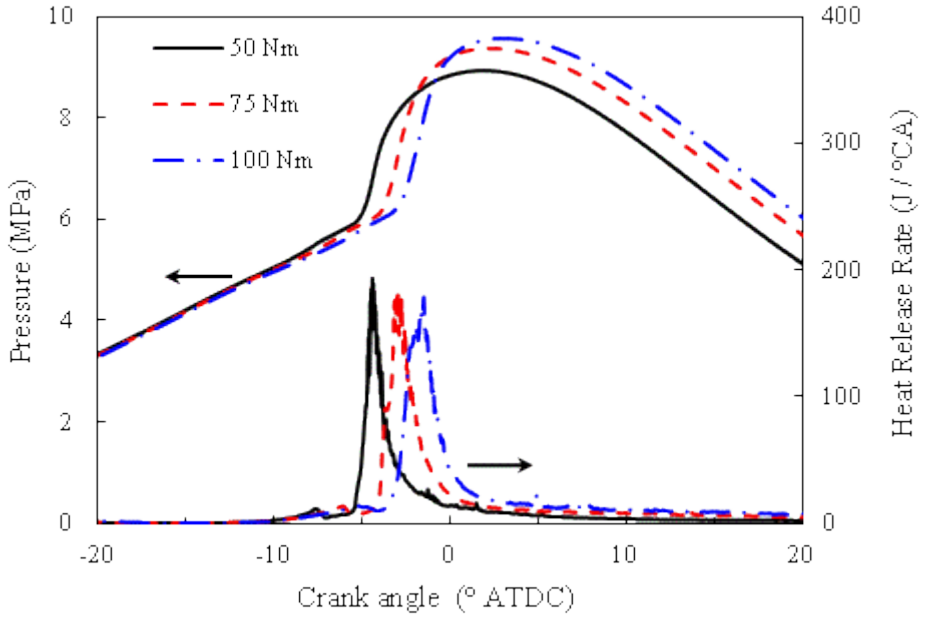

Figure 6.15 In-cylinder pressures and heat release rates for several different engine loads at 1900 rpm

At current operating conditions, fuel consumption increases monotonically with engine load, while combustion phase location retards simultaneously, as shown in Figure 6.16. The incomplete combustion due to rich equivalence ratio causes the significant deterioration in fuel consumption. Although the bulk-gas temperature is higher when more energy released with increased fuelling rate, the benefit for enhancing the oxidations of HC and CO is compensated by the reduced oxygen availability with increased equivalence ratio. Moreover, increased heat loss to cylinder walls and residual heat in exhaust gas due to higher in-cylinder temperature decreases the heat loss efficiency and further increases fuel consumption. Furthermore, the extended combustion duration causes reduction in thermal conversion efficiency due to the expanded variation of combustion volume [Fang et al., 2006]. As fuelling rate increases, lower bulk-air temperature after injection delays the combustion phase. The extended combustion duration also make the 50% burn location retarded. As engine speed increases, the relation between fuel consumption and combustion phase location with engine load does not change but translates in the plot. As discussed in previous section, the engine speed has small effect on fuel consumption. Its influence in combustion phase location is more obvious and translates the trend of fuel consumption against combustion phase location with engine load for about 4 crank angles (1500 rpm to 2500 rpm).

The trade-off between NO_x and soot with increased engine load is illustrated in Figure 6.17. Though greater heat release from increased fuelling leads to higher combustion temperature and maintains the condition of higher temperature for longer time, NO_x emission decrease with engine load. Therefore, higher local equivalence ratio due to the insufficient mixing for

increased fueling amount is considered responsible for suppressing NO_x formation. Conversely, the increased engine load results signification increasing of soot emission due to the reduced oxygen availability. The severity of soot increase depends on engine speed. At lower engine speed, the trend of NO_x-soot trade-off with increased engine load is more flat. The margin of soot increase is significantly smaller than the margin of NO_x decrease when the engine load increases from 50 N·m to 100 N·m at 1500 rpm. As engine speed increases to 2500, the reduction in NO_x emission is accompanied with larger margin of soot increasing with increased engine load. Moreover, the trade-off of NO_x and soot shifts up with increased engine speed. Therefore, the trade-off between NO_x and soot becomes a more serious issue at high speed.

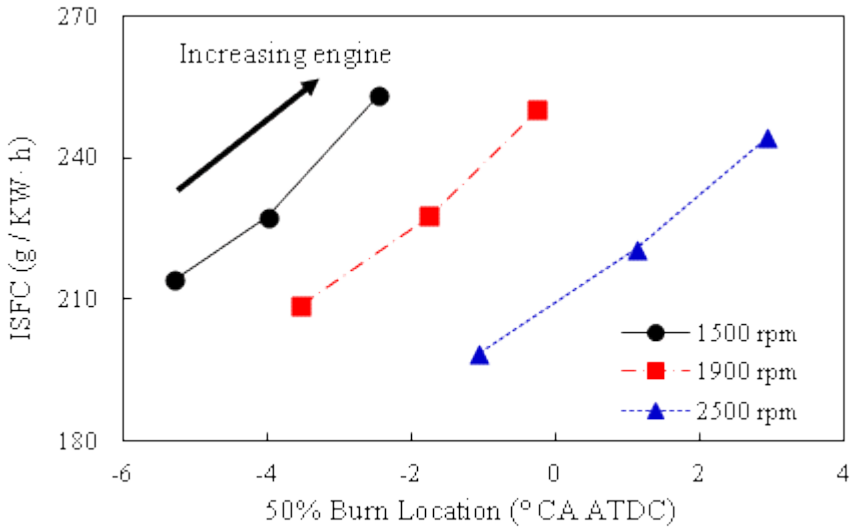

Figure 6.16 The ISFC respects to the combustion phase location with increased engine load at 1500 rpm, 1900 rpm, and 2500 rpm

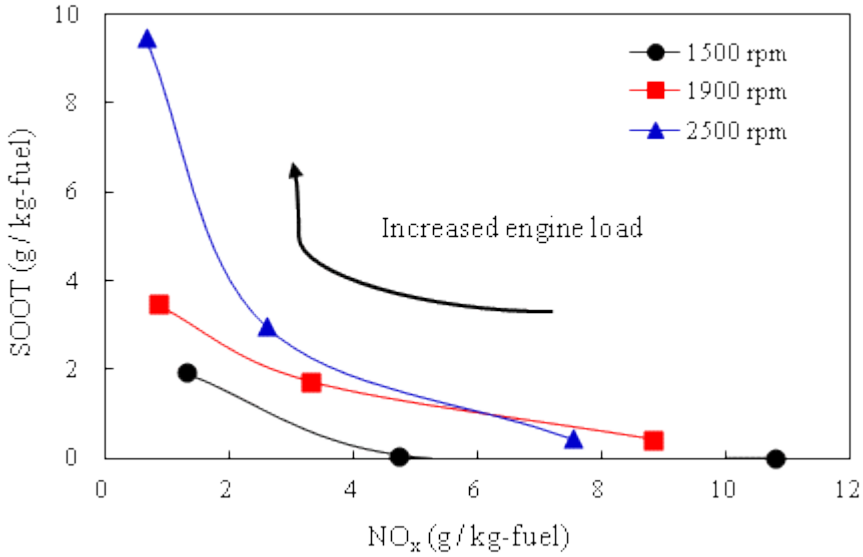

Figure 6.17 The trade-offs of NO_x and soot with increased engine load at 1500 rpm, 1900 rpm, and 2500 rpm

As shown in Figure 6.18 and Figure 6.19, the increased CO and UHC emissions reflect deteriorated combustion efficiency with increased engine load. These two emissions from incomplete combustion show similar trend with engine load. When the load is increased from 50 N·m to 75 N·m, no manifested increases in CO and UHC are observed at any engine speed. Even slightly decrease in CO emission is detected at low engine speed. At 75 N·m, the overall equivalence ratio is about 0.52, which is still considered as "very lean" condition. The reduction in oxygen availability acts no significant influence on oxidation rate. The higher in-cylinder temperature resulted from increased fuel energy improves the completion of combustion at higher engine load. When engine load increases further to 100 N·m, massively increases are observed in both CO and UHC emissions. The studies of Keeler [2008] and Lee et al. [2006] also show that 0.75 is a threshold equivalence ratio. Once the actual equivalence ratio is over that, fuel consumption begins to deteriorate because the mixture is too rich to sustain complete combustion, and CO and UHC increase dramatically. Therefore, the higher fuel consumption at high engine load is mostly from the incomplete combustion under higher equivalence ratio. The trend of CO emission with engine load is much more sensitive to engine speed than UHC. This also proves that reduce time for oxidation is the major reason causing increased CO emission at higher engine speed.

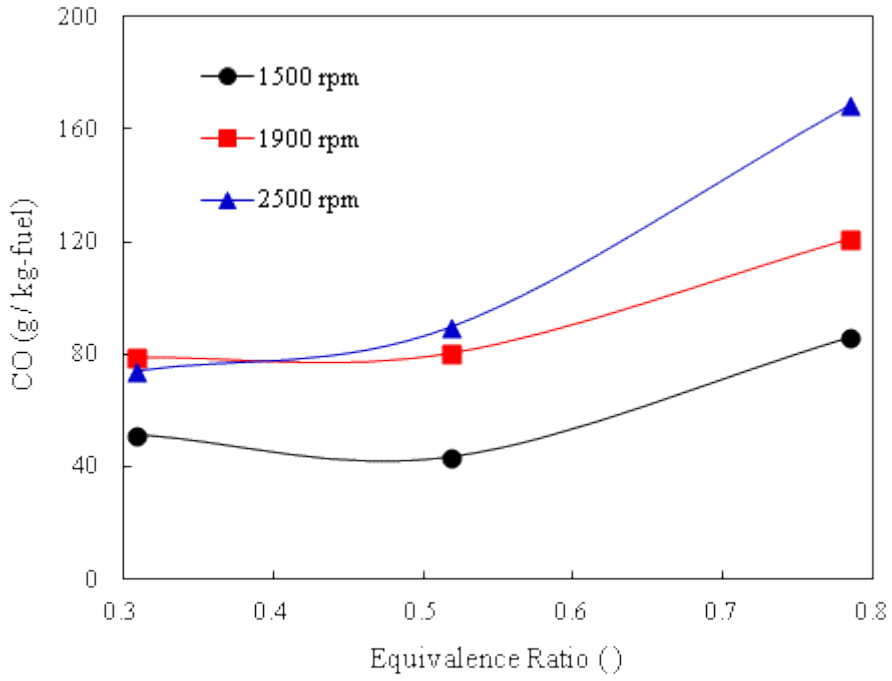

Figure 6.18 Effects of engine load on CO emissions at 1500 rpm, 1900 rpm and 2500 rpm

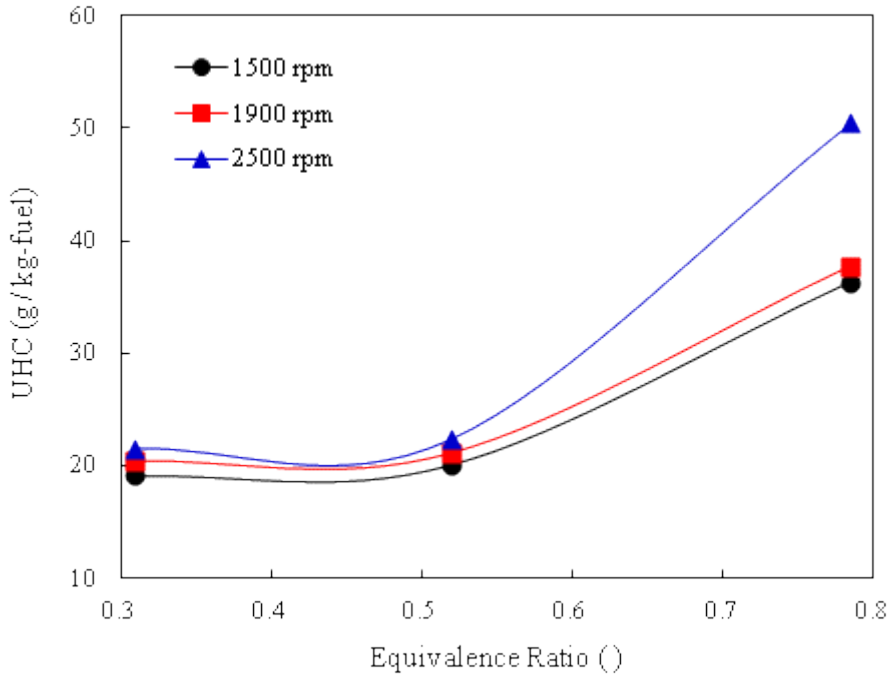

Figure 6.19 Effects of engine load on UHC emissions at 1500 rpm, 1900 rpm and 2500 rpm

6.2.3 Optimization for Load Transition

Table 6.3 gives the parameters for the adjustment of combustion location for different engine loads at 1500 rpm, 1900 rpm and 2500 rpm. The initial 50% burn location is resulted from the sweep of engine loads, as plotted in Figure 6.16. At low engine speed, the combustion locations are mostly advanced from TDC and get retarded with engine load, as shown in Table 6.3 (a). While combustion phase locations are observed retarded to expansion stroke with increased engine loads at 2500 rpm. Regardless the engine speed, for early combustion, slightly decreased intake temperature and considerably increased EGR rate are adopted to delay the combustion phase location toward TDC. For the fuelling rates which represent the expected loads of 125 N ṁ and 150 N ṁ, decreased EGR ratios are adopted to reduce the equivalence ratios to lower than 1. Meantime, the intake temperature is reduced to maintain appropriate ignition delay. After the adjustment, the equivalence ratios at high engine load do not exceed 0.9. As shown in Figure 6.20, the expected loads have been achieved for each engine speed at current equivalence ratios. Normally, the adjusted equivalence ratio for desired combustion phase location of each load reduces as engine speed increases. Minor increases in IMEP are detected at higher engine speed. These are consistent with the discussions in section 6.1.

Table 6.3 Parameters for adjusting combustion phase locations for different engine loads

a) at 1500 rpm

Load (N m)	Intake temperature (K)	EGR rate (%)	Initial 50% burn location (°ATDC)	Equivalence ratio
50	370	63	-5.29	0.439
75	370	52	-3.99	0.637
100	370	45	-2.47	0.853
125	350	35	NA	0.871
150	340	25	NA	0.895

b) at 1900 rpm

Load (N m)	Intake temperature (K)	EGR rate (%)	Initial 50% burn location (°ATDC)	Equivalence ratio
50	350	50	-3.53	0.31
75	390	47	-1.75	0.612
100	380	40	-0.25	0.785
125	360	30	NA	0.824
150	350	18	NA	0.837

c) at 2500 rpm

Load (N m)	Intake temperature (K)	EGR rate (%)	Initial 50% burn location (°ATDC)	Equivalence ratio
50	370	40	-1.06	0.299
75	380	35	1.12	0.485
100	380	25	2.92	0.618
125	380	25	NA	0.816
150	370	15	NA	0.860

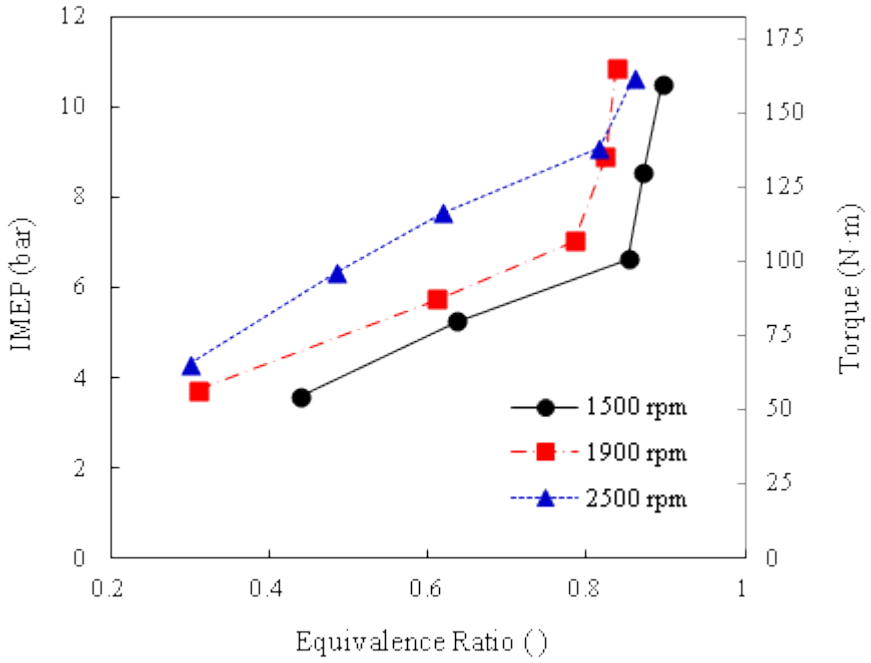

Figure 6.20 The loads under adjusted equivalence ratios at 1500 rpm, 1900 rpm and 2500 rpm

During the engine load sweep, the thermal conversion efficiency is in the range of 44% to 45%, even for the cases with seriously incomplete combustion. Figure 6.21 gives the thermal conversion efficiencies after optimizing combustion phase locations. Engine load shows more significant effects on thermal conversion efficiency, comparing to the effects of speed in Figure 6.7. At lower engine speed of 1500 rpm, the variation in thermal conversion efficiency is smaller than 1%. Also, no monotonically trend can be detected in this variation. The largest difference caused by engine load is shown at 2500 rpm, which is about 5.5%. High engine speed

shows advantages in combustion efficiency at low engine load, while low engine speed is superior at high load. Since almost same combustion phase locations are achieved after optimization, the variations in thermal conversion efficiency is mainly attributed to the effects of combustion duration. Extended combustion duration intends to results more loss in thermal energy during the converting to mechanical work. At 2500 rpm, the combustion duration increases near 2 times when engine load increased from 50 N·m to 150 N·m, whereas only 40% in increase is found at 1500 rpm. Moreover, the unit period in time domain represents more crank angles at higher engine speed, which refers more variations in combustion volume. Then the negative influence in energy converting is magnified at high engine speed.

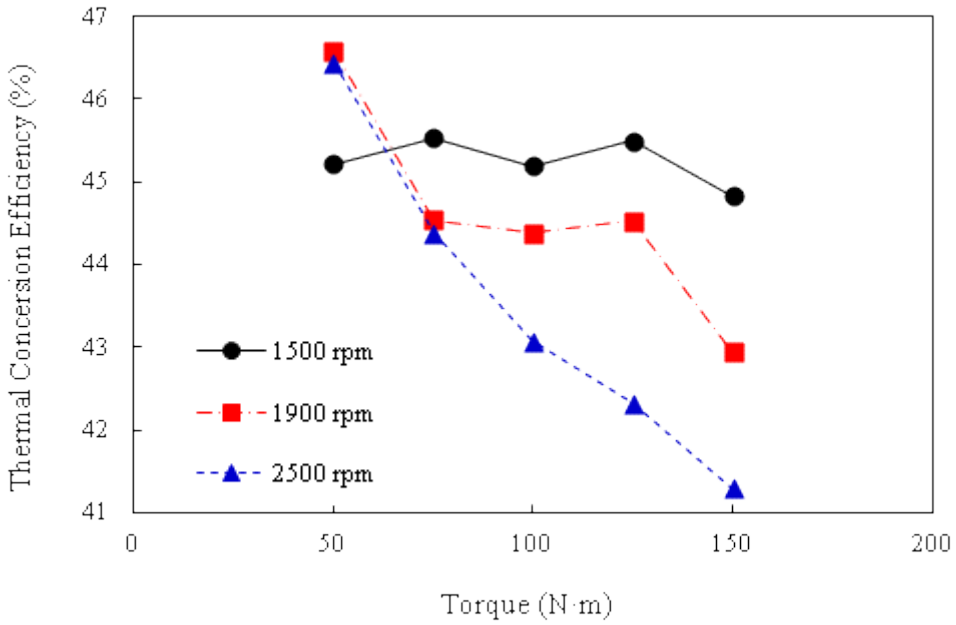

Figure 6.21 Thermal conversion efficiencies at different engine loads after adjustment

The improvements in thermal conversion efficiency are given in Figure 6.22. The variations of improvement shows similar trend to that of the thermal conversion efficiency as illustrated in Figure 6.21. At 1500 rpm, through retarding the combustion phase, 2% to 3% improvement can be achieved. At higher engine speed, no improvement is detected once the engine load is higher than 75 N·m. According to Figure 6.23, the combustion durations start to prolong significantly though optimization when engine load is higher than this level. Therefore, the increased combustion duration is attributed to the deterioration of thermal conversion efficiency at high engine load.

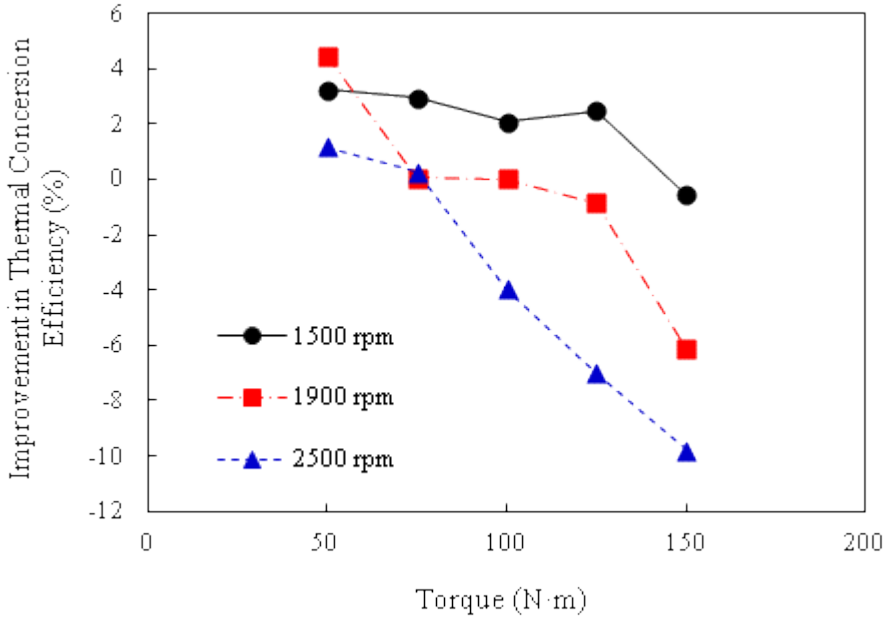

Figure 6.22 Improvements in thermal conversion efficiency at different engine loads after adjustment

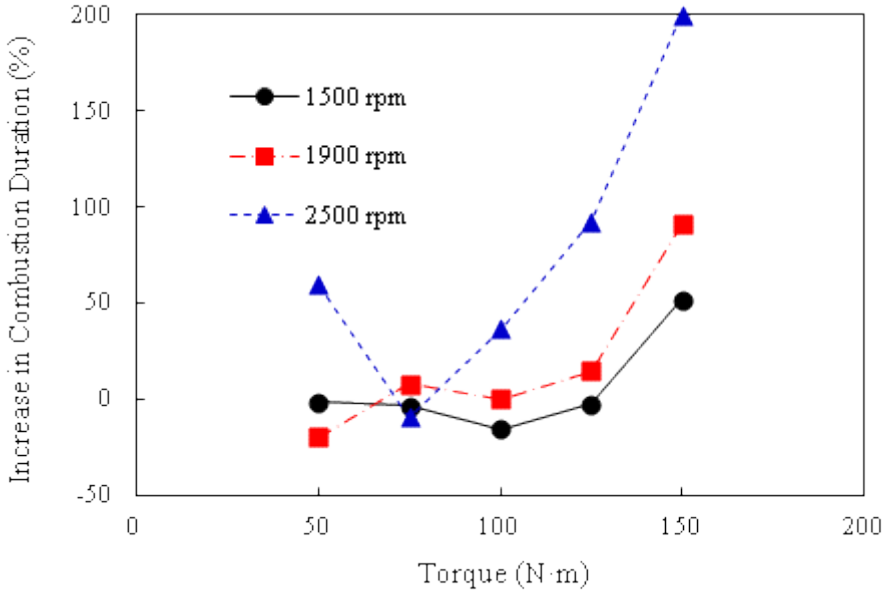

Figure 6.23 Increases in combustion duration at different engine loads after adjustment

Fuel consumptions with increased engine load after the optimization of combustion location are given in Figure 6.24. At 2500 rpm, fuel consumption increases monotonically with equivalence ratio, which is consistent to the effects of reduced thermal conversion efficiency shown in Figure 6.21. When the load increases from 50 N m to 150 N m, the ISFC increases about 20%; while only 11% of reduction in thermal conversion efficiency is observed. The rest penalty in fuel consumption is attributed to the deterioration in heat rejection efficiency. Very small changes are detected in combustion efficiencies, which are in range of 90% to 92% for load

from 50 N m to 150 N m at 2500 rpm. Thus, the increased heat loss to cylinder walls and residual heat in exhaust gas due to higher in-cylinder temperature are considered responsible for the further decreased heat rejection efficiency and the rest penalty in fuel consumption. At 1900 rpm and 1500 rpm, slightly advantages in fuel consumption appear under high load with continuing increased equivalence ratios. No improvement in thermal conversion efficiency is observed at this load, as shown in Figure 6.22. Then enhancement in combustion efficiency is implied for high load at lower engine speed.

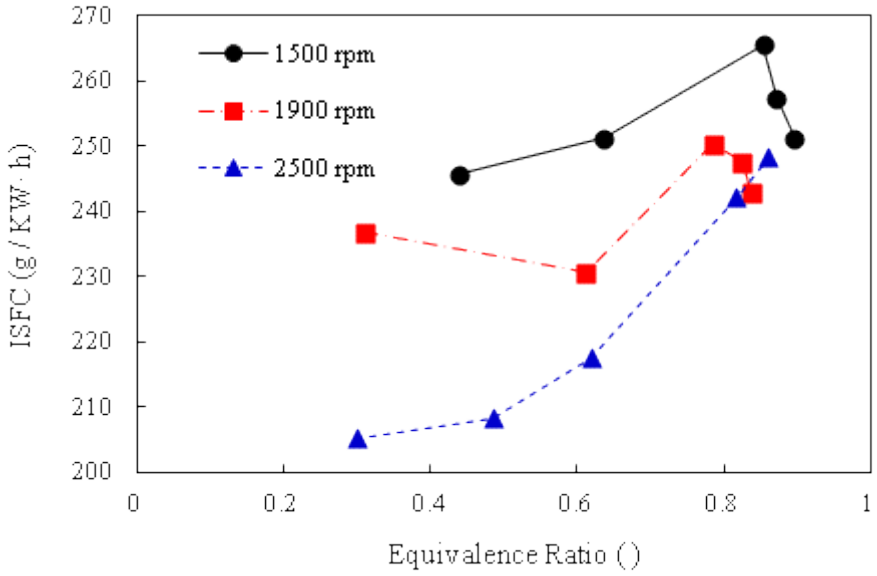

Figure 6.24 Fuel consumptions against euqivalence ratio for a range of engine loads after adjustment

To clarify the effects of combustion phase optimization on fuel consumption, the improvements in ISFC are given against the improvement in thermal conversion efficiency and the improvement in heat rejection efficiency in Figure 6.25 and Figure 6.26, respectively. The improvement of fuel consumption and the improvement of thermal conversion efficiency show reversely relations with engine load. Therefore, it is proved again that heat rejection efficiency has determined effect on fuel consumption for the cases in this study. At 1500 rpm and 1900 rpm, no improvements in fuel consumption are observed with the loads under 100 N m, though up to 5% increases in thermal conversion efficiencies are achieve by optimizing combustion phase location. As shown in Figure 6.26, the gains are cancelled by the deterioration in rejection efficiency, which is about 15% in the same case. As discussed in section 6.1.3, increased equivalence ratios and lower combustion temperatures due to higher EGR rates used during optimization result decreased combustion efficiency. Moreover, the increased EGR rate leads to higher specific heat capacity of the bulk-air. Thus, increased residual heat in exhaust gas leads to decreased heat loss efficiency. For engine loads of 125 N m and 150 N m, the serious incomplete combustion in original load sweep is resolved by reduced EGR rate during

optimization. Therefore, the combustion efficiencies are improved significantly, and massive improvements in fuel consumption are achieved though thermal conversion efficiencies are deteriorated by the prolonged combustion duration. At 2500 rpm, improvement in fuel consumption is detected once engine load is over 75 N m. Reduced EGR rates when advancing the combustion phase location to TDC are attributed to the increases of combustion efficiency, which eventually result in decreased fuel consumptions.

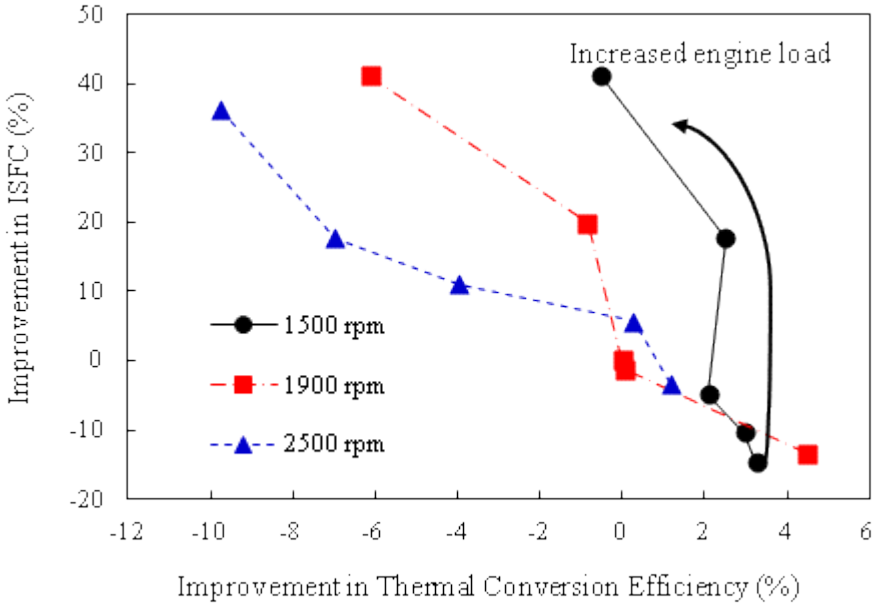

Figure 6.25 Improvement in fuel consumption against improvement in thermal conversion efficiency for a range of engine loads after adjustment

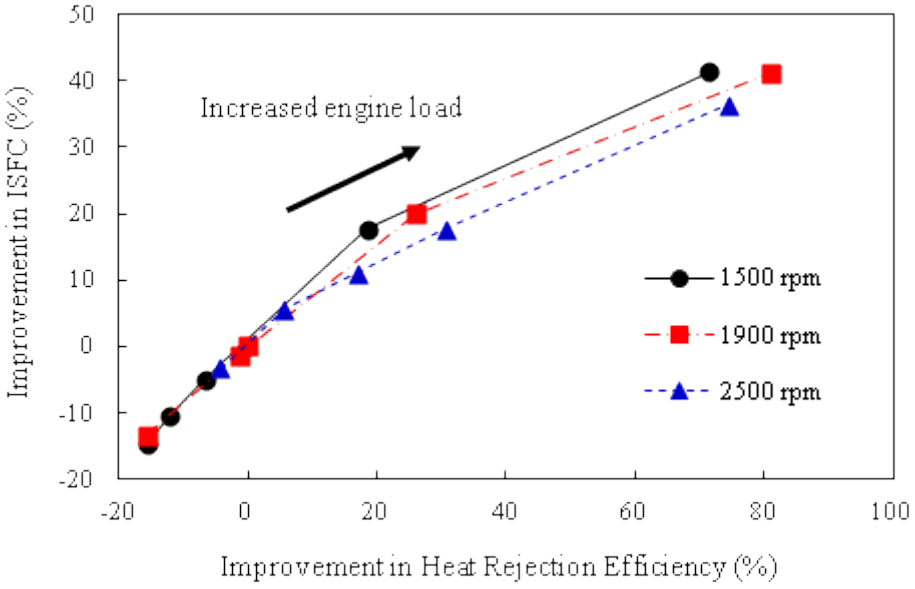

Figure 6.26 Improvement in fuel consumption against improvement in heat rejection efficiency for a range of engine loads after adjustment

The emissions with increased engine load after optimizing combustion phase location are illustrated in Figure 6.27 to 6.30. In contrast to the trends shown in Figure 6.17, NO_x emission increases with engine load though higher equivalence ratio is achieved with the increased fuelling rate, as shown in Figure 6.27. Referring to Table 6.3, at high load (125 N·m and 150 N·m), the variations in equivalence ratio with engine load is small. Thus the increases in NO_x at high loads are attributed to the significant increased combustion temperatures due to the greater chemical energy released from increased fuelling. Since lower adjusted equivalence ratios are adopted for higher engine speed, the trend of NO_x against engine load shifts up as speed increases. With engine load lower than 125 N·m, the NO_x emissions are contained under 3.5 g/kg-fuel at 1500 rpm and 1900 rpm. At high engine speed and load, the peak value of NO_x is about 11 g/kg-fuel.

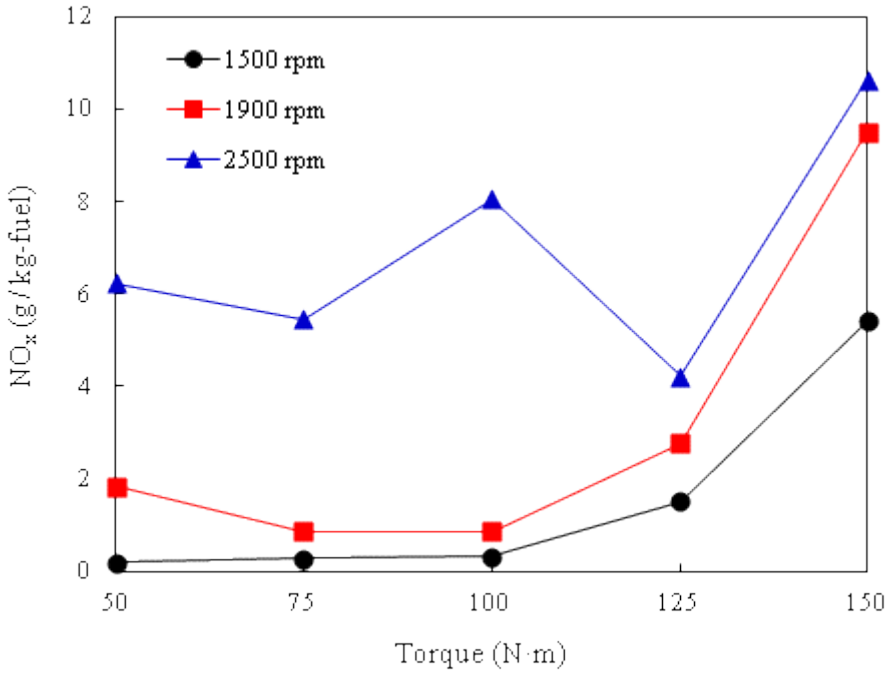

Figure 6.27 NO_x emissions at different engine loads after adjustment

At 1500 rpm and 1900 rpm, no monotonically increases in soot can be seen with increased load though the equivalence ratio is higher, as shown in Figure 6.28. Referring to Table 6.3, relatively cooler EGR is used at high engine load, which is beneficial for suppressing combustion temperature. Therefore, excessively increased soot formation is avoided at high load for these two engine speeds. Conversely, relatively higher temperature of EGR with high equivalence ratio results the highest soot output at 100 N·m. At 2500 rpm, soot emission increases monotonically with engine load. As discussed in section 6.1, the time for mixing is decreased massively at high engine speed. The inferior mixing increases the level of mix-controlled combustion, especially in the cases with high equivalence ratios. And soot formation is more sensitive with equivalence ratio at high engine speed. Dramatically increases

in soot emissions are observed at 125 N m and 150 N m for 2500 rpm. Besides the significantly increased equivalence ratios, relatively warmer EGR is used during optimization, which is assessed to enhance the formation of soot. At 1500 rpm and 1900 rpm, the soot emissions can be constrained under 4 g/kg-fuel for the entire range of load. However, more than 10 g/kg-fuel of soot is formed at high load with engine speed of 2500 rpm, which is too high for current emission criteria.

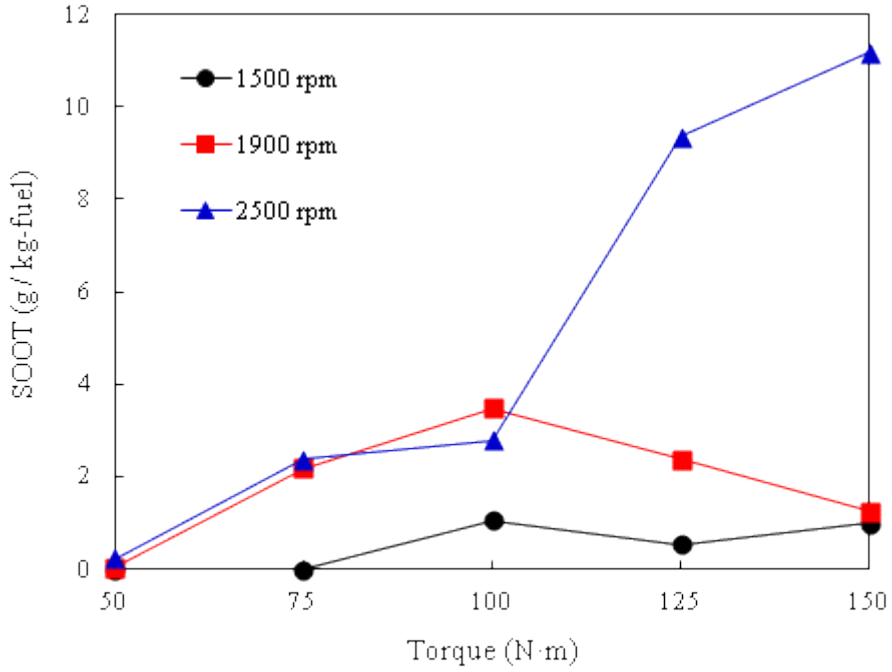

Figure 6.28 Soot emissions at different engine loads after adjustment

For the productions of incomplete combustion, CO emissions decrease with increased load and equivalence ratio, as shown in Figure 6.29. Greater chemical energy released from the increased fuelling rate at higher load leads to increased combustion temperature which accelerates the oxidation of CO. Moreover, significantly increased EGR rates and decreased intake temperatures adopted at low engine loads lead to reduced combustion temperature and eventually hinder the oxidation of CO. However, at high engine speed, massively increased CO emissions are observed at high load. As discussed in section 6.1.2, the reduced time for oxidation is attributed to the increases in CO emission at high speed with high equivalence ratio. Unburned hydrocarbon emissions normally increase with engine load, as given in Figure 6.30. Therefore, the UHC emissions are mainly determined by equivalence ratio. Slightly increased UHC outputs are detected at the lowest engine load, which is assessed to be resulted from low combustion temperature. Higher combustion temperature at high load is attributed for the minor reduction of UHC emission. Because of the relatively lower equivalence using for optimization at high speed, the trend of UHC against engine load moves to lower level at 2500 rpm.

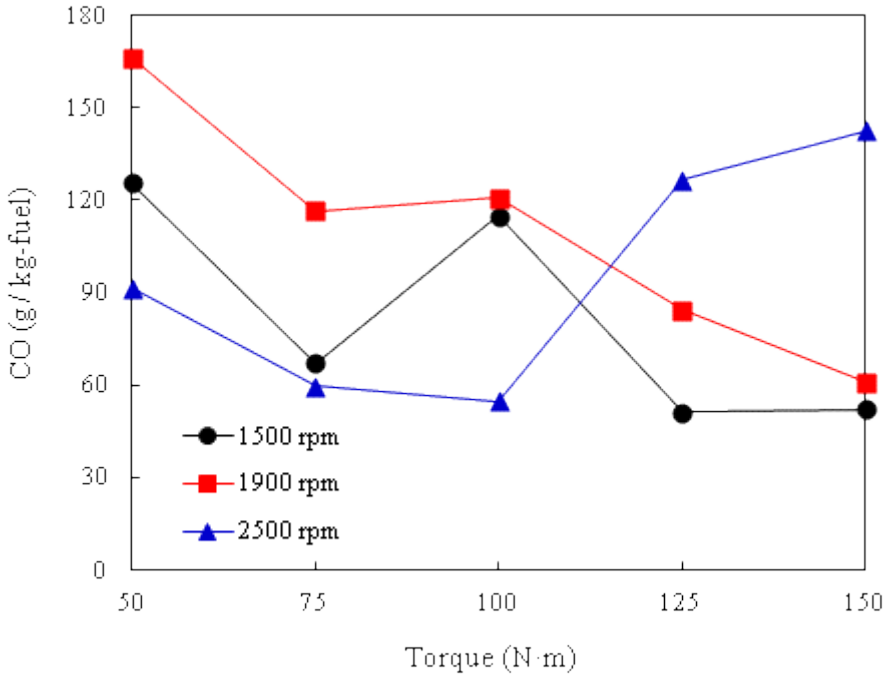

Figure 6.29 CO emissions at different engine loads after adjustment

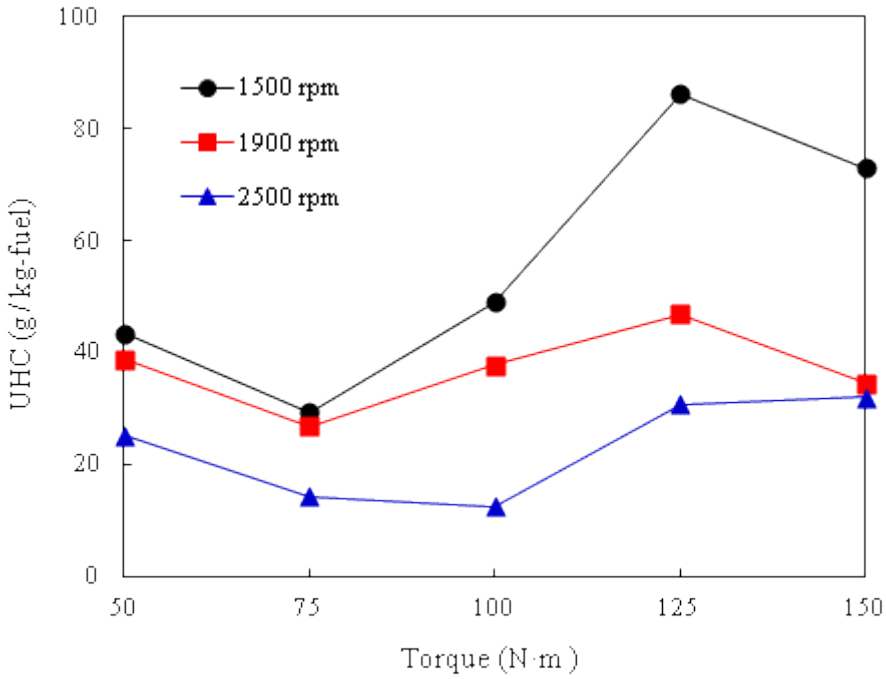

Figure 6.30 UHC emissions at different engine loads after adjustment

During the optimization of combustion phase location, the adopted EGR rates and intake temperatures are changed from the setting of PPCI combustion, as shown in Table 6.2 and 6.3. Therefore, the regimes of combustion with adjusted parameters have to be brought into concern. As discussed in the above sections, in the cases of high engine loads, the characteristics of PPCI combustion become less apparent with significant increased combustion duration and dramatically increased NO_x and soot emissions. In some studies, it is described as a reduction in

the degree of premix combustion or an increase in the proportion of mix-controlled combustion [Keeler and Shayler, 2008; Yun and Reitz, 2007]. In section 6.3, the degree of premix combustion will be further discussed.

6.3 Premixed Combustion Ratio Study

In previous sections, it is shown that the distinct characteristics of PPCI combustion start to fade when the operating conditions approaching the speed or load limit. During these processes, gradual transitions from premixed combustion to mix-controlled combustion are considered happen due to the increasingly rigorous conditions for mixing. Like the study about homogeneity presented in Chapter 4, a method to evaluate the degree of premix combustion is required to discuss. Also, the relations between the regimes of combustion and fuel consumption or emissions are expected to be investigated quantitatively if the method is proposed.

6.3.1 Definition and Formulas

As introduced in the literature review, little pertinent information is found in the available literatures for the definition about the overall degree of premix combustion in PPCI diesel engine. In this study, a factor name Premixed Ratio (*PR*) is proposed trying to quantitatively describe the level of premix, which is derived from the primary definition of combustion stages in diesel engine [Heywood, 1988]. As shown in Figure 6.31, the process of typical conventional diesel combustion can be defined into the following stages: ignition delay (ab), premixed combustion (bc), mix-controlled combustion (cd) and late combustion (de). When the rapid reacted premixed combustion is approaching its end, the rate of heat release drops sharply since the available mixture within flammable range is consumed up. After that, the heat release rate begins to rise again since the mix-controlled combustion starts. The mix-controlled combustion is slow compared to the premixed combustion. Therefore, finding the location of c from the curve of heat release rate is the radical matter to determine the fraction of fuel burned in premixed combustion stage.

For PPCI combustion, it is normally difficult to identify the premix combustion stage from the entire combustion process in the curve of heat release rate. The typical heat release rate diagram of PPCI combustion does not exhibit distinct premixed and diffusion burns as in conventional diesel combustion, as given in Figure 6.32 [Kook et al., 2005]. No clear boundary, i.e. location c, can be detected in the diagram of heat release rate as fuel is injected far advance to the start of combustion. However, the derivative of heat release rate shows that it drops sharply after the location of peak heat release rate and reaches a negative value after couples of crank angles. This process indicates the later stage of premixed combustion where the reacting rate drops rapidly owing to the burning out of flammable mixture. After reaching the lowest value, the derivative begins to increase again which implies the additional heat release from diffusion

combustion. Thus, the location of the lowest value in the derivative of heat release rate is defined as the end of premixed combustion, which is marked as 'c' in Figure 6.32.

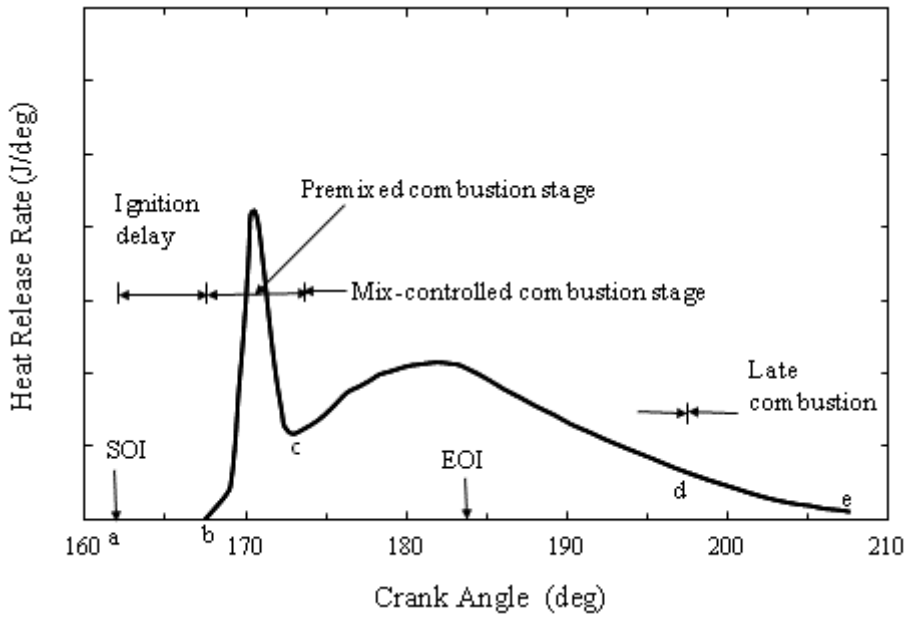

Figure 6.31 Typical DI engine heat release rate diagram identifying different diesel combustion stages [Heywood , 1988]

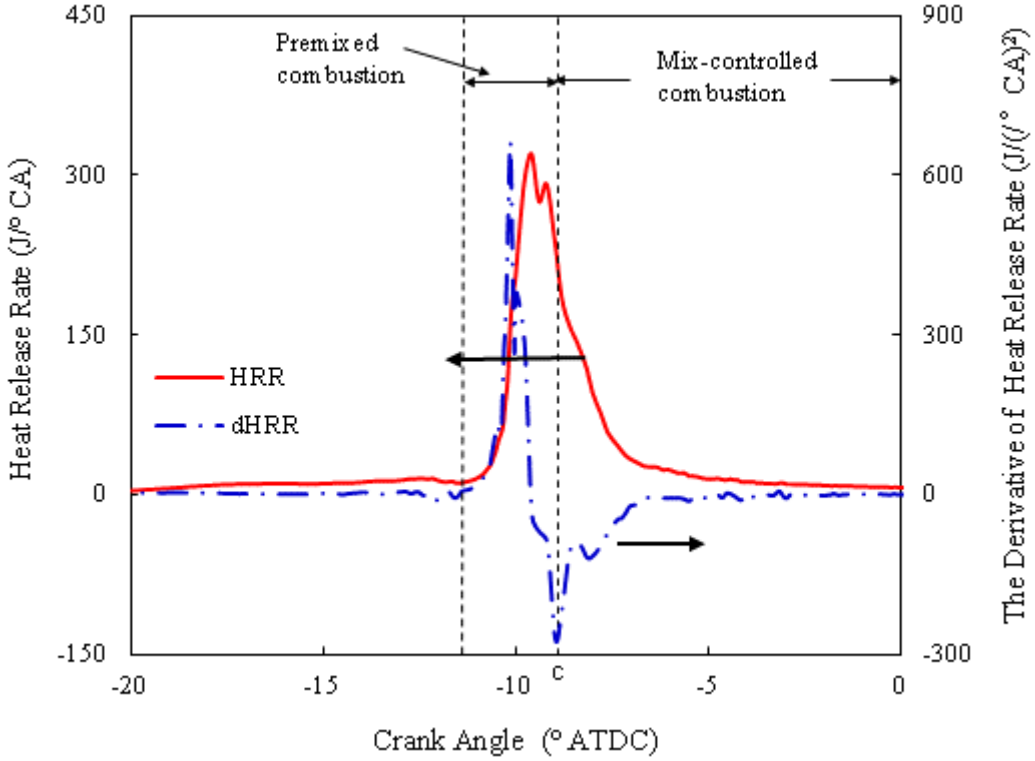

Figure 6.32 Typical heat release rate diagram and the derivative of the heat release rate for PPCI diesel combustion, and the identifying of different combustion stages. Data from the baseline case in Chapter 4, with the 2nd injection timing at -30 °CA ATDC.

Base on the definition of the end of premixed combustion, the total fuel burned before that is defined as a fraction of the total fuel injected, expressed as Premixed Ratio (*PR*):

$$PR = \frac{m_{premix}}{m_{total}} \tag{6.1}$$

where m_{premix} and m_{total} are the fuel burned in premixed combustion stage and the total fuel injected, respectively. In this definition, wall wetting has been considered. Moreover, during the premixed combustion certain fraction of fuel is not completely oxidized to the final product CO_2 but the intermediate product CO. This fraction may increases for PPCI combustion due to the higher dilution level and lower combustion temperature. Therefore, the heat released in premixed combustion stage is much smaller than the energy contained in the fuel burned in this stage. To reveal the fraction of fuel energy released in premixed stage, Premixed Ratio is also calculated by heat in this study, expressed as PR_h:

$$PR_h = \frac{heat_{premix}}{Q_{LHV} m_{total}} \tag{6.2}$$

Where $heat_{premix}$ is the heat released in premixed combustion stage; Q_{LHV} is the lower heating value of fuel.

6.3.2 Injection Strategies and In-Cylinder Conditions

Primarily, the investigation is conducted based on the results received from the parametric study on the combustion performance and emissions in PPCI combustion using split-injection, which is introduced in Chapter 4. In order to gain understandings about the determinants and relative importance of premixed ratio, the sweeps of the 2nd injection timing are conducted under three injection pressures and three EGR rates, as shown in Table 6.4. More details about the operating conditions can be found in Table 4 .1

Table 6.4 Injection pressures and EGR rates for premixed ratio study

Injection Pressure	70 MPa, 110 MPa, 150 MPa
EGR Rate	20%, 35%, 50%

Figure 6.33 shows the premixed ratios by mass and by heat for different injection pressure with varied 2nd injection timing. *PR* shows similar trend with PR_h but with much higher value for each injection pressure. The premixed ratios are sensitive to the 2nd injection timing, which range from 40% to 97% by mass, and 19% to 55% by heat. There are optimal 2nd injection timings for premixed ratios, which are varied for different injection pressure. Before the optimal timing, increased fuel adhering causes less fuel burned during the premixed combustion stage though the ignition delays are longer in these cases with early injection. With retarded 2nd

injection timing, the premixed ratio decreases significantly due to the reduced time for mixing. About 50% reduction from the optimal timing is observed when the 2nd injection timing is retarded to -5 °CA ATDC. Except the cases with the earliest 2nd injection timing, *PR* increases with enhanced injection pressure because it intensifies the air entrainment into spray and provides extra kinetic energy to improve fuel-air mixing. For the cases using the 2nd injection timing at - 30 °CA ATDC, the worse wall impingement caused by higher injection pressure cancel the gain in enhancing mixing. The highest premixed ratio is detected in the case using injection pressure of 150 MPa when 2nd injection is at -20 °CA ATDC, which is 97% by mass and 55% by heat.

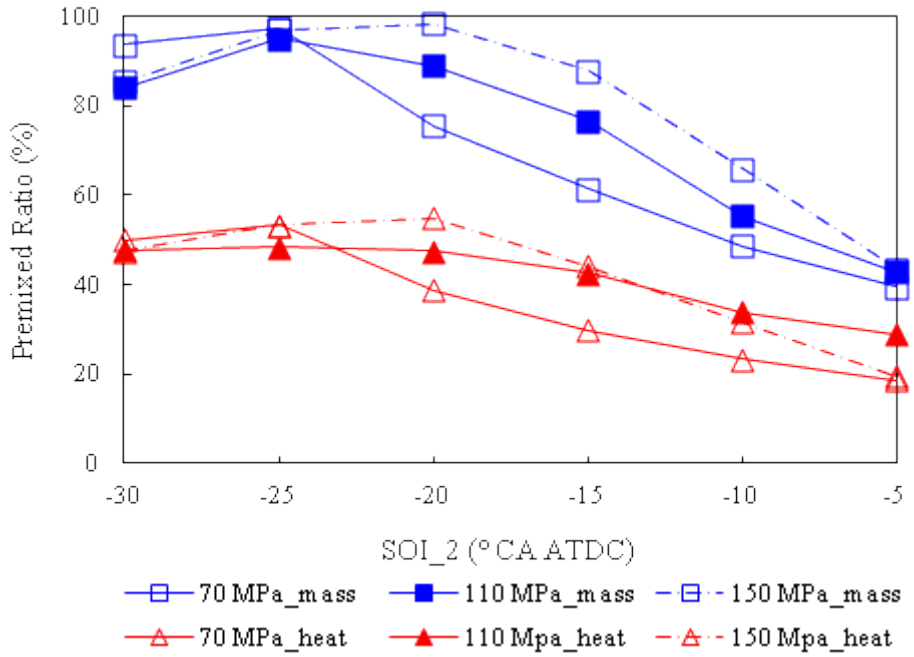

Figure 6.33 The premixed ratios by mass and by heat for the cases of different 2nd injection timings with different injection pressures

The variations of premixed ratio with increased dilution level are illustrated in Figure 6.34. The sensitivity of premixed ratio to injection timing is reduced by the increased EGR rate. With EGR rate of 50%, small variations are observed in premixed ratios which range from 85% to 97% by mass and 36% to 49% by heat. However, at low EGR rate of 20%, the premixed ratios change significantly from 34% to 98% by mass and 18% to 64% by heat. With 2nd injection timing earlier than -25 °CA ATDC, premixed ratio by mass is improved slightly by reduced EGR rate due to the increased oxygen availability which results more flammable mixture. Meantime, greater improvements are observed in premixed ratio by heat, which imply that the combustion is more complete with the relatively lean equivalence ratio. When the 2nd injection timing is retarded after this timing, premixed ratio drops significantly in the case with low EGR rate, while it is still maintained at high level with high EGR rate. With the high dilution level,

the ignition delay is kept sufficient long for mixing owing to the relatively low oxygen availability and reduced in-cylinder temperature due to the increased heat capacity of bulk-air. Therefore, two key factors can maintain combustion at high premixed degree, which are considerable advanced injection timing and high dilution level.

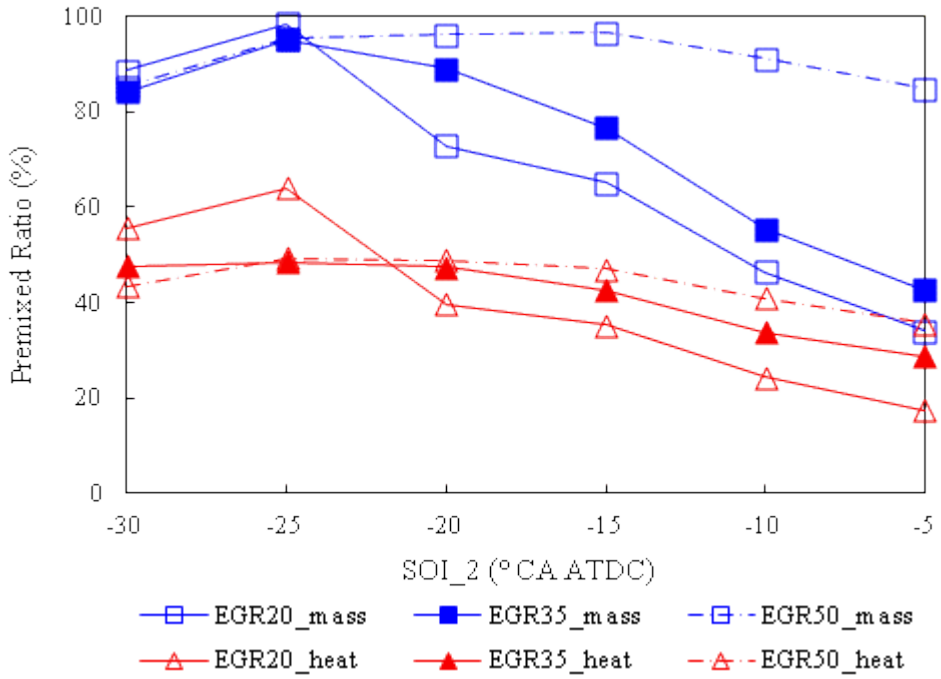

Figure 6.34 The premixed ratios by mass and by heat for the cases of different 2nd injection timings with different EGR rates

Because the fuel consumption is highly depended on the combustion efficiency, it is more sensitive to the premixed ratio by heat rather than by mass. As shown in Figure 6.35, though the dependency on premixed ratio is observed, multiple values of ISFC for same premixed ratio are evident. As discussed in the previous chapters, fuel consumption is determined by the combination of combustion efficiency, heat loss efficiency and thermal conversion efficiency. In general, the fuel consumptions decrease with increased premixed ratio by heat. Firstly, the increased level of premixed combustion leads to reduced combustion duration owing to the shrinking of mix-controlled combustion stage which has slow reaction rate. The shorter combustion duration is beneficial to thermal conversion efficiency. Moreover, greater fuel energy released in premixed combustion stage leads to generates higher bulk-air temperature which is beneficial to accelerate the oxidation rate. The differences in equivalence ratio, heat capacity of bulk-air, fuel distribution, in-cylinder kinetic energy and location of combustion phase are attributed to the variations of fuel consumptions at same premixed ratio.

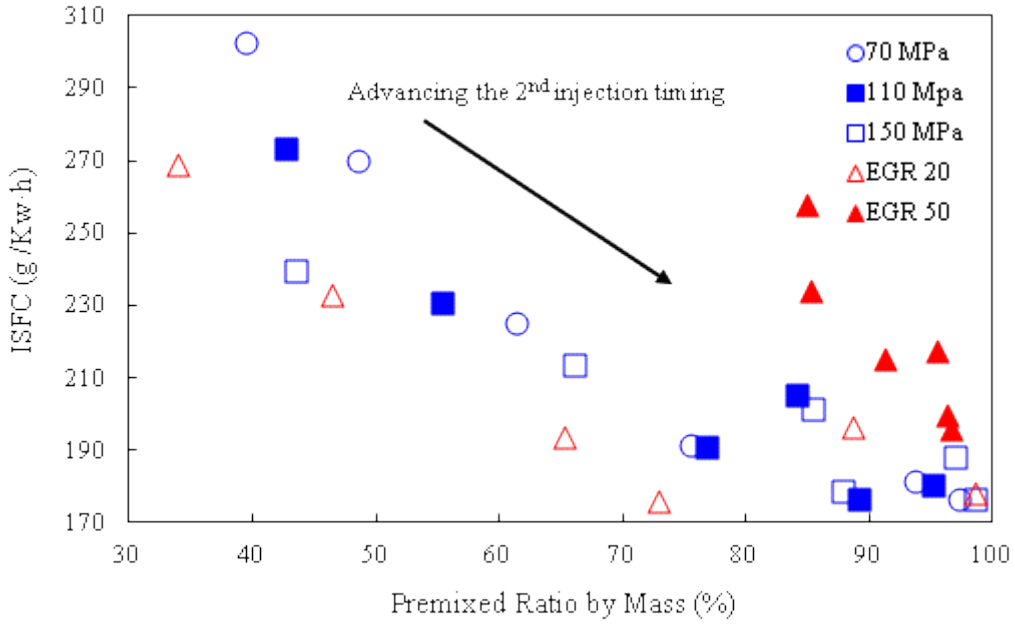

Figure 6.35 The fuel consumptions against the premixed ratios by heat for the cases of different 2nd injection timings with varied injection pressures and EGR rates

The formation of soot is mainly determined by the locally equivalence ratio and combustion temperature. In mix-controlled combustion stage, lager fraction of fuel intends to burn in rich region. Therefore, the amount of fuel consumed in premixed combustion stage is more important than the heat release to concern for discussing the effect of premixed degree on soot emission. As shown in Figure 6.36, no monotonically decreases in soot emissions are observed with increased premixed ratio. However, extremely low soot emissions are still detected at high premixed ratio. When using EGR rate of 50%, significantly high soot emissions are observed though the premixed ratios are higher than 85% in these cases. The low oxygen availability under this high dilution level is considered responsible for the increased formation of soot. Meantime, relatively low soot output is found at low premixed ratio between 30% and 40%. Referring to the discussion in Chapter 4, the decrease of soot is result by the reduced combustion temperature owing to the seriously incomplete combustion. The peak value of soot formation is detected at premixed ratio around 65%, with the 2nd injection timing at -10 °CA ATDC. Higher combustion temperature is attributed to the high level of soot emission at the moderate premixed ratio.

Figure 6.37 and Figure 6.38 give the CO emissions and unburned hydrocarbon emissions against the premixed ratios by heat, respectively. The trends of these two products of incomplete combustion are similar to the trend of fuel consumption, except the responds with EGR rate of 50%. Normally, the increased fractions of fuel energy released in premixed combustion stage decrease the output of CO and UHC, though variable values are seen at same premixed ratio. Extremely low levels of CO and UHC outputs are achieved at high premixed ratio. Because of

the increased oxidations of CO and HC, fuel consumptions are improved significantly, as shown in Figure 6.35. When using EGR rate of 50%, significantly increased CO and UHC emissions are observed since the oxidations of these two emissions are inhibited by the low oxygen availability.

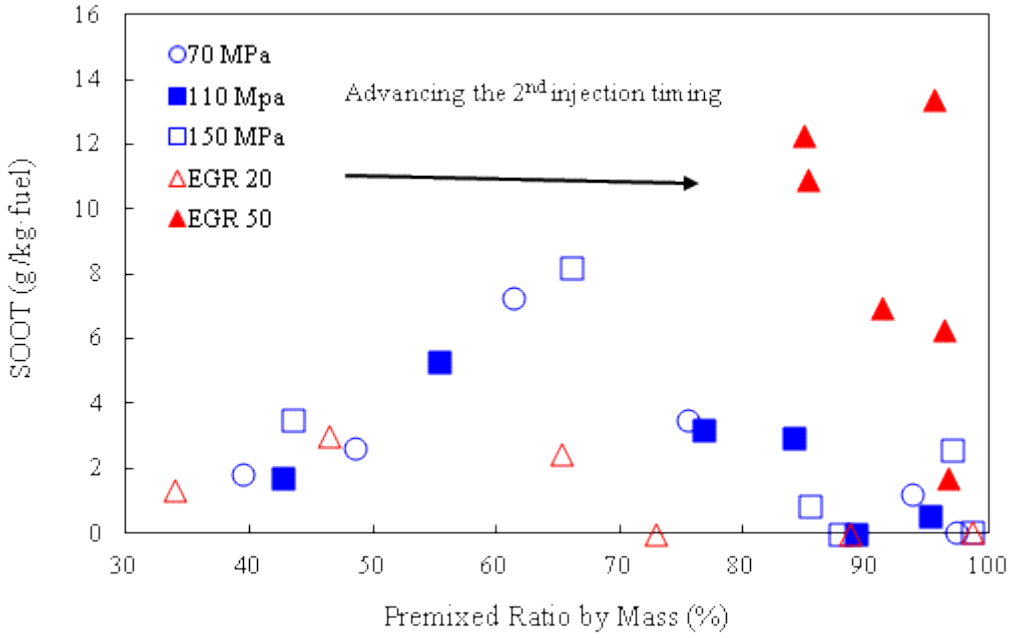

Figure 6.36 The soot emissions against the premixed ratios by mass for the cases of different 2nd injection timings with varied injection pressures and EGR rates

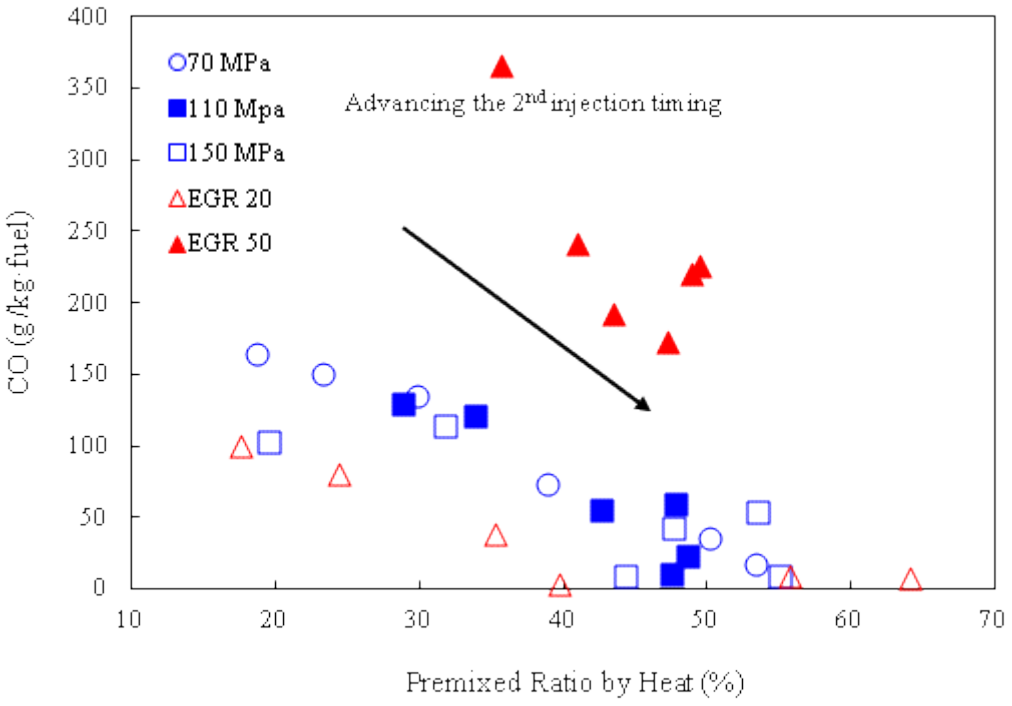

Figure 6.37 The CO emissions against the premixed ratios by heat for the cases of different 2nd injection timings with varied injection pressures and EGR rates

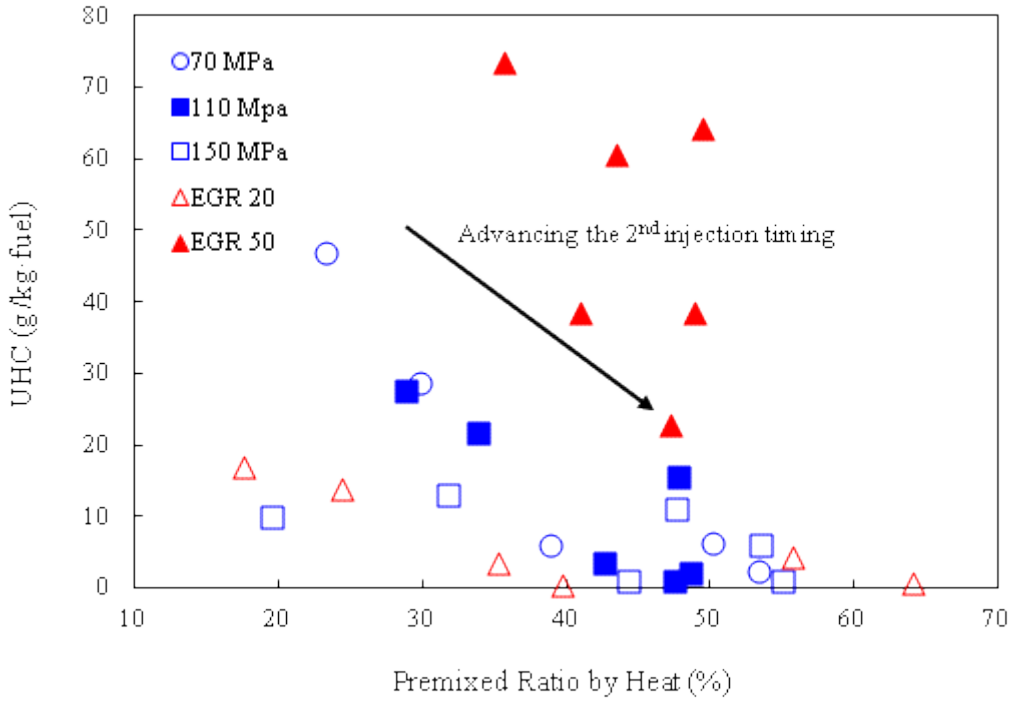

Figure 6.38 The UHC emissions against the premixed ratios by heat for the cases of different 2nd injection timings with varied injection pressures and EGR rates

6.3.3 Correlations of Ignition Delay and Equivalence Ratio

Though the mechanisms determining premixed ratio are complicated, two main factors are considered significantly affect the degree of premix combustion, which are the ignition delay and the equivalence ratio. The ignition delay represents the time period for mixing, whilst the equivalence ratio represents the difficulties for mixing. Figure 6.39 and Figure 6.40 give the premixed ratio respected to the ignition delay by mass and heat, respectively. Generally, premixed ratio constantly increases with ignition delay until ignition delay reaches 15 crank angles. With ignition delay longer than that, the wall wetting gets worse, and it further leads to decreased faction of fuel burned in premixed stage. At same ignition delay, variations of premixed ratios are lager in mass than in heat. These variations are resulted by the differences in kinetic energy introduced by different injection pressures and the differences in oxygen availability caused by different EGR rate. Nevertheless, the relations between ignition delay and premixed ratio can be expected, especially for the ratio by heat. The effects of equivalence ratio on premixed ratio are difficult to be isolated based on current data. Although Figure 6.34 shows increased premixed ratio due to increased EGR rate, significant increased ignition delay is detected owing to the reduced bulk-air temperature.

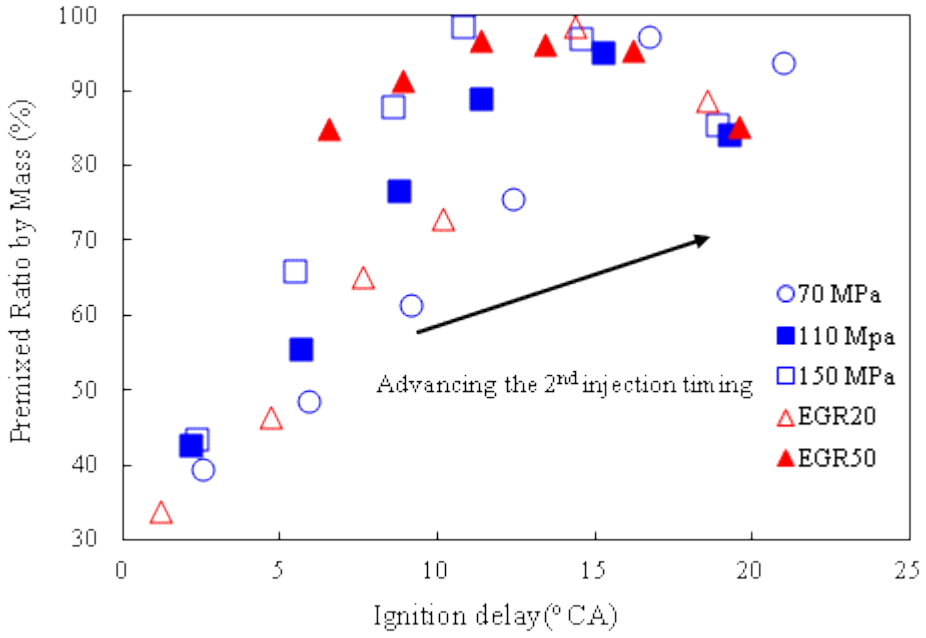

Figure 6.39 The premixed ratios by mass against ignition delay for the cases of different 2nd injection timings with varied injection pressures and EGR rates

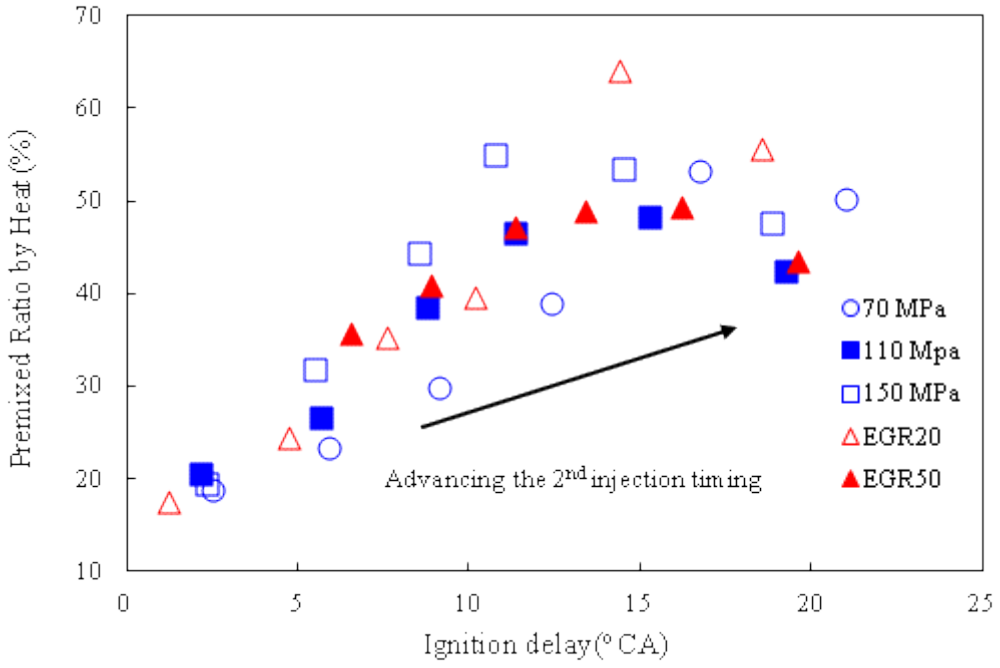

Figure 6.40 The premixed ratios by heat against ignition delay for the cases of different 2nd injection timings with varied injection pressures and EGR rates

A single-zone model proposed by Watson et al. defines the fuel burned in premixed stage as a fraction of total injected fuel, expressed as a proportionality factor, β [Watson, 1980]:

$$\beta = \frac{m_{premix}}{m_{total}} = 1 - \frac{a \cdot \phi^b}{\tau_{id}^c} \tag{6.3}$$

where ϕ is the overall equivalence ratio; τ_{id} is the ignition delay; and a, b, c are empirical constants. They also gave the ranges for a, b, c:

$$0.8 < a < 0.95;\ 0.25 < b < 0.45;\ 0.25 < c < 0.5 \tag{6.4}$$

Therefore, their definition is consistent with the discussion that increased ignition delay is beneficial for achieving higher degree of premix, which is also dependent on overall equivalence ratio. However, this simplified model does not count wall wetting into its functions. Thus, large discrepancies may be resulted when comparing the predicted data of Watson's model with the data of premixed ratio by mass.

The comparison is taken between the predicted values and the premixed ratio by heat defined by equation (6.2), since the incomplete combustion has been considered. Based on the results given in section 6.3.2, the empirical constants a, b and c are determined using the polynomial fitting function of Matlab [2013], as given below:

$$a = 0.573;\ b = 0.148;\ c = 0.244 \tag{6.5}$$

Apparently, these constants are out of the ranges recommended by Watson et al.. Two main reasons are considered responsible for the discrepancies. Firstly, the recommended ranges are achieved on mass fraction, whilst the polynomial fittings are conducted on premixed ratio by heat. Secondly, the model of Watson et al. is proposed on conventional diesel engines, while the cases in this study are mainly operated under PPCI combustion though with different degree of premix. As shown in Figure 6.41 and 6.42, agreements are achieved between the predicted traces and the premixed ratio defined by equation (6.2) with acceptable discrepancies. Therefore, the definition of premixed ratio proposed in this section is considered reveal the correlations between the degree of premix and ignition delay, together with equivalence ratio. As shown in Figure 6.41, the effects of injection pressure are weakened in the predicted traces since the kinetic energy introduced by injection is not considered in the model of Watson et al.. The predictions for different EGR rates are assessed sufficiently accurate, where the advantages of low EGR rate at early injection timing is revealed in the predicted traces.

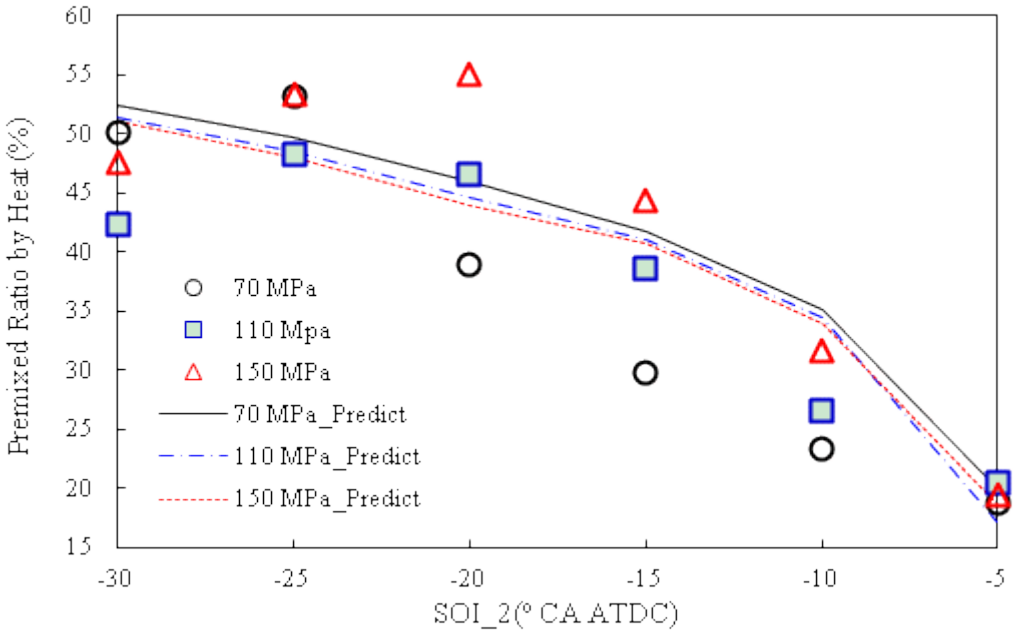

Figure 6.41 The premixed ratios by heat from equation (6.2) and from prediction for the cases of different 2nd injection timings with varied injection pressures

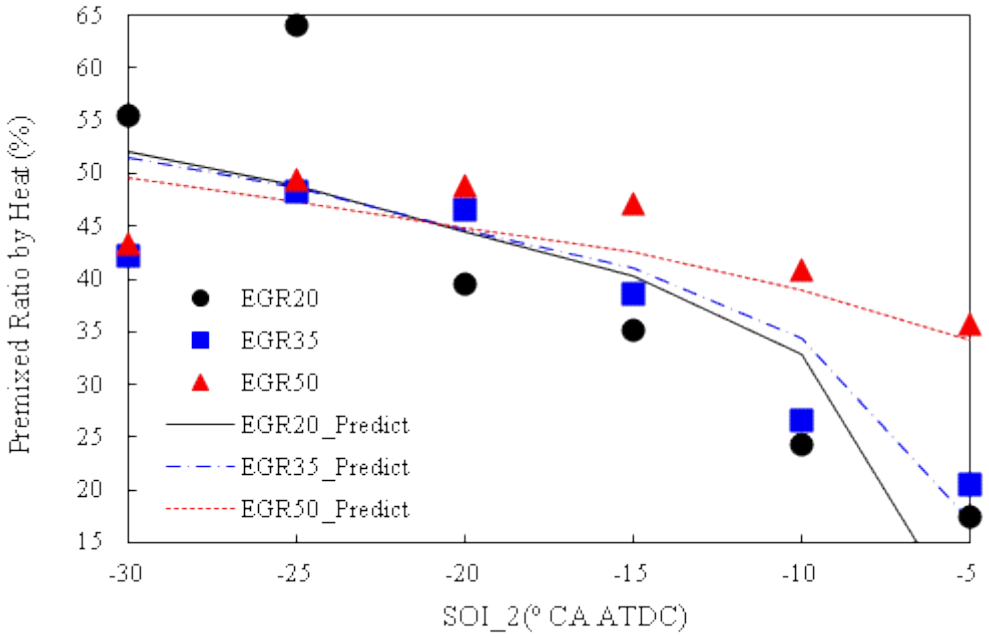

Figure 6.42 The premixed ratios by heat from equation (6.2) and from prediction for the cases of different 2nd injection timings with varied EGR rates

6.3.4 Speed and Load Transitions

Based on the definition of premixed ratio and the related discussions, the degrees of premix at varied engine speeds and loads are evaluated in this section. As shown in Figure 6.43, for the operating conditions listed in Table 6.1, the premixed ratios are of moderate level for different engine speeds, referring to Figure 6.33 and Figure 6.34. The premixed ratios increase with

engine speed within the ranges from 73% to 85% in mass and 31% to 37% in heat. Since the overall equivalence ratios are kept constant during the original sweep of engine speed, the variations in premixed ratios are attributed to the different ignition delays. However, as shown in Figure, the ignition delays decrease of about 0.15 ms from 1500 rpm to 2500 rpm; whilst premixed ratios increase 12% in mass and 6% in heat. This is contrary with the discussion in previous section, which considers that decreased ignition delay results reduced premixed ratio. The increased kinetic energy introduced by enhanced piston motion at higher engine speed is assessed as the reason for these deviations. Moreover, shorter injection duration in crank angle and earlier end of injection lead to worse wall wetting at low engine load because of the longer spray penetration at lower in-cylinder temperature and pressure. In fact, the decrease in ignition delay is minor for increased engine speed compared to the range shown in Figure 6.33 and Figure 6.34. Thus, the effects of ignition delay on premixed ratio are minor with increased engine speed and offset by the effects of increased kinetic energy and reduced wall wetting. Large gaps between the premixed ratio by mass and premixed ratio by heat are observed, which imply significant incomplete combustion happening and massive outputs of CO and UHC.

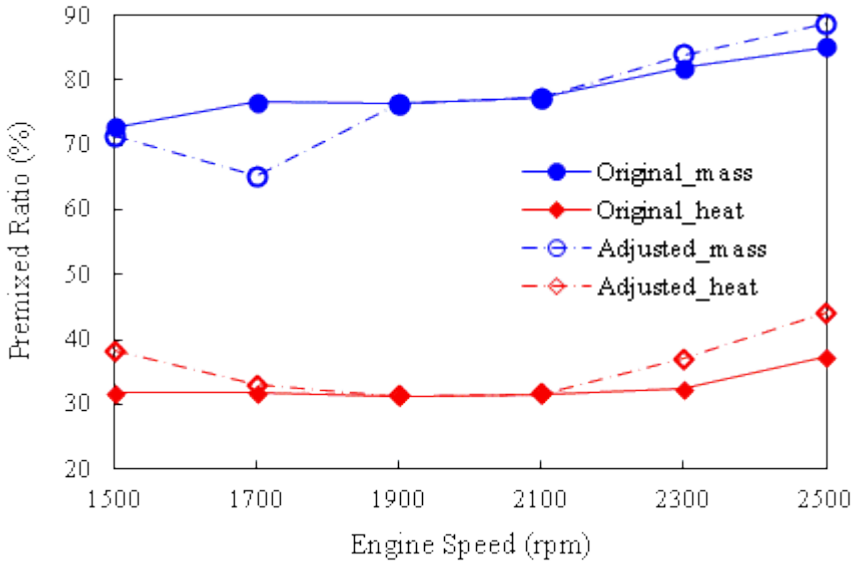

Figure 6.43 The premixed ratios by mass and by heat at different engine speeds for original cases and adjusted cases

After the optimization of location of combustion phase, increased EGR rate results decreased premixed ratio in mass due to the higher equivalence ratio. However, the premixed ratios in heat are increased owing to the high combustion temperature since the combustion phases locate at TDC. At high engine speed, the reduced equivalence ratio results in increased premixed ratio. Moreover, improved completion of combustion leads to further increases in premixed ratio by heat.

Because significant incomplete combustion occurs during the original sweep of engine loads,

the evaluations about premixed ratio are conducted on the cases after the optimization of combustion phase location. As shown in Figure 6.44, the premixed ratios are given against equivalence ratio for increased engine load at 1500 rpm, 1900 rpm and 2500 rpm. Normally, the trend of premixed ratio is flat at moderate engine load for each engine speed; while decreases of premixed ratio are detected at excessive low equivalence ratio around 0.3 and at equivalence ratio higher than 0.82. For the low equivalence cases, optimal combustion phase locations are achieved by retarding ignition though increased EGR rate and reduced intake temperature at low fuelling rate, as shown in Table 6.3. The increased heat capacity and reduced intake temperature lead to lower temperature of bulk-air during fuel evaporation and combustion, and eventually result less flammable mixture at the start of combustion and reduced oxidation rate during premixed combustion. At high load, low EGR rates are adopted in order to avoid deteriorated combustion efficiency and lead to reduced heat capacity of bulk-air. Thus, less time is available for mixing since the ignition limit is reached earlier during the compression stroke. The inferior mixing is considered responsible for the decreased premixed ratio at high load. The increases of premixed ratio in heat at high load of 1500 rpm are assessed result from increased combustion temperature due to greater heat released from higher fuelling. Also, as discussed in previous part, increased engine speed is favorable for increasing the degree of premix because the faster piston motion introduces more intensive kinetic energy and enhances fuel-air mixing.

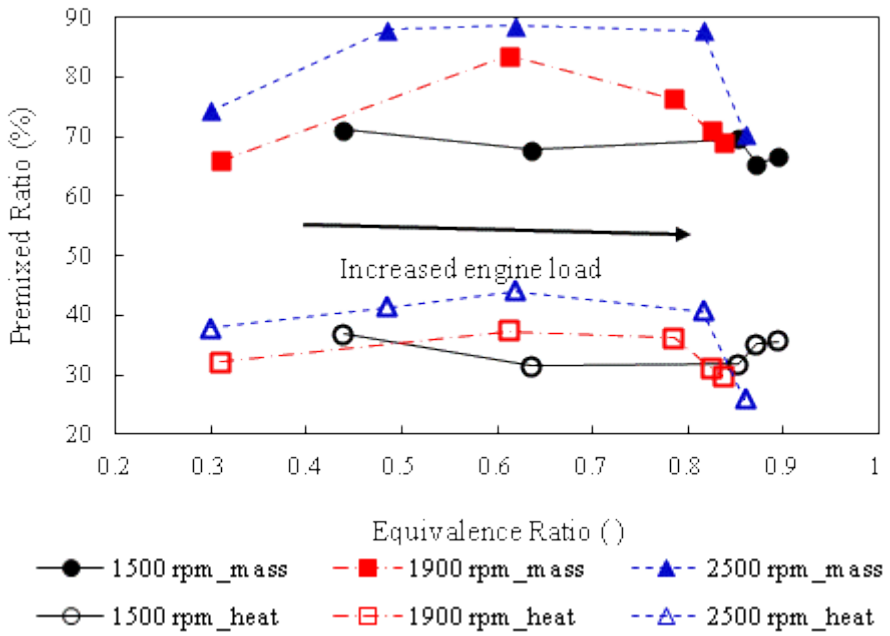

Figure 6.44 The premixed ratios by mass and by heat at different engine loads after adjustment

As shown in Figure 6.45, fuel consumption normally decreases as the degree of premix increases, regardless the engine speed and engine load. However, the reasons for deviations are complicated. Referring to the discussion in section 6.1 and 6.2, with same premixed ratio,

higher engine load intends to results decreased fuel consumption because the oxidation is enhanced due to the increased combustion temperature. Increased engine speed also shows positive effect on fuel consumption since higher kinetic energy is introduced to mixture. Moreover, when large amount of EGR is adopted for optimizing the location of combustion phase, combustion duration intends to prolong and results decreased thermal conversion efficiency at same premixed ratio. Also, the increased heat capacity of bulk-air leads to more heat loss residual in exhaust gas and reduces the heat rejection efficiency of the case using high EGR rate. Therefore, additional fuel consumptions are observed in the cases using increased EGR rate when premixed ratios are same.

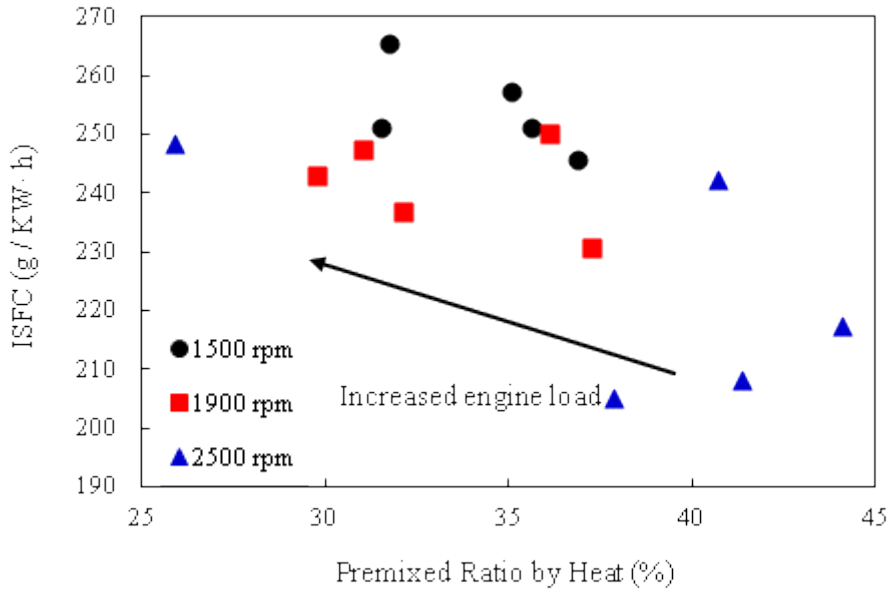

Figure 6.45 The fuel consumptions against the premixed ratios by heat with increased engine load at 1500 rpm, 1900 rpm, and 2500 rpm

No monotonically decreases of soot emissions can be found with increased premixed ratio, as shown in Figure 6.46. Engine speed shows more significant effects on soot emissions. Soot outputs lower than 2 g/kg-fuel are observed mainly at low speed of 1500 rpm. As engine speed increases, the level of soot emissions increases though increased premixed ratio and reduced equivalence ratio are achieved, as shown in Figure 6.44 and Table 6.3. The increased combustion temperature due to greater heat released in the premixed combustion stage is considered responsible for enhancing the formation of soot. Also, near zero soot outputs can be achieved at the lowest engine load of 50 N·m regardless the varied premixed ratio at different speed because the relatively low combustion temperature.

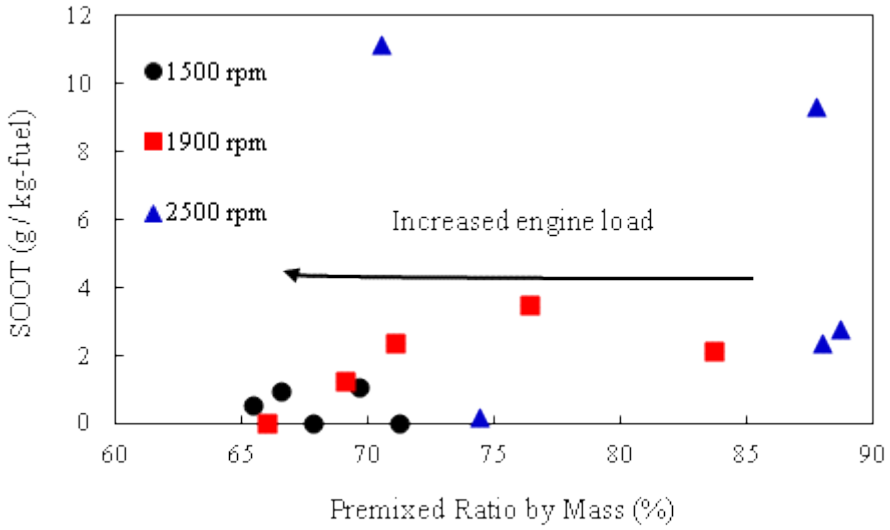

Figure 6.46 The soot emissions against the premixed ratios by mass with increased engine load at 1500 rpm, 1900 rpm, and 2500 rpm

As shown in Figure 6.47, no manifest correlations between CO emissions and premixed ratio can be detected. Referring to Figure 6.29, high EGR rates and low intake temperatures adopted are attributed to the decreased oxidation rates of CO under low engine loads at speeds of 1500 rpm and 1900 rpm, though moderate premixed ratios are achieved at the same time. At 2500 rpm, the reduced time for oxidation is assessed responsible for the increases in CO emission with high equivalence ratio and low premixed ratio. As shown in Figure 6.48, the trend of unburned hydrocarbon is nearly consistent with the trend of ISFC showing Figure 6.45. Increased premixed ratio normally improves the oxidation of hydrocarbon. The two high level outputs of UHC detected at low engine speed are resulted from the inferior evaporation since lower intake temperatures are adopted with high equivalence ratios.

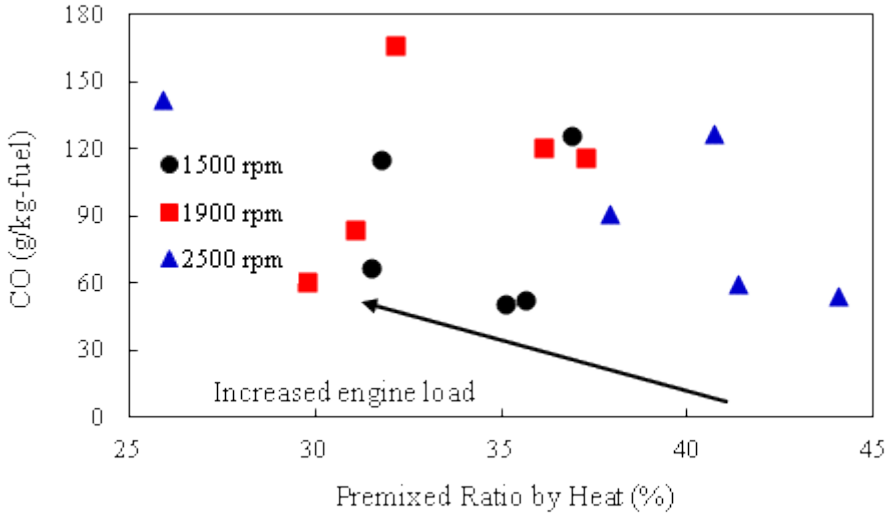

Figure 6.47 The CO emissions against the premixed ratios by mass with increased engine load at 1500 rpm, 1900 rpm, and 2500 rpm

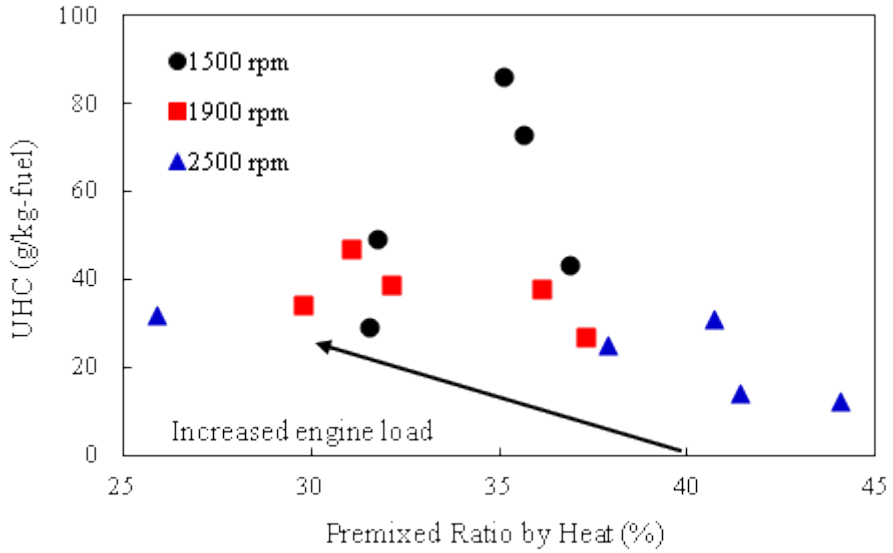

Figure 6.48 The UHC emissions against the premixed ratios by mass with increased engine load at 1500 rpm, 1900 rpm, and 2500 rpm

6.4 Summary

In this chapter, the speed range and load range for the PPCI diesel combustion using split injection are investigated numerically. Primary understandings about the effects of engine speed and load on combustion characteristics and emissions are achieved through the sweep of speed and load. Based on the initially understandings, the methods for optimizing the location of combustion phase are explored. Instead of injection strategy, the adjustments of combustion location are realized by changing EGR rate and initial temperature. The effects of optimization on fuel consumption and emissions are also evaluated. Meantime, a factor named Premixed Ratio (*PR*) is proposed trying to quantitatively describe the level of premix under different operating conditions. The correlations for premixed ratio are studied based on the investigating data about split-injected PPCI diesel combustion which are acquired in Chapter 4. Then the degrees of premix under different operating conditions are investigated using this factor. The relations between premixed ratio and fuel consumption or emissions are discussed in the final part of this chapter.

The following conclusions have been derived from the investigations in this chapter:

1. With same operating parameters, increased engine speed leads to retarded ignition but reduced ignition delay in time domain. Though the time for mixing is reduced, more intensive combustion is detected at higher engine speed with higher peak value of heat release rate in J/ms and shorter combustion duration in ms. Decreased fuel consumption is achieved with increased engine speed, together with decreased NO_x emissions and increased soot, CO and UHC emission.

2. Optimizing the locations of combustion phase at different engine speeds by varied EGR rate and intake temperature cannot assure improvement in thermal conversion efficiency, which is also determined by the length of combustion duration. Extended combustion duration resulted by high EGR rate and low intake temperature cancels the gain in thermal conversion efficiency achieved by optimal combustion location. Larger influences in heat rejection are detected during the optimization, which are considered determine the trend of variations in fuel consumption. Excessively increased NO_x emission is the barrier limit the optimization at high engine speed. However, soot, CO and UHC emissions at high engine speed are suppressed by the optimization.
3. The sweep of engine load shows that the high level of EGR rate limits the implementation of PPCI combustion at high engine load. Fuel consumption, soot, CO and UHC increase significantly with engine load.
4. Significantly reduced EGR rates are adopted for the optimization of combustion location at high engine load. Without additionally reduced intake temperature, the thermal conversion efficiencies decrease massively with engine load at high speed due to the significantly prolonged combustion durations. However, the efficiently improved heat rejection efficiencies due to higher combustion temperature result lower ISFC at high engine speed for almost entire range of loads. The excessively high NO_x and soot emissions at high engine load, especially for high engine speed, imply that the characteristics of PPCI are vanished due to the inferior mixing and significantly increased combustion temperature.
5. The definition of premixed ratio derived from the primary definition of combustion stages in diesel engine is considered to reveal the correlations between the degree of premix and ignition delay, together with equivalence ratio. Moreover, good responds in fuel consumption is observed with premixed ratio based on the data acquired in Chapter 4.
6. Higher premixed ratio is achieved with increased engine speed due to the reduced wall wetting though the ignition delay is reduced slightly. The optimization on the location of combustion phase leads to improved premixed ratio in heat for all speeds.
7. High EGR rate and low intake temperature adopted for the optimization of combustion location at low engine load are attributed to the decrease of premixed ratio owing to the reduced bulk-air temperature for fuel evaporation. Meantime, insufficient time for mixing leads to the reduced premixed ratio at high engine load where low EGR rate is adopted. At high speed and high load, the premixed ratio in heat is reduced to 26%, which can be considered out of the range of PPCI combustion.
8. No monotonically decreases of soot emissions can be found with increased premixed

ratio. Fuel consumption and UHC normally decreases as the degree of premix increases with acceptable discrepancies, regardless the engine speed and engine load.

Chapter 7 Conclusions and Discussion

This study numerically investigated the Partially Premixed Compression Ignition (PPCI) combustion strategy on a high-speed, direct-injection diesel engine aiming to catch up the increasingly stringent emission regulations. A well-established numerical model based on KIVA-3V code coupled with detailed chemistry mechanisms is used for the investigations. The injection strategy using split-injection is adopted since it is indicated to have the potential for further improving the mixing in PPCI combustion [Lee et al., 2006; Park and Bae, 2011]. However, much of the diesel PPCI research has been constrained to the single-injection, and limited pertinent information has been found in available literature explaining the engine performance and emission mechanisms of PPCI using split-injection.

Unlike HCCI combustion, the PPCI diesel combustion adopts moderate early injection and achieves partially stratified mixture prior to ignition. Therefore, PPCI combustion makes it feasible to control the combustion through injection strategy. To realize simultaneously reduced NO_x and soot emissions, the degree of stratification is limited and certainly much less than that in conventional diesel combustion. Thus, the degree of stratification, or in another way the degree of homogeneity is required to be evaluated. This study proposed a definition of Homogeneity Factor (*HF*) to quantitatively evaluate the mixing in PPCI combustion. Also, the relations between the quality of mixing and the characteristics of combustion and emissions are described quantitatively using this factor.

On the other hand, large amount of EGR are usually introduced into intake air in order to achieve prolonged ignition delay and reduced combustion temperature which are important for achieving effective PPCI combustion. However, current researches about the application of EGR in PPCI diesel combustion focus mainly on the overall effects regardless the compositions of EGR. In this study, the effects of the two major constituents, i.e. CO_2 and water vapor, on the engine performance and emission mechanisms of PPCI are numerically investigated.

So far, most studies about PPCI diesel combustion were conducted under moderately low load and moderate speed because the suppressed combustion temperature and sufficient ignition delay for mixing is easy to achieve in this small region of the operating map of diesel engine. It is of great interest to push the current limit of PPCI combustion to higher speed and loads level. Here, the speed range and load range for the PPCI diesel combustion have been investigated when using split injection. To evaluate the degree of premixed combustion, a factor name Premixed Ratio (*PR*) is proposed.

Primarily, the strategy of split-injection was investigated parametrically by analysing the effects of 2^{nd} injection timing, the fuel split proportion, the spray angle and injection pressure on the

combustion performance and emission mechanisms of PPCI. Moreover, the effects of swirl ratio, EGR rate and boost pressure are examined to develop the operating range of PPCI engine. The Homogeneity Factor (*HF*) is proposed to quantitatively characterize mixing under different injection strategies. The following conclusions are reached:

1. The injection strategy influences the combustion and emissions of PPCI diesel combustion. Comparing to the single injection, the split-injection strategy is effective in improving the mixing of fuel and air. This advantage in the formation of mixture is beneficial to remitting the penalty in fuel consumption of the PPCI diesel combustion when pursuing simultaneously reduced NO_x and soot emissions.
2. The parameters of split-injection should be chosen carefully for desired performance of PPCI diesel combustion. According to the findings of this study, the 2nd injection timing should not later than a 'threshold' to keep the engine running under the characteristics of premixed combustion. Meantime, increased fraction of fuel in the 1st injection would increase the homogeneity of mixture before ignition. However, further improvement of the mixing process is required to avoid the increased UHC and CO emission owing to the relatively low temperature during the injection and combustion. With the moderately advanced injection timing, narrow spray angle is not favourable for the reducing of ISFC and emissions in the PPCI diesel combustion. The effects of injection pressure are not significant on most combustion characteristics and emissions for the PPCI diesel combustion, comparing to the standard diesel combustion.
3. For the in-cylinder environment, high swirl ratio is not favourable for improving mixing when using relatively late 2nd injection because the high-speed air flow would trap the fuel inside the eddy. Meantime, various EGR rate and boost pressure are both effective in the control of the combustion phase of PPCI. Nevertheless, the EGR rate would be the more feasible parameter for controlling since its effects on fuel consumption and emissions are not significant until it reaches a certain level (50% in this study).
4. The definition of homogeneity factor (*HF*) proposed in this study shows the capability to quantitatively evaluate the homogeneity of mixture achieved using different injection parameters and under different in-cylinder conditions. It provides a feasible method to compare the quality of mixture between different engines and different operating conditions in same engine. Moreover, the apparent correlation between 50% burn location and the *HF* suggests that the *HF* can be considered as a parameter to indicate the combustion phase location.

In the second part, different EGR compositions with varied fraction of CO_2 or H_2O are applied in PPCI combustion in order to evaluate the effects of EGR constituents on the combustion performance and emissions. Moreover, the parametric study is conducted under a sweep of the

2nd injection timing and EGR rate, in order to achieve understanding of the effects of CO_2 and water vapor in EGR at different operating modes. The following conclusions are reached:

1. The study about the effects of EGR constituents on the performance of PPCI combustion and emissions suggests a method to influence the combustion performance by adjusting the thermal effect of EGR without changing the dilution level.
2. Because of the higher molar heat capacity of CO_2, prolonged ignition delay can be achieved by increasing the fraction of CO_2 in EGR owing to the slower raising of in-cylinder temperature. And lower combustion temperature is also detected for the same reason. These two factors are both beneficial for realising simultaneous reduction of NO_x and soot in the PPCI diesel combustion.
3. Significant increase of fuel consumption is detected in the case using high fraction of CO_2 in EGR when the 2nd injection timing is away from TDC. The excessively low combustion temperature is considered to result the deterioration of fuel efficiency. The improvement in the trade-off between NO_x and soot are more efficient when using the relatively late 2nd injection timing. Meantime, the excessively reduced combustion temperature can result in significant incomplete combustion when using high fraction of CO_2 in EGR at high dilution level.

In the third part, the primary understandings about the effects of engine speed and load on combustion characteristics and emissions are achieved through the sweep of speed and load. Based on the initially understandings, the methods for adjusting the location of combustion phase are explored. Instead of injection strategy, the adjustments of combustion location are realized by changing EGR rate and initial temperature. The effects of adjusting on fuel consumption and emissions are also evaluated. Meantime, a factor named Premixed Ratio (*PR*) is proposed trying to quantitatively describe the level of premix under different operating conditions. The correlations of premixed ratio are studied based on the investigating data about split-injected PPCI diesel combustion which are acquired in Chapter 4. Then the degrees of premix under different operating conditions are investigated using this factor. The relations between premixed ratio and fuel consumption or emissions are discussed. The following conclusions are reached:

1. At high engine speed, the limitations in time for the mixing of fuel-air and the oxidation of soot emission are the major barriers to implementing PPCI diesel combustion. Though decreased fuel consumption is detected at high engine speed, soot, CO and UHC emissions are increased with speed. Meanwhile, the application of high level EGR limits the implementation of PPCI diesel combustion at high engine load.
2. The adjustment of combustion location cannot ensure improvements in the thermal

conversion efficiency, when varied EGR rate and initial temperature are adopted for adjusting. The gain in thermal conversion efficiency achieved by optimized combustion location can be cancelled by the extended combustion duration resulted by high EGR rate and low intake temperature. Moreover, the excessively increased NO_x emission is the barrier limit the optimization at high engine speed. Meantime, both NO_x and soot emissions at high engine load are significantly high, which implies that the advantages of PPCI are vanished due to the inferior mixing and significantly increased combustion temperature.

3. The definition of premixed ratio derived from the primary definition of combustion stages in diesel engine is considered reveal the correlations between the degree of premix and ignition delay, together with equivalence ratio. Moreover, the trend of decrease in fuel consumption with increased premixed ratio is obvious, according to the date acquired in this study. However, no monotonically decreases of soot emissions can be found with increased premixed ratio. At high speed and high load, the premixed ratio in heat is reduced to 26%, which can be considered out of the range of PPCI combustion.

Further recommendation

- The exploring about the effects of variable compression ratios on PPCI combustion would be meaningful for extending the operating range and controlling of combustion. It can be applied by variable valve actuation and will not lead too much extra cost in real engine. Then, it is possible to increase ignition delay without increasing EGR rate or reducing intake temperature. However, the reduced compression ratio may result decreased combustion efficiency.
- The influences on combustion noise are not concluded in this study which could be serious when the degree of premixed combustion increases. Therefore, an extensive evaluation on the combustion noise will improve the completion of the understanding of PPCI diesel combustion.
- The criterion differentiating the PPCI combustion from conventional diesel combustion needs to be improved. According to this study and other literatures [Park and Bae, 2011], relatively long combustion duration exists in PPCI combustion when very low combustion temperature is released by introducing significantly large amount of cool EGR.
- The application of after treatment device, like three-way catalyst, can be investigated since the PPCI diesel combustion has the potential to suppress NO_x and soot emissions at high equivalence ratio near stoichiometric. However, the lighting up of the after treatment device will be a problem since the PPCI combustion usually processes under

low combustion temperature.

- The study of the techniques for improving the fuel economy of PPCI combustion are requested, because its fuel consumption is much higher than that of the conventional diesel combustion according to the results showed in this thesis. The implementation of PPCI diesel combustion will be a challenge if the deterioration in fuel economy cannot be resolved.

References

Abani, N., S. Kokjohn, S. W. Park, M. Bergin, A. Munnannur, W. Ning, Y. Sun and R. D. Reitz (2008). "An Improved Spray Model for Reducing Numerical Parameter Dependencies in Diesel Engine CFD Simulations." SAE 2008-01-0970.

Agrell, F., H.-E. Ångström, B. Eriksson, J. Wikander and J. Linderyd (2003a). Integrated Simulation and Engine Test of Closed Loop HCCI Control by Aid of Variable Valve Timings. SAE 2003-01-0748.

Agrell, F., H.-E. Ångström, B. Eriksson, J. Wikander and J. Linderyd (2003b). Transient Control of HCCI Through Combined Intake and Exhaust Valve Actuation. SAE 2003-01-3172.

Akagawa, H., T. Miyamoto, A. Harada, S. Sasaki, N. Shimazaki, T. Hashizume and K. Tsujimura (1999). Approaches to Solve Problems of the Premixed Lean Diesel Combustion. SAE 1999-01-0183.

Akihama, K., Y. Takatori, K. Inagaki, S. Sasaki and A. M. Dean (2001). Mechanism of the Smokeless Rich Diesel Combustion by Reducing Temperature. SAE 2001-01-0655.

Amsden, A. A. (1993). "KIVA-3: A KIVA Program with Block-Structured Mesh for Complex Geometries." Los Alamos National Laboratory, LA-12503-MS.

Amsden, A. A. (1997). "KIVA-3V: A Block-Structured KIVA Program for Engines with Vertical or Canted Valves." Los Alamos National Laboratory, LA-13313-MS.

Amsden, A. A. (1999). "KIVA-3V, Release 2, Improvement to KIVA-3V." Los Alamos National Laboratory, LA-13608-MS.

Amsden, A. A., P. J. O. Rourke and T. D. Butler (1989). "KIVA-II: A Computer Program for Chemically Reactive Flows with Sprays." Los Alamos National Laboratory, LA-11560-MS.

Azetsu, A. and H. ITO (2007). Effects of CO2 and N2 mixing into Ambient Air on Flame Temperature and Soot Formation in Intermittent Spray Combustion. SAE 2007-01-1844.

Bellman, R. E. and R. H. Pennington (1953). Effects of Surface Tension and Viscosity on Taylor Instability. Santa Monica, Calif: RAND Corporation, RAND Corporation: 403.

Fang, T., R. E. Coverdill, C.-f. F. Lee and R. A. White (2006). Combustion and Soot Visualization of Low Temperature Combustion within an HSDI Diesel Engine Using Multiple Injection Strategy. SAE 2006-01-0078.

Friedrich, I., H. Pucher and T. Offer (2006). Automatic Model Calibration for Engine-Process

Simulation with Heat-Release Prediction. SAE 2006-01-0655.

Golovitchev, V. I. (2000). from http://www.tfd.chalmers.se/~valeri/MECH.html.

Golovitchev, V. I. (2002). "The mechanism of iso-octane." from http://www.tfd.chalmers.se/~valeri/MECH.html.

Han, Z. and R. D. Reitz (1995). "Turbulence Modeling of Internal Combustion Engines Using RNG k-ε Models." Combustion Science and Technology 106(4): 267 -- 295.

Han, Z. and R. D. Reitz (1997). "A temperature wall function formulation for variable-density turbulent flows with application to engine convective heat transfer modeling." International Journal of Heat and Mass Transfer 40(3): 613-625.

Han, Z., Z. Xu and N. Trigui (2000). "Spray/wall interaction models for multidimensional engine simulation." International Journal of Engine Research 1(1): 127 - 146.

Harada, A., N. Shimazaki, S. Sasaki, T. Miyamoto, H. Akagawa and K. Tsujimura (1998). The Effects of Mixture Formation on Premixed Lean Diesel Combustion Engine. SAE 980533.

Hardy, W. L. and R. D. Reitz (2006). A Study of the Effects of High EGR, High Equivalence Ratio, and Mixing Time on Emissions Levels in a Heavy-Duty Diesel Engine for PCCI Combustion. SAE 2006-01-0026.

Hasegawa, R. and H. Yanagihara (2003). HCCI Combustion in DI Diesel Engine SAE 2003-01-0745.

Held, A., P. D. P. Taylor and C. Ingelbrecht (1999). "Measuring Metal Homogeneity in a Matrix via the Measurement of the Ratio Metal to Matrix Oxide Using ICP-MS." Fresenius J Anal Chem 364: 437~439.

Helmantel, A. (2008). Reduction of NOx Emissions from a Light Duty DI Diesel Engine in Medium Load Conditions with High EGR Rates SAE 2008-01-0643

Heywood, J. B. (1988). Internal combustion engine fundamentals, McGraw-Hill Science/Engineering/Math.

Horibe, N., S. Harada, T. Ishiyama and M. Shioji (2009). "Improvement of premixed charge compression ignition-based combustion by two-stage injection." International Journal of Engine Research 10(2): 71-80.

Hu, B. and C. J. Rutland (2006). Flamelet Modeling with LES for Diesel Engine Simulations. SAE 2006-01-0058.

Hu, B., C. J. Rutland and T. A. Shethaji (2008). Combustion Modelling of Conventional Diesel-type and HCCI-type Diesel Combustion with Large Eddy Simulations. SAE

2008-01-0958.

Husberg, T., S. Gjirja, I. Denbratt and J. Engström (2005). Fuel Equivalence Ratio and EGR Impact on Premixed Combustion Rate and Emission Output on a Heavy-Duty Diesel Engine. SAE 2005-24-046.

Hyvonen, J., G. Haraldsson and B. Johansson (2003). Operating range in a Multi Cylinder HCCI engine using Variable Compression Ratio. SAE 2003-01-1829.

Iida, N. (1993). Surrounding Gas Effects on Soot Formation and Extinction - Observation of Diesel Spray Combustion Using a Rapid Compression Machine. SAE 930603.

Jacobs, T. J., S. V. Bohac, D. N. Assanis and P. G. Szymkowicz (2005). Lean and Rich Premixed Compression Ignition Combustion in a Light-Duty Diesel Engine. SAE 2005-01-0166.

Jafari, A. and S. K. Hannani (2006). "Effect of fuel and engine operational characteristics on the heat loss from combustion chamber surfaces of SI engines." International Communications in Heat and Mass Transfer 33(1): 122-134.

Jia, M., Z. Peng and M. Xie (2008a). Evaluation of Breakup Models and Application to the Mixture Preparation Process for Diesel HCCI Engines. SAE 2008-01-0023.

Jia, M., M. Xie and Z. Peng (2008b). Prediction of the Operating Range for a HCCI Engine Based on a Multi-zone Model. SAE 2008-01-1663.

Jia, M., Z. J. Peng and M. Z. Xie (2009). "Numerical investigation of soot reduction potentials with diesel homogeneous charge compression ignition combustion by an improved phenomenological soot model." Proceedings of the Institution of Mechanical Engineers, Part D: Journal of Automobile Engineering 223(3): 395-412.

Jia, M. and M. Xie (2006). "A chemical kinetics model of iso-octane oxidation for HCCI engines." Fuel 85(17-18): 2593-2604.

Jia, M., M. Xie and Z. Peng (2008c). Prediction of the Operating Range for a HCCI Engine Based on a Multi-zone Model. SAE 2008-01-1663.

Kaario, O., E. Antila, K. Lehto, V. Vuorinen and M. Larmi (2009). Computational Considerations of Fuel Spray Mixing in an HCCI Operated Optical Diesel Engine.

Kamimoto, T. and M.-h. Bae (1988). High Combustion Temperature for the Reduction of Particulate in Diesel Engines. SAE 880423.

Kanda, T., T. Hakozaki, T. Uchimoto, J. Hatano, N. Kitayama and H. Sono (2005). PCCI Operation with Early Injection of Conventional Diesel Fuel. SAE 2005-01-0378.

Kazakov, A. and D. Foster (1998). Modeling of soot formation during DI diesel combustion

using a multi-step phenomenological model. SAE 982463.

Kee, R. J., F. M. Rupley, E. Meeks and J. A. Miller (1996). "CHEMKIN-III: A FORTRAN CHEMICAL KINETICS PACKAGE FOR THE ANALYSIS OF GAS-PHASE CHEMICAL AND PLASMA KINETICS." Sandia National Laboratories, SAND96-8216.

Keeler, B. and P. J. Shayler (2008). Constraints on Fuel Injection and EGR Strategies for Diesel PCCI-Type Combustion. SAE 2008-01-1327.

Kerschgens, B., C. Felsch, A. Vanegas and N. Peters (2009). Applying an Interactively Coupled CFD-Multi-Zone Approach to Study the Effects of Piston Bowl Geometry Variations on PCCI Combustion. SAE 2009-01-1955.

Khan, I. M., G. Greeves and C. H. T. Wang (1973). Factors Affecting Smoke and Gaseous Emissions from Direct Injection Engines and a Method of Calculation. SAE 730169.

Kim, D., I. Ekoto, W. F. Colban and P. C. Miles (2008). In-cylinder CO and UHC Imaging in a Light-Duty Diesel Engine during PPCI Low-Temperature Combustion. SAE 2008-01-1602.

Kim, Y.-J., S. H. Lee and N.-H. Cho (1999). "Effect of Air Motion on Fuel Spray Characteristics in a Gasoline Direct Injection Engine."

Kimura, S., O. Aoki, Y. Kitahara and E. Aiyoshizawa (2001). Ultra-Clean Combustion Technology Combining a Low-Temperature and Premixed Combustion Concept for Meeting Future Emission Standards. SAE 2001-01-0200.

Kimura, S., O. Aoki, H. Ogawa, S. Muranaka and Y. Enomoto (1999). New Combustion Concept for Ultra-Clean and High-Efficiency Small DI Diesel Engines. SAE 1999-01-3681.

Kiplimo, R., E. Tomita, N. Kawahara and S. Yokobe (2012). "Effects of spray impingement, injection parameters, and EGR on the combustion and emission characteristics of a PCCI diesel engine." Applied Thermal Engineering 37(0): 165-175.

Koci, C. P., Y. Ra, R. Krieger, M. Andrie, D. E. Foster, R. M. Siewert and R. P. Durrett (2009). Multiple-Event Fuel Injection Investigations in a Highly-Dilute Diesel Low Temperature Combustion Regime. SAE 2009-01-0925.

Kokjohn, S. L. and R. D. Reitz (2008). A Computational Investigation of Two-Stage Combustion in a Light-Duty Engine. SAE 2008-01-2412

Kokjohn, S. L. and R. D. Reitz (2010). Characterization of Dual-Fuel PCCI Combustion in a Light-Duty Engine.

Kong, S.-C., C. D. Marriott, R. D. Reitz and M. Christensen (2001). Modeling and Experiments of HCCI Engine Combustion Using Detailed Chemical Kinetics with Multidimensional CFD.

SAE 2001-01-1026.

Kong, S.-C., Y. Ra and R. D. Reitz (2005a). "Performance of multi-dimensional models for simulating diesel premixed charge compression ignition engine combustion using low- and high-pressure injectors." International Journal of Engine Research 6(5): 475-486.

Kong, S.-C., Y. Sun and R. D. Reitz (2005). "Modeling Diesel Spray Flame Lift-Off, Sooting Tendency and NOx Emissions Using Detailed Chemistry With Phenomenological Soot Model." ASME Conference Proceedings 2005(41847): 149-157.

Kook, S., C. Bae, P. C. Miles, D. Choi, M. Bergin and R. D. Reitz (2006). The Effect of Swirl Ratio and Fuel Injection Parameters on CO Emission and Fuel Conversion Efficiency for High-Dilution, Low-Temperature Combustion in an Automotive Diesel Engine. SAE 2006-01-0197.

Kook, S., C. Bae, P. C. Miles, D. Choi and L. M. Pickett (2005). The Influence of Charge Dilution and Injection Timing on Low-Temperature Diesel Combustion and Emissions. SAE 2005-01-3837.

Ladommatos, N., S. M. Abdelhalim, H. Zhao and Z. Hu (1996a). The Dilution, Chemical, and Thermal Effects of Exhaust Gas Recirculation on Diesel Engine Emissions - Part 1: Effect of Reducing Inlet Charge Oxygen. SAE 961165.

Ladommatos, N., S. M. Abdelhalim, H. Zhao and Z. Hu (1996b). The Dilution, Chemical, and Thermal Effects of Exhaust Gas Recirculation on Diesel Engine Emissions - Part 2: Effects of Carbon Dioxide. SAE 961167.

Ladommatos, N., S. M. Abdelhalim, H. Zhao and Z. Hu (1997a). The Dilution, Chemical, and Thermal Effects of Exhaust Gas Recirculation on Diesel Engine Emissions - Part 3: Effects of Water Vapour. SAE 971659.

Ladommatos, N., S. M. Abdelhalim, H. Zhao and Z. Hu (1997b). The Dilution, Chemical, and Thermal Effects of Exhaust Gas Recirculation on Disesel Engine Emissions - Part 4: Effects of Carbon Dioxide and Water Vapour. SAE 971660.

Lapuerta, M., J. M. Salavert and C. Doménech (1995). Modeling and Experimental Study About the Effect of Exhaust Gas Recirculation on Diesel Engine Combustion and Emissions. SAE 950216.

Launder, B. E. and D. B. Spalding (1974). "The numerical computation of turbulent flows." Computer Methods in Applied Mechanics and Engineering 3(2): 269-289.

Lázaro, J. L., J. L. García-Bernad, C. Pérez, J. Galindo, H. Climent and F. J. Arnau (2002). "Cooled EGR Modulation: A Strategy to Meet EURO IV Emission Standards in Automotive DI

Diesel Engines." SAE 2002-01-1154.

Lechner, G. A., T. J. Jacobs, C. A. Chryssakis, D. N. Assanis and R. M. Siewert (2005). Evaluation of a Narrow Spray Cone Angle, Advanced Injection Timing Strategy to Achieve Partially Premixed Compression Ignition Combustion in a Diesel Engine. SAE 2005-01-0167.

Lee, S. and R. D. Reitz (2006a). Spray Targeting to Minimize Soot and CO Formation in Premixed Charge Compression Ignition (PCCI) Combustion with a HSDI Diesel Engine SAE 2006-01-0918.

Lee, S., M. A. G. D. and R. D. Reitz (2006b). Stoichiometric Combustion in a HSDI Diesel Engine to Allow Use of a Three-way Exhaust Catalyst. SAE 2006-01-1148.

Lee, S.-S. (2006). Investigation of Two Low Emissions Strategies for Diesel Engines; Premixed Charge Compression Ignition (PCCI) and Stoichiometric Combustion, UNIVERSITY OF WISCONSIN - MADISON. Doctor of Philosophy 78~103.

Lewander, M., B. Johansson, P. Tunestål, N. Keeler, S. Tullis, N. Milovanovic and P. Bergstrand (2009). Evaluation of the Operating Range of Partially Premixed Combustion in a Multi Cylinder Heavy Duty Engine with Extensive EGR SAE 2009-01-1127.

Martin, G. C., C. J. Mueller, D. M. Milam, M. S. Radovanovic and C. R. Gehrke (2008). Early Direct-Injection, Low-Temperature Combustion of Diesel Fuel in an Optical Engine Utilizing a 15-Hole, Dual-Row, Narrow-Included-Angle Nozzle. SAE 2008-01-2400.

MathWorks. (2013). "Help Documents for Statistics Toolbox." from http://www.mathworks.com/.

Miles, P. C. (2000). The Influence of Swirl on HSDI Diesel Combustion at Moderate Speed and Load. SAE 2000-01-1829.

Miles, P. C., D. Choi, S. Kook, M. J. Bergin and R. D. Reitz (2005). The Influence of Flow Structures and Mixing on Low-Temperature Diesel Combustion, 5th Symposium in Lund Institute of Technology.

Munnik, F., K. A. Sjoland and U.Watjen (2000). "Using microprobe distribution maps to determine homogeneity and correlation between elements." Nuclear Instruments and Methods in Physics Research B 161-163: 348~353.

Naber, J. D. and R. D. Reitz (1988). Modelling engine spray/wall impingement. SAE 880107.

Nagle, J. and R. F. Strickland-Constable (1962). Oxidation of carbon between 1000℃ and 2000℃, Pergamon Press.

Nakagome, K., N. Shimazaki, K. Niimura and S. Kobayashi (1997). Combustion and Emission

Characteristics of Premixed Lean Diesel Combustion Engine. SAE 970898.

Nandha, K. P. and J. Abraham (2002). Dependence of Fuel-Air Mixing Characteristics on Injection Timing in an Early-Injection Diesel Engine. SAE 2002-01-0944.

Neely, G. D., S. Sasaki, Y. Huang, J. A. Leet and D. W. Stewart (2005). New Diesel Emission Control Strategy to Meet US Tier 2 Emissions Regulations. SAE 2005-01-1091.

Neoh, K. G., J. B. Howard and A. F. Sarofim (1985). "Effect of oxidation on the physical structure of soot." Symposium (International) on Combustion 20(1): 951-957.

Nordin, P. A. N. (2001). Complex chemistry modeling of diesel spray combustion. Go ̈teborg, Sweden, Chalmers University of Technology. PhD.

Okude, K., K. Mori, S. Shiino and T. Moriya (2004). Premixed Compression Ignition (PCI) Combustion for Simultaneous Reduction of NOx and Soot in Diesel Engine. SAE 2004-01-1907.

Opat, R., Y. Ra, M. A. G. D., R. Krieger, R. D. Reitz, D. E. Foster, R. P. Durrett and R. M. Siewert (2007). Investigation of Mixing and Temperature Effects on HC/CO Emissions for Highly Dilute Low Temperature Combustion in a Light Duty Diesel Engine. SAE 2007-01-0193.

O'Rourke, P. J. (1981). Collective Drop Effects on Vaporizing Liquid Spray. Technical Report Los Alamos National Laboratory.

O'Rourke, P. J. and A. A. Amsden (2000). A Spray/Wall Interaction Submodel for the KIVA-3 Wall Film Model. SAE 2000-01-0271.

Park, Y. and C. Bae (2011). "Influence of EGR and Pilot Injection on PCCI Combustion in a Single-Cylinder Diesel Engine." SAE 2011-01-1823.

Patel, A., S.-C. Kong and R. D. Reitz (2004). Development and Validation of a Reduced Reaction Mechanism for HCCI Engine Simulations. SAE 2004-01-0558

Patterson, M. A. and R. D. Reitz (1998). Modeling the Effects of Fuel Spray Characteristics on Diesel Engine Combustion and Emission. SAE 980131.

Peng, Z. and M. Jia (2008). "An investigation and evaluation of variable-valve-timing and variable-valve-actuation strategies in a diesel homogeneous charge compression ignition engine using three-dimensional computational fluid dynamics." Proceedings of the Institution of Mechanical Engineers, Part D: Journal of Automobile Engineering 222(6): 1047 - 1064.

Reitz, R. D. (1987). "Modeling Atomization Processes in High-Pressure Vaporization Sprays." Atomization and Spray Technology 3(4): 309 -- 337.

Reitz, R. D. and F. V. Bracco (1986). Mechanisms of Breakup of Round Liquid Jets. The Encyclopedia of Fluid Mechanics. N. P. Cheremisinoff. 3: 223 -- 249.

Reitz, R. D. and R. Diwakar (1987). Structure of High-Pressure Fuel Sprays. SAE 870598.

Ricardo. (2006). from http://www.ricardo.com/engineeringservices/engine.aspx?page=hydra.

Ricart, L. M., R. D. Reitz and J. E. Dec (2000). "Comparisons of Diesel Spray Liquid Penetration and Vapor Fuel Distributions With In-Cylinder Optical Measurements." Journal of Engineering for Gas Turbines and Power 122(4): 588 -- 595.

Richter, M., R. Collin, J. Nygren, M. Alden, L. Hildingsson and B. Johansson (2005). "Studies of the Combustion Process with Simultaneous Formaldehyde and OH PLIF in a Direct-Injected HCCI Engine." JSME International Journal Series B Fluids and Thermal Engineering 48(4): 701-707.

Rogers, G. F. C. and Y. R. Mayhew (1994). Thermodynamic and Transport Properties of Fluids : SI Units, Wiley-Blackwell.

Ryan, T. W. and T. J. Callahan (1996). Homogeneous Charge Compression Ignition of Diesel Fuel. SAE 961160.

Siewert, R. M. (2007). Spray Angle and Rail Pressure Study for Low NOx Diesel Combustion. SAE 2007-01-0122.

Sjoberg, M. and J. E. Dec (2007). EGR and Intake Boost for Managing HCCI Low-Temperature Heat Release over Wide Ranges of Engine Speed. SAE 2007-01-0051.

Smith, G. P., D. M. Golden, M. Frenklach, N. W. Moriarty, B. Eiteneer, M. Goldenberg, C. T. Bowman, R. K. Hanson, S. Song, W. C. Gardiner, V. V. Lissianski and Z. Qin. (2000). from http://www.me.berkeley.edu/gri_mech/.

Tao, F., D. E. Foster and R. D. Reitz (2006). Soot Structure in a Conventional Non-Premixed Diesel Flame. SAE 2006-01-0196.

Torralba, J. M., F.VELASCO, J. M. RUIZ-ROMÄN, L. E. G. CAMBRONERO and J. M. RUIZ-PRIETO (1996). "Reliability and Homogeneity study of sintered steels through the Weibull statistic." Journal of Materials Science Letters 15: 2015~2017.

Walls, J. R. and R. F. Strickland-Constable (1964). "Oxidation of carbon between 1000-2400 ℃." Carbon 1(3): 333-334, IN323, 335-338.

Walter, B. and B. Gatellier (2002). Development of the High Power NADI Concept Using Dual Mode Diesel Combustion to Achieve Zero NOx and Particulate Emissions. SAE 2002-01-1744.

Watson, N., A. D. Pilley and M. Marzouk (1980). A Combustion Correlation for Diesel Engine

Simulation. SAE 800029.

Westbrook, C. K. (2000). "CHEMICAL KINETICS OF HYDROCARBON IGNITION IN PRACTICAL COMBUSTION SYSTEMS." Proceedings of the Combustion Institute 28: 1563 -- 1577.

Xu, M., K. Nishida and H. Hiroyasu (1992). A Practical Calculation Method for Injection Pressure and Spray Penetration in Diesel Engines. SAE 920624.

Yun, H. and R. D. Reitz (2007). "An Experimental Investigation on the Effect of Post-Injection Strategies on Combustion and Emissions in the Low-Temperature Diesel Combustion Regime." Journal of Engineering for Gas Turbines and Power 129: 279.

Zhao, H. (2007). HCCI and CAI engines for the automotive industry. H. Zhao. Abington, Woodhead Publishing Limited: 241-266.